Synthesis and Characterization of Homopolymers and Copolymers via ROMP Based on High-Strain Cyclic Alkenes as Potential Candidates for Organic Electronics and Electro-Optic Device Applications

マフムード, バスユーニ

九州大学
KYUSHU UNIVERSITY

Synthesis and Characterization of Homopolymers and Copolymers via ROMP Based on High-Strain Cyclic Alkenes as Potential Candidates for Organic Electronics and Electro-Optic Device Applications

by

MAHMOUD BASYOUNI

A Dissertation Submitted to Chemistry and Materials Science Major, Department of Interdisciplinary Engineering Sciences, Interdisciplinary Graduate School of Engineering Sciences, Kyushu University, Japan
For the Degree of

Doctor of Philosophy

Sep 2025

Abstract

This thesis investigates the synthesis and characterization of homopolymers, and copolymers derived from high-strain cyclic alkenes via ring-opening metathesis polymerization (ROMP), employing various generations of Grubbs catalysts. The research focuses on developing polymeric materials with potential applications in organic electronics and electro-optic devices. The study includes the synthesis of poly(*p*-phenylenevinylene) (PPV) derivatives, where the effect of different linking groups, particularly alkyl groups, on the properties of the synthesized PPV polymers was explored. A key aspect of the research also involves evaluating commercially effective methods for benzyne rearrangement in the synthesis of PPV derivatives. Further, the research covers the synthesis of homopolymers such as carbazole-functionalized norbornene dicarboximide (CA-NDI) and adamantane-functionalized norbornene dicarboximide (Ad-NDI) and explores copolymerization strategies to enhance the thermal stability of PPV derivatives. In the final part of this thesis, efforts were focused on optimizing the polymerization and copolymerization of donor and acceptor monomers using the ROMP technique. Two homopolymers were synthesized individually from a carbazole hexyl-based donor (CAH-NDI) and a triazine-based acceptor (DCT-NDI), respectively. Furthermore, a series of copolymers was prepared by varying the feed ratios of the donor and acceptor monomers. The goal was to study how monomer structure and composition affect the polymerization behavior, control over molecular weight, and final polymer properties. This study provides valuable insights into the design and synthesis of donor–acceptor polymers via ROMP, contributing to the development of functional materials with tunable characteristics for future high-performance applications.

Acknowledgments

In the name of Allah, the Most Gracious, the Most Merciful. All praise and gratitude are due to Allah, who has guided me at every step and blessed me with the strength and perseverance to complete this doctoral journey. His mercy and blessings have been the true foundation of all my achievements.

I would like to express my sincere and profound gratitude to my supervisor, **Associate Professor Andrew Spring**, for his exceptional mentorship, unwavering support, and constant encouragement throughout my doctoral studies at Kyushu University. His guidance, insightful feedback, and belief in my potential have been invaluable to both my academic and personal growth. I will remain forever grateful for his mentorship.

I am also deeply thankful to **Associate Professor Hiroshi Furuno**, who shared the laboratories with Spring Sensei's group, for his valuable discussions and support throughout my PhD journey. His insights added meaningful depth to my research experience.

My sincere thanks go to the **Albrecht Research Group** for providing access to their facilities and for their kind guidance throughout my research. I am also grateful to the **Adachi Research Group** for their collaboration and generous support, which greatly enriched the technical scope of my project.

I also appreciate the companionship and contributions of my labmates in the Spring research group at IGSES Keisuke Nomura, Yuto Goroumaru,

Mohamed Ezzat, and Mohammed Fouad. **Keisuke** and **Yuto** made my daily life in Japan much easier, especially during my first semester, by helping me navigate and manage various tasks until I became more independent. **Ezzat** and **Fouad** provided invaluable support and collaboration in drafting our manuscripts; through these efforts, we helped each other grow as researchers. Working alongside such dedicated and supportive colleagues has been both a pleasure and an inspiration.

To my beloved family, I owe everything. My deepest gratitude goes to my parents, **Zakaria** and **Saeida**, for their lifelong sacrifices, endless support, and unwavering belief in my dreams. From the very beginning, you stood beside me with patience, prayers, and unconditional love. You taught me the values of hard work, honesty, and perseverance, and you never stopped encouraging me to aim higher, even when the road was uncertain. Every achievement I've made is rooted in the strength and foundation you gave me. I hope this accomplishment brings you pride and joy, as it is truly a reflection of your lifelong dedication and love.

To my wife, **Warda,** thank you for standing by me, believing in me, and walking with me through every step of this long and challenging journey. From the very beginning, you were not only my partner but my anchor, my closest friend, and my greatest source of strength. When I faced setbacks, you reminded me of my worth. When I doubted myself, you lifted me with

your words, your patience, and your unwavering faith in me. You endured sacrifices, moments of distance, stress, and uncertainty all without complaint just so I could focus on building our future. You celebrated the small wins with me. This achievement is not mine alone, it belongs to us. You helped me realize this dream, and I am eternally grateful. I am proud to call you, my wife. I love you.

To my lovely daughters, **Leen** and **Jannah** you are the joy of my life and the driving force behind everything I strive for. Your laughter, curiosity, and pure hearts have given me strength during the most difficult moments. Even when you were too young to understand, your presence reminded me of what truly matters. I dedicate this achievement to you both, with all my love. I hope you grow up strong, kind, and brave, and that you pursue your dreams with confidence and passion. I have always tried to be the kind of father you can one day be proud of, and I will continue doing my best for you. May your lives be filled with happiness, purpose, and endless love. I will always be proud of you.

I am also thankful to my sister **Sameha** and her family **Shawkat**, **Camellia**, and their newest joy, baby **Youssef,** for their constant love, encouragement, and support. Sameha is like a daughter to me; I love her deeply and wholeheartedly. I truly wish her and her beautiful family all the happiness and blessings life can offer.

In addition to my academic journey, I have had the honor of serving as the representative of the Egyptian Students Association in Japan – Kyushu branch (ESAJ-K), Chikushi Campus, for the academic year April 2024 to March 2025. This role allowed me to support fellow Egyptian students, foster cultural exchange, and contribute to the sense of community within our campus.

I would also like to extend my sincere thanks to Associate Professor **Abdelrahman Zakaria** at Kyushu University for his generous support and guidance during my PhD journey. His encouragement and advice were deeply appreciated and contributed meaningfully to my academic progress.

Lastly, I am grateful to the Japanese Ministry of Education, Culture, Sports, Science, and Technology **(MEXT)** for their financial support throughout my postgraduate studies. I also extend my appreciation to Kyushu University, especially the Interdisciplinary Graduate School of Engineering Sciences and the Department of Chemistry and Materials Science for providing an excellent academic environment and invaluable resources during my doctoral journey.

This journey has been long and filled with challenges. I began pursuing my PhD in 2019 at the College of Chemistry, Huazhong Agricultural University in Wuhan, China. However, the outbreak of the COVID-19 pandemic forced us to return to Egypt, and I was unable to complete my studies there. Despite

this setback, I refused to give up. With determination and hard work, I secured a new opportunity to begin my doctoral studies again.

For that, I would like to sincerely thank myself for the persistence and resilience it took to restart and carry this dream to completion. And to my wife, Warda, your strength, encouragement, and belief in me throughout this uncertain and difficult time were essential. Without your support, I could not have made it this far. This achievement is not mine alone; it is ours.

Mahmoud

Publications

[1] **M.Z. Basyouni**, K. Nomura, Y. Goroumaru, M.F. Radwan, M.E. Abdu, A.M. Spring, Controlled Synthesis of PPV Oligomers by ROMP: Impact on Optical, Structural, and Thermal Properties, Chem. Pap. 79 (2025).

[2] **M.Z. Basyouni**, M.E. Abdu, M.F. Radwan, A.M. Spring, Ring-opening metathesis polymerization of homo- and copolymers Based on p -phenylenevinylene and norbornene-dicarboximide: Enhanced thermal stability for optoelectronic applications, J. Mol. Struct. 1338 (2025) 142296.

[3] **M.Z. Basyouni**, M.F. Radwan, M.E. Abdu, A.M. Spring, Synthesis, Characterization, and Optical Properties of Carbazole-Functionalized Poly(norbornene-dicarboximide) by ROMP, Evergreen 11 (2024) 207–213.

[4] **M.Z. Basyouni**, M.E. Abdu, M.F. Radwan, A.M. Spring, From monomer to polymer: Controlled synthesis and comprehensive analysis of poly(p-phenylene vinylene) via ROMP, J. Mol. Struct. 1310 (2024) 138001.

[5] **M.Z. Basyouni**, M.E. Abdu, M.F. Radwan, A.M. Spring, ROMP-Based Synthesis and Characterization of Donor-Acceptor Norbornene Copolymers, Polym. Bull. (Submitted).

Conferences

[1] **M.Z. Basyouni**, M.F. Radwan, M.E. Abdu, A.M. Spring, Concise Review of TADF: Basic Principles, Material Design, Prospective Applications, and the Role of ROMP in Polymer Synthesis, Int. Exch. Innov. Conf. Eng. Sci. 10 (2024) 597–601.

[2] **M.Z. Basyouni**, J. Ye, A.M. Spring, Conjugated Polymers and ROMP: Synthesis, Applications, and Prospects for Technological Innovations, Int. Exch. Innov. Conf. Eng. Sci. 9 (2023) 405–411.

Joint Research

[1] M.E. Abdu, M.F. Radwan, D.A. Elsayed, W.S. Shehab, W.A. Zordok, **M.Z. Basyouni**, A.M. Spring, Controlled synthesis, characterization and computational studies of novel homo and random Co-polymers from carbazolovinylene and phenothiazinovinylene via ROMP chemistry, Polyer. 333 (2025) 128590.

[2] M.F. Radwan, M.E. Abdu, M.M. Elkady, **M.Z. Basyouni,** A.M. Spring, Living ROMP of N -phenothiazinyl norbornene-dicarboximide homopolymer: Synthesis, characterization, and physical behavior insights, Polymer. 321 (2025) 128115.

Table of Contents

List of Schemes

List of Figures

List of Tables

Abbreviations

ROMP	Ring opening metathesis polymerization
OLEDs	Organic light emitting diodes
NDI	Norbornene dicarboximide
CA	Carbazole
Ad	Adamantane
LEDs	Light-emitting diodes
ATRP	Atom transfer radical polymerization
RAFT	Reversible addition fragmentation chain transfer
NMP	Nitroxide mediated polymerization
ADMET	Acyclic diene metathesis polymerization
G1	Grubbs catalyst first generation
G2	Grubbs catalyst second generation
G3	Grubbs catalyst third generation
NHC	N-heterocyclic carbene
S_0	Ground singlet state
S_1	Excited singlet state
T_1	Triplet state
ISC	Intersystem crossing
RISC	Reverse intersystem crossing
ICT	Intramolecular charge transfer
OPV	Organic photovoltaic
OFET	Organic field-effect transistors
VOCs	Volatile organic compounds
GPC	Gel permeation chromatography
DP	Degree of polymerization (DP)
λ_{max}	Wavelength of maximum absorption
λ_{ex}	Excitation wavelength
s	Singlet (NMR)
d	Doublet (NMR)
dt	Doublet of triplets (NMR)
t	Triplet (NMR)

m	Multiplet (NMR)
PDI	Polydispersity index
TGA	Thermogravimetric analysis
DSC	Differential Scanning Calorimetry
NMR	Nuclear magnetic resonance
UV-vis	Ultraviolet-visible
CV	Cyclic voltammetry
TLC	Thin layer chromatography
Tg	Glass transition temperature
Td	Decomposition temperature
Mn	Number average molecular weight
Mw	Weight average molecular weight
DCE)	Dichloroethane
δ	Chemical shift
^{o} C	Degrees Celsius
THF	Tetrahydrofuran
MS	Mass spectrometry
HOMO	Highest occupied molecular orbital
LUMO	Lowest unoccupied molecular orbital
DCC	*N,N'*-dicyclohexylcarbodiimide
DCM	Dichloromethane
DMF	Dimethylformamide
EVE	Ethyl vinyl ether
D.MWD	Differential molecular weight distribution
E_g^{op}	Optical bandgaps
TCT	Trichlorotriazine
PLQYs	Photoluminescence quantum yields

List of synthesized monomers & polymers

M_1	(2*Z*,5*Z*)-12,15-bis(octyloxy)-1,4(1,4)-dibenzenacyclohexaphane-2,5-diene (DO-PCPD)
M_2	2-[(2-Ethylhexyl)oxy]-5-methoxy-dibenzenacyclohexaphane-2,5-diene (EHM-PCPD)
M_3	2-(9*H*-carbazol-9-yl)ethyl 3-((3a*R*,4*S*,7*R*,7a*S*)-1,3-dioxo-1,3,3a,4,7,7a-hexahydro-2*H*-4,7-methanoisoindol-2-yl)propanoate (CA-NDI)
M_4	(3a*R*,4*S*,7*R*,7a*S*)-2-((1*S*,3*S*)-adamantan-1-yl)-3a,4,7,7a-tetrahydro-1*H*-4,7-methanoisoindole-1,3(2*H*)-dione (AD-NDI)
M_5	2-(6-(9*H*-carbazol-9-yl) hexyl)-3a,4,7,7a-tetrahydro-1*H*-4,7-methanoisoindole-1,3(2*H*)-dione (CAH-NDI)
M_6	2-(2-((4,6-dichloro-1,3,5-triazin-2-yl)oxy)ethyl)-3a,4,7,7a-tetrahydro-1*H*-4,7-methanoisoindole-1,3(2*H*)-dione (DCT-NDI)
P_1	poly(2,5-Dioctyloxy-*p*-Phenylenevinylene) DO-PPV
P_2	poly (2-[(2-Ethylhexyl)oxy]-5-methoxy- *p*-phenylenevinylene) EHM-PPV
P_3	poly(CA-NDI)
P_4	poly(Ad-NDI)
P_5	CA-NDI / DO-PPV Random Copolymer
P_6	CA-NDI / EHM-PPV Random Copolymer
P_7	poly (carbazole hexyl-norbornene dicarboximide) (CAH-NDI)
P_8	Synthesis of poly (dichlorotriazine-norbornene dicarboximide) (DCT-NDI)
P_9	CAH-NDI / DCT-NDI Random Copolymer M_5:M_6 0.9:0.1
P_{10}	CAH-NDI / DCT-NDI Random Copolymer M_5:M_6 0.7:0.3
P_{11}	CAH-NDI / DCT-NDI Random Copolymer M_5:M_6 0.5:0.5
P_{12}	CAH-NDI / DCT-NDI Random Copolymer M_5:M_6 0.3:0.7

Chapter 1

Introduction

1.1. Overview of Polymeric Materials

Polymers are a cornerstone of modern life, ubiquitous in applications ranging from packaging and textiles to medical devices and advanced electronics[1–4]. Their versatility stems from a combination of properties such as thermal stability, mechanical strength, chemical resistance, and cost-effectiveness. Polymers are found everywhere, from everyday items like plastic bottles and car tires to cutting-edge materials used in renewable energy and environmental sustainability. By tailoring the composition and structure of polymers, scientists have developed materials suited for diverse needs, such as eco-friendly packaging, high-strength composites, and flexible electronics [5–7].

Historically, polymers were primarily associated with electrical insulation. This changed dramatically with the groundbreaking discovery of conductive polymers in the late 1970s by Heeger, Shirakawa, and MacDiarmid, who demonstrated that polyacetylene could achieve electrical conductivity through doping[8,9]. This milestone earned the researchers the Nobel Prize in Chemistry in 2000 and revolutionized the field of materials science. Unlike traditional polymers, conjugated polymers possess alternating single and double bonds in their backbone, granting them unique electronic and optical properties[10–13]. These materials bridge the gap between metals and semiconductors, combining the processability and lightweight nature of polymers with the electronic capabilities of semiconductors[14].

The development of conjugated polymers has unlocked numerous possibilities in electronic and optoelectronic applications. Their tunable properties have been harnessed in light-emitting diodes (LEDs), organic solar cells, and transistors, offering significant advantages over inorganic counterparts. Conjugated polymers enable large-area device fabrication using solution processing techniques, such as spin-coating and printing, which are cost-efficient and scalable. Moreover, their chemical structures can be easily modified to optimize performance for specific applications, making them highly adaptable materials for the rapidly evolving demands of organic electronics[15,16].

The discovery of electroluminescence in conjugated polymers further propelled their application in light-emitting devices. Organic light-emitting diodes (OLEDs), for example, have garnered attention for their potential in creating flexible, lightweight, and large-area displays. Unlike inorganic LEDs, OLEDs based on conjugated polymers

offer simpler processing methods and lower manufacturing costs, along with the ability to fine-tune their emission properties through synthetic design[17,18].

Despite these advancements, challenges remain in improving the stability, efficiency, and performance of conjugated polymers. Efforts to address these challenges have focused on developing new synthetic methods, such as controlled polymerization techniques, to achieve precise control over molecular weight, composition, and microstructure. The integration of donor-acceptor systems, such as poly(*p*-phenylenevinylene) (PPV) derivatives and norbornene-dicarboximide (NDI) monomers, offers a promising strategy for designing materials with enhanced optoelectronic properties and environmental stability[19].

1.2. Bibliometric Analysis

Bibliometric analysis is a valuable tool for visualizing research trends, identifying influential materials, and mapping interdisciplinary applications within a scientific domain[20]. In this study, VOSviewer software was employed to analyze and visualize data extracted from the Web of Science database, focusing on the field of polymer science. To understand the general research development, a search was conducted using the term "polymer" covering the period from 2015 to 2025. The resulting bibliometric map is shown in (Figure 1. 1).

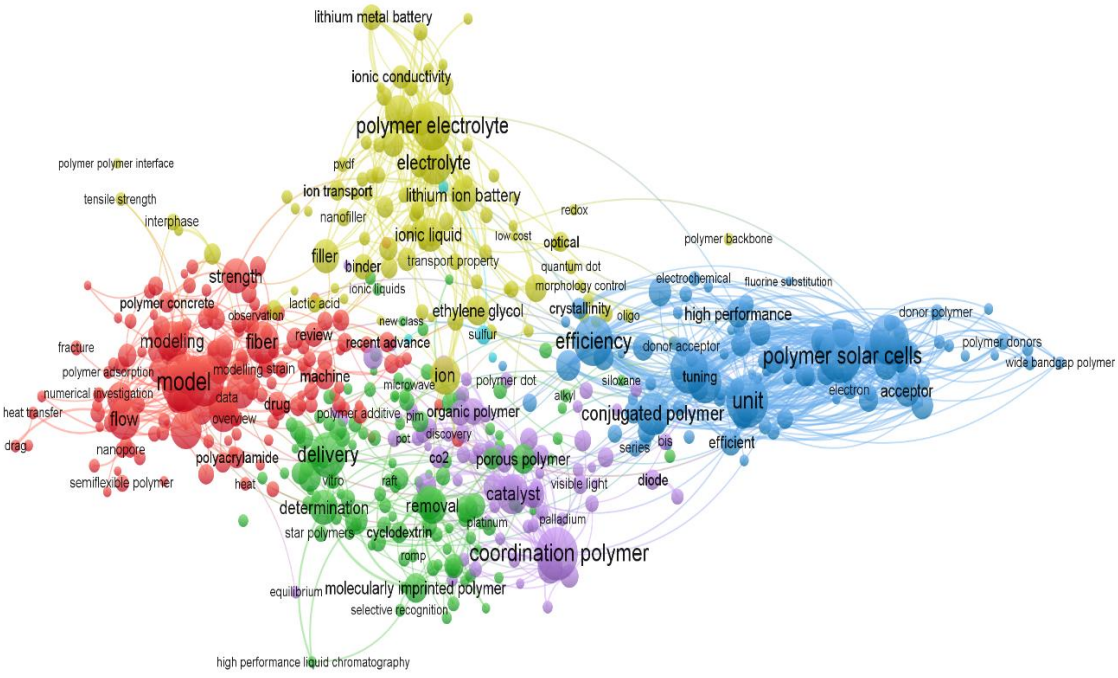

Figure 1. 1 Network Visualization of Terms Associated with 'Polymer' Research (2015–2025).

This map reveals the dominant research directions over the last decade. Notably, a large blue cluster indicates a high level of interest in conjugated polymers, suggesting their importance within the broader field of polymer science.

Further exploration was performed using the terms “conjugated polymer” and “poly(*p*-phenylenevinylene) (PPV)” to examine the diversity of materials and applications within this subfield.

As illustrated in (Figure 1. 2), the keyword co-occurrence analysis for “conjugated polymer” reveals a rich variety of materials and associated technologies. Conjugated polymers are frequently linked to applications such as organic photovoltaics (OPVs), organic field-effect transistors (OFETs), sensors, and light-emitting devices. Among the materials that frequently appear are polythiophenes, carbazoles, and donor–acceptor type polymers. Notably, poly (PPV) and its derivatives also emerge as prominent materials due to their excellent optoelectronic properties.

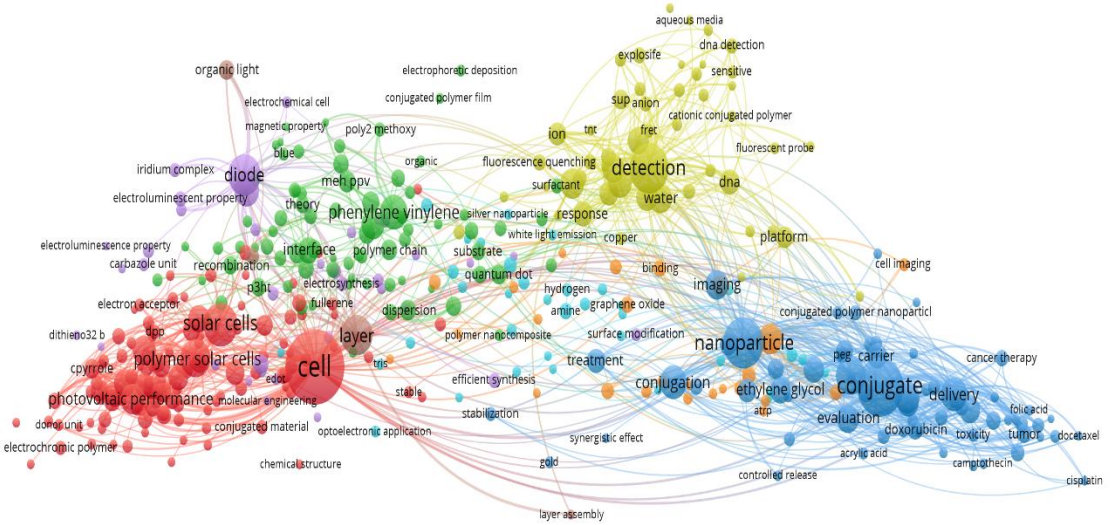

Figure 1. 2 Network Visualization of Terms Associated with 'Conjugated Polymer' Applications and Materials.

In (Figure 1. 3), the bibliometric map based on “poly(p-phenylenevinylene)” demonstrates the significant role of PPVs in organic optoelectronics. Strong links are observed with keywords like OLEDs, photoluminescence, electroluminescence, and emission efficiency. This confirms the enduring importance of PPV derivatives in light-emitting materials and devices, owing to their high photoluminescence quantum yield, good film-forming properties, and synthetic versatility.

In summary, the bibliometric analysis confirms that conjugated polymers, particularly PPVs, have been pivotal in advancing polymer-based materials for optoelectronic applications, while maintaining a prominent position in the broader landscape of polymer science over the past decade.

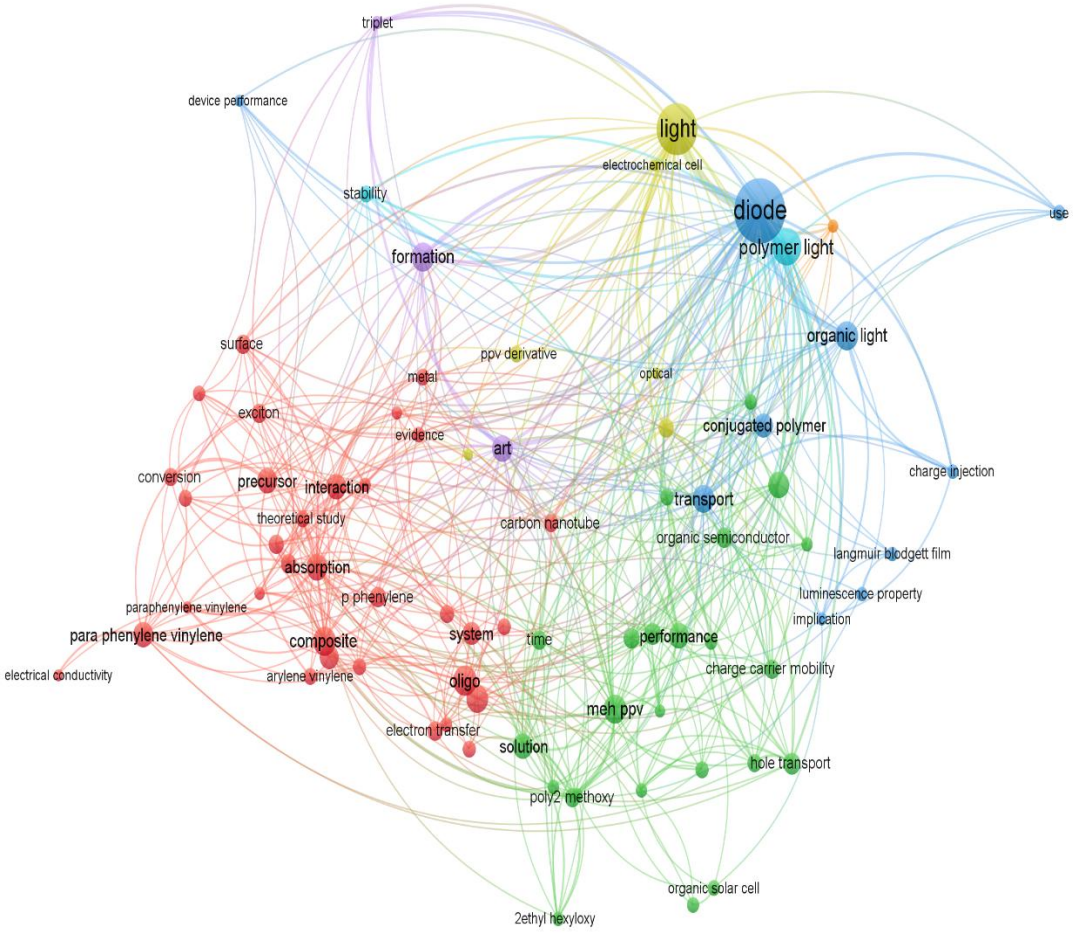

Figure 1. 3 Network Visualization of Terms Associated with PPV in Organic Electronic Applications.

1.3.Classification of Polymers

A polymer is composed of a series of monomer units that are covalently bonded together. The properties of the material can be controlled by altering factors such as the type of monomers used, the way they are connected, and the length of the polymer chains. There are several methods for synthesizing polymers, which can generally be categorized into two main types: addition polymerization and condensation polymerization (Scheme 1. 1).

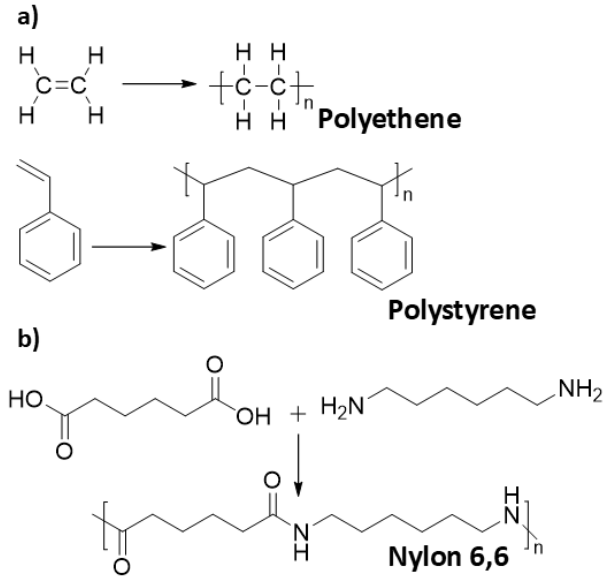

Scheme 1. 1 Illustration of (a) addition polymerization for synthesizing polyethene, polystyrene and (b) condensation polymerization for producing nylon 6,6.

Condensation polymerization, also known as step-growth polymerization, occurs when two bifunctional monomers or polymer segments react to forming an extending polymer chain, accompanied by the release of a small molecule as a byproduct. While water is the most commonly released byproduct in these reactions, other small molecules may also be produced depending on the specific type of condensation reaction [21].

In contrast, addition polymerization involves the successive addition of monomer units to the growing polymer chain without the generation of any byproducts. In this process, the repeating unit retains the same molecular structure as the initial monomer [22]. Unlike condensation polymers, which involve the loss of a small molecule, addition polymers incorporate all atoms of the monomer into the polymer chain. A familiar example of an addition polymer is polyethylene, formed by the covalent bonding of ethylene (C_2H_4) units into long chains. Other examples include butyl rubber (used in tires), polyacrylates (used in paints), and polystyrene (used in packaging).

Polymeric materials go beyond simple linear chains of monomers and can include cyclic and branched structures, cross-linked network polymers, and polymers with polymeric repeating units, such as graft copolymers. Additionally, when multiple types of monomers are used, polymers can exhibit diverse structural arrangements, including

block copolymers (AAABBB), alternating copolymers (ABABAB), and random copolymers (ABAABABBA)[23].

1.3.1. Molecular Weight of Polymers

In contrast to conventional organic molecules, polymers lack a precise molecular formula or fixed molecular weight. Instead, they are defined by a molecular weight distribution, which represents the number of polymer chains (n_i) with a specific molecular weight (M_i). The number-average molecular weight (M_n) is the average molecular weight of the polymer chains, weighted by the mole fraction of each chain ($x_i = n_i / \sum n_i$) It can be expressed as:

$$M_n = \sum x_i M_i = \frac{\sum niMi}{\sum ni}$$

In contrast, the weight-average molecular weight (M_w) considers the weight fraction ($w_i = niMi / \sum niMi$), giving greater importance to longer polymer chains. The equation for M_w is:

$$M_w = \sum wiMi = \frac{\sum niMi^2}{\sum niMi}$$

The dispersity (Đ), defined as the ratio of M_w to M_n, indicates the uniformity of the polymer's molecular weight distribution:

$$Đ = \frac{Mw}{Mn}$$

A dispersity of Đ=1 denotes a monodisperse polymer where all chains are identical in molecular weight. Such uniformity is rare, occurring only in certain natural polymers like DNA. Synthetic polymers, on the other hand, are typically polydisperse, with Đ > 1.

The degree of polymerization (DP), which represents the average number of repeating units in a polymer chain, is calculated by dividing the number-average molecular weight by the molecular weight of the repeating unit (m_{RU}):

$$DP = \frac{Mn}{m_{RU}}$$

1.3.2. Polymer Formation Mechanisms

Polymers are formed through two primary mechanisms: step-growth polymerization and chain-growth polymerization, corresponding to the two major polymer classes, condensation and addition polymers.

Step-growth polymerization, often associated with condensation reactions, involves a gradual increase in molecular weight over time. In this mechanism, all monomers are equally reactive, and polymerization begins with the rapid disappearance of monomers as they combine to form small oligomers. The formation of high-molecular-weight polymers occurs only at advanced stages of the reaction, as the oligomers link together. A distinguishing feature of this process is the release of small molecules, such as water, as byproducts (Figure 1. 4 a).

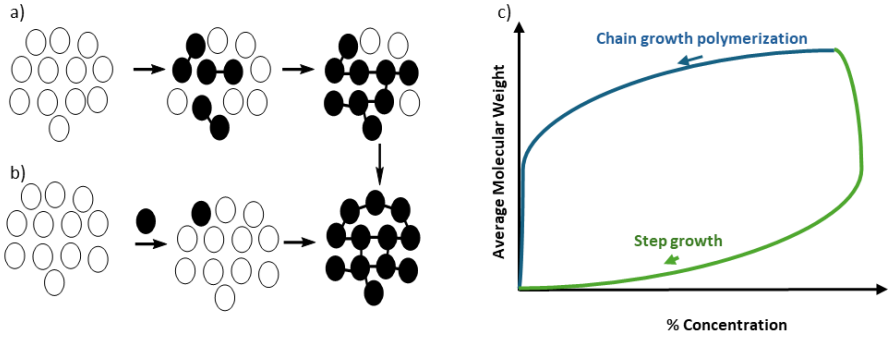

Figure 1. 4 a) Representative diagram for step-growth polymerization, b) Representative diagram for chain-growth polymerization. c) Average molecular weight vs monomer concentration curves for chain growth and step-growth polymerizations.

In chain-growth polymerization, which is characteristic for addition reactions, occurs through the sequential addition of monomer units to a growing polymer chain. The process begins with the generation of an active initiating species, which can be a radical, cation, anion, or coordination complex. These species react with monomers, often derivatives of ethylene, to create an active chain that propagates. Unlike step-growth polymerization, chain-growth mechanisms exhibit a steady decrease in monomer concentration throughout the reaction, without the abrupt disappearance seen in step-growth mechanisms (Figure 1. 4 b)).

Stages of Chain-Growth Polymerization

The mechanism of chain-growth polymerization can be divided into three stages: initiation, propagation, and termination (Figure 1. 5):

Initiation: This stage involves two steps. First, an initiator decomposes or reacts to form an active species (I*). The active species then reacts with a monomer to create an active monomer complex (M_xI^*), marking the start of the polymer chain. The rate of initiator

activation (k_a) is typically slower than the rate of monomer activation (k_i), ensuring that monomers preferentially add to growing chains rather than initiating new ones.

Propagation: The growing polymer chain reacts with additional monomers to form longer chains ($P_{x+1}I^*$). This process continues until the monomer is exhausted or the chain undergoes termination. The rate constant for this step is denoted as (k_p)

Termination: Polymerization terminates when the active species is neutralized. Termination can occur through bimolecular processes, such as radical recombination, or through interactions with impurities, such as oxygen. The overall termination rate is characterized by the rate constant (k_t)

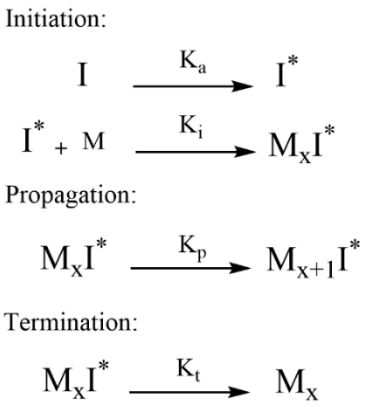

Figure 1. 5 Generalized initiation, propagation, and termination steps in an addition polymerization process, with * denoting an active species.

1.3.3.Controlled Polymerization Methods

Controlled polymerizations represent a specialized class of addition polymerizations characterized by a low rate of termination. These polymerizations offer several desirable features, such as the ability to predetermine the degree of polymerization, narrow molecular weight distributions, and well-defined polymer end groups that remain reactive for further propagation. When termination is nearly eliminated, polymer chains are referred to as "living," allowing for the potential reactivation of chains by introducing additional monomers. The degree of polymerization is typically determined by the stoichiometric ratio of monomer to initiator, multiplied by the monomer conversion (p), where $0 < p < 1$.

$$DP=\frac{[M]0}{[I]0}\ p = \frac{[M]0-[M]}{[I]0}$$

A key characteristic of controlled polymerizations is the linear relationship between the average molar mass and monomer conversion. Minimal termination ensures that the concentration of propagating radicals remains consistent with the initial concentration of the initiator, resulting in a first-order kinetic process.

$$-\frac{d[M]}{dt} = k_{app}[M] \Rightarrow ln\left(\frac{[M]0}{[M]}\right) = k_{app}t$$

Controlled polymerization methods include several techniques that allow precise control over polymer molecular weight, architecture, and end-group functionality. Common techniques are Atom Transfer Radical Polymerization (ATRP), Reversible Addition-Fragmentation Chain Transfer (RAFT) Polymerization, and Nitroxide-Mediated Polymerization (NMP), which all rely on reversible deactivation mechanisms to regulate chain growth and minimize termination. Additionally, metathesis-based methods such as ROMP and Acyclic Diene Metathesis Polymerization (ADMET) are widely used, with ROMP being especially versatile for synthesizing polymers with well-defined architectures using high-strain cyclic alkenes and transition metal carbene catalysts.

ROMP is central to this thesis, and its mechanisms, catalyst systems, and applications in synthesizing homopolymers and copolymers for potential use in organic electronics and electro-optic devices will be discussed in detail in subsequent sections.

1.3.4. Ring-opening metathesis polymerization

ROMP is a form of chain-growth polymerization that uses transition metal catalysts, predominantly those based on ruthenium, without the involvement of radicals. Pioneered by Grubbs, ROMP leverages the release of ring strain in cyclic olefins, such as norbornene and cyclobutene, to drive the polymerization forward. Monomers with significant ring strain (>5 kcal/mol) are particularly suitable for this process. The development of Grubbs catalysts has significantly enhanced ROMP applicability, progressing through three generations. The first-generation catalyst (G1) proved effective for a wide range of monomers, while the second-generation catalyst (G2) introduced N-heterocyclic carbene (NHC) ligands, replacing weaker phosphine ligands. This modification improved both stability and activity but faced limitations in initiation speed, affecting molecular weight control. The third-generation catalyst (G3) further refined these characteristics by incorporating brominated pyridines, achieving faster

initiation and superior control, making it ideal for complex macromonomers (Figure 1. 6).

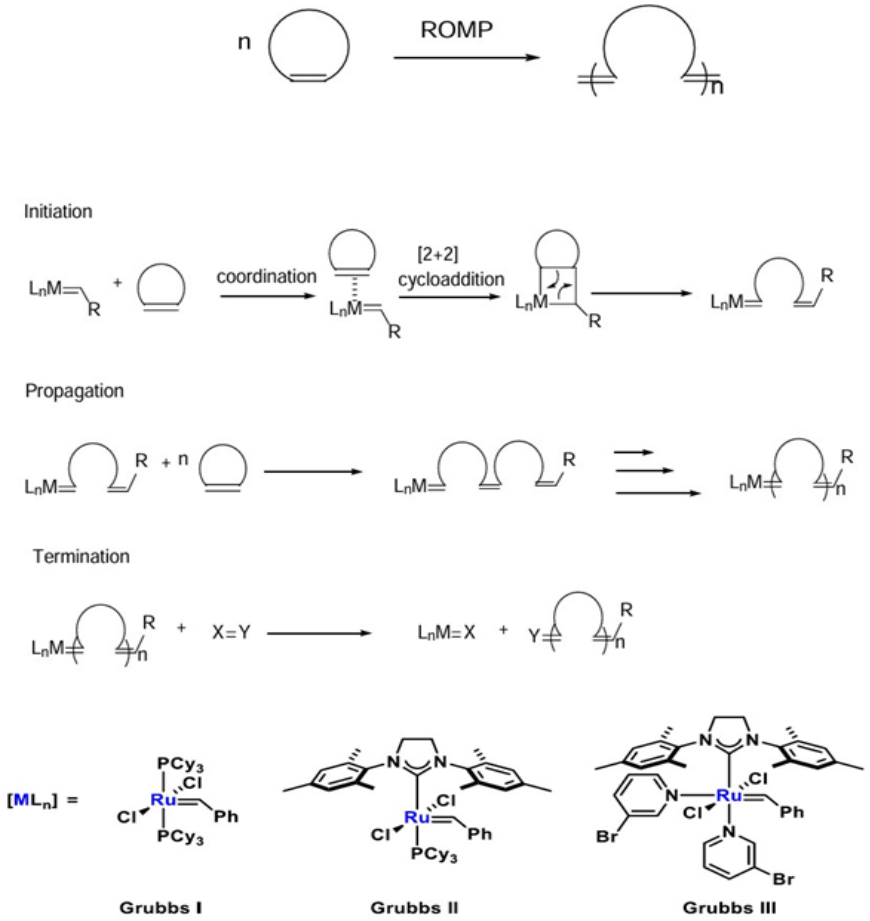

Figure 1. 6 Mechanism of ROMP and three generations of Grubbs metathesis catalysts

Mechanistically, ROMP involves three steps: initiation, propagation, and termination. Initiation begins with the coordination of the cyclic olefin to the metal alkylidene catalyst, followed by a [2+2] cycloaddition to form a metallacyclobutane intermediate. Cycloreversion then produces the active metal alkylidene species, enabling the propagation stage. During propagation, monomers are sequentially added to the growing polymer chain. Termination is typically achieved by introducing a quenching agent, such as ethyl vinyl ether, which deactivates the catalyst and stabilizes the polymer. ROMP is often considered living polymerization due to its ability to maintain active chain ends in the absence of impurities, enabling the synthesis of block copolymers when new monomers are introduced. Despite its classification as a controlled polymerization method with low dispersity, challenges such as chain backbiting and the

need for rapid quenching remain. The process's versatility, functional group tolerance, and capacity to produce well-defined polymers with narrow molecular weight distributions underscore its importance in polymer chemistry. ROMP has become a powerful tool for the synthesis of advanced materials, particularly in organic electronics and electro-optic applications, aligning closely with the focus of this study.

1.4. Conjugated Polymers

CPs are organic materials distinguished by a sequence of alternating σ and π bonds along their central structure. The appealing optical and electrochemical characteristics arise from the existence of a delocalized π-electron cloud along the backbone of these compounds (Figure 1. 7). [10,13,24–26].

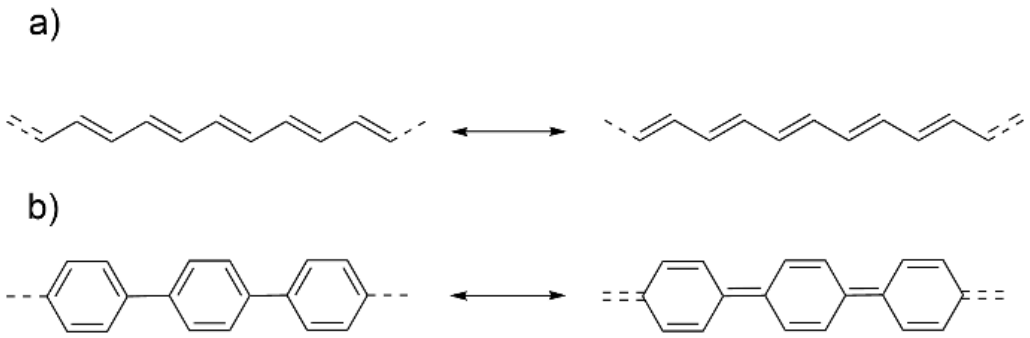

Figure 1. 7 Representation of the resonance structures of a) poly(acetylene), b) poly(*p*-phenylene).

In 1977, Alan MacDiarmid and Hideki Shirakawa[8] discovered and pioneered the conducting nature of CPs, a groundbreaking achievement that earned them the chemistry Nobel Prize in 2000. Since then, CPs have garnered substantial attention due to their promising technological potential. CPs can be obtained with different backbone chains, such as poly (PPV), polyfluorene (PF), polythiophene (PTh), poly(*p*-phenylene) (PPP), poly(*p*-phenylene ethynylene) (PPE), and polypyrrole (PPy).[26], etc. as shown in (Figure 1. 8). The fundamental feature of CPs can be described as a sequence of alternating double (or triple) and single bonds. This arrangement not only provides thermodynamic stability to the structure but also imparts specific properties, such as the capacity to absorb and emit light or conduct electrical charges. These distinctive characteristics make these materials highly versatile and valuable for diverse applications in chemical, biological, and material science fields. Among these, poly (PPV) stands out due to its unique properties and applications. PPV is notable for its

electroluminescent capabilities, making it a key material in the development of light-emitting diodes

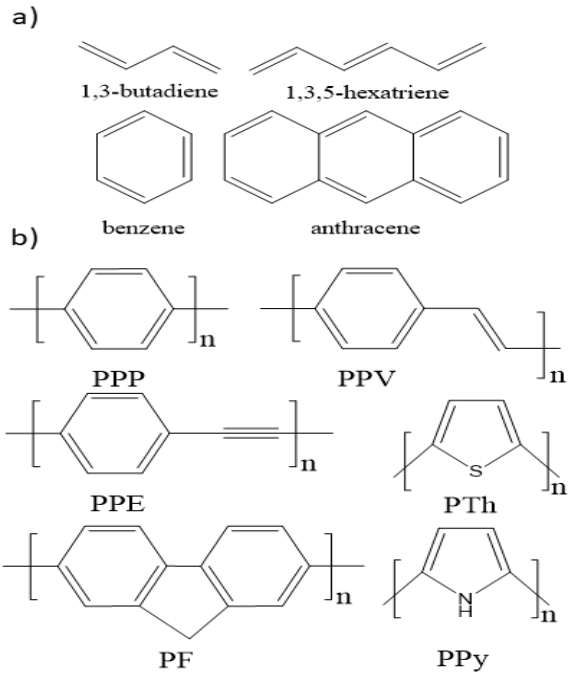

Figure 1. 8 Overview of the most important a) conjugated molecules; b) conjugated polymer backbones.

1.4.1. Electronic Structure and Excitation Mechanisms

The unique electrical behavior of conjugated polymers stems from their molecular architecture, where alternating single and double bonds create a delocalized electron network. This electron delocalization occurs through parallel alignment of p-orbitals in sp^2-hybridized carbon atoms, forming an extended π-system along the polymer backbone (Figure 1. 9).

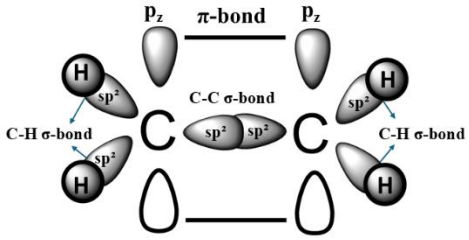

Figure 1. 9 Molecular orbital configuration showing σ and π bonding in conjugated systems

The alignment of p-orbitals in conjugated polymers creates an extended delocalized π-electron system along the polymer backbone, leading to the formation of distinct

electronic energy bands. In this configuration, the highest occupied molecular orbitals (HOMO, π-orbitals) constitute the valence band, while the lowest unoccupied molecular orbitals (LUMO, π*-orbitals) form the conduction band. The energy separation between these bands, known as the bandgap (Eg), typically ranges from 1-3.5 eV (Figure 1. 10) and serves as the fundamental parameter governing the material's semiconducting properties and electrical characteristics.

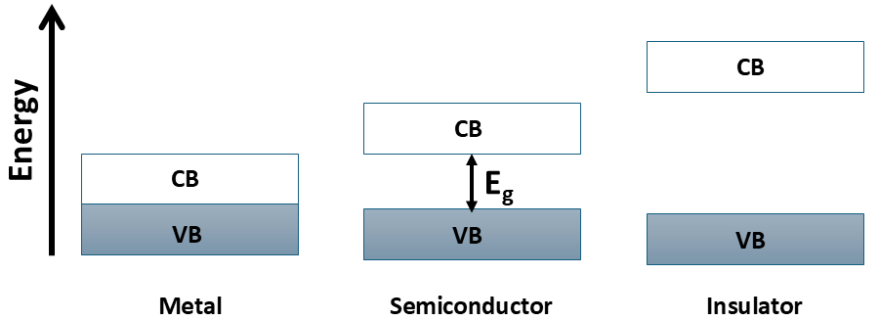

Figure 1. 10 Energy band diagram illustrating the electronic structure of different material classes

Upon absorption of a photon with energy equal to or greater than the bandgap, an electron is promoted to the LUMO, leaving behind a hole in the HOMO. This creates an exciton a bound electron hole pair within the polymer chain. These excitons can migrate along the polymer backbone or between chains and are essential for the operation of devices.

The electronic structure can be further modulated via chemical doping. *n*-type doping introduces additional electrons, while *p*-type doping creates holes, both enhance charge carrier density and significantly improves electrical conductivity sometimes to levels comparable to those of metals.

Moreover, the planar and rigid nature of conjugated backbones promotes strong π–π stacking interactions between polymer chains, facilitating charge transport. However, excessive stacking can hinder solubility and processability. To mitigate this, side chains such as alkyl groups are often introduced to improve solubility and film formation without severely compromising the electronic properties.

Due to these tunable electrical and optical properties, conjugated polymers are widely applied in organic electronics, such as OLEDs, OPVs, and OFETs.

1.4.2. Luminescent Properties of Conjugated Polymers

The luminescence of conjugated polymers arises from their extended π-conjugated systems, which allow for efficient electronic excitation and radiative decay. Upon photoexcitation, electrons are promoted from the ground singlet state (S_0) to the first excited singlet state (S_1), initiating a series of photophysical processes that are conventionally illustrated using a Jablonski diagram (Figure 1. 11). Three primary pathways govern the fate of the excited electron: (i) Fluorescence, wherein the electron relaxes radiatively from S_1 to S_0, emitting a photon on the nanosecond timescale; (ii) Phosphorescence, which involves intersystem crossing (ISC) from S_1 to the triplet state (T_1), followed by spin-forbidden radiative decay back to S_0, typically occurring on a microsecond to second timescale; and (iii) Thermally Activated Delayed Fluorescence (TADF), in which the electron undergoes reverse intersystem crossing (RISC) from T_1 back to S_1 and subsequently emits via fluorescence.

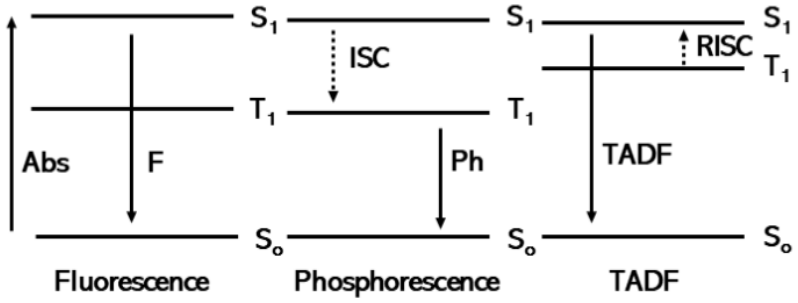

Figure 1. 11 Jablonski Diagram Highlighting Deactivation Mechanisms from the Excited State in Conjugated Polymers.

The occurrence and efficiency of each pathway are strongly influenced by the electronic structure of the polymer, the surrounding environment, and temperature. In conjugated polymers, strong π–π* transitions facilitate high molar extinction coefficients and generally efficient fluorescence. The incorporation of donor–acceptor segments, molecular rigidity, and intramolecular charge transfer (ICT) characteristics can modulate the singlet–triplet energy gap (ΔE_{ST}), thereby impacting the probability of ISC and RISC events. Although phosphorescence and TADF are more common in small-molecule systems or specialized heavy-metal complexes, understanding these processes in conjugated polymers provides valuable insight for designing advanced photonic and optoelectronic materials.

1.4.3.Poly (*p*-phenylene vinylene) (PPV): Synthesis Methods

Poly (PPV) is one of the most widely studied conjugated polymers due to its excellent optoelectronic properties, including high photoluminescence quantum yield and charge transport capabilities. Since its discovery, various synthetic routes have been developed to produce PPV and its derivatives, each with unique advantages and challenges. The primary methods for synthesizing PPV include the following:

1.4.3.1.Wessling-Zimmerman Method

The Wessling-Zimmerman method is one of the earliest and most extensively utilized approaches for synthesizing PPV [27]. It employs the precursor polymer method, where a soluble precursor polymer is synthesized first and then thermally converted into PPV. This process typically involves the polymerization of a sulfonium salt monomer, such as *p*-xylene bis (tetrahydrothiophenium chloride), via a nucleophilic substitution reaction to produce a soluble precursor polymer. Upon heating, this precursor undergoes thermal elimination, resulting in the formation of the conjugated PPV backbone along with the release of small molecules such as tetrahydrothiophene and hydrogen chloride (Scheme 1. 2).

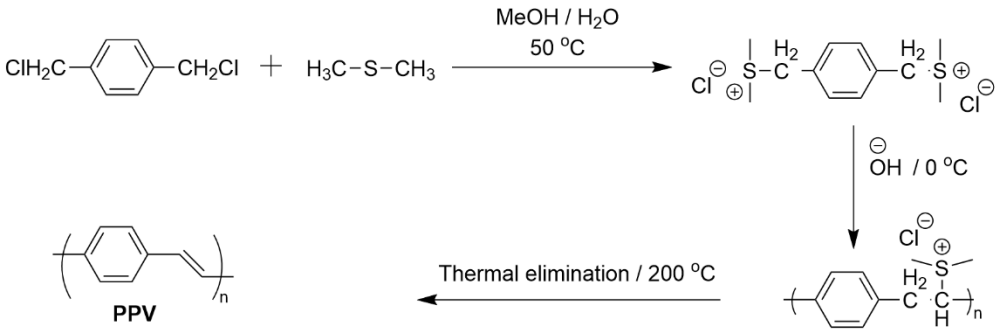

Scheme 1. 2 Wessling method for PPV synthesis.

While this method enables the fabrication of high-quality PPV thin films with well-defined conjugation, it is highly sensitive to temperature control during the thermal elimination step. Improper conditions can introduce defects in the polymer backbone or cause degradation.

1.4.3.2.Gilch Polymerization

The Gilch polymerization method was employed to achieve the PPV in organic solvent units was the polymerization of symmetrical *α,α′*- dichloro *p*-xylylene as a monomer in

the presence of a significant excess of potassium tert-butoxide (K*t*BuO) act as a strong base (Scheme 1. 3), which was authorized by Gilch and Wheelwright in 1966[28]. However, the main complaint with such an approach is that extreme physical gelation during the growth radical chain caused the progress to an extremely high molecular weight polymer [29]. A further limitation of the Gilch pathway that a number of head–head and tail–tail defects will be built in the structure during the propagation reaction, besides these reasons, they were given a detrimental effect on the polymer's opto-electric characteristics.

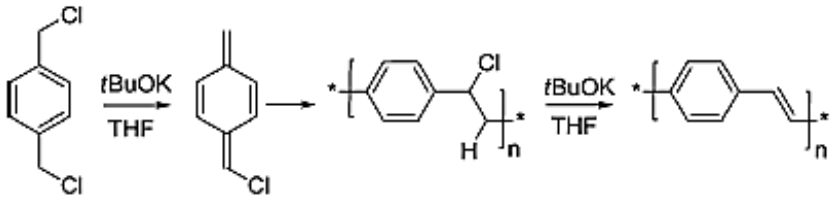

Scheme 1. 3 Gilch polymerization of PPV.

1.4.3.3.Heck Coupling Polymerization

Heck coupling polymerization utilizes a palladium-catalyzed coupling reaction between aryl halides and vinyl monomers to synthesize PPV derivatives[30]. This method is particularly attractive due to its functional group tolerance, which allows for the incorporation of a variety of substituents along the PPV backbone, thereby tailoring the material's optoelectronic properties. Despite its versatility, the Heck coupling method is less commonly used due to its reliance on expensive palladium catalysts and the harsh reaction conditions that can limit the types of monomers that can be employed **(**Scheme 1. 4**).**

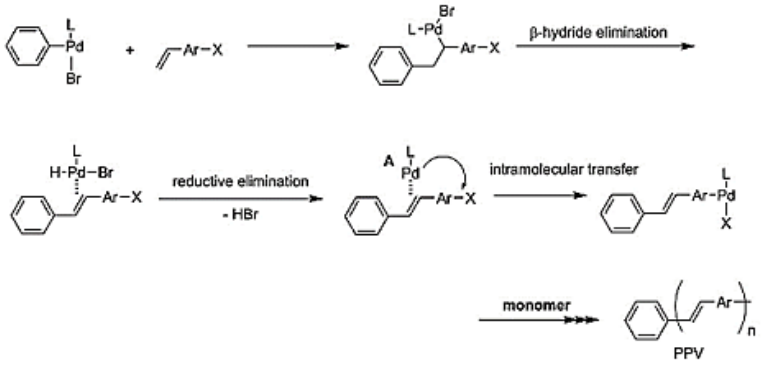

Scheme 1. 4 Heck coupling for PPV synthesis.

1.4.3.4.Wittig and Horner-Wadsworth-Emmons Reactions

The Wittig reaction and its modified version, the Horner-Wadsworth-Emmons (HWE) reaction, offer another synthetic route for PPV[31]. These methods involve the coupling of phosphonium ylides or phosphonate esters with aromatic dialdehydes to form the conjugated polymer through the creation of vinyl linkages between the monomer units. The stereoselectivity of these reactions enables precise control over the cis/trans configuration of the vinylene groups, making them particularly suitable for designing PPV derivatives with specific electronic properties. However, the moisture and air sensitivity of these reactions, as well as the need for stoichiometric amounts of reagents, can pose challenges, often resulting in the formation of byproducts (
Scheme 1. 5).

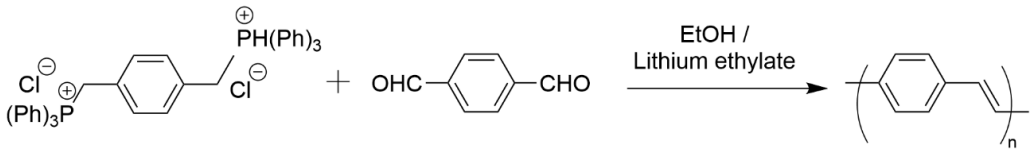

Scheme 1. 5 Wittig and Horner-Wadsworth-Emmons Reactions.

1.4.3.5.ROMP for synthesizing PPVs

ROMP is a powerful polymerization technique that utilizes the high ring strain of cyclic olefins to produce well-defined polymers. Although not a conventional method for synthesizing PPV, ROMP has been explored for creating PPV like structures by polymerizing norbornene derivatives and subsequently introducing vinylene linkages through post-polymerization modifications (Scheme 1. 6).

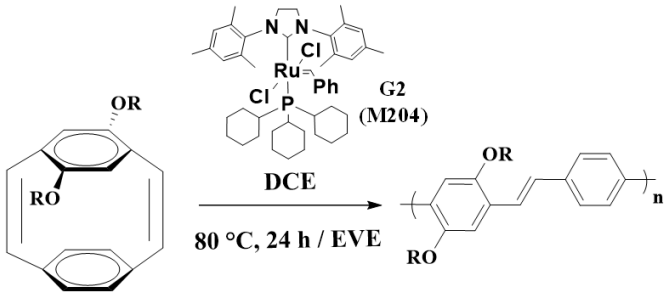

Scheme 1. 6 ROMP method for PPV synthesis.

One of the key advantages of ROMP is its ability to precisely control molecular weight and polymer architecture, leading to materials with narrow molecular weight

distributions and tunable properties. The use of highly efficient ruthenium-based Grubbs catalysts further enhances its versatility, enabling living polymerization characteristics and functional group tolerance. However, the reliance on specialized catalysts, high cost and the need for complex post-polymerization modifications have traditionally limited the large-scale applicability of ROMP for PPV synthesis[32].

1.4.4.Applications of conjugated polymers

1.4.4.1.Organic Light-Emitting Diodes (OLEDs)

Conjugated polymers have revolutionized display technology through their implementation in OLEDs, where their unique optoelectronic properties enable efficient conversion of electrical energy into light[33]. These materials form the basis of a technology that surpasses conventional displays in key aspects, including viewing angles, contrast ratios, and power efficiency. The pioneering work of Tang and Vanslyke[34] established the viability of organic semiconductors for light emission, using precisely engineered small molecules with controlled molecular architectures [35,36].

The fundamental operation of OLED devices involves the generation and recombination of electron-hole pairs within nanoscale organic layers positioned between conductive electrodes (Figure 1. 12). Modern OLED architecture incorporates multiple functional layers - including charge injection, transport, and blocking layers - all carefully optimized to maximize exciton formation and radiative recombination in the emissive layer. A primary design consideration involves mitigating the naturally high electrical resistance of organic semiconductors through strategic layer sequencing and interfacial engineering.

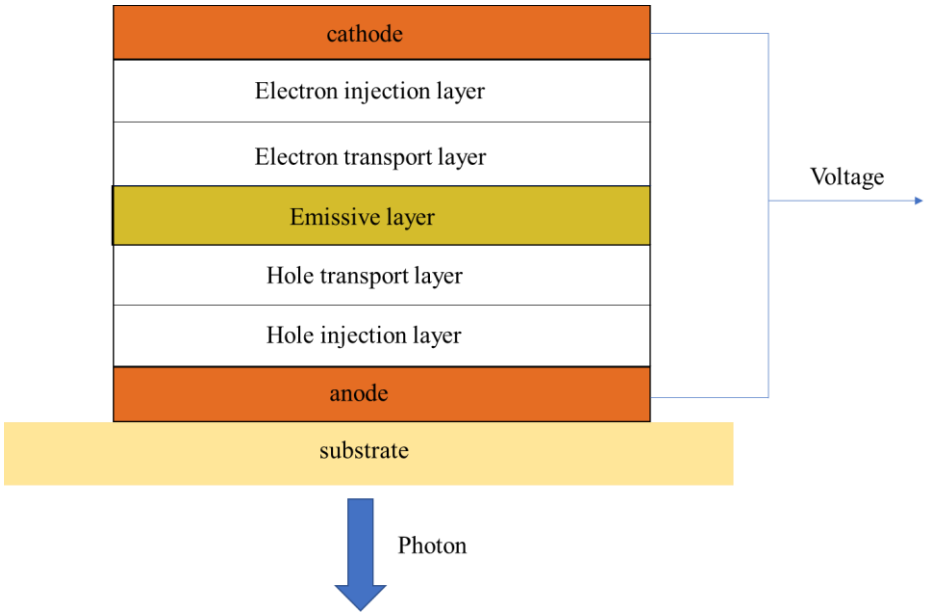

Figure 1. 12 Schematic drawing of a polymer light emitting device.

OLED materials derive their distinctive characteristics from conjugated molecular structures containing extended π-electron systems, frequently modified with heteroatomic functional groups. Their relatively low thermal stability (with decomposition temperatures generally under 350°C) presents processing limitations but enables deposition on temperature-sensitive substrates. This property has facilitated the development of groundbreaking applications including:

- Ultra-thin, flexible displays for wearable electronics
- Transparent smart windows with integrated lighting
- Lightweight, large-area illumination panels
- Mechanically robust displays for automotive applications

Conjugated polymers offer particular advantages for OLED implementation, primarily due to their chemically tunable electronic band structures, which allow for precise control over optoelectronic properties such as emission wavelength and charge mobility. Optimized systems exhibit exceptional luminescent efficiencies, with quantum yields often exceeding 80%, making them ideal candidates for high-brightness, energy-efficient devices. Furthermore, their compatibility with solution-based fabrication methods include spin coating, inkjet printing, and roll-to-roll processing facilitates scalable, low-cost production on flexible and large-area substrates. These attributes have positioned CP-based OLEDs as a leading technology for next-generation visual

displays in consumer electronics. Simultaneously, ongoing research continues to extend their application potential into fields such as solid-state lighting, biomedical imaging, and wearable photonic devices. The development of novel polymer structures and advanced device architectures holds promise for further improvements in key performance metrics, including operational lifetime, efficiency, and color purity[37–40].

1.4.4.2.Organic Photovoltaic Cells (OPVs).

Conjugated polymers have significantly advanced OPV technologies by enabling lightweight, flexible, and low-cost solar cells with tunable optical and electronic properties. These materials support solution-based fabrication and compatibility with plastic substrates, making them ideal for wearable devices, portable power sources, and building-integrated applications. Recent developments in donor–acceptor systems, particularly the combination of conjugated polymer donors with non-fullerene acceptors, have boosted power conversion efficiencies beyond 18%.

The schematic below (Scheme 1. 7) highlights common OPV device structures, including conventional and inverted layouts, along with fabrication methods such as spin coating, hybrid evaporation-solution processing, and blade coating. These scalable techniques are key to transitioning OPVs from lab research to commercial deployment. Continued research focuses on improving stability, morphology control, and environmentally friendly processing to unlock the full potential of OPVs in sustainable energy solutions[41–43].

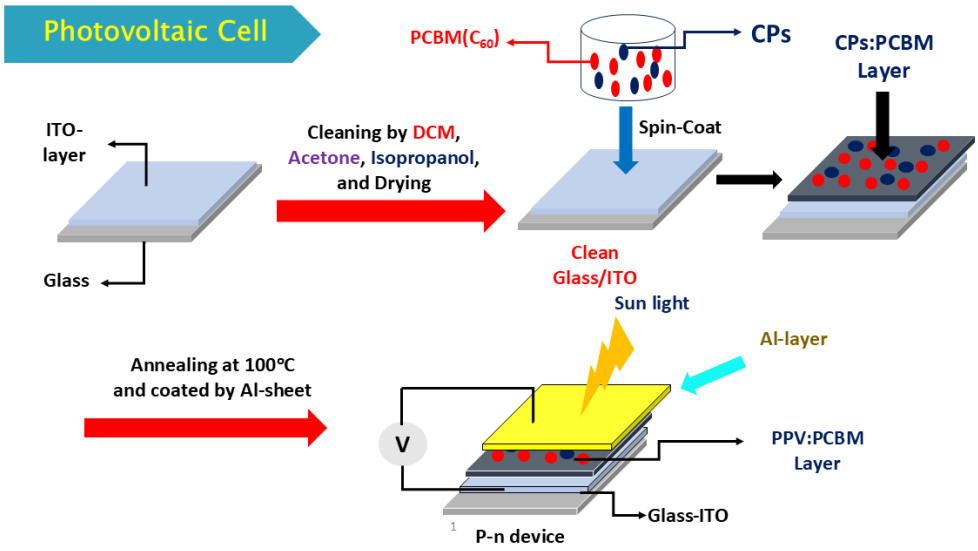

Scheme 1. 7 Schematic overview of OPVs device configurations and representative fabrication methods used for their development.

1.4.4.3.Organic Field-Effect Transistors (OFETs).

OFETs are foundational components in the field of flexible and printed electronics. These three-terminal devices—comprising an organic semiconductor, gate dielectric, and source/drain/gate electrodes offer a platform for both practical applications and fundamental studies of charge transport in π-conjugated systems (Figure 1. 13). Since their inception in the 1980s, OFETs have facilitated significant progress in understanding structure–property relationships in organic semiconductors.

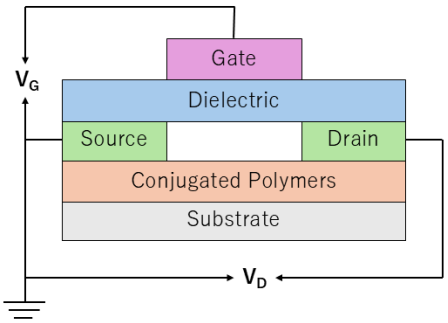

Figure 1. 13 Schematic representation of an organic field-effect transistor (OFET) structure

Performance parameters such as field-effect mobility (μ), often exceeding 10 $cm^2 V^{-1} s^{-1}$ in advanced systems, on/off current ratios of 10^3 to 10^8, and tunable threshold voltages underscore their technological relevance. The widely adopted bottom-gate top-contact architecture highlights the importance of energy level alignment at the

semiconductor–dielectric interface for efficient charge accumulation and injection. Recent innovations involve high-mobility conjugated polymers—such as diketopyrrolopyrrole (DPP)-based copolymers and indacenodithiophene derivatives paired with engineered dielectric materials for enhanced performance and low-voltage operation.

These advances have enabled a range of applications, including flexible displays and biosensors. Current challenges include improving environmental stability, ensuring large-area uniformity, and achieving high reproducibility for circuit integration. Emerging frontiers explore neuromorphic systems via ionic-gated OFETs and ambipolar semiconductors for complementary logic. Overall, OFETs continue to serve both as practical tools in wearable and flexible electronics and as insightful probes into organic charge transport behavior[44–48].

1.4.4.4.Sensors.

Sensors are devices that detect external stimuli such as temperature changes, gas exposure, humidity and convert them into electrical or optical signals for information processing, monitoring, and control. Conjugated conductive polymers have become essential materials in sensor technologies due to their exceptional sensitivity and versatility (Figure 1. 14).

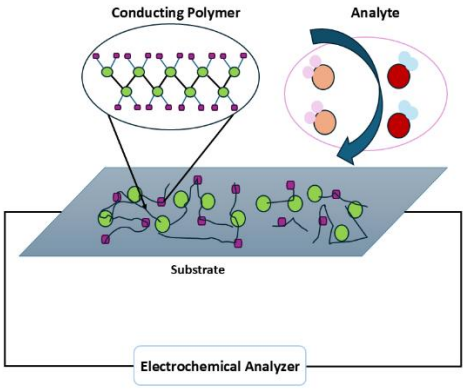

Figure 1. 14 Schematic representation of an electrochemical sensor with a conducting polymer and target analyte.

These polymers respond to various stimuli like light, gases, anions, and solvents by altering their electrical conductivity or optical appearance. For instance, highly sensitive and selective sensors for volatile organic compounds (VOCs) have been developed using blends of poly(3-hexylthiophene) with solid-state ionic liquids. The strong

interaction between the conjugated polymer and the ionic liquid enables precise modulation of conductivity under an applied electric field, allowing reliable detection of different VOCs based on their polarity.

Conjugated polymers also exhibit visual responses, such as temperature-dependent color changes. Polydiacetylene (PDA)-based materials, for example, can shift from blue to purple when heated, driven by structural changes in their conjugated backbones. These thermochromic properties open up applications in biosensors, thermal indicators, smart coatings, and packaging materials.

Additionally, conjugated polymers show great potential for chemical sensing. Certain diketopyrrolopyrrole-based polymers can selectively detect fluoride ions by undergoing a visible color change, offering high sensitivity and the ability to extract target anions from solutions. Recent advancements also include the development of insulated conjugated bimetallopolymers, which enhance the stability, responsiveness, and tunability of sensors[49–53].

1.5.Non-Conjugated Polymers

Unlike conjugated polymers, which possess extended π-electron delocalization along their backbones, non-conjugated polymers consist of σ-bonded saturated carbon chains that lack delocalized electronic structures (Figure 1. 15). As a result, these materials are typically electrically insulating and do not exhibit intrinsic optical or electronic activity. However, their chemical versatility, mechanical robustness, and thermal stability make them indispensable in various industrial and research applications.

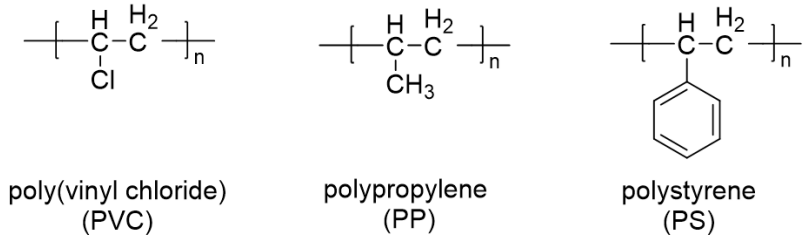

Figure 1. 15 structure of some common non conjugated polymers

Non-conjugated polymers can serve as flexible and inert scaffolds, which can be chemically modified to introduce functional side groups that impart desired electronic, optical, or structural characteristics. This design strategy allows for the creation of hybrid materials that combine the processability and stability of traditional polymers

with the electronic functionality of conjugated systems, achieved through the incorporation of conjugated or photoactive pendants.

One significant advantage of non-conjugated backbones is their greater freedom in tuning polymer architecture and solubility, especially through post-polymerization functionalization or monomer design. Additionally, living or controlled polymerization techniques, such as ROMP, have expanded the scope of non-conjugated polymers by enabling the precise incorporation of functional groups with high fidelity and low dispersity.

Within this context, poly (NDIs) has emerged as a promising class of non-conjugated polymers. Their strained cyclic norbornene structure is highly reactive toward ROMP, facilitating the synthesis of well-defined polymers with tailored molecular properties. Through pendant functionalization, these materials can be engineered to exhibit tunable photophysical, electrochemical, and morphological behaviors, thus bridging the gap between purely insulating polymers and electronically active materials.

1.5.1.Poly (Norbornene-dicarboximides) as a Model System

Poly (NDIs) represents a highly adaptable group of non-conjugated polymers (Scheme 1. 8), widely studied due to their ease of synthesis and structural versatility. Originally introduced by Asrar in 1992[54], these materials are typically synthesized via ROMP of NDI monomers, which are often prepared through Diels–Alder reactions [2].

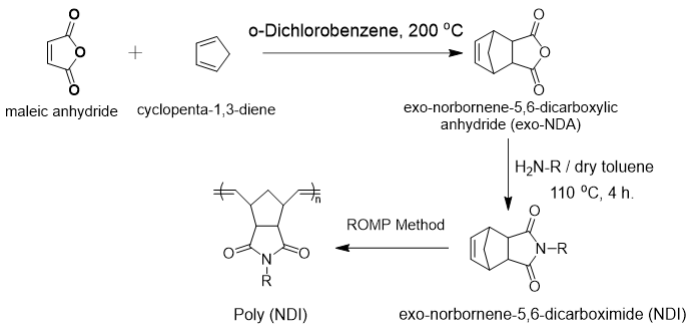

Scheme 1. 8 General scheme for synthesis NDI.

The use of Grubbs catalysts facilitates a living polymerization process, yielding well-defined polymers with low dispersity (Đ < 1.2) and controllable molecular weights[23]. A key advantage of poly (NDIs) lies in their capacity for N-substitution, enabling the fine-tuning of physical properties. For example, the rigid cyclic backbone contributes

to high glass transition temperatures (Tg ≈ 150–300 °C), while functional side groups can modify optical transparency, refractive index, and mechanical properties such as modulus (2–4 GPa). Furthermore, their low moisture uptake and excellent processability make them attractive candidates for advanced functional materials.

1.5.2.Functionalization Strategies and Advanced Applications

Functionalization is a powerful strategy in polymer chemistry, enabling the introduction of specific chemical groups onto a polymer backbone or side chain to tailor physical, chemical, or biological properties[55,56]. This approach offers several advantages, including enhanced solubility, improved compatibility with other materials, and the ability to impart targeted functionalities such as conductivity, fluorescence, or responsiveness to external stimuli. By carefully selecting and positioning functional moieties, polymers can be designed to meet the stringent requirements of diverse applications, ranging from optoelectronics and separation membranes to biomedical devices and sensors. Functionalization also plays a crucial role in enabling post-polymerization modifications, offering flexibility in material design and facilitating the development of modular and adaptive systems.

In the context of non-conjugated systems, functionalization becomes even more critical, as it allows these electronically inert backbones to acquire advanced characteristics typically associated with conjugated materials. Among these, poly (NDIs) has emerged as a highly tunable and versatile class of non-conjugated polymers. The imide linkage in NDI units provides a convenient handle for side-chain engineering, enabling the introduction of a wide variety of functional groups without compromising backbone integrity. Through ROMP, these side-functionalized monomers can be polymerized into well-defined architectures with controllable molecular weights and narrow dispersity.

Recent developments have demonstrated the successful incorporation of photoactive, redox-active, and bio interactive moieties onto poly (NDI)s, broadening their utility in optoelectronic devices, chemical sensing, and biological interfaces. Their non-conjugated nature provides high transparency and excellent insulating behavior, which is advantageous for applications such as dielectric layers in organic transistors and protective coatings. Moreover, amphiphilic or stimuli-responsive side chains have enabled the formation of nanostructured morphologies and "smart" materials that respond to environmental triggers like pH, temperature, or light. These properties have

positioned functionalized poly (NDI)s at the frontier of materials innovation, offering a flexible platform for developing next-generation functional polymers across multiple disciplines.

1.6. Literature Review and Research Gap

Poly (PPV) and its derivatives are among the most widely explored conjugated polymers due to their luminescence, electrical conductivity, and tunable optical properties. These features make them attractive for applications in OLEDs, OFETs, and OPVs devices. Since the first reports on their synthesis, researchers have developed several synthetic routes, each presenting specific advantages and limitations. The ability to tailor the polymer structure and optical response through molecular design and synthetic strategy remains a central focus of PPV research[57–65].

Suzuki coupling has been utilized to synthesize PPV derivatives by forming C–C bonds between aryl halides and boronic acids or esters in the presence of a palladium catalyst. This method is renowned for its functional group tolerance, mild reaction conditions, and high yield (Scheme 1. 9). Suzuki polymerization enables the integration of electron-rich and electron-deficient units within the polymer backbone, allowing precise tuning of electronic and optical properties. However, it shares the common challenge of palladium residue contamination and sometimes low molecular weight products due to side reactions and incomplete coupling[66].

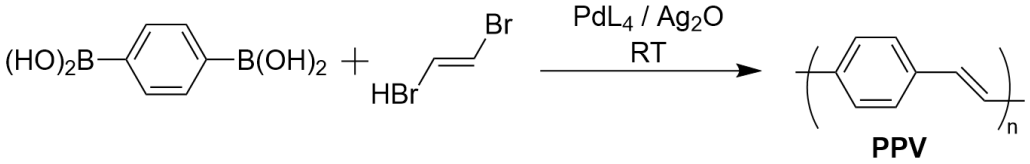

Scheme 1. 9 Suzuki polymerization for synthesizing PPV

The McMurry reaction involves the reductive coupling of aromatic aldehydes or ketones using low-valent titanium species to form alkenes. When applied to the synthesis of PPV-type materials, McMurry coupling enables the direct formation of vinylene linkages, offering a metal-free approach to conjugated polymers (Scheme 1. 10). Although this method avoids the use of expensive catalysts, it often requires harsh conditions, and the yields can be inconsistent. Moreover, achieving high molecular weight polymers with this technique remains difficult, and side reactions such as over-

reduction or oligomerization can affect the purity and performance of the resulting materials[67].

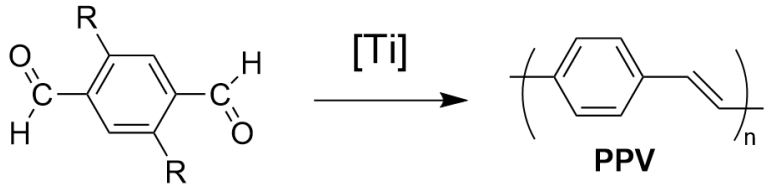

Scheme 1. 10 McMurry reaction for synthesizing PPV

Electro-polymerization offers a unique approach to synthesizing conjugated polymers like PPV by applying an electrical potential to induce polymer growth directly on an electrode surface (Scheme 1. 11). This technique allows for in-situ film deposition with controlled thickness and doping levels, making it advantageous for device fabrication. Furthermore, it provides a pathway for patterning and integration into microelectronic architectures. However, electro-polymerization is often limited by poor structural control, difficulties in scaling up, and challenges in achieving uniform film morphology, particularly for bulk material applications[68].

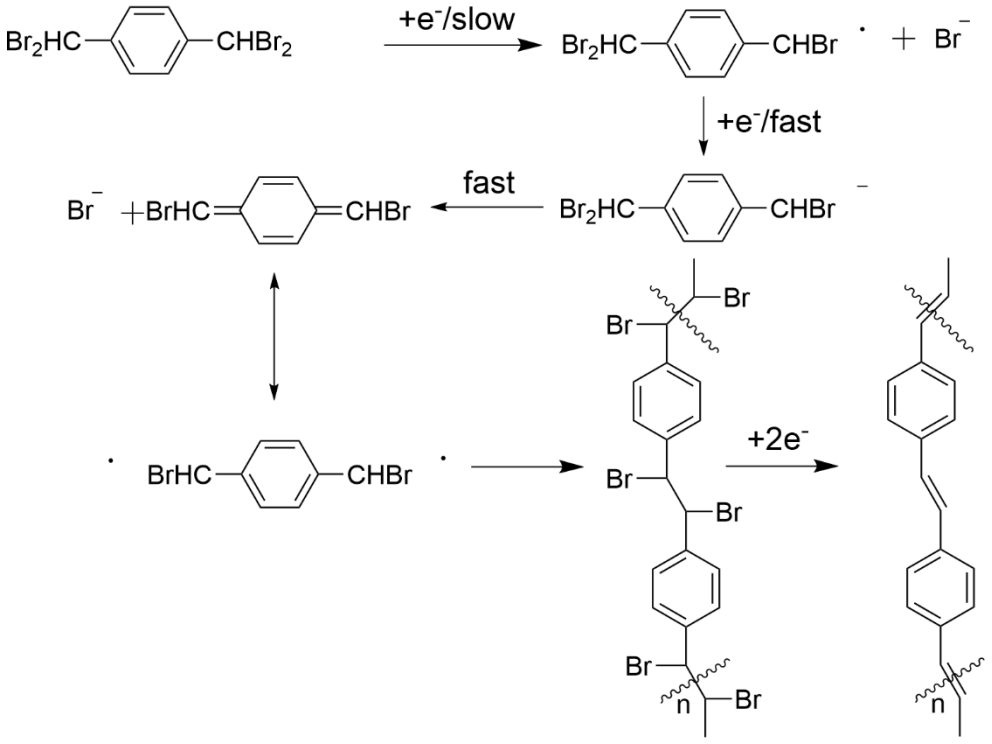

Scheme 1. 11 Electro-polymerization for synthesizing PPV

Early synthetic approaches included the Wessling-Zimmerman precursor route, which involves the synthesis of a soluble sulfonium-based precursor polymer followed by

thermal elimination to produce the conjugated PPV backbone (Scheme 1. 2). While this method offers good film-forming ability, it suffers from limitations such as temperature sensitivity and the risk of incomplete elimination, which can compromise the purity and conjugation length of the final polymer[69,70].

The Gilch polymerization is one of the most extensively used methods due to its simplicity and ability to produce high-molecular-weight PPV (Scheme 1. 3). This method uses strong bases such as potassium tert-butoxide to dehydrohalogenate α,α'-dihalogenated p-xylenes. Despite its efficiency, the Gilch route often leads to structural defects such as head-to-head and tail-to-tail linkages, as well as uncontrolled molecular weight and gelation, which can negatively affect the polymer's performance[71].

Heck coupling polymerization, based on palladium-catalyzed cross-coupling between aryl halides and vinyl monomers, provides structural versatility and the ability to introduce functional groups (Scheme 1. 4). However, the requirement for expensive catalysts and harsh reaction conditions limit its scalability and applicability[27].

The Wittig and Horner-Wadsworth-Emmons (HWE) reactions have also been employed for the synthesis of PPVs. These reactions enable the formation of vinylene linkages through the condensation of phosphonium ylides or phosphonate esters with aromatic aldehydes (Scheme 1. 5). The advantages include better control over stereochemistry and conjugation, but the reactions are sensitive to moisture and require stoichiometric reagents, making them less practical for large-scale synthesis[72].

Among these various techniques, ROMP method has gained attention for its potential to address several challenges inherent in traditional methods. ROMP utilizes strained cyclic olefins and transition-metal catalysts, such as Grubbs' ruthenium-based complexes, to achieve living polymerization with control over molecular weight and dispersity. Recent studies have explored the use of cyclophane-based norbornene diene monomers for ROMP, which after polymerization can be post-modified to install vinylene units, resulting in PPV-like structures[73].

The chosen monomer structure in ROMP plays a pivotal role in defining the polymer's conjugation pattern, packing, and emission characteristics. For instance, 1,4-dicyclohexadiene-based norbornene derivatives have been examined for their ability to yield rigid, planar backbones conducive to strong π-π stacking and high photoluminescence. Post-polymerization modifications, such as oxidative elimination,

convert the non-conjugated diene units into extended vinylene linkages[74–76], effectively generating a PPV-like conjugated polymer with improved optical properties.

1.7.Thesis's Motivation and Objective

The advancement of organic semiconducting materials has opened new frontiers in the development of flexible, lightweight, and cost-effective electronic devices. Among these materials, poly (PPV) derivatives and norbornene-based polymers stand out due to their promising optoelectronic and thermal properties, structural versatility, and compatibility with solution-based processing techniques. However, further optimization of their molecular design and synthesis methods remains essential to enhance their performance and expand their applicability in next-generation technologies, such as OLEDs, OPVs, and OFETs.

This thesis is motivated by the growing demand for well-defined, soluble, and thermally stable conjugated polymers with tailored structural and electronic properties. A key focus of this work is to explore both traditional and advanced synthetic strategies to develop functional polymers that can meet these criteria. In particular, we aim to leverage ROMP, a powerful and versatile polymerization technique that allows for precise control over molecular weight, dispersity, and architecture, to construct novel polymeric systems based on norbornene monomers.

The primary objective of this thesis is to design, synthesize, and fully characterize a series of novel conjugated polymers based on PPV and NDI frameworks. As part of this effort, we first synthesized a series of PPV derivatives through established commercial methods. These PPV based materials were then subjected to comprehensive structural, thermal, and optical characterization to evaluate their fundamental properties and identify opportunities for further improvement.

Building on this foundation, we developed a set of norbornene-functionalized monomers and employed Grubbs second-generation catalyst to carry out ROMP and construct various polymer systems, including homopolymers and random copolymers. The synthesized polymers were designed to incorporate electron-donating and electron-accepting units, bulky side chains, and rigid frameworks to influence solubility, thermal behavior, and optoelectronic characteristics.

The specific aims of this research are as follows:

- To synthesize and characterize PPV derivatives using commercial methods, focusing on understanding the influence of side-chain variations on solubility, film-forming properties, and structural features.
- To develop a series of ROMP-based homopolymers, including carbazole- and admentyl-functionalized norbornene monomers, and analyze their molecular weights, dispersity, thermal stability, and absorption/emission behavior.
- To synthesize random copolymers aiming to combine the thermal robustness of NDIs with the optoelectronic benefits of PPVs.
- To investigate the effects of molecular design and polymer architecture on the performance relevant properties of the synthesized materials, using various analytical techniques such as GPC, NMR, TGA, DSC, and UV-Vis absorption.

Overall, this thesis seeks to provide a systematic investigation into the design, synthesis, and characterization of functional conjugated polymers, bridging the gap between conventional synthesis methods and advanced living polymerization techniques. The results are expected to contribute to the broader field of organic electronics by offering new material insights and synthetic routes for producing well-defined, high-performance polymeric semiconductors.

1.8. Organization of the Thesis

This thesis is organized into seven chapters, each of which systematically presents the progression of the research, from the motivation and materials used to the synthesis, analysis, and final conclusions. Below is a summary of the contents of each chapter:

Chapter 1 Introduction

This chapter presents the background, motivation, and objectives of the research. It provides an overview of conjugated polymers, particularly poly (PPV) derivatives and norbornene-based systems synthesized via ROMP. A dedicated section, *Literature Review and Research Gap*, is included to comprehensively discuss the evolution of PPV synthesis methods, their corresponding optical properties, and the limitations of existing techniques. This section critically identifies the research gap and positions the relevance of ROMP as a versatile synthetic platform for next-generation optoelectronic materials.

Chapter 2 Materials & Instrumentation

This chapter details the materials, synthetic techniques, and characterization methods used throughout the thesis. It includes commercial synthetic strategies for PPV

derivatives and the preparation of ROMP-based polymers using Grubbs catalysts. Comprehensive characterization techniques such as NMR, FTIR, GPC, TGA, DSC, UV–Vis spectroscopy, fluorescence spectroscopy, and cyclic voltammetry are described.

Chapter 3 Precise Synthesis and Characterization of Poly (*p*-phenylene vinylene) Polymers Using ROMP

focuses on the synthesis and characterization of two poly(*p*-phenylenevinylene) (PPV) derivatives P_1 (DO-PPV) and P_2 (EHM-PPV) using ROMP. These polymers, featuring symmetric and asymmetric side chains respectively, displayed excellent solubility, narrow PDIs (1.22 for P_1 and 1.09 for P_2), and promising photoluminescence. Optical and electrochemical measurements revealed tunable band gaps, confirming their suitability for optoelectronic applications. This chapter highlights the impact of alkyl side-chain engineering on polymer properties.

Chapter 4 Thermal Stability and Solubility of Poly (norbornene-dicarboximide) Derivatives: Synthesis and Characterization of Carbazole and Adamantyl Pendants

presents the synthesis and analysis of two poly (NDI) derivatives P_3 (CA-NDI) and P_4 (AD-NDI) via ROMP using the Grubbs 3rd generation catalyst G3. P_3 incorporates carbazole side groups, while P_4 features bulky adamantane units. Both polymers exhibited high thermal stability, good solubility, and controlled molecular weights with narrow PDIs. Characterization techniques (NMR, GPC, FT-IR, DSC, TGA, UV-vis) confirmed their structural and functional performance.

Chapter 5 ROMP of *p*-Phenylenevinylene and Norbornene-Dicarboximide Copolymers: Toward Enhanced Thermal Stability

describes the synthesis of two random copolymers, P_5 (CA-NDI/DO-PPV) and P_6 (CA-NDI/EHM-PPV), aiming to combine the thermal robustness of NDIs with the optoelectronic benefits of PPVs. Synthesized via ROMP using the Grubbs 2nd generation catalyst G2. Both copolymers showed strong absorption (~450 nm), fluorescence (~530 nm), and high thermal stability (up to 421.7 °C). The results emphasize the effectiveness of ROMP in producing versatile copolymers with balanced properties for electronic devices.

Chapter 6 ROMP-Based Synthesis and Characterization of Donor-Acceptor Norbornene Copolymers

This chapter presents the synthesis and characterization of donor and acceptor-type polymers, along with their copolymers, using ROMP. A donor-type monomer (CAH-NDI, M_5), featuring a carbazole moiety connected via a flexible alkyl spacer, was polymerized to yield polymer P_7. The effect of polymerization time and conditions on molecular weight and dispersity was investigated to optimize the polymerization process.

Additionally, an acceptor-type monomer (DCT-NDI, M_6), incorporating a triazine unit, was polymerized to form P_8. Following this, random copolymers (P_9–P_{12}) were synthesized using various molar ratios of CAH-NDI and DCT-NDI monomers to study the impact of composition on the resulting material properties.

All polymers were characterized by standard techniques including NMR, GPC, and UV-vis to evaluate their structural and optical features. This chapter highlights the modular approach to designing donor-acceptor type materials and provides insights into tuning polymer properties through monomer selection and feed ratio adjustment.

Chapter 7 Conclusions, Recommendations, and Future Work

Finally, this thesis concludes with a summary of key findings, practical recommendations for optimizing ROMP-based polymer design, and a future outlook focused on developing solution-processable multi-resonance TADF pendant polymers for next-generation ultra-low power OLED applications.

Chapter 2

Materials & Instrumentation

Unless explicitly stated, all chemicals were utilized in their as-received state from Sigma-Aldrich, Tokyo Chemical Industry, Fujifilm Wako, and Kanto Chemical, without additional purification. Thin-layer chromatography on LC Silica gel 60 F_{254} 25 Aluminium sheets 20 x 20 was employed to monitor the progress of most reactions. Preparative separations were conducted through column chromatography using silica gel Wakosil(R) with a particle size range of 60 to 210 μm. Polymerizations were executed using a Radleys Carousell 12 under a nitrogen atmosphere.

The ^{1}H and ^{13}C nuclear magnetic resonance (NMR) spectra were acquired in deuterated chloroform encompassing both one-dimensional (1D) and two-dimensional (2D) techniques, and chemical shifts were referenced to tetramethylsilane (TMS) as an internal standard, using a Nihon Denshi JEOL JNM-LA400 spectrometer operating at 400 MHz and 600 MHz, with Chemical shifts expressed in parts per million (ppm) relative to the residual solvent peak. All coupling constants (*J* values) are presented in hertz (Hz), and multiplicity abbreviations such as s (singlet), d (doublet), dt (doublet of triplets), t (triplet), and m (multiplet) are utilized.

High-resolution mass spectrometry (HRMS) was conducted on a Nihon Denshi JEOL MStation JMS700.

The molecular weights and polydispersity of polymers were determined using Gel Permeation Chromatography (GPC) with a Shodax GPC K-804L column on a JASCO LC2000 liquid chromatography system, with tetrahydrofuran (THF) serving as the eluent.

UV absorption spectra were recorded on a Shimadzu UV-Vis spectrometer 1240, with a standard concentration of 5 mg/100 ml THF. Fluorescence spectra were measured using JASCO FP-8600 fluorometer. Phosphorescence spectra were recorded on a Hamamatsu Photonics PMA12 C10027-01 with a 340 nm LED (Thorlabs M340L5) as the excitation source.

Cyclic voltammogram traces were recorded using a conventional three-electrode configuration with an electrochemical analyzer (ECstat-302, EC frontier, JPN) with a glassy carbon (7.07 mm^2) working electrode, a Pt wire counter electrode, and Ag/Ag^+ reference electrode, and the ferrocene/ferrocenium (Fc/Fc^+) external reference. Acetonitrile was used as solvent and 0.1 M tetrabutylammonium hexafluorophosphate ($TBAPF_6$) was used as the supporting electrolyte.

Glass transition temperature (Tg) was determined by Differential Scanning Calorimetry (DSC) using Seiko Instruments Inc SII-DSC 6220, under nitrogen atmosphere at heating rate 10 ° C/min. Decomposition temperature (Td) was carried out by Thermogravimetric Analysis (TGA), Rigaku Thermoplus TG8110 instrument, using a nitrogen flow of 100 cc/min and a temperature ramp rate of 10℃/min.

Chapter 3

Precise Synthesis and Characterization of Poly (*p*-phenylene vinylene) Polymers Using ROMP

This chapter explores the synthesis, characterization, and photophysical evaluation of two soluble poly (PPV) derivatives, each prepared through ROMP. The first derivative, poly(2,5-dioctyloxy-*p*-phenylenevinylene) (DO-PPV) P_1, and the second, poly(2-[(2-ethylhexyl)oxy]-5-methoxy-*p*-phenylenevinylene) (EHM-PPV) P_2, feature distinct alkyl substituents dioctyl and ethylhexyl chains, respectively. Both polymers exhibited excellent solubility in various organic solvents and displayed narrow polydispersity indices (PDI), indicative of controlled polymerization. DO-PPV had a PDI of 1.22, while EHM-PPV exhibited a lower PDI of 1.09, indicating a higher degree of molecular weight uniformity. Optical band gaps ranged from 2.21 to 2.25 eV in thin films and 2.07 to 2.19 eV in solution for DO-PPV, while EHM-PPV demonstrated slightly higher optical band gaps, ranging from 2.32 to 2.37 eV. Electrochemical studies using cyclic voltammetry revealed band gaps of 2.37 eV and 2.19 eV for DO-PPV and EHM-PPV, respectively, further underscoring their potential for optoelectronic applications. Both polymers exhibited promising fluorescence activity in solution and thin-film states, suggesting their suitability for OLEDs and related devices. This chapter highlights the influence of alkyl chain structure on the optoelectronic properties of PPV derivatives, offering valuable insights into the rational design of conjugated polymers for advanced applications.

Two notable PPV derivatives include poly(2,5-dioctyloxy-*p*-phenylenevinylene) (DO-PPV) and poly(2-[(2-ethylhexyl)oxy]-5-methoxy-*p*-phenylenevinylene) (EHM-PPV). These polymers differ in the alkyl side chains attached to their backbones, with DO-PPV incorporating dioctyl groups and EHM-PPV featuring ethylhexyl and methoxy substituents. With its symmetric dioctyl groups, DO-PPV is well-known for its excellent solubility in organic solvents and ability to form uniform thin films. EHM-PPV, on the other hand, introduces an asymmetric ethylhexyl group and methoxy group in para position, offering enhanced molecular packing and tunable optoelectronic properties. These structural differences make EHM-PPV particularly interesting for applications requiring precise control over band gaps and fluorescence activity.

In this study, both DO-PPV and EHM-PPV were synthesized using ROMP. This robust method enables precise control over polymer architecture, molecular weight, and dispersity. The use of 2nd generation Grubbs catalyst G2 ensured high efficiency and

narrow polydispersity indices (PDIs), with values of 1.22 for DO-PPV and 1.09 for EHM-PPV.

This chapter provides a detailed investigation of the synthesis, characterization, and photophysical properties of these PPV derivatives. Their optical and electrochemical band gaps, fluorescence emission, and solubility were evaluated to assess their potential for use in OLEDs and other optoelectronic applications. The findings underscore the critical role of side-chain engineering in tuning the properties of conjugated polymers for advanced technological applications.

First synthetic route for Synthesis of Poly(2,5-Dioctyloxy-*p*-Phenylenevinylene) (DO-PPV)

3.1.Synthesis of DO-Paracyclophanediene Monomer (M_1).

(Scheme 3. 1) illustrates the synthesis of the DO-[2.2] paracyclophane-1,9-diene (PCPD) monomer. The process begins with the cyclization of key starting materials to form an intermediate compound. This intermediate undergoes several reactions, including rearrangement, oxidation, and elimination steps, leading to the formation of the desired PCPD monomer. Each synthesized structure was confirmed by NMR spectroscopy (both proton and carbon) and MS. The final product is then purified through column chromatography and recrystallization. Characterization techniques are employed to confirm the structure and purity of the synthesized compound.

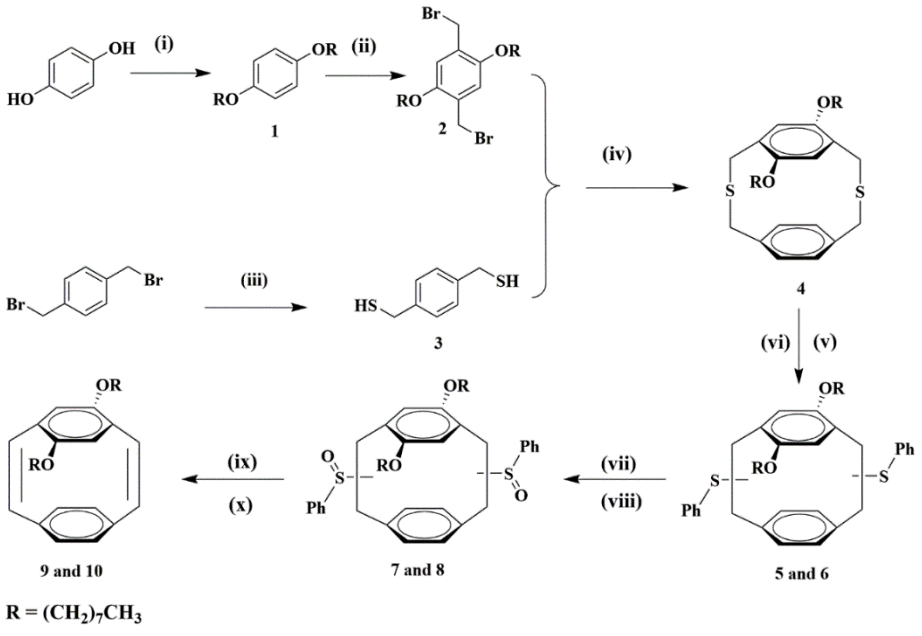

Scheme 3. 1 Synthesis of DO-Paracyclophanediene Monomer M_1.

(i) 1-bromooctane, K_2CO_3, HBr, Acetonitrile, 80 °C, 48 h; (ii) Paraformaldehyde, Acetic acid, 70°C, 6 h; (iii) a-Thiourea, Ethanol, 90 °C, 5 h; b- $KOH_{(aq.)}$, 110 °C, 2 h; c-H_2SO_4, RT, 1 h; (iv) $KOH_{(alc.)}$, Benzene, RT, 72 h; (v) TBAF, TMS-PTFMS, Dry THF, RT, 6 h; (vi) anhydrous 1.2-dichloroethane, isoamyl nitrite, anthranilic acid, under N_2, 90 °C, 2 h; (vii) *m*-ClPBA, Chloroform, 0 °C, 1 h, (vii) Benzene / acetic acid, H_2O_2, RT, 12 h; (xi) Cs_2CO_3, *o*-xylene, 150 °C, 20 h; (x) DMF, nitrogen stream, 155 °C, 20 h

3.1.1.Synthesis of 1,4-bis(dioctyloxy)benzene compound (1).

A mixture of 1,4-hydroquinone (20.00 g, 0.1816 mol), 1-bromooctane (87.69 g, 0.4540 mol), and potassium carbonate (62.75 g, 0.4540 mol) was refluxed in acetonitrile (200 ml) for about 48 hours. The resultant mixture was cooled followed by stirred in de-ionized water for 30 minutes at room temperature to afford a dark brown precipitate which collected, washed several times by de-ionized water and dried at 50°C. Then, the crude material was purified by dissolving in the minimum amount of hot hexane and re-precipitated by using excess of stirred methanolic solution to produce a brown precipitate which filtered, washed with methanol, and dried at 50°C to give a pale brown solid in (53 g, 80%) yield. EI-MS calculated for $C_{22}H_{38}O_2$ *m/z*: 334.00; Found: *m/z* 334.00. ^{1}H NMR (400 MHz, Chloroform-d) δ 6.83 (d, J = 15.1 Hz, 4H), 3.89 (t, J = 6.6 Hz, 4H), 1.70-1.77 (m, 4H), 1.27-1.47 (m, 20H), 0.88 (t, J = 6.6 Hz, 6H) ppm.^{13}C NMR (101 MHz, Chloroform-d) δ 153.03, 115.47, 68.33, 32.04, 29.49, 29.34, 26.36, 22.47, 13.95 ppm. (S3. 1)**.**

3.1.2.Synthesis of 1,4-bis(bromomethyl)-2,5-bis(octyloxy)benzene compound (2).

A mixture of product **1** (21.29 g, 0.1195 mol), paraformaldehyde (7.35 g 0.2451 mol) was dissolved in (300 ml) acetic acid. A solution of hydrobromic acid (42.5 ml) (33 wt. % in acetic acid) was added and the mixture was stirred for 6 hours under refluxing system. The reaction mixture was cooled to RT and the suspension was poured onto de-ionized water, the precipitate was isolated by filtration and washed with de-ionized water. The dark brown residue was dissolved in hot chloroform, then poured onto methanol to form a solid white precipitate, which can be repeated for a white loose solid in (28 g, 75.5%) yield. EI-MS calculated for $C_{24}H_{40}Br_2O_2$ *m/z*: 520.00; Found: *m/z* 520.14. ^{1}H-NMR (400 MHz, Chloroform-d) δ 6.85 (s, 2H), 4.53 (s, 4H), 3.98 (t, *J* = 6.4 Hz, 4H), 1.81 (dq, *J* = 8.2, 6.5 Hz, 4H), 1.63 –1.21 (m, 20H), 0.98 –0.73 (m, 6H)

ppm.^{13}C NMR (101 MHz, Chloroform-d) δ 1150.75, 127.46, 114.48, 68.56, 32.10, 29.02, 28.92, 25.62, 22.39, 14.20 ppm. (S3. 2).

3.1.3.Synthesis of 1,4-Benzenedimethanethiol compound (3).

A deoxygenated ethanolic solution (200 ml) containing 1,4-Bis(dibromomethyl)benzene (17.8 g, 0.056 mol) and thiourea (9.8 g, 0.13 mol) was refluxed for 5 hours to give a suspension which cooled to room temperature and the solvent was removed in vacuo. A solution of deoxygenated water (200 ml) containing Sodium hydroxide (12.6 g, 0.22 mol) was added to the residue followed by refluxing for 2 hours. The reaction mixture was cooled to room temperature, neutralized with 50% aqueous H_2SO_4, and extracted with chloroform (3 × 100 ml). The organic layer was dried over $MgSO_4$, filtered, and the solvent removed in vacuo. The resulting solid was crystallized from mixed solutions of (chloroform / methanol) to afford a white powder in (9 g, 94%) yield. EI-MS calculated for $C_8H_6S_2$ *m/z:* 170.00; Found: *m/z* 170.00. ^{1}H NMR (400 MHz, Chloroform-d) δ 7.26 (d, J = 6.9 Hz, 4H), 3.72 (d, J = 7.8 Hz, 4H), 1.74 (t, J = 7.5 Hz, 2H) ppm.^{13}C NMR (101 MHz, Chloroform-d) δ 139.39, 127.89, 28.19 ppm. (S3. 3).

3.1.4.Synthesis of Thiacyclophane compound (4).

Compound **2** (10 g, 0.019 mol) and Compound **3** (3.27 g, 0.019 mol) were dissolved in deoxygenated benzene (500 ml). This solution was added extremely slowly dropwise using a pressure-equalizing dropping funnel to a stirred solution of Potassium Hydroxide (4.31 g, 0.077 mol) in deoxygenated ethanol (1000 ml), over 72 hours at RT. After a further 3 hours, the solvent was evaporated, the residue dissolved in chloroform and water, washed with water and brine in an organic layer which dried by using anhydrous Na_2SO_4, and the solvent evaporated to give a yellow oil which purified using column chromatography ($CHCl_3$: Hexane, 20:80) yielding a colorless oil (6.31 g, 62%). EI-MS calculated for $C_{32}H_{48}O_2S_2$ *m/z*: 528.00; Found: *m/z* 528.8. ^{1}H NMR (400 MHz, Chloroform-d) δ 6.92 (dd, *J* = 36.7, 7.8, 2.0 Hz, 4H), 6.42 (s, 2H), 4.28 (d, *J* = 14.8 Hz, 2H), 3.94 (t, *J* = 9.2, 6.5 Hz, 4H), 3.87 –3.72 (m, 4H), 3.35 (d, *J* = 14.8 Hz, 2H), 1.82 (dd, *J* = 13.2, 7.1, 4.3 Hz, 4H), 1.57(dp, *J* = 12.8, 4.0 Hz, 4H), 1.48 –1.29 (m, 8H), 0.97 –0.87 (m, 6H)ppm.^{13}C NMR (101 MHz, Chloroform-d) δ 149.82, 135.62, 129.08,

128.23, 124.93, 114.46, 68.20, 38.02, 32.03, 31.22, 29.61, 26.55, 22.83, 14.29ppm. (Figure 3.4).

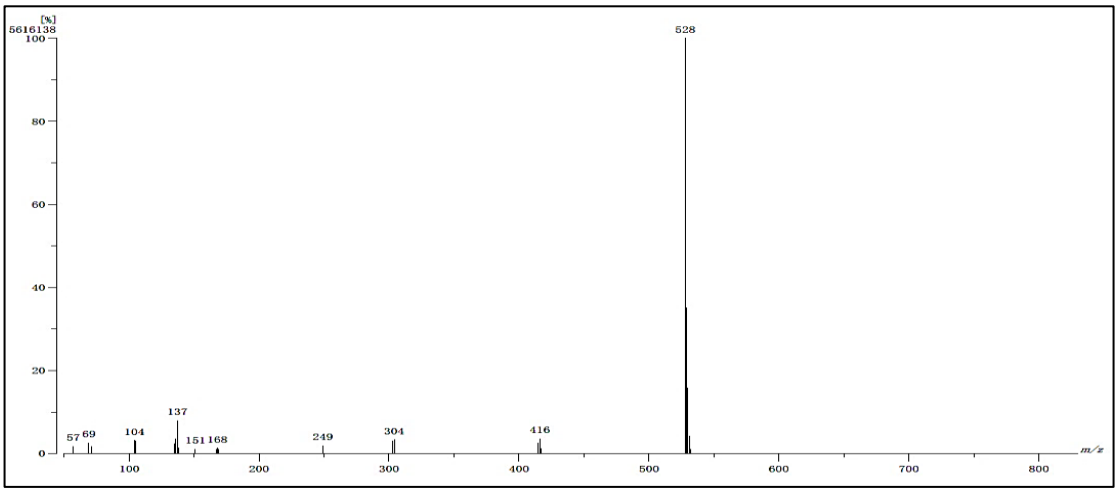

(a)

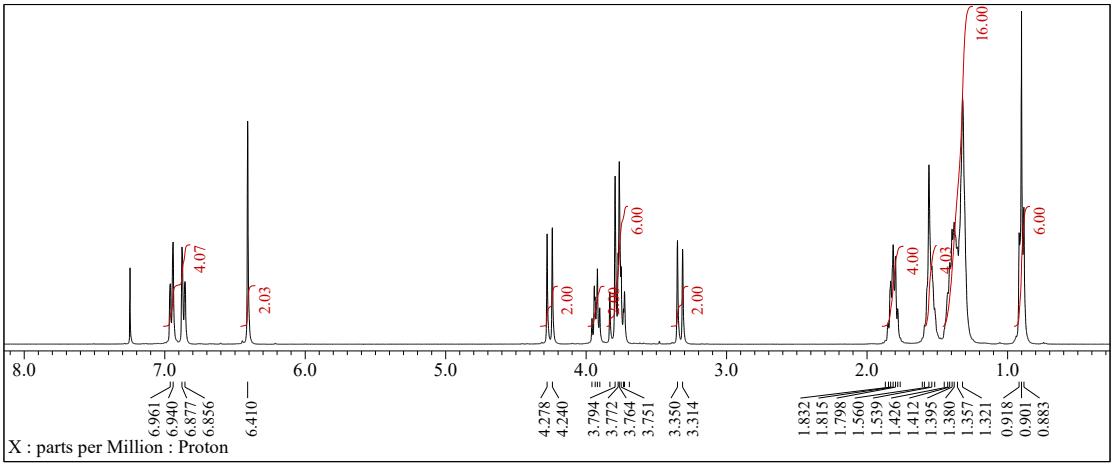

(b)

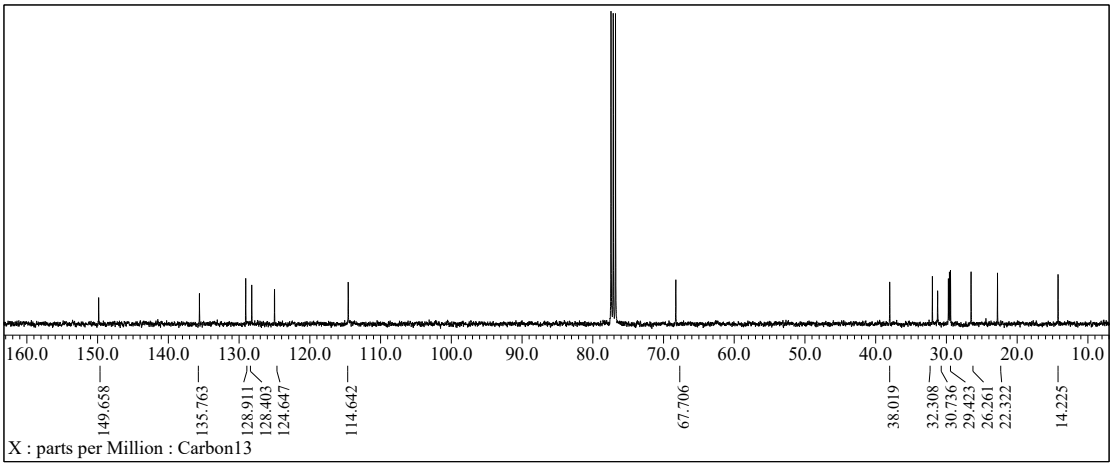

(c)

Figure 3. 1 a) EI-MS spectrum of compound 5; b) ^{1}H NMR spectrum; c) ^{13}C NMR spectrum.

3.1.5.Benzyne-induced Pummerer rearrangement of compound (5).

A mixture of the DO-Thiacyclophane **4** (1 g, 0.0037 mol) and 2-(trimethylsilyl) phenyltrifluoromethanesulfonate (1.4 g, 0.0094 mol) in dry THF (100 ml) was stirred at room temperature for few minutes. Then, a solution of Tetrabutylammonium fluoride trihydrate (TBAF·$3H_2O$) (1.78 g, 0.009189 mol) in dry THF (10 ml) added dropwise using over a period of 5 hours. The resulting solution stirred for 1 additional hour then evaporated to produce brown oil. The crude material was purified by column chromatography ($CHCl_3$: Hexane, 30:70) yielding a pale yellow oil (1.2 g, 94%). EI-MS calculated for $C_{44}H_{56}O_2S_2$ *m/z*: 680.00; Found: *m/z* 680.01. (S3. 4).

3.1.6.Benzyne Induced Stevens Rearrangement compound (6).

The DO-Thiacyclophane **4** (3.57 g, 0.00675 mol) and Anthranilic acid (2.77 g, 0.02 mol) were dissolved in anhydrous 1,2-Dichloroethane (100 mL) and heated to 90^{o}C under nitrogen with a condenser. At the reflux point, Isoamyl nitrite (3.16 g, 0.027 mol) was added by syringe very slowly over a period of at least 60 minutes. The resulting solution was heated at 90^{o}C for 1 additional hour and then evaporated to produce brown oil. The crude material was purified by column chromatography (DCM: Hexane, 30:70) yielding a pale-yellow oil (1.5 g, 42%). EI-MS calculated for $C_{44}H_{56}O_2S_2$ *m/z*: 680.37; Found: *m/z* 680. (S3. 5)**.**

3.1.7.Oxidation of phenyl sulfides of compound (7).

Stirring the rearrangement product **5** (1.2 g, 0.0018 mol) in chloroform (15 ml) and the solution maintained at 0 ˚C. After that, a solution of 3-Chloroperoxybenzoic Acid (*m*-CPBA) (0.6 g, 0.0035 mol) was slowly added over approximately 10 minutes and the reaction mixture stirred for an additional 30 minutes at 0 ˚C. Then, quenched by a saturated sodium bicarbonate solution followed by extracted via chloroform, collected the organic phase and washed with de-ionized water (3x100 ml) and dried by anhydrous $MgSO_4$, and evaporated to give a (1.25 g, 96%) yield of the desired product as a clear yellow oil. EI-MS calculated for $C_{44}H_{56}O_4S_2$ *m/z*: 712.00; Found: *m/z* 712.05. (S3. 6).

3.1.8.Oxidation of phenyl sulfides of compound (8).

The Stevens rearrangement product **6** (0.75 g, 0.0011 mol) was dissolved in a mixture of benzene (30 ml) and acetic acid (5 ml). The mixture was stirred for 10 minutes and

then cooled to approximately 0 ˚C using an ice bath. Hydrogen peroxide (0.112 g, 0.0033 mol) was dissolved in acetic acid (5ml) and added dropwise by syringe over a period of 30 minutes in air. The vessel was allowed to warm at room temperature and stirred for 12 hours in air. Then, quenched by a saturated sodium bicarbonate solution followed by extracted via chloroform, collected the organic phase and washed with de-ionized water (3x100 ml) and dried by anhydrous $MgSO_4$, and evaporated to give a (0.355 g, 46.6 %) yield of the desired product as a clear yellow oil. EI-MS calculated for $C_{44}H_{56}O_4S_2$ *m/z*: 712.05; Found: *m/z* 712.00. (S3. 7).

3.1.9.Synthesis of (2Z,5Z)-12,15-di(octyloxy)-1,4(1,4)-dibenzenacyclohexaphane-2,5-diene (PCPD) compound (9) (M_1).

Heating under reflux a mixture of compound **7** (0.7 g, 0.00098 mol) and Cs_2CO_3 (1.3 g, 0.0039 mol) was dissolved in *o*-xylene for 4 hours. The reaction was cooled, filtered, and solvent removed to form a dark brown oil, which was then purified using column chromatography ($CHCl_3$: Hexane, 10:90) to afford a colorless viscous oil in (0.3 g, 75%) yield, EI-MS calculated for $C_{32}H_{44}O_2$ *m/z*: 460.00; Found: *m/z* 460.70. ^{1}H NMR (400 MHz, Chloroform-d) δ7.06 –6.95 (m, 2H), 6.85 (d, J = 10.0 Hz, 2H), 6.67 –6.60 (m, 2H), 6.58 –6.51 (m, 2H), 5.52 (s, 2H), 3.58 –3.43 (m, 4H), 1.54 –1.39 (m, 4H), 1.32 –1.00(m, 20H), 0.68 –0.60 (m, 6H) ppm.^{13}C NMR (101 MHz, Chloroform-d) δ 152.46, 138.34, 135.62, 134.54, 131.43, 129.18, 127.61, 120.40, 69.21, 31.96, 29.71, 26.31, 22.78, 14.23ppm. (Figure 3. 2).

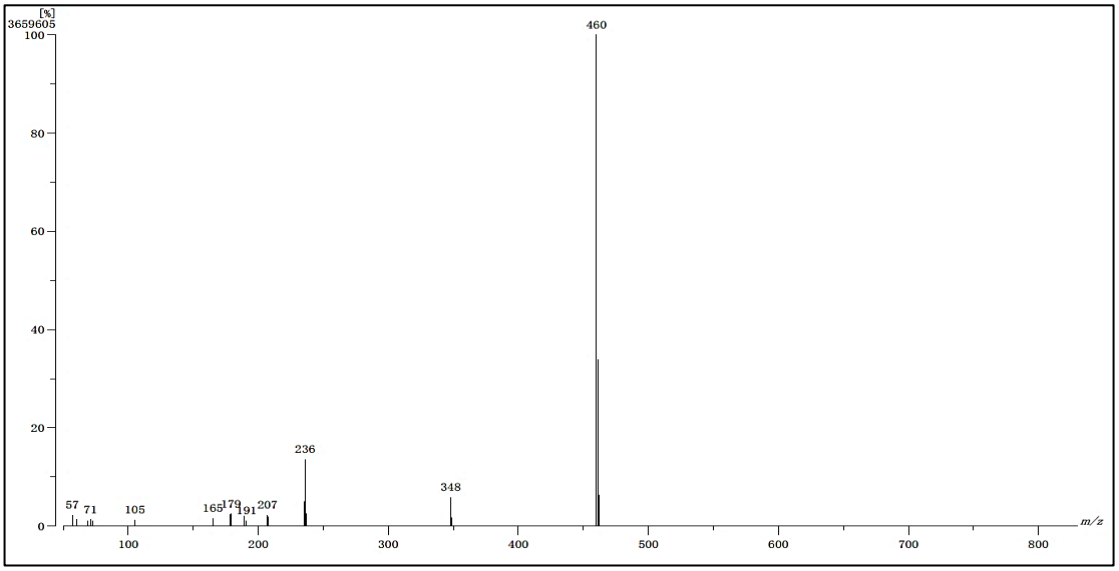

(a)

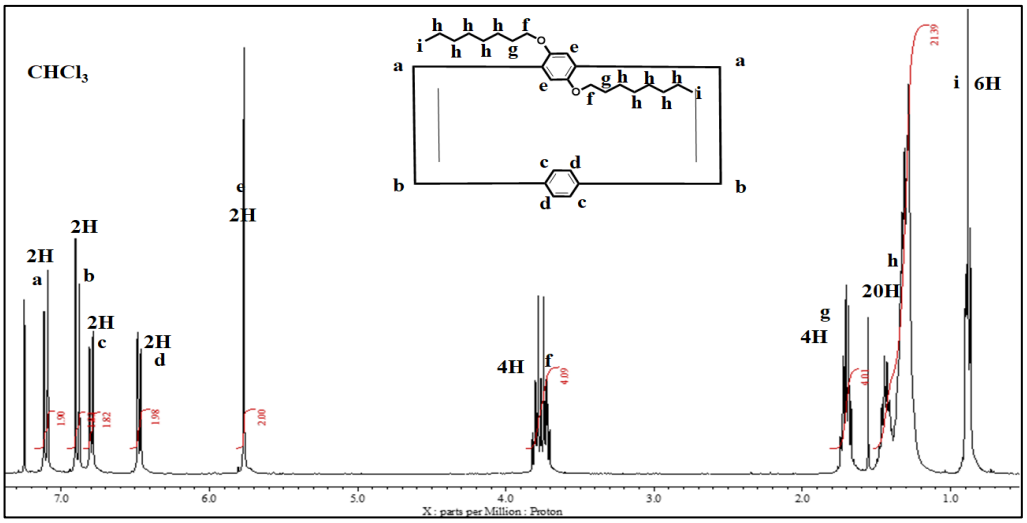

(b)

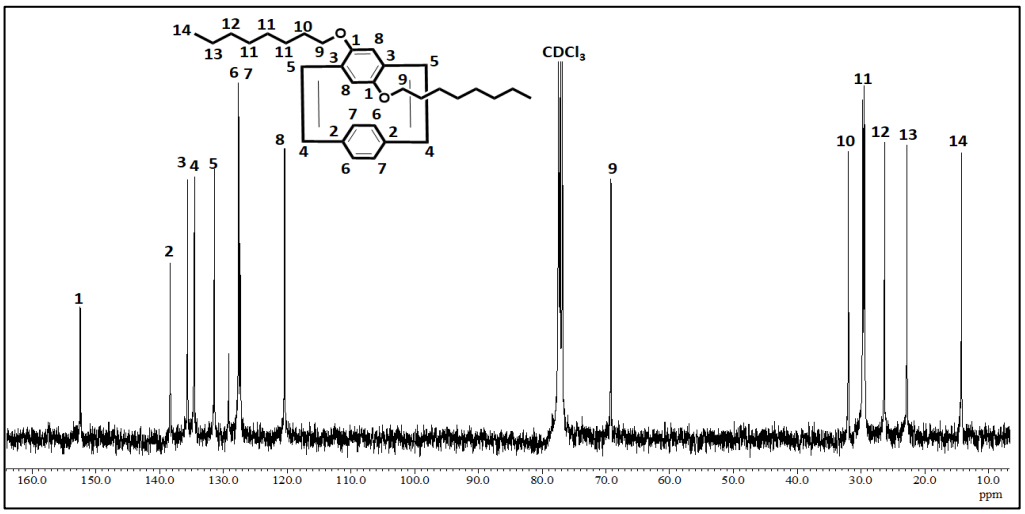

(c)

Figure 3. 2 Compound 9 (M_1) a) EI-MS spectrum; b) ^{1}H NMR spectrum; c) ^{13}C NMR spectrum.

3.1.10.Synthesis of (2Z,5Z)-12,15-di(octyloxy)-1,4(1,4)-dibenzenacyclohexaphane-2,5-diene (PCPD) compound (10) (M_1).

The oxidation product **8** (0.36 g, 0.000505 mol) was dissolved in DMF (40 ml) the mixture was stirred at room temperature for 5 minutes. The solution was then heated to 155°C with a nitrogen stream for a period of 20 hours. The solution was allowed to cool and washed with dilute aqueous HCL and extracted into chloroform, dried with sodium sulfate to give yellow oil. The crude material was purified using column chromatography (DCM: Hexane, 10:90) to afford a colorless viscous oil in (0.22 g,

61 %) yield, EI-MS calculated for $C_{32}H_{44}O_2$ *m/z*: 460.00; Found: *m/z* 460.70. ^{1}H NMR (400 MHz, Chloroform-d) δ 7.10 (d, J = 10.1 Hz, 2H), 6.89 (d, J = 10.1 Hz, 2H), 6.79 (d, J = 8.2 Hz, 2H), 6.47 (d, J = 8.2 Hz, 2H), 5.76 (s, 2H), 3.70-3.82 (m, 4H), 1.67-1.74 (m, 4H), 1.24-1.56 (m, 20H), 0.86-0.92 (m, 6H) ppm. ^{13}C-NMR (101 MHz, Chloroform-d) δ 152.39, 138.31, 135.60, 134.51, 131.39, 127.58, 127.30, 120.29, 77.43, 77.12, 76.79, 69.15, 31.95, 29.69, 29.52, 29.38, 26.29, 22.78, 14.24. (Figure 3. 3).

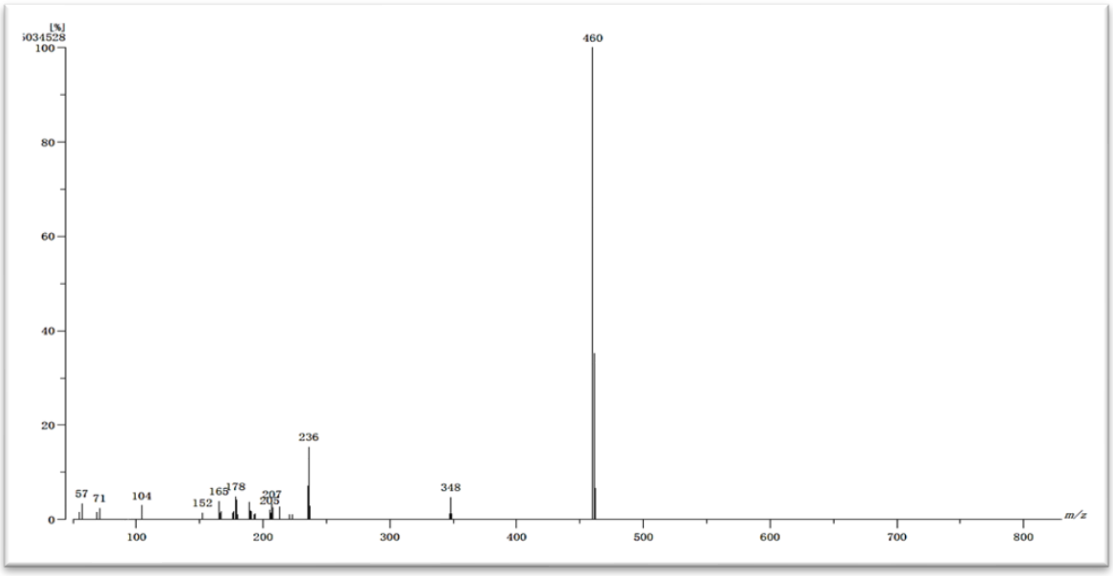

(a)

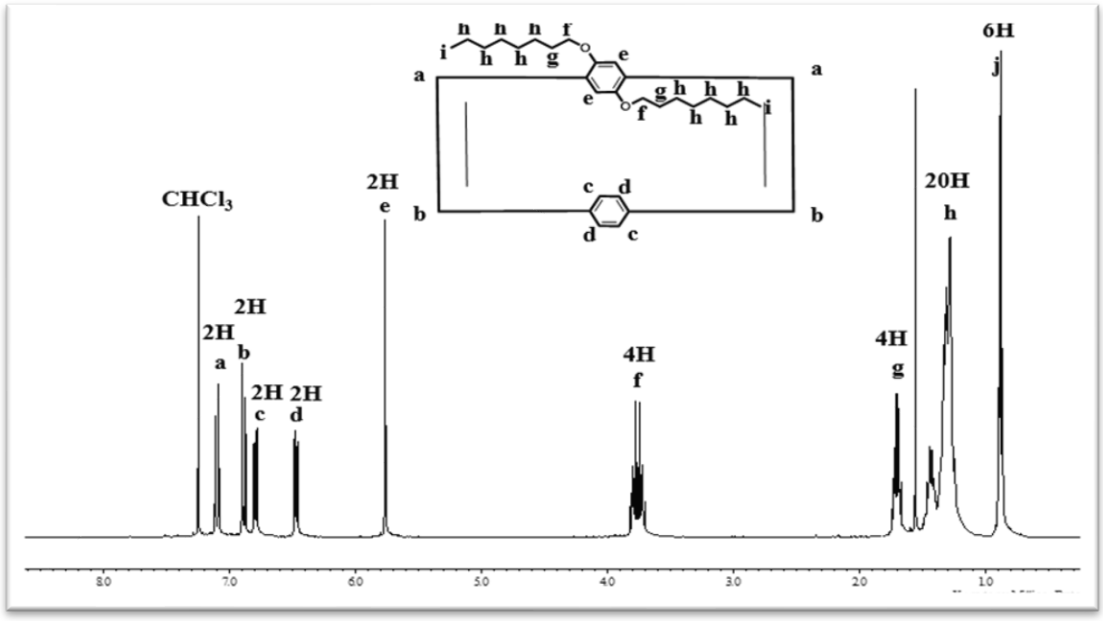

(b)

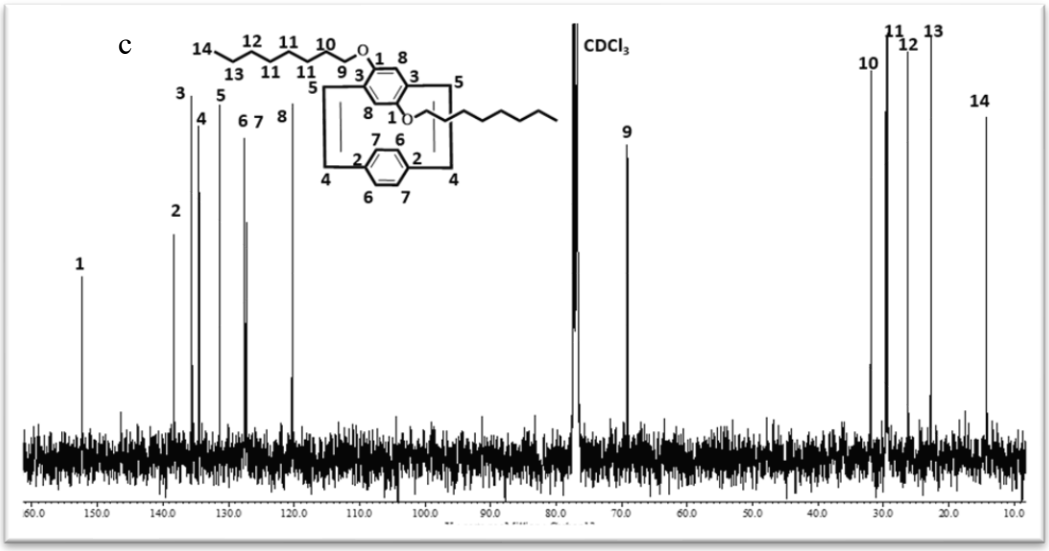

(c)

Figure 3. 3 Compound 10 (M_1) a) EI-MS spectrum; b) ^{1}H NMR spectrum; c) ^{13}C NMR spectrum.

3.2.Synthesis of Poly(2,5-Dioctyloxy-*p*-Phenylenevinylene) (11) (P_1).

In a dry Radleys Carousell tube under a nitrogen atmosphere, tetrahydrofuran (10 ml) solution containing DO-PCPDE monomer (**M_1**) (0.30 g, 6.5118x10^{-4} mol) was stirred for 10 minutes at 60˚C to fully dissolve. Then, G2 catalyst (18.42 mg, 2.1706x10^{-5}mol) was dissolved in dry Tetrahydrofuran (2 ml) under nitrogen and was quickly transferred by syringe to the polymerization vessel, then, the mixture was stirred at 60˚C for 24 hours. The mixture was then allowed to cool to RT, and the polymerization was quenched by adding excess ethyl vinyl ether (2 ml). The reaction mixture was allowed to proceed for an additional 1 hour. In order to remove the deactivated catalyst the polymerization mixture was passed through silica, the solvent was removed, and the pure polymer was dried in a vacuum oven at 40˚C for 12 hours. The pure product was exposed to 365nm light to convert the *cis-trans* structure in the polymer to the all-trans structure. (S3. 8).

^{1}H NMR (400 MHz, Chloroform-d) δ 7.53 –7.49 (m, 2H), 7.33 (d, 3H), 7.25 (s, 3H), 7.21 (d, J = 4.4 Hz, 2H), 7.09 (d, J = 16.7 Hz, 2H), 6.98 (s, 2H), 6.86 –6.44 (m, 6H), 3.97 (t, J = 6.9 Hz, 4H), 3.71 (t, J = 7.3 Hz, 4H), 1.47 –1.38 (m, 24H), 0.83 (t, J = 26.3 Hz, 6H).

3.3.Results and discussion.

(Scheme 3. 1) illustrates the steps involved in producing the DO-PCPD monomer (**M1**). In order to prevent the formation of oligomers and polymers, an equimolar amount of 1,4-bis(bromomethyl)-2,5-bis(octyloxy)benzene **2** and 1,4-Benzenedimethanethiol **3** were cyclized at a high dilution in the presence of aqueous potassium hydroxide for at least three days. This process produced the intermediate material, dithiaparacyclophane **4**. The benzyne rearrangement of compound **4** using benzyne-induced rearrangement Pummerer and Stevens methods also yielded bisphenylsulfides. Compounds **5** and **6** were obtained with a yield of 94% and 42% respectively after purification *via* flash column chromatography. Characterizing the mixture of isomers by NMR spectroscopy was challenging due to a large number of overlapping signals. The ESI mass spectrum of the benzyne rearrangement products exhibited a molecular ion at m/z 680 for both methods.

Compound **7** was synthesized by treatment with *m*-CPBA to give corresponding disulfoxides Then, Compound **7** was heated at reflux in *o*-xylene with Cesium Carbonate. Following purification by column chromatography and recrystallization, a 75% yield of the DO-PCPD monomer (**M1**) **9** was obtained. Oxidation of the phenyl sulfides by treatment with 35% w/w hydrogen peroxide in a 1:6 ratio of acetic acid/benzene solution gave the desired bis(sulfoxide) compound 8. Pyrolysis of the bis(sulfoxide) mixture was carried out in DMF solution under reflux with a nitrogen purge for 20 hours, and the crude compound was then chromatographed in hexane to give the monomer (**M1**)**10** in an overall yield of 46.6%. Then the monomer followed by the polymerization process utilizing G2 catalyst, and it was ultimately quenched by adding excess ethyl vinyl ether. (Scheme 3. 2)

Scheme 3. 2 DO-PPV homopolymer P_1 Using the G2 Catalyst

(Figure 3. 2) illustrates the ^{1}H NMR spectrum of the DO-PCPD monomer **9** in chloroform-d. Four doublets corresponding to the *cis*-vinylic hydrogens were observed at chemical shifts of 7.06, 6.95, 6.85, and 6.67 ppm. Two additional doublets were attributed to the hydrogens of the substituted phenyl ring at 6.95 and 6.41 ppm. Additionally, the hydrogens in the non-substituted phenyl ring manifested as a doublet at 6.47 ppm, integrating two hydrogens. One of the two aromatic hydrogens of the substituted phenyl ring appeared as a singlet at 5.52 ppm. Signals below 2 ppm in all three spectra corresponded to hydrogens of the long alkyl chain, except for methylene hydrogens linked to oxygen atoms. Furthermore, (Figure 3. 2) exhibited a peak with a molecular weight of 460 (M+) visible in the EI-MS analysis, indicative of the full formation of the desired monomer **9**. Similarly, monomer **10** exhibited nearly identical data in (Figure 3. 3). (S3. 8) (a and b) display the polymer $\mathbf{P_1}$ ^{1}H NMR spectra. The peaks at 3.97 and 3.71 ppm, respectively, are the methylene hydrogens bound to the oxygen adjacent to the *trans*- and *cis*-vinylenes. At 6.86 and 6.44 ppm, the signals of hydrogens for *cis*-vinylene and *o*-phenyl to the *cis*-vinylene were detected. Furthermore, peaks corresponding to the hydrogens for *trans*-vinylene and o-phenyl for *trans*-vinylene are seen at 7.53 and 7.49 ppm, respectively.

As shown in (Figure 3. 4), the polymer exhibited a reasonable number-average molecular weight (M_n) value of 27483 g/mol obtained from GPC analysis. So, the polydispersity index (PDI) can be calculated as 1.22 with a yield of 91%. It can be generally considered to be a narrow molecular weight distribution, which is important for use in electronic and optoelectronic applications, such as solar cells, light-emitting diodes, and field-effect transistors, where their good film forming properties are highly dependent on their molecular weight and the uniformity of their structure

In these applications, a low PDI value is desirable, as it can lead to more consistent and stable electronic properties in the final device with minimal quenching. Additionally, a comparison analysis was conducted on the end products of the polymer produced through ROMP and the Gilch method [77,78]. The findings indicated that the PPV derivative obtained exhibited superiority in terms of PDI, polymer purity, yield, and applications such as OLEDs.

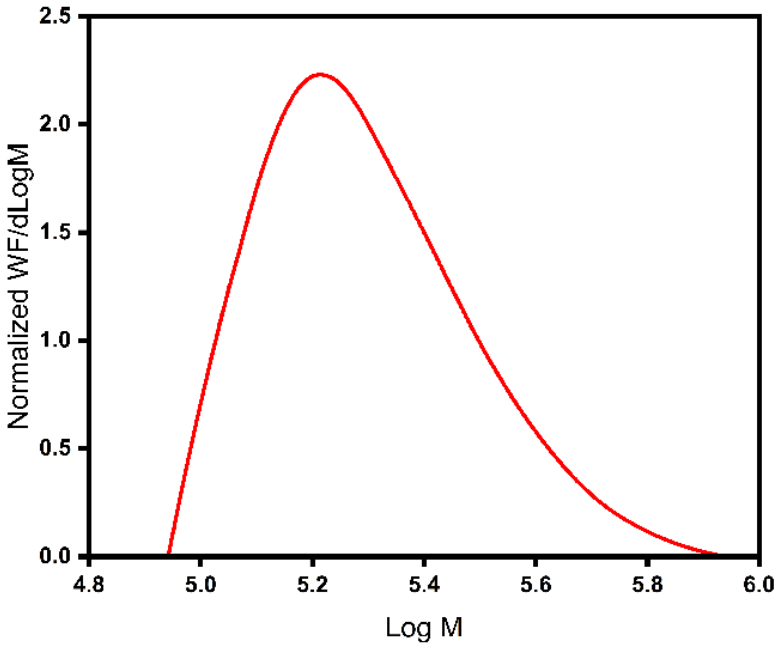

Figure 3. 4 Molecular weight distribution of polymer P_1.

P_1 absorption spectra were measured in the variable solutions including $CHCl_3$, C_6H_5Cl, and THF. Furthermore, (Table 3. 1) provides a summary of associated optoelectronic properties.

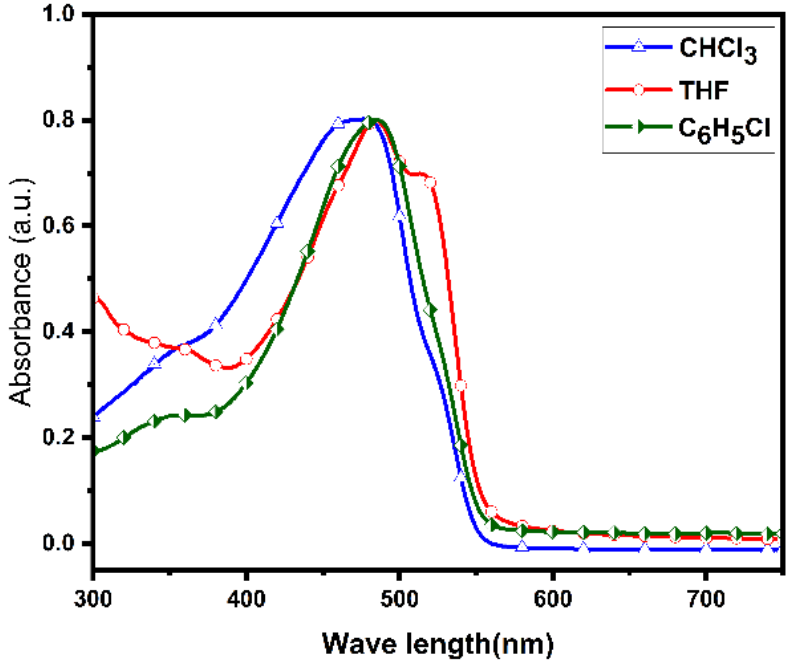

Figure 3. 5 Absorption profile of the polymer P_1.

UV-vis absorption maxima (λ_{max}) in the range of 470.90 – 485.70 nm were shown by the PPV in varied solutions. As presented major absorption peaks for $CHCl_3$ and C_6H_5Cl have been found at 470.90 and 485.70 nm, correspondingly (Figure 3. 5).

Remarkably, THF had a strong band of absorption at 485.00 nm in addition to its tiny shoulder peaks at 515.00 nm. The thin film UV-vis absorption of PPV derivatives emerged (Figure 3. 6). In this instance, the PPV homopolymer showed a broader band compared to the solution because of the polymer chains solid-state aggregation[79], and (λ_{max}) values were discovered at 480.16 nm.

The photoluminescence emission spectra of **P_1** were obtained by irradiative excitation at their respective wavelengths of the absorption maximum in variable solutions at concentrations 10^{-6} M at room temperature.

Table 3. 1 Optical Properties of the Polymer P_1

Polymer P_1	**solvent**	**UV-Vis Absorption**				**Fluorescence Emission**
		$\lambda_{(max)}$, nm	$\lambda_{(onset)}$, nm	E_g^{op} (eV)	E_g^{op} Tauc plot	$\lambda_{(em)}$ nm
Solution	C_6H_5Cl	485.7	552.8	2.24	2.17	539
	THF	485	556.7	2.23	2.19	545
	DCM	470.9	551	2.25	2.18	558.6
Thin film	C_6H_5Cl	480.1	561	2.21	2.07	647.85

In addition, the casting thin film is provided in (Figure 3. 6), and their data are displayed in (Table 3. 1). The highest emission bands in various solutions were observed in the region of approximately 539.0–555.8 nm. When $CHCl_3$ was stimulated at λ_{max} (470.00 nm), the λ_{em} maximum (558.65 nm) was reached.

Hence in this instance, THF and C_6H_5Cl share the identical excited λ_{max} at 480.00 nm in addition to having respective λ_{em} maximum values of 539.07 nm and 545.00 nm (Figure 3. 7).

Furthermore, the emission maximum λ_{em} was noticed at (647.85 nm) when the thin film was included at the excited λ_{max} (480 nm), and noticed that, in comparison to the emission maxima of different solutions, the λ_{em} in the thin film was more-red shifted, so this observation suggests that reduce the energy gap between the relaxed S^1 and S^0.

Therefore, the optical band gap (E_g^{op}) of the **P1** was determined by two methods one of those using the absorption onsets (λ_{onset}) according to this equation: (E_g^{op}) = 1240/λ_{onset} in addition to Tauc plot (Figure 3. 8).

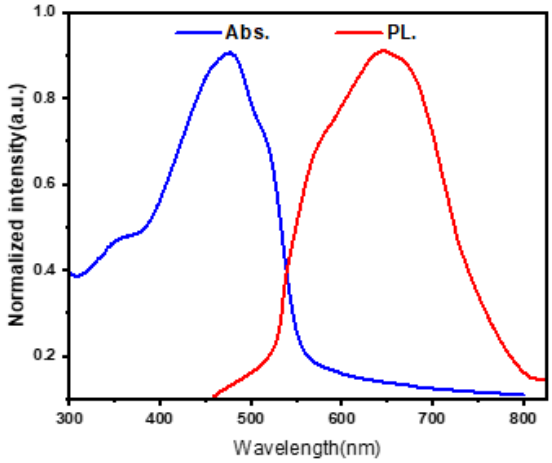

Figure 3. 6 Thin film Absorption and emission of P_1.

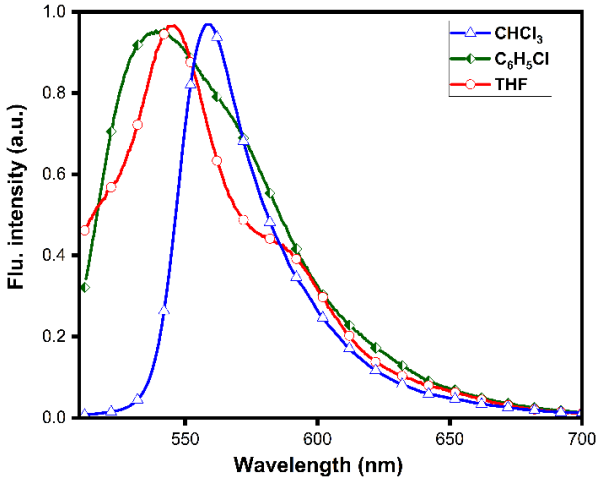

Figure 3. 7 Emission profile of the polymer P_1.

The onsets thin film in addition to, onsets of $CHCl_3$, C_6H_5Cl, and THF absorptions (λ_{onset}) of DO-PPV **P1** were estimated to be near 561.01, 551.06, 552.80 and 556.70 nm, respectively. Therefore, their E_g^{op} was anticipated to be among 2.21 - 2.25 eV. On the other hand, the Tauc plot E_g^{op} approach estimates a trend by linearly extending to zero of the linear regions of the $(\alpha hv)^{1/2} = f(hv)$ curves. In which hv is the energy of the photon and α is the absorption coefficient. Additionally, the Tauc plot was represented in the range of 2.07 to 2.19 and (Table 3. 1) displays the E_g^{op} for both thin-film and variable solutions.

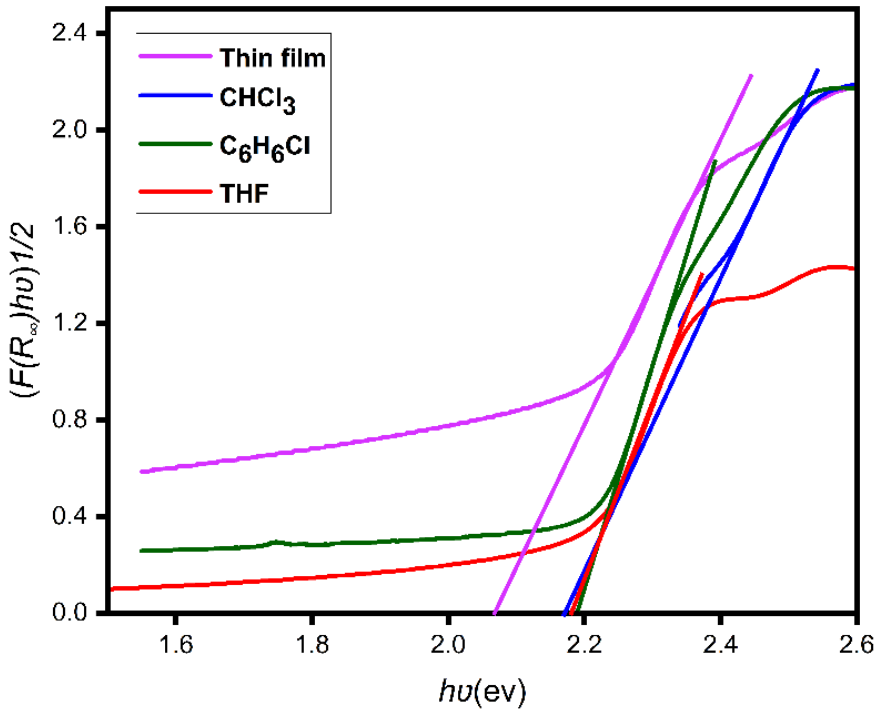

Figure 3. 8 Tauc plot band gap of P_1

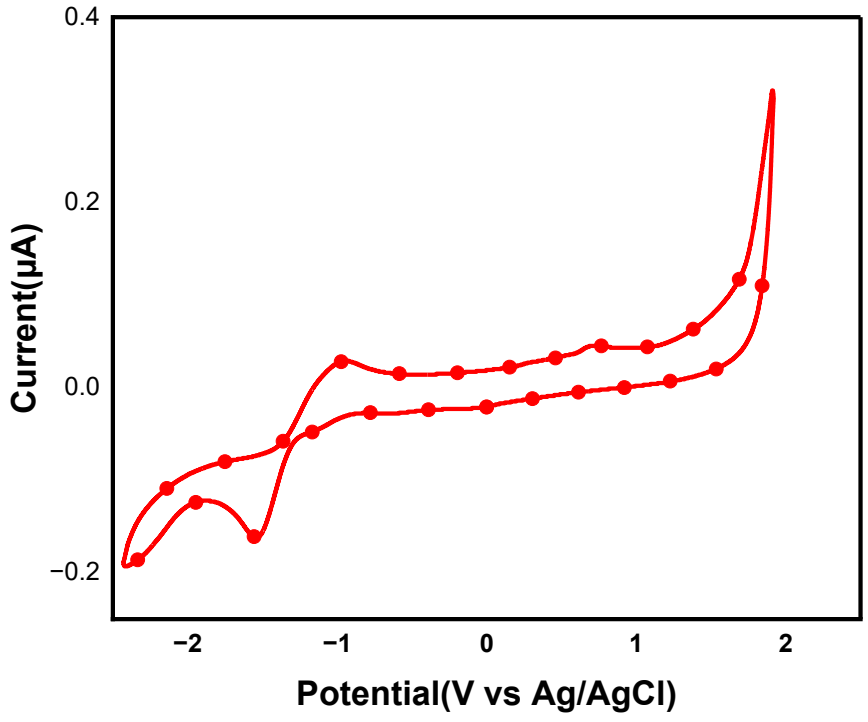

Figure 3. 9 Cyclic voltammograms for polymer on a Pt electrode in an acetonitrile solution containing 0.1M NBu_4PF_6 of P_1

The polymers electrochemical characteristics were assessed via cyclic voltammetry in solid-state conditions, employing tetrabutylammonium hexafluoride in acetonitrile (0.1 M) as the electrolyte. The polymer films were deposited onto a glassy carbon working electrode. The estimated energy levels for E_{HOMO} and E_{LUMO} are approximately -5.94 and -3.58 eV for **P_1**, respectively (Figure 3. 9).

By applying the equation for the difference between the HOMO and LUMO energy levels, we determined that the electrochemical band gap is 2.37 eV, which closely aligns with the energy obtained from the optical band gap [80].

The thermal stability of polymer **P_1** was assessed using thermogravimetric analysis (TGA) performed under a nitrogen atmosphere with a constant heating rate of 10 °C/min. The resulting data are illustrated in (Figure 3. 10).

For polymer **P_1**, the thermogram displays a two-step degradation process. The initial decomposition begins at approximately 193.1 °C, with a minor mass loss of 2.86%, likely caused by the release of low-molecular-weight side fragments. A second, more substantial degradation occurs at 265.9 °C, resulting in a 38.4% mass reduction, which is mainly attributed to the thermal cleavage of alkyl side chains.

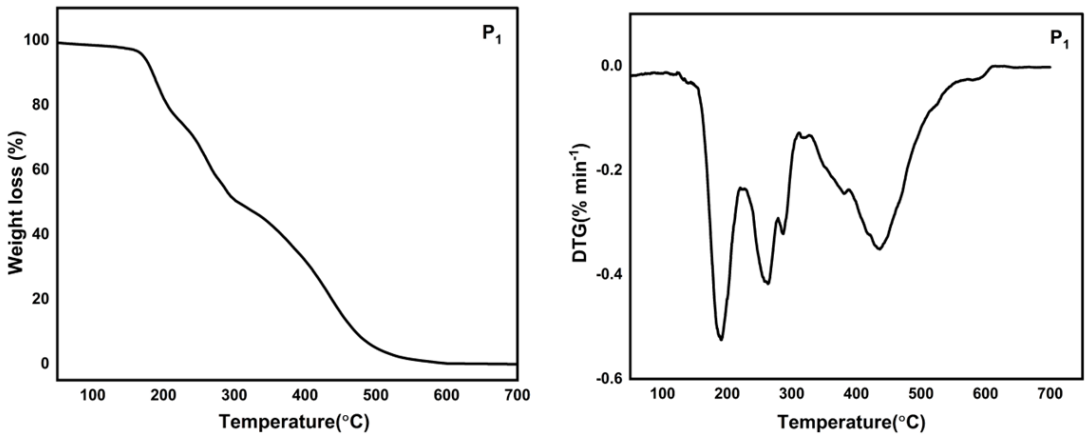

Figure 3. 10 a) TGA, and b) DTG curves for polymer P_1.

Second synthetic route for Synthesis of poly(2-[(2-ethylhexyl)oxy]-5-methoxy-*p*-phenylenevinylene) (EHM-PPV) (P_2)

3.4.Synthesis of EHM-Paracyclophanediene Monomer (M_2)

(Scheme 3. 3) illustrates the steps involved in synthesizing the EHM-Paracyclophanediene (EHM-PCPD) monomer. The process begins with the cyclization of key intermediates under controlled conditions to form a stable cyclic precursor.

Subsequent oxidation steps introduce sulfoxide functionalities, followed by elimination reactions to generate the desired conjugated structure. Each step in the synthesis was optimized to ensure high purity and yield, and the final structure was confirmed using NMR spectroscopy and mass spectrometry (MS).

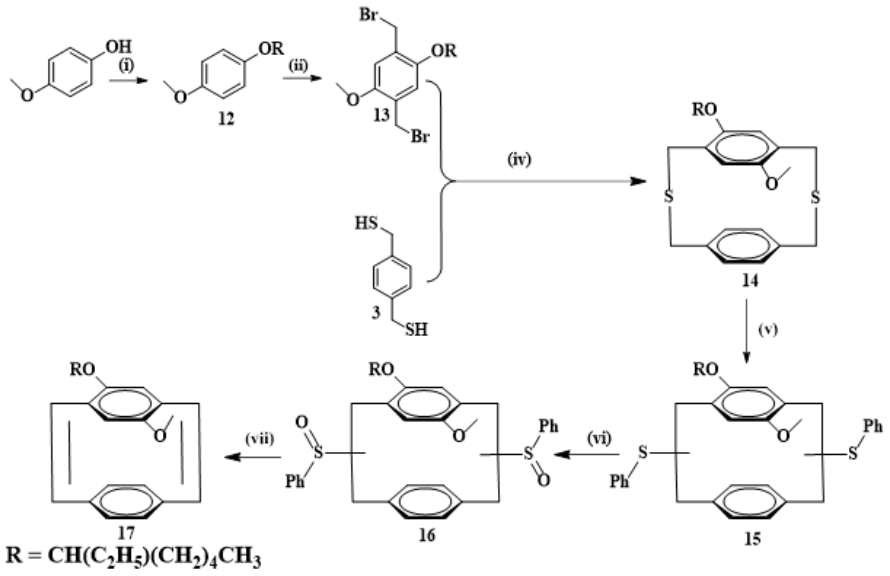

Scheme 3. 3 Synthesis of EHM-Paracyclophanediene Monomer M_2.

(i) 2-ethylhexylbromide, K_2CO_3, Acetonitrile, 80 ^oC, 48 h. (ii) $(CH_2O)n$, HBr, Acetic acid, 65 ^oC, 4 h. (iii) a-Thiourea, Ethanol, 90 ^oC, 5 h; b- KOH (aq.), 110 ^oC, 2 h; c-H_2SO_4, RT, 1 h. (iv) Alc.KOH, Benzene, RT, 72 h. (v) DCE, Isoamyl nitrite, Anthranilic acid, 90 ^oC, 2 h. (vi) Benzene / Acetic acid, H_2O_2, RT, 12 h. (vii) DMF, 155 ^oC, 20 h.

3.4.1.4.1 Synthesis of (R)-1-((2-ethylhexyl) oxy)-4-methoxybenzene (12).

A mixture of 4-methoxyphenol (10.00 g, 0.08 mol), 2-ethylhexylbromide (18.66 g, 0.096 mol), and potassium carbonate (13.35 g, 0.096 mol) was refluxed in acetonitrile (200 ml) for about 48 hours. The resultant mixture was cooled followed by stirring in de-ionized water for 30 minutes at room temperature to afford a dark brown precipitate which collected, washed several times by de-ionized water and dried at 50°C. Then, the crude was purified by dissolving in the minimum amount of hot hexane and re-precipitated by using excess of stirred methanolic solution to produce a brown precipitate which filtered, washed with methanol, and dried at 50°C to give a white solid in (17 g, 88 %) yield. EI-MS calculated for $C_{22}H_{38}O_2$ *m/z*: 236.35; Found: *m/z* 236.00.

^{1}H NMR (400 MHz, Chloroform-d) *δ 6.86 (d, J = 2.3 Hz, 4H), 3.82 (d, J = 4.6 Hz, 2H), 3.78 (s, 3H), 1.70-1.79 (m, 1H), 1.60-1.30 (8H), 0.93-0.98 (m, 6H))* ppm.^{13}C NMR (101 MHz, Chloroform-d) *δ 153.69, 115.50, 114.67, 71.01, 55.52, 39.16, 30.42, 28.77, 24.25, 23.22, 13.99, 10.54* ppm (S3. 9).

3.4.2.Synthesis of (R)-1,4-bis(bromomethyl)-2-((2-ethylhexyl)oxy)-5-methoxybenzene (13)

A mixture of product **12** (10 g, 0.004 mol), paraformaldehyde (2.54 g 0.0084 mol) was dissolved in (50 ml) acetic acid. A solution of hydrobromic acid (16 ml) (33 wt. % in acetic acid) was added and the mixture was stirred for 6 hours under refluxing system. The reaction mixture was cooled to RT and the suspension was poured onto de-ionized water, the precipitate was isolated by filtration and washed with de-ionized water. The dark brown residue was dissolved in hot hexane, then poured onto chilled methanol to form a solid white precipitate, which can be repeated for a white loose solid in (9.7 g, 54.3%) yield. EI-MS calculated for $C_{24}H_{40}Br_2O_2$ *m/z*: 422.2; Found: *m/z* 422.00 ^{1}H-NMR (400 MHz, Chloroform-d) δ *6.85 (d, J = 3.7 Hz, 2H), 4.52 (s, 4H), 3.79-3.87 (m, 5H), 1.73 (td, J = 11.9, 6.0 Hz, 1H), 1.32-1.58 (m, 8H), 0.91 (td, J = 14.8, 7.8 Hz, 6H) ppm.*^{13}C NMR (101 MHz, Chloroform-d) *δ 150.70, 127.51, 113.80, 70.83, 55.89, 39.12, 30.31, 28.29, 23.72, 22.67, 13.20, 10.31 ppm.*(S3. 10).

3.4.3.Synthesis of Thiacyclophane compound (14).

Compound **13** (9.6 g, 0.023 mol) and Compound **3** (3.9 g, 0.023 mol) were dissolved in deoxygenated benzene (500 ml). This solution was added extremely slowly dropwise using a pressure-equalizing dropping funnel to a stirred solution of Potassium Hydroxide (5.1 g, 0.077 mol) in deoxygenated ethanol (1000 ml), over 72 hours at RT. After a further 3 hours, the solvent was evaporated, the residue dissolved in chloroform and water, washed with water and brine in an organic layer which dried by using anhydrous Na_2SO_4, and the solvent evaporated to give a yellow oil which purified using column chromatography ($CHCl_3$: Hexane, 20:80) yielding a colorless oil (3.44 g, 35%). EI-MS calculated for $C_{32}H_{48}O_2S_2$ *m/z*: 430.2; Found: *m/z* 430.00. ^{1}H NMR (400 MHz, Chloroform-d) *δ 6.74-6.94 (m, 4H), 6.43 (d, J = 11.4 Hz, 2H), 4.24 (t, J = 14.2 Hz, 2H), 3.76 (s, 3H), 3.64 (td, J = 8.3, 3.2 Hz, 2H), 3.35 (d, J = 14.6 Hz, 2H), 0.88-1.77 (m, 15H)* ppm.^{13}C NMR (101 MHz, Chloroform-d) *δ 149.69, 135.59, 129.11, 128.25,*

128.18, 127.43, 124.28, 114.64, 113.71, 69.81, 55.68, 39.96, 37.98, 31.22, 29.26, 24.42, 23.25, 14.29, 11.22 ppm. (Figure 3.20).

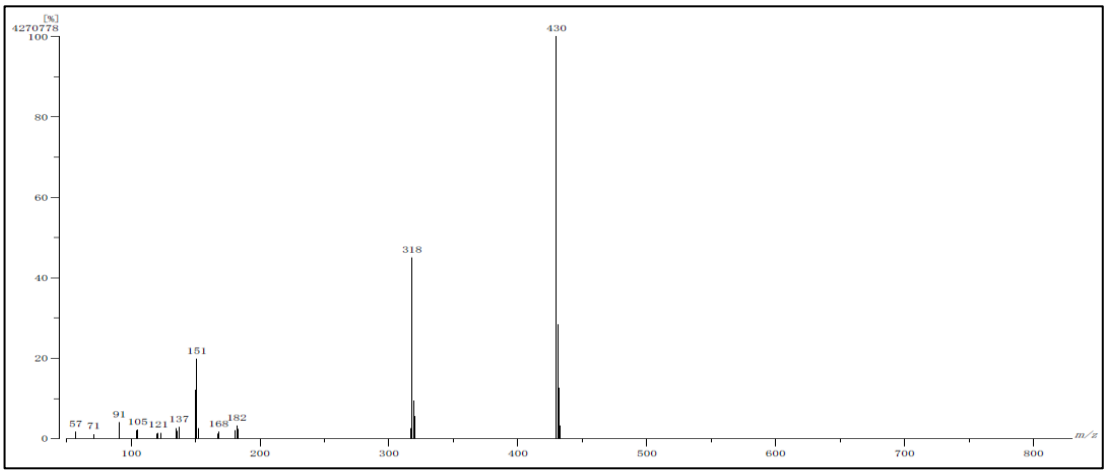

(a)

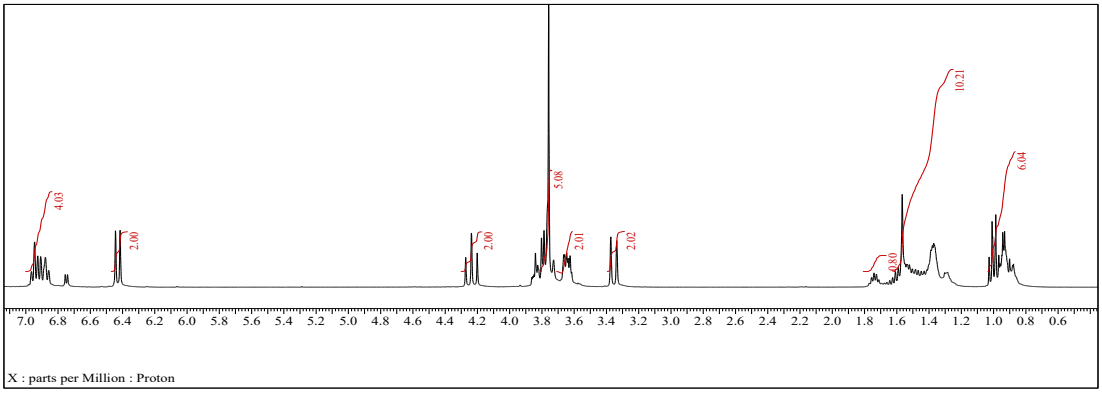

(b)

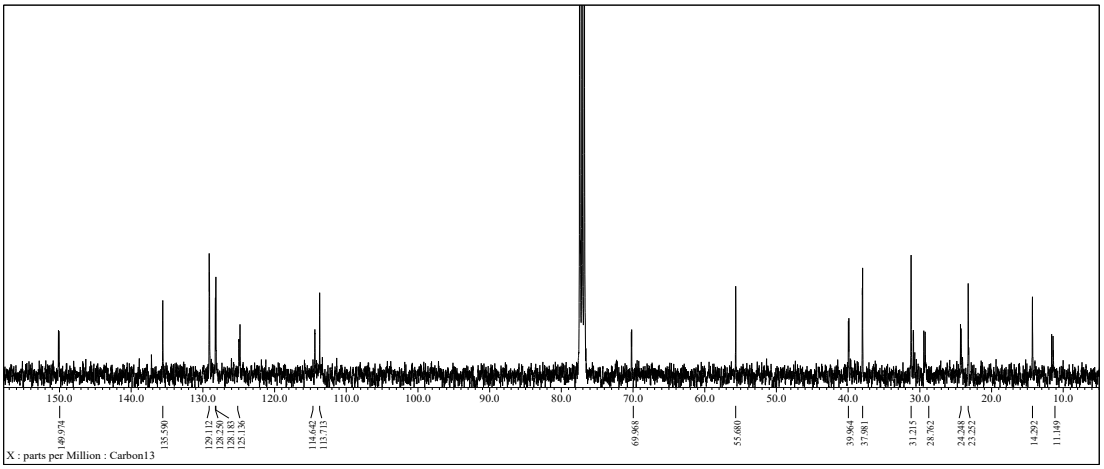

(c)

Figure 3. 11 Compound 14 a) EI-MS spectrum; b) ^{1}H NMR spectrum; c) ^{13}C NMR spectrum.

3.4.4.Benzyne rearrangement compound (15).

The Thiacyclophane **14** (3.1 g, 0.0072 mol) and Anthranilic acid (3.46 g, 0.025 mol) were dissolved in anhydrous 1,2-Dichloroethane (100 mL) and heated to 90^{o}C under nitrogen with a condenser. At the reflux point, Isoamyl nitrite (3.37 g, 0.0288 mol) was added by syringe very slowly over a period of at least 60 minutes. The resulting solution was heated at 90^{o}C furthermore 1 hour and then evaporated to produce brown oil. The crude material was purified by column chromatography (DCM: Hexane, 30:70) yielding a pale-yellow oil (1.86 g, 44.5 %). EI-MS calculated for $C_{44}H_{56}O_2S_2$ *m/z*: 582.86; Found: *m/z* 582.00 (S3. 11).

3.4.5.Oxidation of phenyl sulfides of compound (16).

The Steves rearrangement product **15** (1.86 g, 0.0032 mol) was dissolved in a mixture of benzene (30 ml) and acetic acid (5 ml). The mixture was stirred for 10 minutes and then cooled to approximately 0 $^{\circ}$C using an ice bath. Hydrogen peroxide (0.33 g, 0.0096 mol) was dissolved in acetic acid (5ml) and added dropwise by syringe over a period of 30 minutes in air. The vessel was allowed to warm to room temperature and stirred for 12 hours in air. Then, quenched by a saturated sodium bicarbonate solution followed by extracted via chloroform, collected the organic phase and washed with de-ionized water (3x100 ml) and dried by anhydrous $MgSO_4$, and evaporated to give a (0.95 g, 48.2 %) yield of the desired product as a clear yellow oil. EI-MS calculated for $C_{44}H_{56}O_4S_2$ *m/z*: 614.86; Found: *m/z* 472.00 (S3. 12).

3.4.6.Synthesis of substituted 2-[(2-Ethylhexyl)oxy]-5-methoxy-dibenzenacyclohexaphane-2,5-diene EHM-PCPD compound (17) (M_2)

The oxidation product **16** (0.36 g, 0.000505 mol) was dissolved in DMF (40 ml) the mixture was stirred at room temperature for 5 minutes. The solution was then heated to 155ºC with a nitrogen stream for a period of 20 hours. The solution was allowed to cool and washed with dilute aqueous HCL and extracted into chloroform, dried with sodium sulfate to give yellow oil. The crude material was purified using column chromatography (DCM: Hexane, 10:90) to afford a colorless viscous oil in (0.22 g, 25 %) yield, EI-MS calculated for $C_{25}H_{30}O_2$ *m/z*: 362.51; Found: *m/z* 362.00. ^{1}H NMR (400 MHz, Chloroform-d) δ*7.30-7.32 (m, 2H), 7.28 (d, J = 0.0 Hz, 2H), 7.23 (d, J = 7.3 Hz, 4H), 6.92 (d, J = 10.1 Hz, 2H), 6.49 (d, J = 8.2 Hz, 1H), 5.80 (d, J = 9.1 Hz, 1H),*

4.08 (s, 1H), 3.68 (s, 3H), 1.27-1.48 (m, 10H), 0.85-0.97 (m, 6H) ppm. ^{13}C NMR (101 MHz, Chloroform-d) δ*152.60, 150.28, 131.45, 129.48, 126.93, 124.46, 119.47, 118.49, 71.72, 55.91, 31.42, 30.20, 29.05, 26.40, 23.93, 23.20, 14.25, 11.09 ppm* (Figure 3. 12).

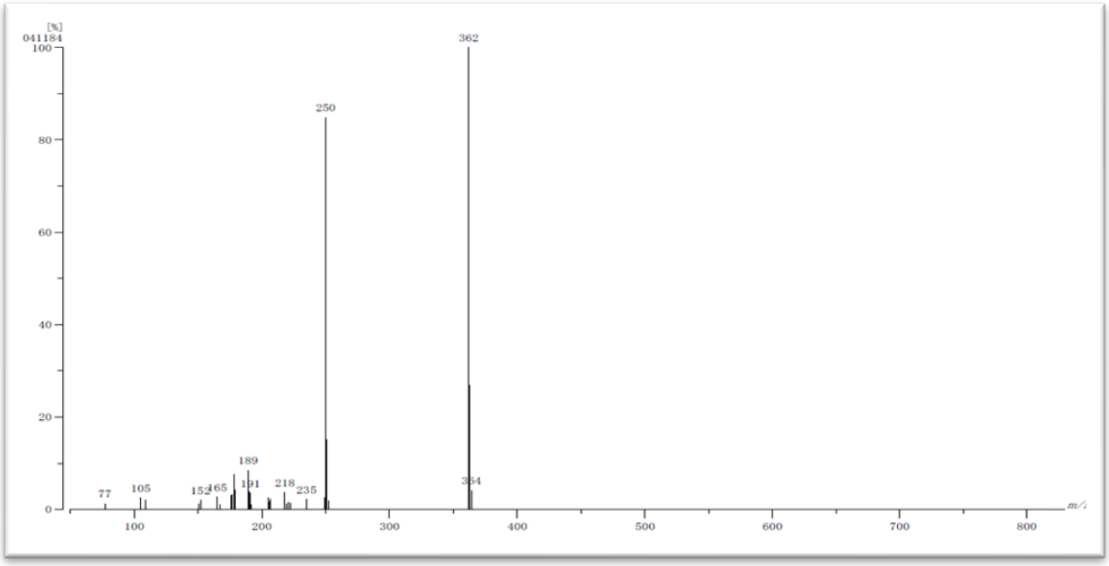

(a)

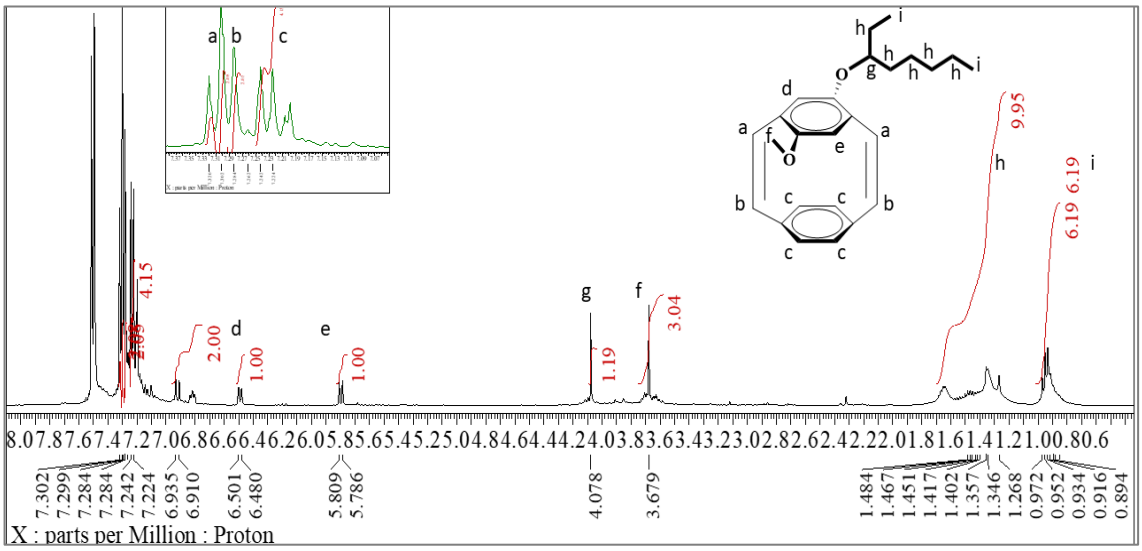

(b)

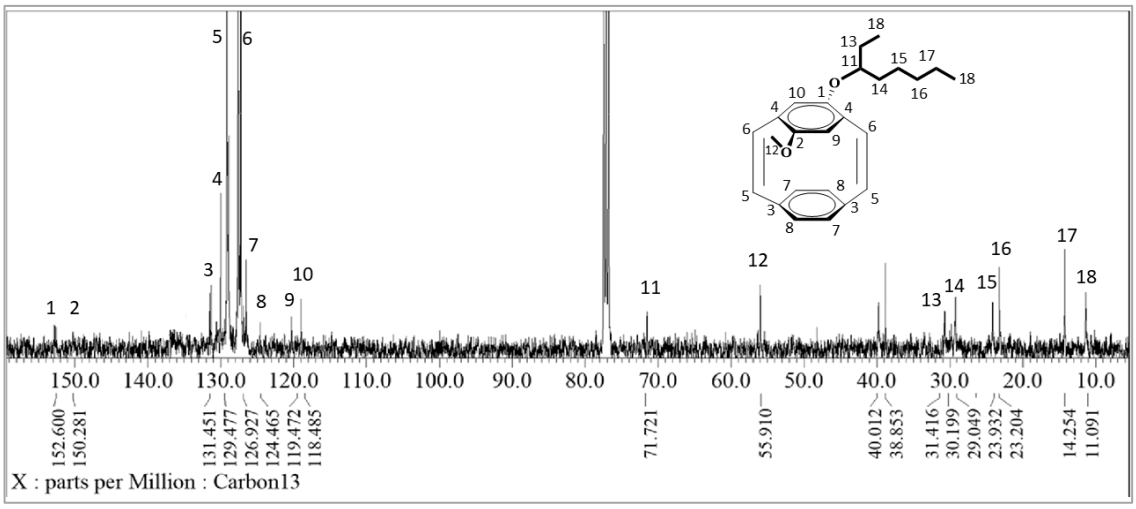

(c)

Figure 3. 12 Compound 17 (M_2) a) EI-MS spectrum; b) ^{1}H NMR spectrum; c) ^{13}C NMR spectrum.

3.5.Synthesis of poly (2-[(2-Ethylhexyl)oxy]-5-methoxy- *p*-phenylenevinylene) EHM-PPV (P_2).

In a nitrogen atmosphere within a dry radleys Carousel tube, a solution was prepared using anhydrous 1,2-dichloroethane (DCE) (1 ml) containing 30 mg (0.083 mmol) of EHM-PCPD monomer (**M_2**). This mixture was stirred for 10 minutes at 60°C to ensure the monomer was fully dissolved. Subsequently, G_2 (3.5 mg) was introduced, dissolved in 0.2 mL of anhydrous DCE and stirred for at least 10 minutes prior to incorporation into the monomer solution, which was kept at 60°C for 24 hours. Following this period, the reaction mixture was allowed to cool to room temperature, and the polymerization process ended capped by adding an excess of EVE (2 ml). Following an extra 2 hours of stirring at ambient temperature, the reaction mixtures were concentrated using a vacuum. The crude products were re-dissolved in minimum amount of DCM and then precipitated into methanol to remove any residual ruthenium complexes. This process yielded the polymer with a 91% yield. The purified product will then be subjected to 365 nm light exposure to convert the polymer cis-trans configuration into the all-*trans* form.

3.6.Results and discussion.

3.6.1.The structural characterization of the EHM-PCPD monomer & synthesized polymer P_2 by ROMP.

the monomer underwent homopolymerization **P_2** using the G_2 catalyst, which was finally terminated by the addition of EVE (Scheme 3. 4).

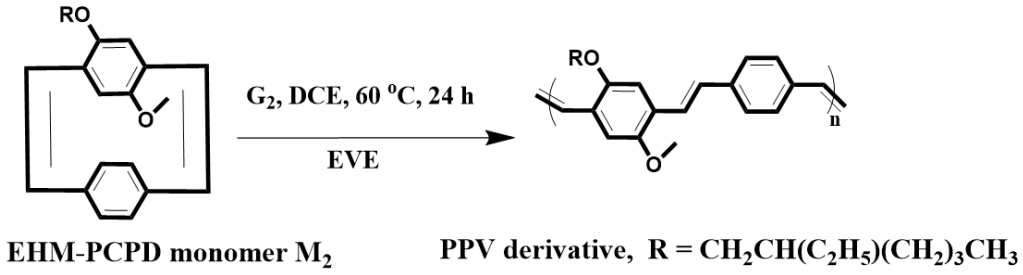

Scheme 3. 4 EHM-PPV homopolymer P_2 using the G2 catalyst.

GPC analysis was performed using THF as the eluent to determine the molecular weight of the synthesized polymer **P_2** shown in (Figure 3. 13). The polymer exhibited a number average molecular weight (*Mn*) of 22270 g/mol with a polydispersity index (PDI) of 1.09.

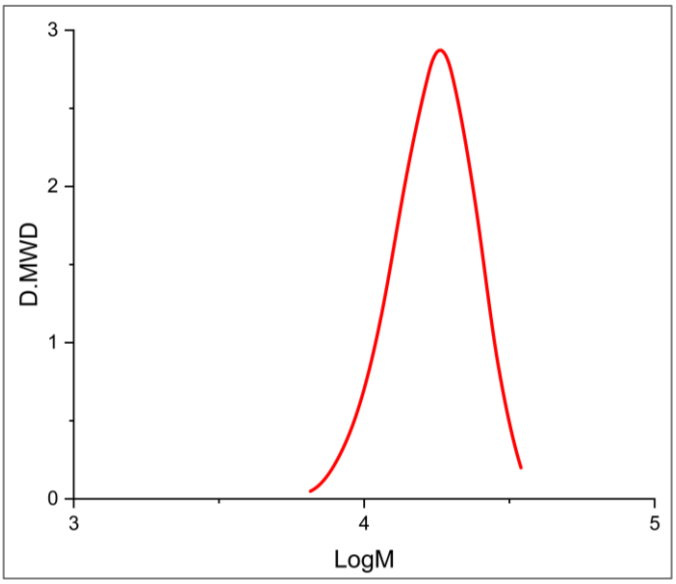

Figure 3. 13 Molecular weight distribution of polymer P_2

3.6.2.Characterization of the synthesized polymers by ^{1}H NMR Spectroscopy

The ^{1}H NMR spectra of the synthesized polymer **P_2** recorded in $CDCl_3$, are shown in (Figure 3. 14). The *trans-vinylene* and other aromatic protons are observed at chemical

shifts above 7.00 ppm. A broad peak at 3.35 ppm appears corresponding to the methylene protons and methyl groups attached to oxygen atoms. Alkyl chain protons resonate at chemical shifts below 2.00 ppm.

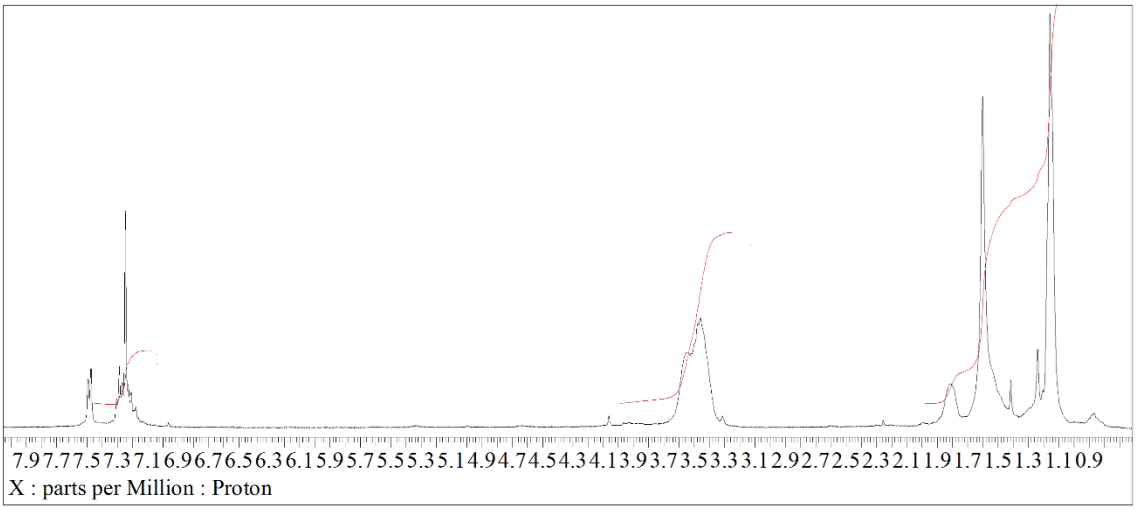

Figure 3. 14 ^{1}H NMR spectrum of P_2

3.6.3. Optical properties of the polymer P_2.

(Figure 3. 15) displays the absorption spectra of **P_2** in chlorobenzene, THF, and DCM, each at a concentration of 5×10^{-8} M. In all three solvents, **P_2** predominantly shows a single absorption peak at 468 nm. The *p*-phenylenevinylene backbone is primarily responsible for this absorption due to its conjugated nature, which allows for efficient π–π* transitions (Table 3. 2).

Table 3. 2 Optical Properties of the Polymer P_2.

Polymer No.	solvent	UV-Vis Absorption			Fluorescence Emission
		$\lambda_{(max)}$, nm	$\lambda_{(onset)}$, nm	E_g^{op} (eV)	$\lambda_{(em)}$, nm
P_2	C_6H_5Cl	468	533.0	2.32	516
	THF	483	524.5	2.36	513
	DCM	466	523.5	2.37	511

The absorption and fluorescence emissions of the polymers showed minimal deviation across the solvents.

The absorption maxima (λ_{max}) ranged between 466 nm and 483 nm across the solvents, while the fluorescence emission peaks were observed at 516 nm (C_6H_5Cl), 513 nm (THF), and 511 nm (DCM) (Figure 3.27).

Overall, the optical bandgaps (E_g^{op}) calculated from the onset of absorption (λ_{onset}) also showed minimal variation, with the values ranging from 2.32 eV to 2.43 eV for all polymers.

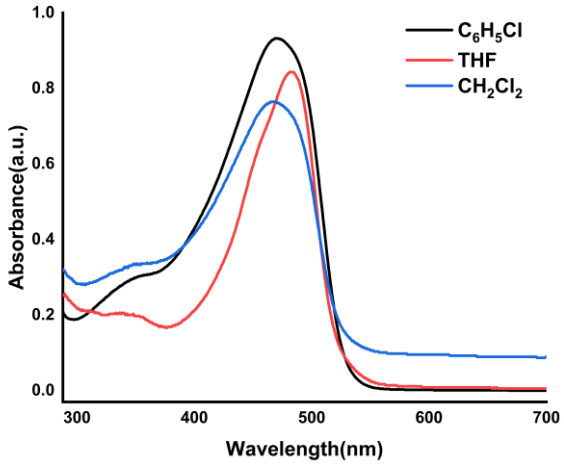

Figure 3. 15 UV of (P_1) In C_6H_5Cl &THF&DCM.

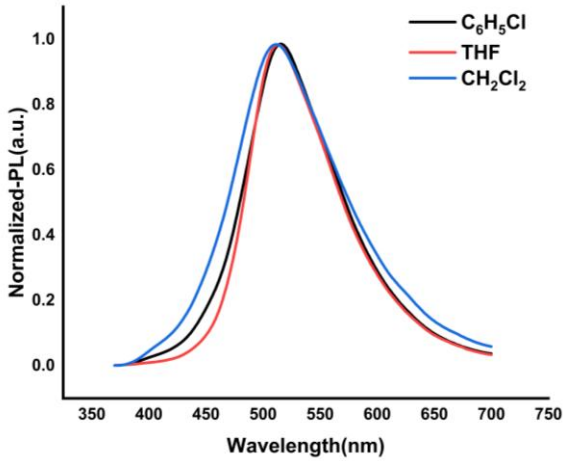

Figure 3. 16 PL of (P_1) In C_6H_5Cl &THF&DCM.

3.6.4.Electrochemical properties of the polymer P_2.

The electrochemical properties of polymer were evaluated using cyclic voltammetry (CV), with results shown in (Figure 3. 17) and summarized in (Table 3. 3).

Table 3. 3 Electrochemical properties of the polymer P_2

Polymers	$[O]_{onset}$ (V)	$[R]_{onset}$ (V)	HOMO (eV)	LUMO (eV)	E_g (eV)
P_2	0.81	- 1.38	5.61	3.42	2.19

The HOMO and LUMO energy levels for this polymer were derived from their oxidation and reduction onsets, leading to electrochemical band gaps of 2.19 eV for P_2.

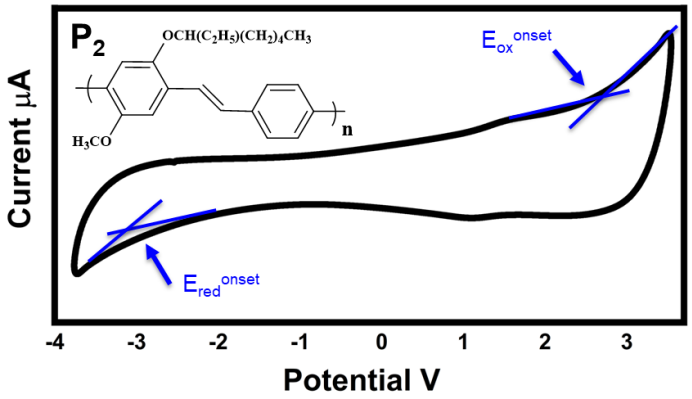

Figure 3. 17 CV curve for P_2 and band gap.

3.6.5.Thermal behavior of the polymer P_2.

The thermal stability of the synthesized polymer **P_2** was investigated through thermogravimetric analysis (TGA) under a nitrogen atmosphere at a heating rate of 10 °C/min. The results are presented in (Figure 3. 18) The TGA results reveal two stages of decomposition. The first stage occurs at 177.2 °C, accompanied by a 2.7 % weight loss, likely due to the volatilization of small side groups. The second stage, at 299.5 °C, leads to a more significant 29.7% weight loss, which is attributed to the breakdown of alkoxy side chains. After this, the polymer stabilizes, with a minor residual mass loss of 2.1% and a char yield of 97.9%, indicating reasonable thermal stability.

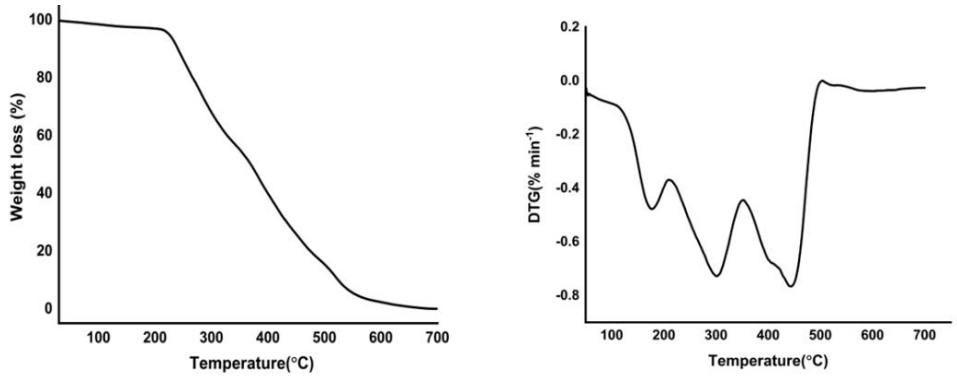

Figure 3. 18 a) TGA, and b) DTG curve for polymer P_2.

3.7.Conclusion.

This study focused on the synthesis, characterization, and optical evaluation of two soluble poly (*p*-phenylene vinylene) (PPV) derivatives: poly(2,5-dioctyloxy-*p*-phenylenevinylene) (DO-PPV, P_1) and poly(2-[(2-ethylhexyl)oxy]-5-methoxy-*p*-phenylenevinylene) (EHM-PPV, P_2). The monomer for P_1 was synthesized via two methods for benzyne rearrangement: the induced-benzyne Pummerer rearrangement and the benzyne Stevens rearrangement. However, the Stevens rearrangement proved to be a more cost-effective approach. The synthesis of the monomer for P_2 exclusively utilized the benzyne Stevens rearrangement, ensuring an efficient and economical pathway. Both monomers were subsequently polymerized using G2 catalyst via ROMP, yielding soluble polymers with narrow polydispersity indices (PDI), measured at 1.22 for P_1 and 1.09 for P_2.

The optical properties revealed distinct behaviors for each polymer. DO-PPV (P_1) exhibited maximum absorption peaks ranging from 470.9 to 485.7 nm in solution and 480.16 nm in the thin film. The fluorescence emission varied from 539 nm to 558.6 nm in solution, with a significant red shift to 647.85 nm in the thin film. Its optical band gaps (Eg^{op}) ranged from 2.21 to 2.25 eV in solution, with a Tauc plot estimation of 2.07 eV in the thin film. EHM-PPV (P_2), on the other hand, displayed absorption maxima between 466 and 483 nm in solution, with fluorescence emission peaking between 511 and 516 nm. Its optical band gaps (Eg^{op}) in solution ranged from 2.32 to 2.37 eV, demonstrating slightly higher values compared to P_1, which may be attributed to the polymers structural and electronic uniformity.

These findings demonstrate that structural variations, such as dioctyl and ethylhexyl substituents, significantly influence the polymers optical and electronic properties. The innovative combination of the benzyne Stevens rearrangement and ROMP, particularly in the cost-effective synthesis of P_2, underscores the potential for tailoring conjugated polymers for OLEDs and other advanced optoelectronic applications.

Chapter 4

Thermal Stability and Solubility of Poly (norbornene-dicarboximide) Derivatives: Synthesis and Characterization of Carbazole and Adamantyl Pendants

This chapter focuses on synthesizing, characterizing, and analyzing a new series of thermally stable and soluble poly (NDI) derivatives designed for advanced functional applications. The central aim of this chapter is to explore the role of pendant groups and their impact on the polymer's properties, including its solubility, thermal stability, and optical characteristics. The synthesis of two distinct NDI monomers, M_3 and M_4, functionalized with carbazole and adamantane groups, respectively, serves as the basis for developing these polymers.

Poly (NDI) derivatives are promising candidates for various applications due to their excellent processability, stability, and the ability to undergo controlled polymerization via ROMP. By incorporating different pendant groups onto the norbornene backbone, it is possible to modulate the physical, electronic, and optoelectronic properties of the resulting polymers. In particular, the carbazole-functionalized poly (CA-NDI), which was synthesized through the Grubbs 3rd generation initiator G3, demonstrates not only exceptional solubility in a variety of solvents but also significant thermal stability, making it ideal for applications in high-performance electronics and optoelectronics.

The second polymer, based on adamantane-functionalized poly (AD-NDI), was synthesized to explore the effect of bulky, rigid adamantane groups on the polymer's thermal and solubility properties. Both polymers exhibit controlled polymerization, as evidenced by narrow molecular weight distributions (low polydispersity index) and high molecular weights, a testament to the precision afforded by ROMP using the Grubbs initiator. These polymers were characterized using a combination of techniques, including NMR, GPC, FT-IR, DSC, and UV-vis spectroscopy, to investigate their chemical structure, molecular weight, thermal properties, and optical behavior.

The results of this study indicate that the incorporation of carbazole and adamantane pendant groups into the poly (NDI) backbone significantly affects the polymers properties, including their solubility, thermal stability, and optical characteristics. These findings offer important insights into the design of new materials for use in high-performance applications such as organic semiconductors, optoelectronics, and photovoltaic devices.

First synthetic route for Synthesis of Carbazole-NDI monomer

4.1.Synthesis of Carbazole-NDI Monomer (CA-NDI) (M_3)

(Scheme 4. 1) illustrates the synthetic route employed to prepare the carbazole-functionalized CA-NDI monomer. The process begins with the synthesis of an exo-norbornene-5,6-dicarboxylic anhydride precursor (1) through the reaction of maleic anhydride with dicyclopentadiene under high temperature conditions. This precursor is then reacted with a commercially available amino acid precursor under reflux, leading to the formation of a NDI derivative (2).

In the subsequent step, the carbazole moiety is introduced into the NDI structure through a coupling reaction using a base catalyst and a carbazole-based reagent. The reaction is carried out at low temperatures to ensure precise functionalization and to prevent undesired side reactions.

The CA-NDI monomer is finalized through purification steps, including column chromatography and recrystallization, yielding a white solid product. Structural confirmation was achieved using NMR, MS, and elemental analysis (EA).

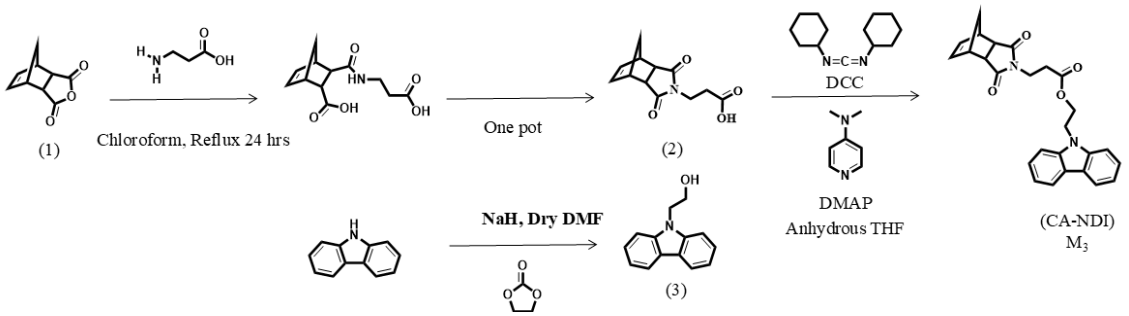

Scheme 4. 1 Synthesis Carbazole-NDI Monomer M_3.

4.1.1. Synthesis of precursor (1)

The synthesis of exo-norbornene-5,6-dicarboxylic anhydride (1) proceeded as follows: Maleic anhydride MA (188.20 g, 1.92 mol) was dissolved in 200 ml of o-dichlorobenzene. The solution was raised to a temperature of 200 °C. Simultaneously, dicyclopentadiene was warmed in a water bath at 45 °C to facilitate melting, enabling easy pouring. The melted dicyclopentadiene (128.60 g, 0.97 mol) was then gradually introduced into the pre-stirred solution using a funnel. following the complete addition, the product was additionally heated to 200 °C. for an extra two hours. The heated mixture was transferred into a beaker and gradually cooled to room temperature. The crystals obtained were filtered and rinsed with 100 ml o-dichlorobenzene. To obtain the desired exocyclic isomer, the crystals were recrystallized from chlorobenzene two or three times as required to

obtain a high purity in a yield of around 40%. LRMS (EI+) computed for $C_9H_8O_3$: m/z 164; Determined m/z 164. ^{1}H NMR (400 MHz, $CDCl_3$): δ 6.30 (s, 2H), 3.41 (s, 2H), 2.98 (s, 2H), 1.63 (d, J = 9.6 Hz, 1H), 1.39 (d, J = 10.1 Hz, 1H) ppm. ^{13}C NMR (101 MHz, Chloroform-d) δ: 171.80, 138.02, 48.85, 46.93, 44.19 (S4. 1).

4.1.2.Synthesis of precursor (2)

Precursor (1) (10.00 g, 0.061 mol) was dissolved in 100 mL of $CHCl_3$ at room temperature, and beta-alanine (5.44 g, 0.061 mol) was gradually introduced into the stirred solution under a nitrogen atmosphere. The mixture underwent reflux for 24 hours. Removal of the solvent by rotary evaporator gave the crude product a clear viscous oil. The pure product was obtained by column chromatography in 90% $CHCl_3$ and 10% CH_3OH. The white solid was then recrystallized from hexane and the minimum amount of tetrahydrofuran in a yield of 57%. LRMS (EI+) computed for $C_{12}H_{13}NO_4$: m/z 236; Determined m/z 236. ^{1}H-NMR (400 MHz, $CDCl_3$) δ: 6.24 (s, 2H), 3.74 (t, J = 7.3 Hz, 2H), 3.23 (s, 2H), 2.55-2.66 (m, 4H), 1.47 (d, J = 10.1 Hz, 1H), 1.20 (d, J = 9.6 Hz, 1H) ppm. ^{13}C NMR (101 MHz, Chloroform-d) δ: 178.01, 176.26, 137.93, 47.90, 45.25, 42.83, 34.18, 31.80. (S4. 2).

4.1.3.Synthesis of 2-Carbazole-9-yl-ethanol (CA-OH) (3)

The synthesis of (CA-OH), designated as precursor (3), was carried out as follows: Dry DMF (20 mL) and sodium hydride (NaH, 60% dispersion in paraffin oil, 3.98 g, 0.2 mol) were added to a 3-neck round-bottom flask equipped with a stirring mechanism. The reaction mixture was cooled to 0 °C using a chiller. A solution of carbazole (8.35 g, 0.1 mol) in dry DMF (20 mL) was added dropwise using a pipette while maintaining the temperature at 0 °C. The resulting suspension was stirred for 30 minutes. Subsequently, a solution of ethylene carbonate (10 g, 0.11 mol) in DMF (20 mL) was added dropwise to the mixture. The reaction was allowed to proceed with continuous stirring at 0 °C for 12 hours. Upon completion, the crude product was extracted using chloroform and washed with deionized water to remove impurities. Purification was achieved via column chromatography, starting with 0% THF and gradually increasing to 20%. The purified product, initially obtained as a clear oil, was further dried under vacuum, converting it into a solid. Recrystallization from hexane with a minimal amount of THF yielded fine needle-like white crystals. LRMS (EI+) computed for $C_{14}H_{13}NO$: m/z 211; Determined m/z 211 ^{1}H-NMR (400 MHz, $CDCl_3$) δ 8.09 (d, J = 7.8 Hz, 2H), 7.41-7.49 (m, 4H), 7.21-7.24 (m, 2H), 4.45 (t, J = 5.5 Hz, 2H), 4.02 (t, J = 5.5 Hz, 2H) ppm. ^{13}C NMR (101 MHz,

Chloroform-d) δ: 140.55, 126.07, 122.96, 120.19, 119.31, 108.87, 61.83, 45.34 (Figure 4. 1).

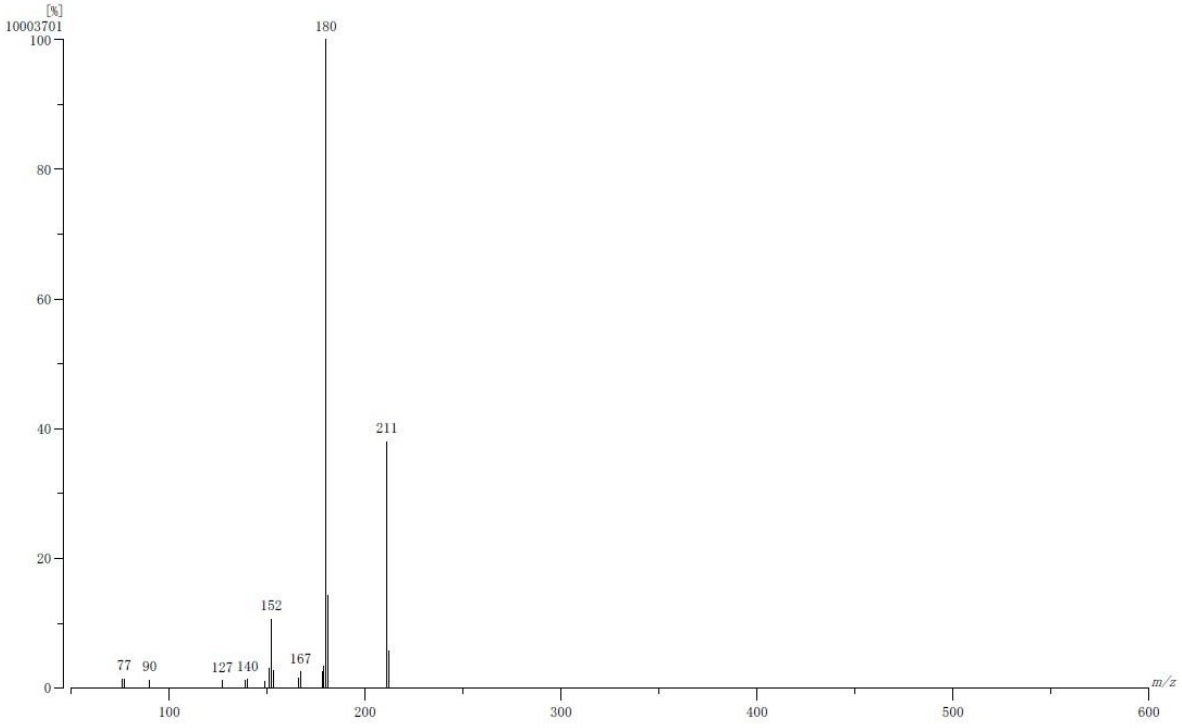

(a)

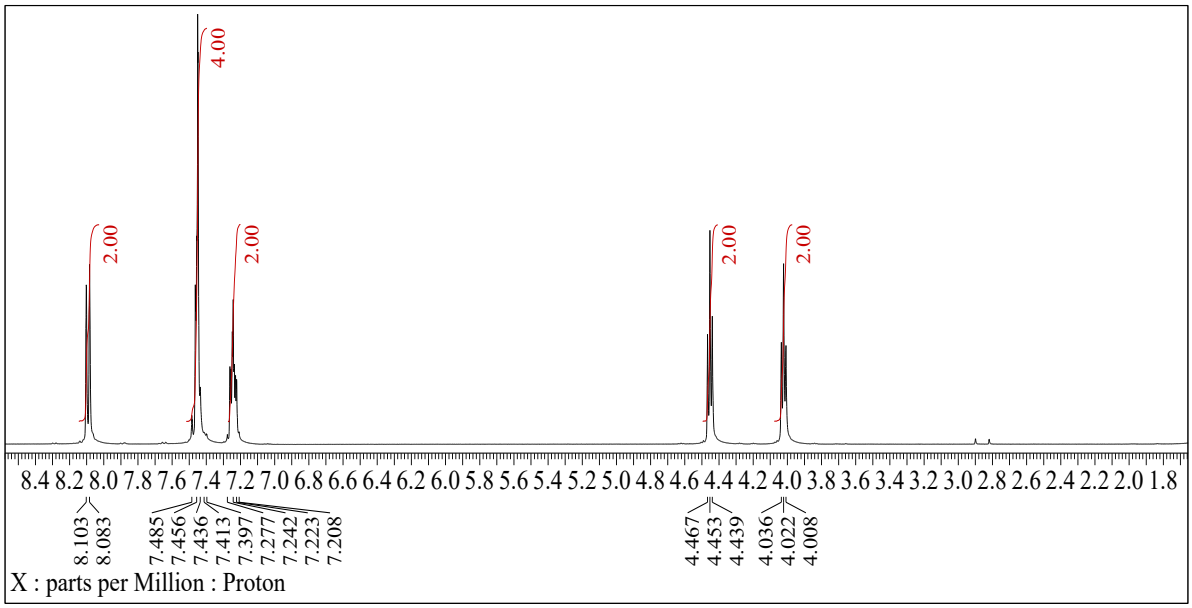

(b)

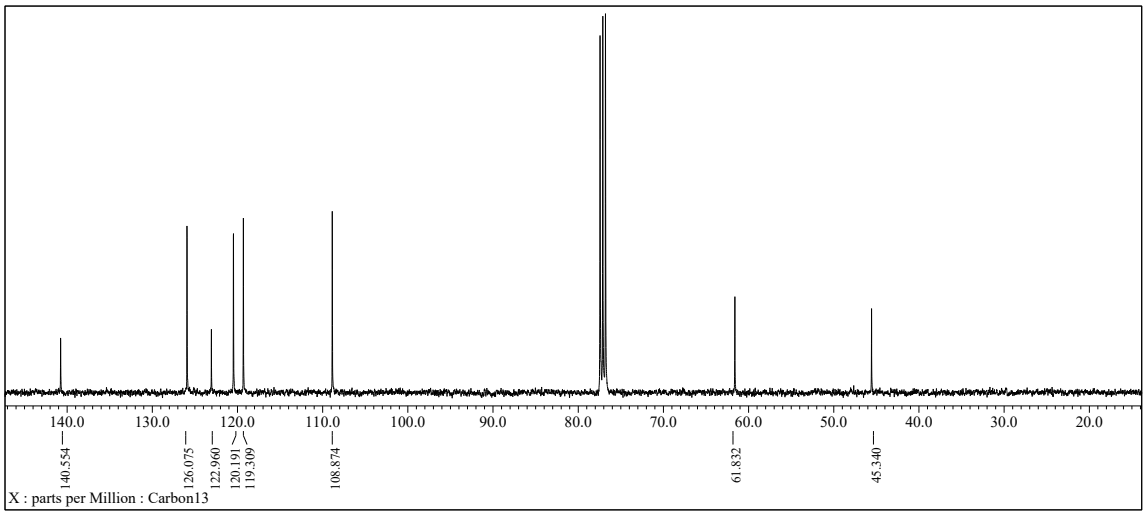

(c)

Figure 4. 1 a) EI-MS spectrum, b) ^{1}H NMR spectrum, and c) ^{13}C NMR spectrum of precursor 3.

4.1.4. Synthesis of Monomer (CA-NDI) (M_3)

A mixture of precursor (3) (4.49 g, 0.021 mol), DMAP (2.59 g, 0.021 mol), DCC (4.38 g, 0.021 mol), and precursor (2) (5.00 g, 0.021 mol) was mixed and chilled to -5 °C under a nitrogen atmosphere. Cooled THF (50 ml) was then rapidly injected into the reaction vessel. After 2 hours of stirring at this temperature initiated the formation of a white precipitate. The mixture underwent an additional 24 hours of stirring at -5 °C, following which the tetrahydrofuran was evaporated. The unrefined material underwent purification through column chromatography, employing a solvent blend of 20% THF and 80% Hex. Subsequently, it underwent drying in a vacuum oven at 45 °C for 24 hours. the material transformed into a white solid, yielding 43%. LRMS (EI+) computed for $C_{26}H_{24}N_2O_4$: m/z 428; computed m/z 428. ^{1}H NMR (400 MHz, $CDCl_3$) δ: 8.08 (d, J = 7.8 Hz, 2H), 7.41-7.47 (m, 4H), 7.25 (d, J = 7.8 Hz, 2H), 6.24 (s, 2H), 4.44-4.57 (m, 4H), 3.67 (d, J = 13.7 Hz, 2H), 3.21 (t, 2H), 2.48-2.53 (m, 4H), 1.44 (d, J = 10.1 Hz, 1H), 1.18 (d, J = 10.1 Hz, 1H) ppm. ^{13}C NMR (101 MHz, Chloroform-d) δ 177.37, 170.47, 140.47, 137.87, 126.08, 123.07, 120.36, 119.18, 108.31, 62.36, 47.58, 45.39, 42.43, 40.16, 34.10, 31.95 (Figure 4. 2).

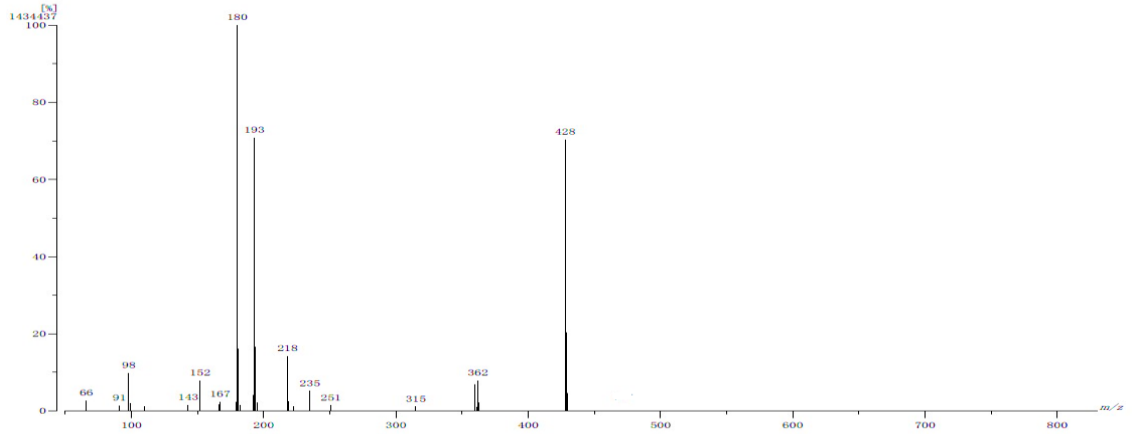

(a)

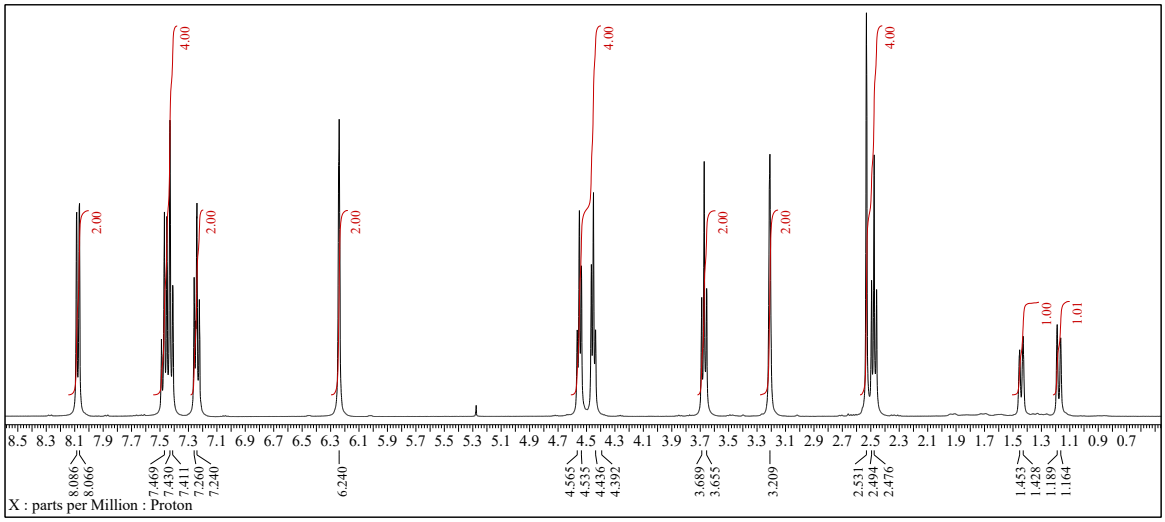

(b)

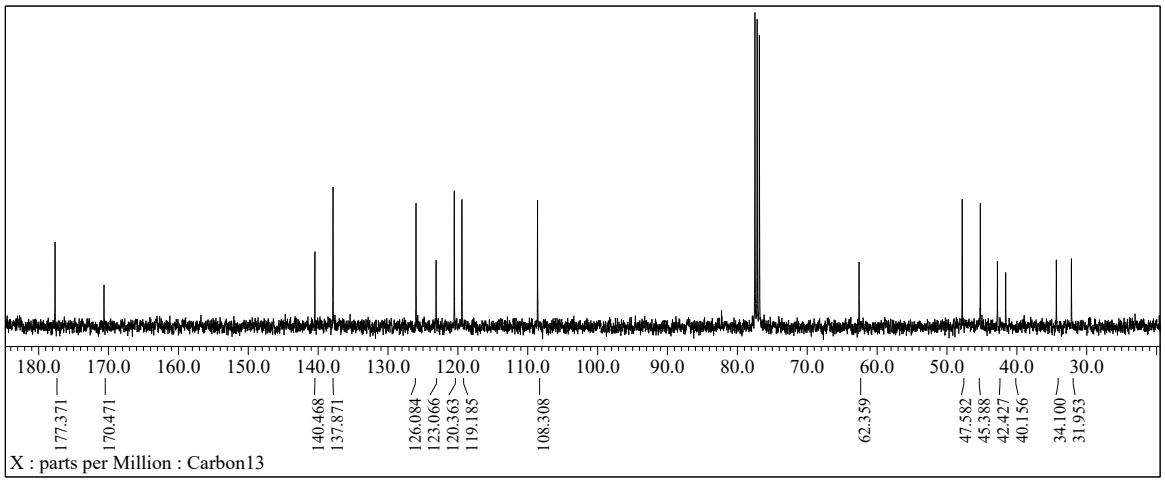

(c)

Figure 4. 2 a) EI-MS spectrum, b) ^{1}H NMR spectrum, and c) ^{13}C NMR spectrum of monomer (M_3).

4.2. Synthesis of Polymer poly(CA-NDI) P_3

The carbazole-pendant monomer CA-NDI (M_3) (0.50 g, 0.00116 mol) was moved to a Schlenk tube, which was then flushed with nitrogen. Subsequently, 10 ml of dry chloroform was injected using a syringe. After approximately 10 minutes of stirring to ensure the solid completely dissolved, the Grubbs 3rd generation initiator G3 (10.32 mg, 1.16 x 10^{-5} mol) dissolution in 2 ml of dry $CHCl_3$ was swiftly injected. The polymerization proceeded for 12 hours at room temperature to ensure full conversion of the monomer. To terminate the living polymerization, 4 ml of degassed EVE was injected. The quenching reaction was allowed to progress for one more hour, following which the polymer was isolated through multiple reprecipitations into stirred methanol, subsequent filtration, and drying in a vacuum oven at 45 °C for 24 hours, resulting in a pure polymer with a yield of 90%.^{1}H NMR (400MHz, $CDCl_3$) δ: 8.03 (d, J = 17.8 Hz, 2H), 7.08-7.41 (m, 9H), 5.45 (d, J = 81.9 Hz, 2H), 4.34-4.49 (m, 4H), 3.57 (d, J = 30.2 Hz, 2H), 2.37-3.11 (m, 6H), 2.02 (d, J = 71.8 Hz, 1H), 1.32 (d, J = 54.9 Hz, 1H) ppm (Figure 4. 3).

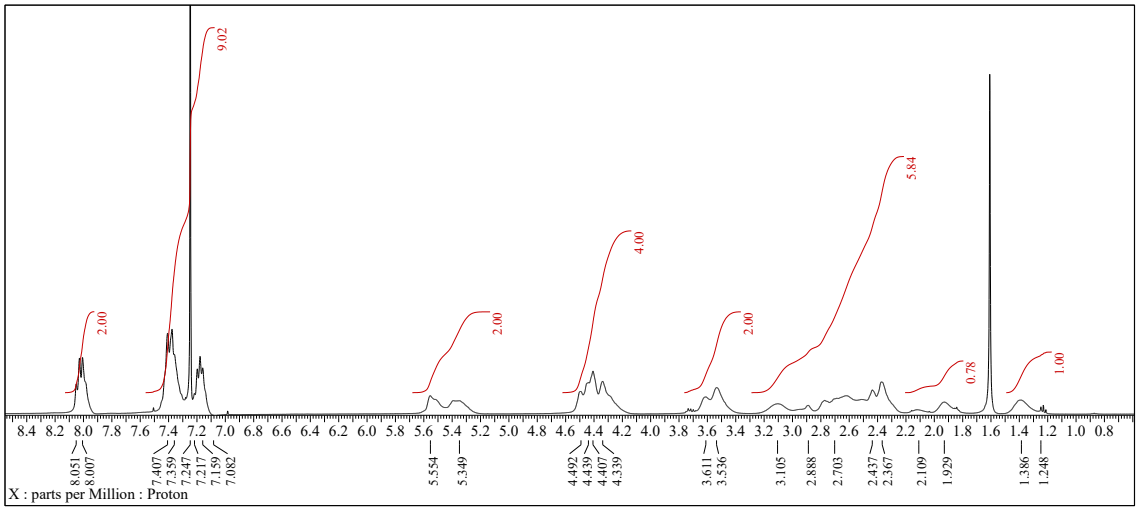

Figure 4. 3 ^{1}H NMR spectrum of polymer (P_3).

4.3.Results and Discussion

4.3.1.Monomer Synthesis and Characterization

Organic photorefractive materials have been known for several decades and are unique in that they can undergo a temporary change in their refractive index upon exposure to certain wavelengths of light. This phenomenon has been particularly useful in the development of holographic imaging. As in many areas of organic electronics, organic materials have been a research focus due to their tunability, and ease of processing

compared to inorganic alternatives. Non-conjugated polymers with pendant carbazole groups, such as poly(vinyl carbazole), have been extensively studying for their electronic properties. The ROMP technique is an excellent method to produce well-controlled homo-, block-, and random copolymers. For the preparation of non-conjugated materials, NDIs serve as excellent, easily functionalized monomers. Hence, the synthesis of carbazole-pendant NDI monomers is particularly valuable for integration into more intricate systems.

The synthesis of CA-NDI monomer (M_3) was achieved through a multi-step reaction, including the esterification of NDI carboxylic acid (NDI-COOH) and 2-carbazole-9-yl-ethanol (CA-OH). Initially, a Diels–Alder reaction between maleic anhydride and cyclopentadiene under high-temperature conditions yielded a mixture of endo- and exo-norbornene-5,6-dicarboxylic anhydride. This mixture underwent multiple crystallization steps to isolate the pure *exo*-isomer (*exo*-NDA), as endo-derivatives exhibit reduced reactivity due to steric hindrance around the olefin. Eliminating the endo isomer facilitates a cleaner polymerization profile for the final NDI monomer [81].

Next, exo-NDA was refluxed with β-alanine in dry chloroform for 24 hours, affording NDI-COOH as the first precursor for the esterification step. Meanwhile, (CA-OH), was synthesized through the alkylation of carbazole with 2-ethylene carbonate in dry DMF in the presence of sodium hydride as a reducing agent, forming the second precursor for esterification.

The final step involved a one-pot esterification reaction catalyzed by DMAP and DCC, a well-established method for N-protected amino acids. The reaction was conducted in THF, a suitable solvent for dissolving NDI-COOH and CA-OH. A DCC/DMAP solution was added dropwise over two hours at -5°C to minimize side product formation. Despite some dicyclic urea formation, indicating esterification progress, the reaction mixture gradually warmed to room temperature and stirred for 24 hours, with TLC monitoring to ensure complete reactant consumption. The dicyclic urea was filtered out, and the solvent was evaporated, yielding a white solid product. Column chromatography was used for purification, yielding the final CA-NDI monomer (M3).

The ^{1}H NMR spectrum of M_3 confirms the presence of 11 distinct proton environments. The carbazole peaks appear as two doublets and one multiplet at δ 8.08–7.25 ppm, indicative of the aromatic environment of the carbazole moiety. The two alkenic protons of the NDI monomer correspond to a prominent singlet at δ 6.24 ppm.

Furthermore, the multiple peaks at 4.57–4.44 ppm (J = 7.8 Hz) are characteristic of the NCH_2CH_2 methylene groups linked to the carbazole moiety. The peak at 3.67 ppm (J = 13.7 Hz) corresponds to the methylene hydrogens attached to the carbonyl ester group. The triplet peak at 3.21 ppm is characteristic of the NCH_2 methylene groups linked to the NDI moiety. The spectrum also shows a triplet of a doublet at 2.48–2.53 ppm, corresponding to the hydrogen ring-bridging environments. Signals below 2 ppm are attributed to the methylene hydrogens of the bicyclic molecule in the NDI moiety. the ^{13}C-NMR spectrum of the synthesized monomer which includes peaks at 177.37, 170.47, and 137.87 ppm which are attributed to two carbonyl-NDI groups, one carbonyl-ester group, and olefin carbon atoms, respectively. Low resolution (EI) mass spectrometry revealed a strong peak at 428 confirming the correct molecular composition of $C_{26}H_{24}N_2O_4$.

4.3.2. Polymer poly (CA-NDI) P_3 Synthesis and Characterization

The polymerization of the CA NDI monomer in its pure form occurred at room temperature for a duration of 12 hours under a nitrogen atmosphere. Previous experimentation suggested that achieving full polymerization of NDI monomers typically took place in around an hour when employing the Grubbs 1st generation initiator G1. The G3 initiator is recognized for demonstrating similar kinetics, displaying tolerance to bulky substituents, and leading to a cis-trans vinylene configuration. The prolonged reaction period of 12 hours was chosen to ensure complete consumption of the sizable and sterically hindered CA-NDI monomer (Scheme 4. 2). Additionally, at room temperature, occurrences of backbiting are believed to be minimal, resulting in a few disadvantages associated with an extended reaction time. The ^{1}H NMR spectrum of the poly (CA-NDI) P_3 can be observed in figure (Figure 4. 3), there are 12 proton environments, however, due to the broad nature of most peaks as can be expected from an NMR spectrum of a polymer it is difficult to assign precisely.

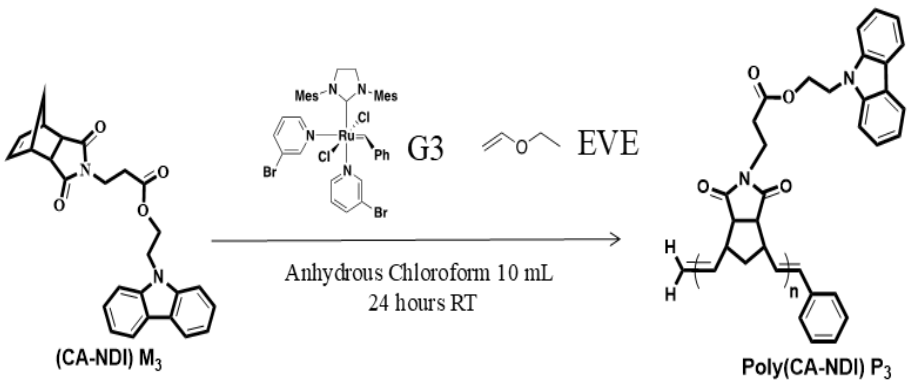

Scheme 4. 2 CA-NDI homopolymer P_3 using the G3 catalyst.

Peaks of notes include the broad but sharp multiplet at 8.03 - 7.08 ppm corresponding to the carbazole protons. The NDI alkenic protons are clearly visible as a broad doublet at 5.45 ppm. The doublet corresponds to both *cis* and *trans* vinylene linkages which are in an approximately 1:1 ratio as is expected from the G3 initiator.

The GPC analysis of poly (CA-NDI) (P_3) revealed a number-average molecular weight (M_n) of 26,820 g/mol with a narrow polydispersity index (PDI) of 1.11, confirming the well-controlled polymerization process at room temperature. A plot of differential molecular weight distribution (D.MWD) vs. log(M) is shown in (Figure 4. 4)

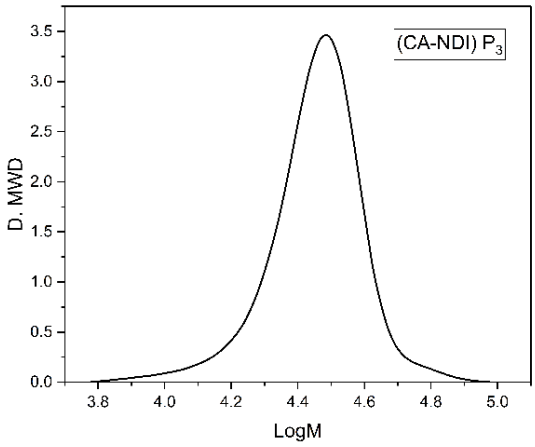

Figure 4. 4 Molecular weight distribution of polymer P_3.

(Figure 4. 5) shows the DSC measurement of the polymer, analysis revealed a Tg of 116.7 °C. This relatively low Tg may be attributed to the flexible linker group between the NDI unit and the carbazole. Shortening of this linker may allow the Tg to be raised, if the application so required.

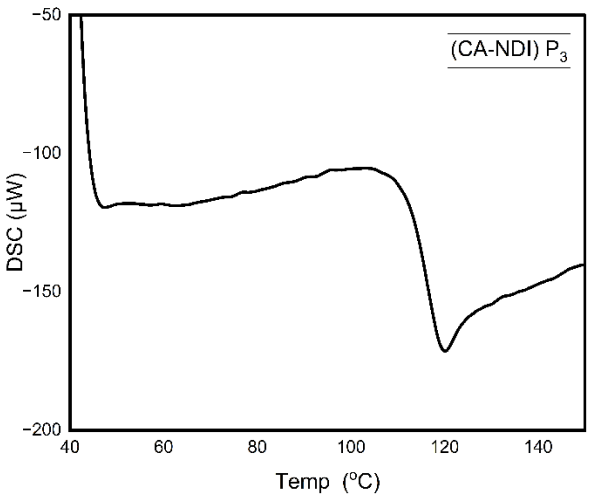

Figure 4. 5 DSC analysis of polymer P_3.

The thermal stability of the synthesized polymer **P3** was investigated through TGA under a nitrogen atmosphere at a heating rate of 10 °C/min. The results are presented in (Figure 4. 6). For **P3**, Thermogravimetric analysis (TGA) revealed an initial mass loss of approximately 2% at 168.4 °C, which is likely due to moisture uptake. Minor thermal degradation began just above 295 °C, with the primary decomposition temperature (T_{d1}) observed at around 422 °C, corresponding to a substantial weight loss of 88.8%. This initial degradation phase is primarily attributed to the breakdown of the ester bond linking the carbazole unit to the NDI moiety. This interpretation is consistent with the known thermal fragility of the ester group, which typically decompose at lower temperatures than the main polymer chain. As a result, the cleavage of these ester linkages precedes the degradation of the more stable polymer backbone. A second decomposition step (T_{d2}) occurred at approximately 534 °C, accompanied by a further mass loss of 95.4%. This high-temperature degradation is attributed to the decomposition of the robust polymer backbone structure, ultimately leading to the formation of minimal char residue. Overall, these findings indicate that the polymer exhibits excellent thermal stability, with a relatively low residual content, across different degrees of polymerization.

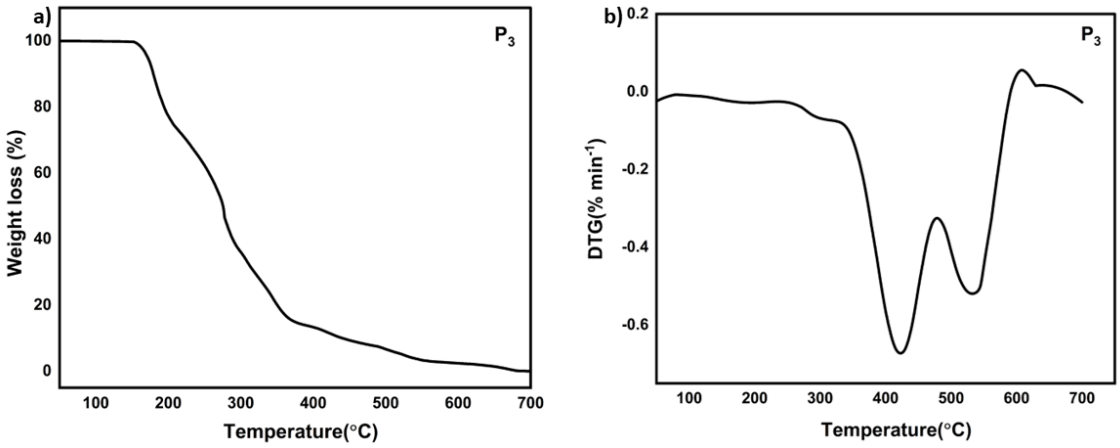

Figure 4. 6 a) TGA, and b) DTG curves for polymer P_3.

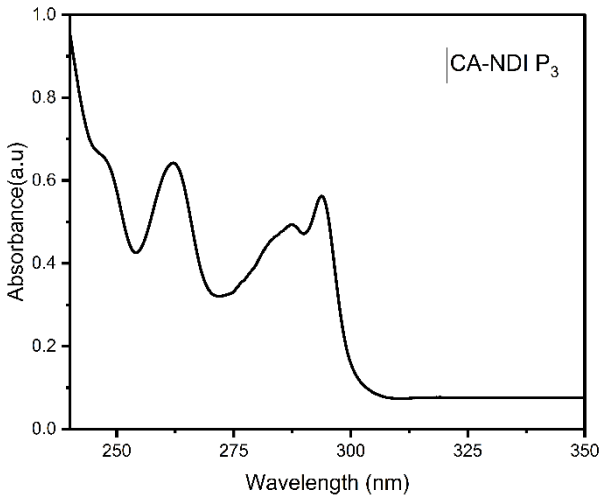

Figure 4. 7 UV-vis analysis of polymer P_3.

The UV-Vis absorption spectrum of poly CA-NDI (P_3) exhibited three main absorption peaks at 264 nm, 287.7 nm, and 293.8 nm, all attributed to the π–π* transitions of the carbazole moiety (Figure 4. 7). Notably, the spectrum does not show any n–π* transitions, indicating minimal electronic delocalization within the polymer. The overall absorption intensity is relatively weak, suggesting that the non-conjugated polymer backbone limits electronic interactions between the chromophores.

Second synthetic route for Synthesis of Admentyl-NDI monomer

4.4.Synthesis of Adamantly-NDI Monomer (AD-NDI) (M_4)

(Scheme 4. 3) illustrates the synthetic route employed to prepare the Adamantly functionalized AD-NDI monomer M_4. The process begins with the synthesis of an exo-norbornene-5,6-dicarboxylic anhydride precursor (5) through the reaction of maleic anhydride with dicyclopentadiene under high temperature conditions. This precursor then

reacted with a adamantylamine precursor under reflux, leading to the formation of a norbornene- Adamantly-amic acid (6).

In the subsequent step, the triethylamine is introduced into the norbornene- Adamantly-amic acid.

The Ad-NDI monomer is finalized through purification steps, including column chromatography and recrystallization, yielding off white solid product. Structural confirmation was achieved using NMR, MS.

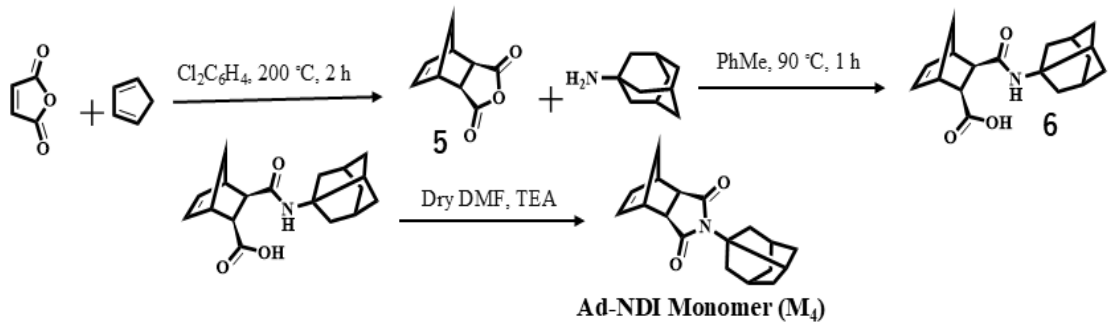

Scheme 4. 3 Synthesis Admentyl-NDI Monomer M_4.

4.4.1.Synthesis of *exo*-norbornene-5,6-dicarboxylic anhydride (*exo*-NDA) 5

Into a solution of maleic anhydride (90.00 g, 0.9178 mol) in *o*-dichlorobenzene (100 ml) at 200 ˚C, dicyclopentadiene (60.67 g, 0.4589 mol) was added slowly. The solution was heated for 2 hours at 200 ˚C, transferred into a beaker, and left to cool to room temperature gradually. To obtain the crystals of exo isomer, the formed precipitate was filtered, rinsed with *o*-dichlorobenzene, recrystallized three times, and dried in a vacuum oven at 50 ˚C for 12 hours to afford the white crystalline solid in 40% yield. EI-MS calculated for $C_9H_8O_3$ *m/z*: 164.16; Found: *m/z* 164. ^{1}H NMR (400 MHz, Chloroform-d) δ 6.38-6.24 (2H), 3.49-3.35 (2H), 3.05-2.90 (2H), 1.71-1.57 (1H), 1.46-1.34 (1H) ppm.^{13}C NMR (101 MHz, Chloroform-d) δ 171.80, 138.02, 48.85, 46.93, 44.19 ppm. (S4. 3)**.**

4.4.2.Synthesis of adamantly-amic acid 6

Adamantyl amine (10.13 g, 0.0670 mol) was added slowly to a heated solution of *exo*-NDA **3** (10.00 g, 0.0609 mol) in toluene (400 ml), then the reaction was continued under heating at 90 ˚C for 1 hour. After that, the solution was cooled slowly to room temperature, filtered off, washed with a little cold toluene, collected, and dried in a vacuum oven at 60 ˚C overnight to afford adamantly-amic acid as a white precipitate in a 95% yield. The sample was characterized by ^{1}H NMR (400 MHz, Chloroform-d) δ ^{1}H-NMR (400 MHz, Chloroform-d) δ 6.13 (s, 2H), 2.82 (s, 2H), 2.61 (s, 2H), 2.37 (d, J = 9.6 Hz, 2H), 2.16-

2.19 (m, 4H), 1.89 (d, J = 32.5 Hz, 6H), 1.55 (s, 6H), 1.14 (d, J = 8.2 Hz, 2H) ppm.^{13}C NMR (101 MHz, Chloroform-d) δ 175.17, 172.07, 138.43, 51.02, 47.16, 46.73, 45.09, 43.91, 41.31, 36.66, 29.33 ppm (S4. 4).

4.4.3.Synthesis of Ad-NDI Monomer (7) (M_4)

A mixture of Adamantly-amic acid **5** (15.00 g, 0.0475 mol) and triethylamine (7.21 g, 0.0713 mol) in dry DMF (100 ml) was heated at 120 ˚C for 3 hours under nitrogen and was stirred at room temperature for 12 hours followed by precipitation into the water to afford the crude product which filtered off, washed with excess water, and dried with an aspirator. The obtained off-white solid was recrystallized from hot ethanol with a minimum amount of THF to give a white crystalline solid Ad-NDI **M_1** that dried under vacuum at 50 ˚C for 12 hours in 78 % yield. EI-MS calculated for $C_{19}H_{23}NO_2$ *m/z*: 297.4; Found: *m/z* 297. ^{1}H NMR (400 MHz, Chloroform-d) δ: 6.27-6.17 (2H), 3.23-3.13 (2H), 2.49-2.41 (2H), 2.39-2.28 (6H), 2.17-2.01 (3H), 1.76-1.58 (6H), 1.46-1.18 (2H). ^{13}C NMR (101 MHz, Chloroform-d) δ 175.17, 171.71, 138.43, 51.02, 47.47, 46.73, 45.58, 44.01, 41.41, 36.23, 28.96 ppm (Figure 4. 8).

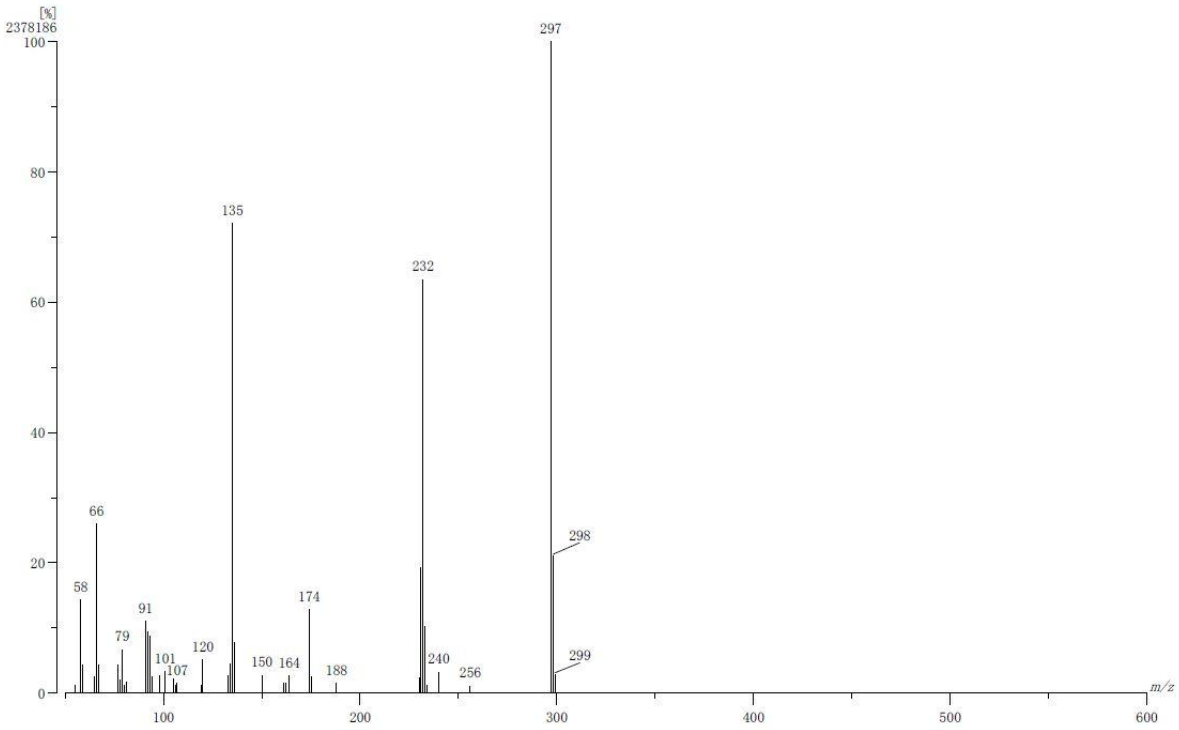

(a)

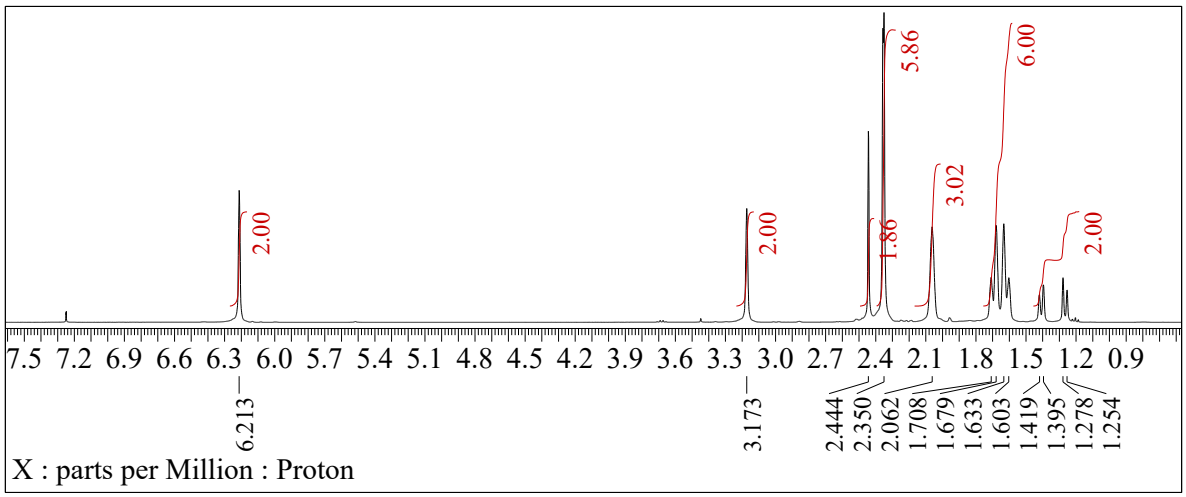

(b)

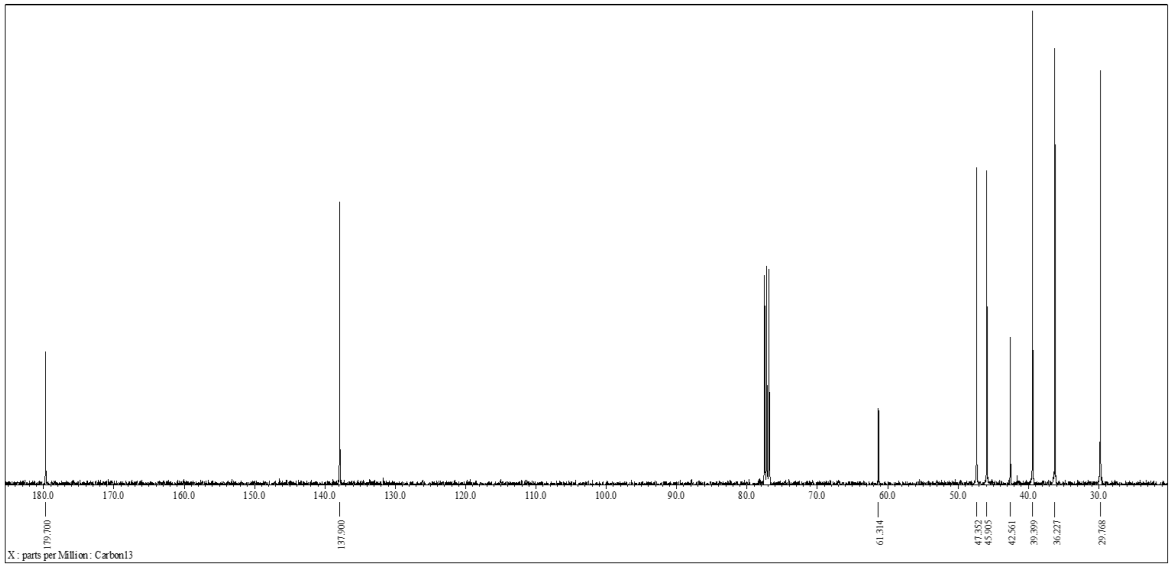

(c)

Figure 4. 8 a) EI-MS spectrum, b) ^{1}H NMR spectrum, and c) ^{13}C NMR spectrum of monomer (M_4).

4.5. Synthesis of poly (Ad-NDI) P_4

The polymerization process was carried out as follows: Under nitrogen atmosphere, the monomer **M_4** 1g was transferred to dry Schlenk tubes and degasses dry chloroform (10 ml) were injected into the mixture and stirred for 10 minutes at room temperature to complete dissolving of solids. After that, The Grubbs 3rd generation initiator was weighed into separate vials, dissolved in anhydrous chloroform (2 ml) under nitrogen, and quickly injected into the polymerization tube, and the mixture was stirred at room temperature for 24 hours. After this time, the polymerization was quenched by adding excess ethyl vinyl

ether to the mixture, which was allowed to proceed for an additional hour. The green-blue solution was precipitated into excess stirred methanol, filtered off, and dried in a vacuum oven for 12 hours at 40 ˚C (S4. 5).

4.6.Results and Discussion

4.6.1.Monomer Synthesis and Characterization

The adamantyl-functionalized NDI monomer (M_4), abbreviated as AD-NDI, was synthesized via a three-step synthetic route as shown in (Scheme 4. 3).

The first step involved the preparation of exo-norbornene-5,6-dicarboxylic anhydride (exo-NDA) through a Diels–Alder reaction between maleic anhydride and dicyclopentadiene in o-dichlorobenzene at 200 °C. The product was purified by recrystallization to yield a white crystalline solid. Characterization by EI-MS revealed a molecular ion peak at m/z 164, consistent with the expected mass. Key ^{1}H NMR signals included vinylic protons around δ 6.3 ppm and bridgehead methylene protons between δ 3.4–2.9 ppm. The ^{13}C NMR spectrum confirmed the presence of anhydride carbonyl and olefinic carbons.

In the second step, the condensation of exo-NDA with adamantylamine under reflux in toluene gave the intermediate adamantyl-amic acid in high yield. The product appeared as a white solid, and its structure was confirmed by the presence of characteristic peaks in the ^{1}H NMR spectrum, including the norbornene vinylic protons at δ 6.1 ppm and multiple signals for adamantyl protons below 2 ppm. The ^{13}C NMR supported successful formation of the amic acid intermediate 175,172 ppm corresponding to carbon atom of carboxylic group and amide group respectively, also found peak at 138 for olefinic carbons.

Finally, imidization was achieved by treating the amic acid with triethylamine in dry DMF at 120 °C under nitrogen, followed by overnight stirring at room temperature. The product was precipitated in water and recrystallized to afford the AD-NDI monomer (M_4) as a white crystalline solid in 78 % yield.

Structural confirmation was supported by EI-MS, which showed a molecular ion at m/z 297 (calcd for $C_{19}H_{23}NO_2$). In the ^{1}H NMR spectrum, the vinylic protons appeared at δ 6.2–6.3 ppm, and signals attributed to adamantyl and norbornene protons were observed between δ 3.2–1.2 ppm. The ^{13}C NMR showed disappear imide carbonyls peak at 172 ppm with strong peak at 179 ppm resonances consistent with anhydride carbonyl, olefinic carbons, and the aliphatic skeleton. These results confirm the successful synthesis of M4.

4.6.2.Polymer poly (Ad-NDI) P_4 Synthesis

The polymerization of the pure Ad-NDI monomer (M_4) was carried out at room temperature under a nitrogen atmosphere for 12 hours. Although earlier trials indicated that full conversion of NDI-based monomers could typically be achieved within an hour using the first-generation Grubbs catalyst (G1), the third-generation catalyst (G3) was selected for this study. G3 is known for exhibiting comparable polymerization kinetics, greater tolerance to bulky groups, and favoring the formation of polymers with cis/trans vinylene linkages. Given the significant steric hindrance of the Ad-NDI monomer, an extended reaction time of 12 hours was employed to ensure complete monomer consumption (Scheme 4. 4). Furthermore, conducting the reaction at room temperature minimizes backbiting side reactions, thus making the prolonged duration less problematic. The ^{1}H NMR spectrum of the resulting poly (Ad-NDI) P_4 is shown in (S4. 5). As is typical for polymers, the spectrum exhibits broad signals, which makes it challenging to assign individual proton environments with high precision.

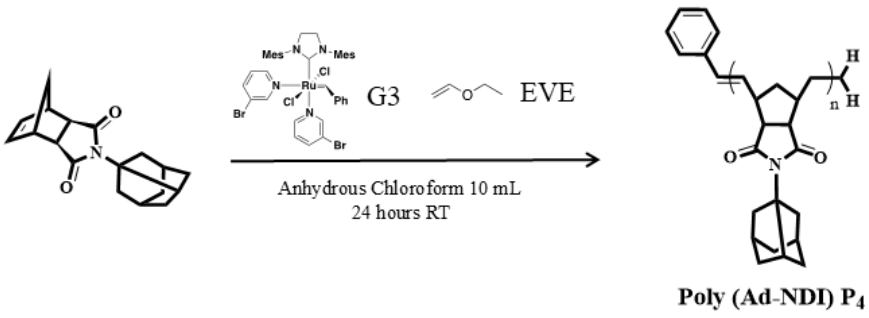

Scheme 4. 4 Ad-NDI homopolymer P_4 using the G3 catalyst.

Due to the living nature of polymerization, which is driven by the release of ring strain in the monomer, the molecular weight of the resulting polymer can be precisely controlled. To obtain a high-quality film suitable for use as an electro-optic (EO) host, poly (Ad-NDI) (P_4) was synthesized and characterized. GPC analysis revealed a number-average molecular weight (M_n) of 30,689 g/mol and a narrow polydispersity index (PDI) of 1.2, indicating a well-controlled polymerization process carried out at room temperature. The differential molecular weight distribution (D.MWD) as a function of log(M) is presented in (Figure 4. 9).

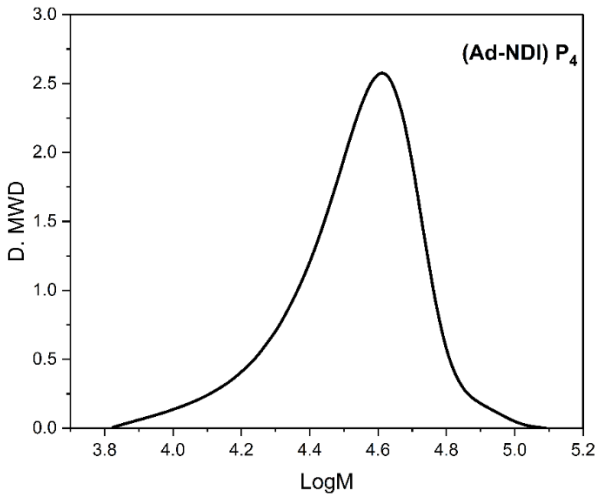

Figure 4. 9 Molecular weight distribution of polymer P_4.

One of the key thermal properties of polymeric materials is the glass transition temperature (Tg), which was evaluated for polymer (P_4) using differential scanning calorimetry (DSC). The measurement was conducted under a nitrogen atmosphere by heating the sample from 50 °C to 350 °C at a rate of 10 °C/min. As shown in (Figure 4. 10) the Tg of P_4 was observed at 210 °C, indicating good thermal stability. The thermal decomposition temperature (T_d) was assessed by TGA. Prior to analysis, the sample was preheated to 100 °C for 30 minutes to eliminate any residual volatile compounds. The Td, defined as the temperature corresponding to 10% weight loss, was found to be 385 °C. [82].

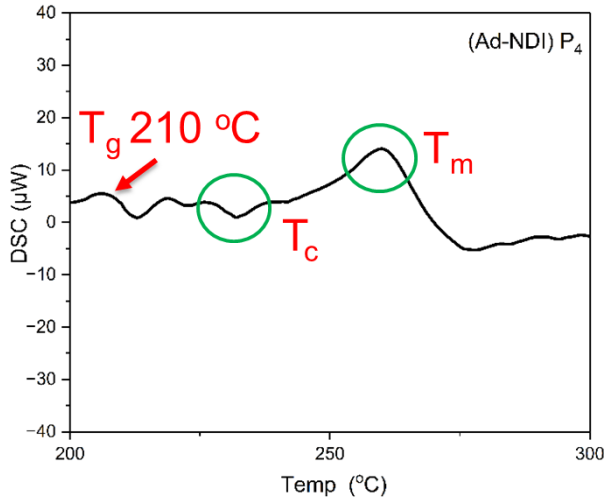

Figure 4. 10 DSC analysis of polymer P_4.

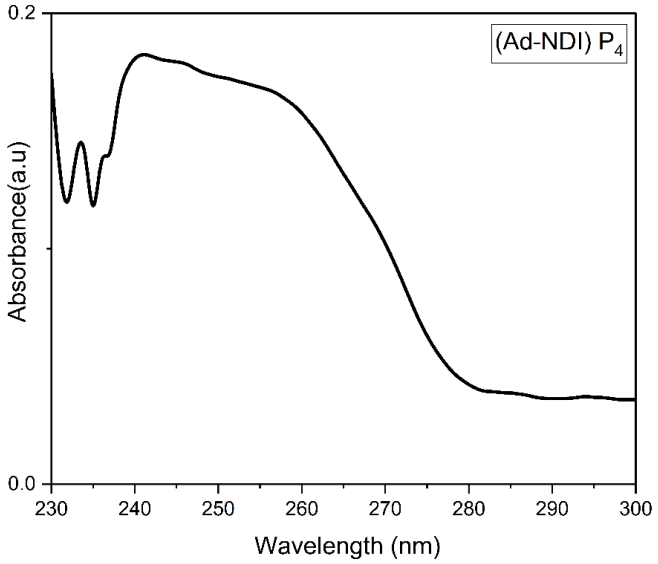

Figure 4. 11 UV-vis analysis of Poly (Ad-NDI) P_4

The UV–Vis absorption spectrum of poly (Ad-NDI) (P_4) was recorded in chloroform to evaluate its optical characteristics and identify the wavelength region where the polymer absorbs light. As shown in (Figure 4. 11), P_4 exhibits a broad absorption band extending from 241 nm to 259 nm, which is attributed to the π–π* transitions localized on the electron-deficient NDI units. The breadth of this band rather than a sharp peak suggests a distribution of conformations or slight aggregation even in dilute solution, although the bulky, non-conjugated adamantyl side chains themselves do not participate in these electronic transitions. This spectroscopic fingerprint confirms that the NDI chromophore dominates P_4 optical response.

Because P_4 absorption is confined to the UV region and does not extend into the visible unlike the carbazole-bearing CA-NDI (M_3) monomer—Chapter 5 focuses exclusively on M_3 for copolymerization with PPV derivatives, omitting M_4 from further optoelectronic studies.

4.7. Conclusion

This chapter successfully demonstrated the synthesis, characterization, and thermal and solubility analysis of two novel poly (NDI) derivatives functionalized with carbazole (CA-NDI) and adamantyl (AD-NDI) pendant groups. Both polymers were synthesized via ROMP using the Grubbs 3rd generation (G3) catalyst, yielding well-defined polymers with controlled molecular weights and narrow polydispersity indices PDI.

The carbazole-functionalized poly (NDI) (P_3) exhibited excellent solubility in common organic solvents, attributed to the bulky, planar carbazole moieties that disrupt polymer

chain packing. Thermal analysis revealed a Tg of 116.7 °C, while TGA demonstrated high thermal stability, with decomposition initiating at 295 °C and the primary degradation occurring at 422 °C. The UV-vis spectrum confirmed the presence of π–π* transitions associated with the carbazole chromophores, suggesting potential optoelectronic applications.

In contrast, the adamantyl-functionalized poly (NDI) (P_4) displayed enhanced rigidity due to the bulky, three-dimensional adamantyl groups, resulting in a higher Tg compared to P_3. GPC analysis confirmed a well-controlled polymerization, with a molecular weight (Mn) of 30,689 g/mol and a PDI of 1.2. The thermal stability of P_4 was also notable, with decomposition occurring at elevated temperatures, making it suitable for high-performance applications requiring thermal resistance. The comparative study of these two polymers highlights the significant influence of pendant group structure on polymer properties:

Carbazole pendants enhance solubility and introduce optoelectronic characteristics, making P_3 suitable for organic electronics and photorefractive materials.

Adamantyl pendants improve thermal stability and rigidity, positioning P_4 as a candidate for high-temperature applications. Overall, this work provides valuable insights into the structure-property relationships of functionalized poly (NDI derivatives, demonstrating their potential in advanced material applications, including organic semiconductors, optoelectronic devices, and high-performance polymers. Future studies could explore copolymerization strategies to combine the beneficial properties of both pendant groups or investigate their performance in device applications.

Chapter 5

ROMP of *p*-Phenylenevinylene and Norbornene-Dicarboximide Copolymers: Toward Enhanced Thermal Stability

In this chapter we synthesized random copolymers based on PPVs derivatives and NDI using ROMP technique with Grubbs 2nd generation catalyst (G2). The copolymerization of CA-NDI and PPV derivatives was aimed at enhancing the thermal stability of the resulting materials, which hold promise for organic electronic and electro-optic device applications. The UV-Vis spectroscopy indicated absorption maxima of 457 nm for **P_5**, and 449 nm for **P_6**, while the optical band gaps ranged from 2.32 eV to 2.42 eV. Photoluminescence (PL) studies revealed emission peaks of 536 nm for **P_5**, and 526 nm for **P_6**. CV measurements revealed electrochemical band gaps of 2.33 eV for **P_5**, and 2.34 eV for **P_6**, closely aligning with optical measurements. Thermal stability was evaluated by thermogravimetric analysis (TGA), which demonstrated high decomposition temperatures for both copolymers, ranging from 299.5 °C to 421.7 °C. These results demonstrate that incorporating CA-NDI enhances the thermal stability of PPV derivatives.

Two notable materials in this field are NDI) and poly (*p*-phenylene vinylene) (PPVs). NDIs are highly valued in materials science due to their exceptional thermal stability, optical transparency, and versatile functionalization capabilities[83–86]. These polymers can be easily modified to incorporate various functional groups, enhancing their applicability in different fields such as electro-optics technologies, and coatings[87–89]. NDIs exhibit excellent film-forming abilities, making them ideal for creating uniform, defect-free films necessary for high-performance optical and electronic devices. Additionally, their elevated glass transition and thermal decomposition temperatures ensure long-term stability and durability in demanding applications[90,91].

PPVs are renowned for their outstanding semiconducting properties, making them essential for use in organic electronic devices. PPVs have a conjugated backbone that allows for efficient charge transport, which is crucial for electronic applications[92–95]. They also possess unique optical properties, such as a localized band gap within the visible region, making them suitable for light emission and sensing applications[96–98]. The ability to tailor their electronic and optical properties through chemical modifications further enhances their versatility and utility in advanced material applications[99–104].

Combining NDIs and PPVs through random copolymerization can create materials that merge the best features of both. Using ROMP with the Grubbs catalyst is a powerful way to synthesize these random copolymers[105]. ROMP is highly efficient and can polymerize a wide range of monomers under mild conditions[106,107,116,108–115], making it a versatile tool in polymer chemistry[117]. The Grubbs catalyst, a ruthenium-based compound, is particularly effective in initiating and controlling the polymerization

process, ensuring high yields and uniform polymer structures[118]. This method is especially advantageous for creating random copolymers, as it allows for the incorporation of different monomer units in a controlled manner, resulting in materials with customized properties suited for particular applications [31,119].

In this work, we synthesized random copolymers Carbazole NDI (CA-NDI) / 2,5-dioctyloxy-*p*-phenylenevinylene (DO-PPV) (**P_5**) and CA-NDI / EHM-PPV (**P_6**) using ROMP with the G2. These copolymers are expected to demonstrate enhanced thermal stability, which is a key feature of PPVs, while also incorporating the functional advantages of NDIs. This chapter provides insights into the synthesis and characterization of these NDI-PPV-based copolymers, which represent a promising class of materials for next-generation organic electronics.

5.1.Synthesis of poly CA-NDI / DO-PPV Random Copolymer (P_5).

The two monomers, CA-NDI (M_3) (85 mg, 0.2 mmol) and DO-PCPD (M_1) (92 mg, 0.2 mmol), were combined in 2 ml of dry DCE and placed in a dry Carousell tube in a nitrogen atmosphere. The mixture was stirred for 10 minutes at room temperature to achieve complete dissolution. A solution of the G2 (0.43 mg) was prepared in 0.4 ml of anhydrous DCE and stirred for at least 10 minutes. This initiator solution was then added to the monomer solution, and the mixture was heated at 60 °C to facilitate polymerization for 24 hours. The reaction was monitored by TLC until all monomers were consumed. After cooling to room temperature, excess EVE (2 ml) was introduced to halt the reaction. Following an additional 2 hours of stirring at room temperature, the mixtures were concentrated under reduced pressure. The crude products were then re-dissolved in DCM and precipitated into methanol to remove ruthenium complexes. The final polymer was obtained with a yield of 94%.

5.2.Synthesis of poly CA-NDI / EHM-PPV Random Copolymer (P_6).

The two monomers, CA-NDI (M_3) (24 mg, 0.055 mmol) and EHM-PCPD (M_2) (20 mg, 0.055 mmol), were dissolved in 2 ml of anhydrous DCE and transferred to a dry Carousell tube under a nitrogen atmosphere. The mixture was stirred at room temperature for 10 minutes to ensure complete dissolution. A solution of the G2 generation catalyst (0.43 mg) was prepared in 0.4 ml of dry DCE and stirred for at least 10 minutes. This initiator solution was then added to the monomer mixture, and the polymerization reaction was conducted at 60 °C for 24 hours. The progress of the reaction was monitored by TLC. After the monomers were completely consumed, the reaction mixture was cooled to room

temperature, and an excess of EVE (2 ml) was added to terminate the polymerization. The mixture was stirred for an additional 2 hours at room temperature before being concentrated under reduced pressure. The crude products were re-dissolved in DCM and precipitated into methanol to eliminate any ruthenium complexes. The resulting polymer was obtained with a yield of 95%.

5.3.Results and discussion.

5.3.1. The structural characterization of the synthesized polymers (P_5, P_6) by ROMP

(**P_5** and **P_6**) were synthesized through ROMP of the individual monomers (**M_1**, **M_2** and **M_3)** using the G2 initiator in anhydrous DCE at 60 °C. The initial monomers to initiator ratio are 20:1, with an equal molar ratio set to be a random distribution of resulting copolymers (Scheme 5. 1). Once the monomers were fully reacted, the mixtures were terminated by the addition of an excess of EVE. The resulting crude polymers, **P_5** and **P_6**, were purified simply by precipitating into methanol.

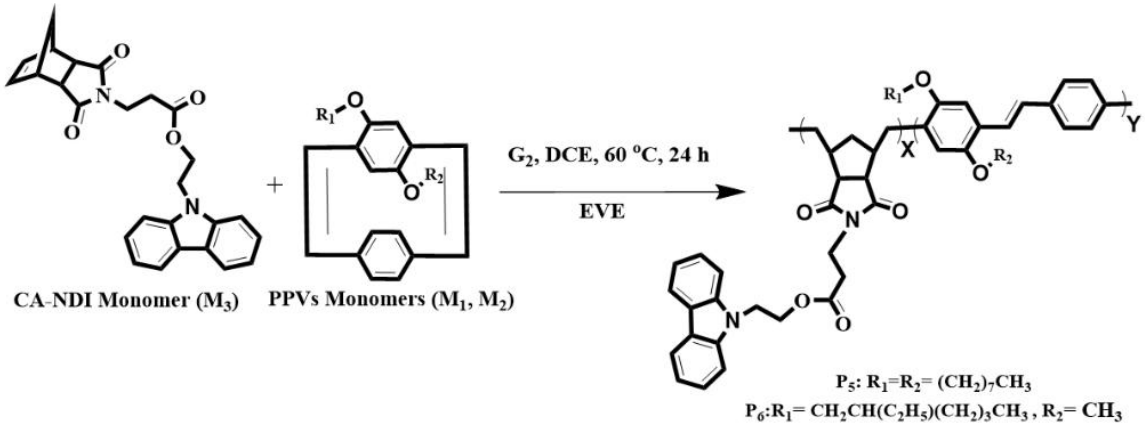

Scheme 5. 1 CA-NDI / PPVs Random copolymer using the G2 catalyst.

GPC analysis was performed using THF as the eluent to determine the molecular weight and distribution of the synthesized polymers **P_5**, and **P_6** shown in (Scheme 5. 1). random copolymer **P_5** had an *Mn* of 16.67 kDa and a PDI of 1.95, while random copolymer **P_6**, showed an *Mn* of 40.33 kDa and a PDI of 2.65.

All synthesized polymers exhibited monomodal molecular weight distributions and relatively low polydispersity indices (PDIs), suggesting effective control over chain growth and a high efficiency of chain transfer by the Grubbs initiator during the polymerization process. The copolymers **P_5** and **P_6** contained NDI moieties, which possess higher ring strain, resulting in faster polymerization rates but relatively broader PDIs due to less control over chain growth (Figure 5. 1).

Table 5. 1 GPC data for synthesized polymers (P_5 &P_6)

Polymer Samples	GPC data purified				Yield
	$M_{n(calc.)}$ (KDa)	$M_{n(obs.)}$ (KDa)	$M_{w(obs.)}$ (KDa)	PDI (M_w/M_n)	%
P_5	9.32	14.67	38.95	1.95	94
P_6	7.34	40.33	78.56	2.65	95

The narrow molecular weight distributions observed with THF as the eluent reflect efficient control over polymerization, although a slight broadening of distributions was noted with increasing monomer conversion.

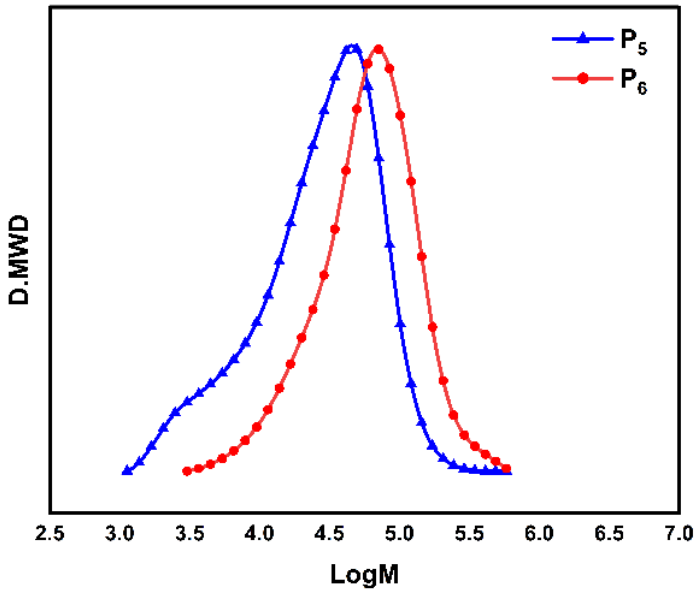

Figure 5. 1 Molecular weight distribution of polymers P_5, P_6 (GPC in THF).

This highlights the robustness of ROMP in achieving controlled polymer structures even under complex conditions. Overall, these results underscore the advantages of using ROMP with G2, such as precise control over PDI, efficient chain growth, and high-yield production of well-defined polymers.

5.3.2. Characterization of the synthesized polymers by ^{1}H NMR Spectroscopy

The ^{1}H NMR spectra of the synthesized polymers **P_5**, **P_6** recorded in $CDCl_3$, are shown in (Figure 5. 2), (Figure 5. 3) respectively. The *trans-vinylene* and other aromatic protons are observed at chemical shifts above 7.00 ppm. A broad peak at 3.35 ppm appears in all polymers, corresponding to the methylene protons and methyl groups attached to oxygen

atoms. Alkyl chain protons resonate at chemical shifts below 2.00 ppm. peaks are seen for the carbazole and NDI units. A distinct peak around 8.00 ppm is assigned to the aromatic protons of the carbazole moiety. The NDI alkenic protons are observed as a triplet between 5.56 and 5.38 ppm, while the triplet at 4.4 ppm is attributed to the carbazole linking protons. The NDI linking protons resonate at 3.97 ppm. Based on the ^{1}H NMR data, we can conclude that the copolymerization reaction proceeded successfully.

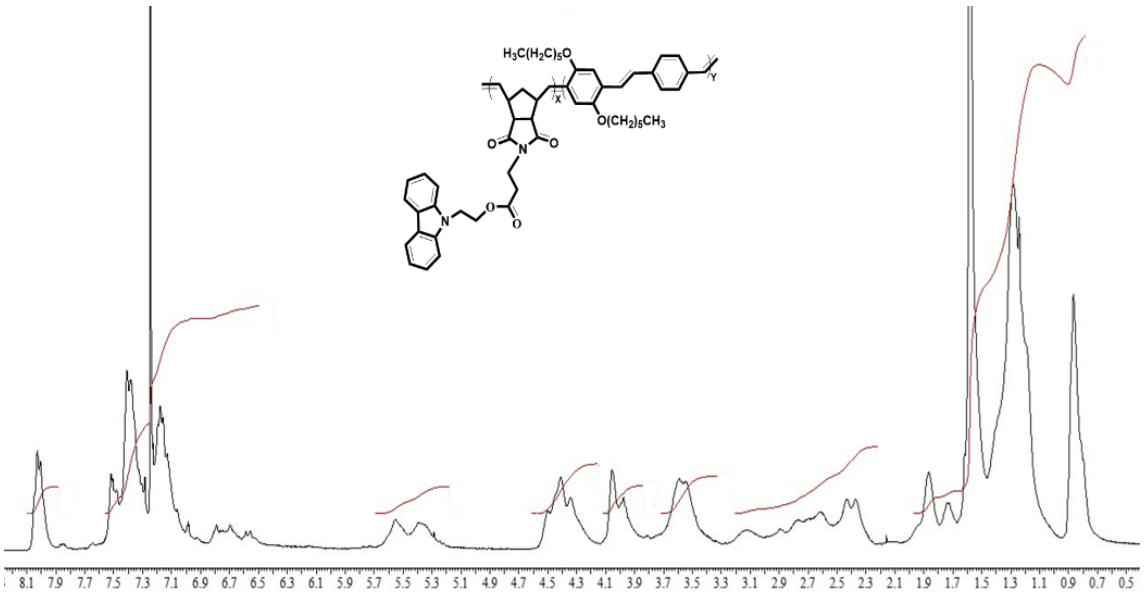

Figure 5. 2 ^{1}H NMR spectrum of P_5.

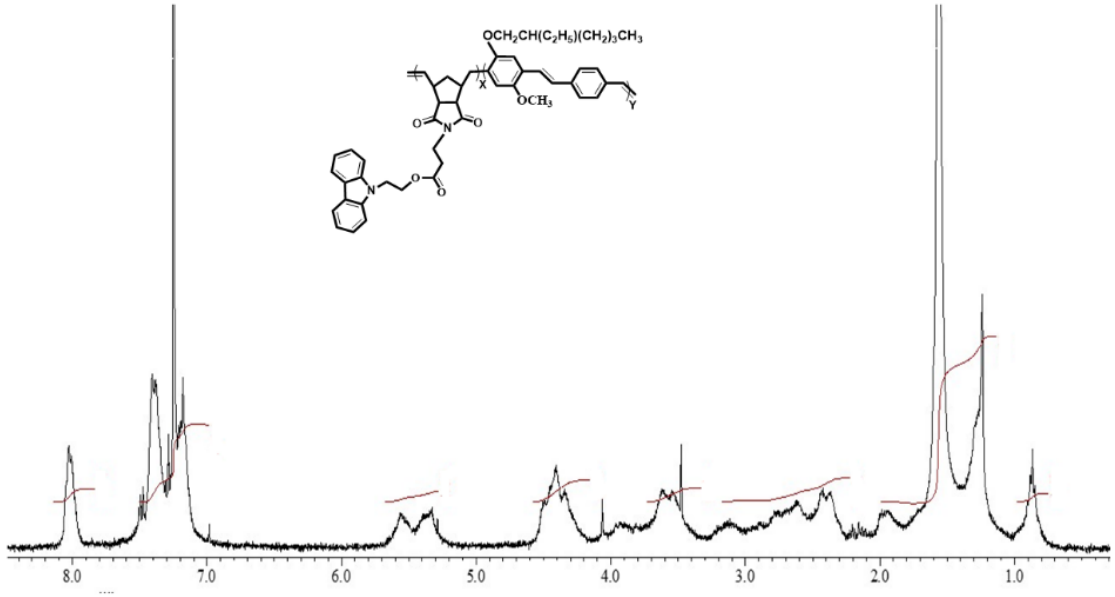

Figure 5. 3 ^{1}H NMR spectrum of P_6.

5.3.3. Optical properties of the polymers (P_5 &P_6)

The UV-Vis absorption and fluorescence emission spectra of the synthesized copolymers **P_5** and **P_6** were analyzed in three solvents—chlorobenzene (C_6H_5Cl), tetrahydrofuran (THF), and dichloromethane (DCM) to assess their optical properties and solvent-dependent behavior. The measurements were performed at a polymer concentration of 5×10^{-8} M, and the results are summarized in (Table 5. 2).

Table 5. 2 Physical properties of the synthesized polymers (P_5 &P_6)

Polymer No.	solvent	UV-Vis Absorption			Fluorescence Emission
		$\lambda_{(max)}$, nm	$\lambda_{(onset)}$, nm	E_g^{op} (eV)	$\lambda_{(em)}$, nm
P_5	C_6H_5Cl	457	527.2	2.35	536
	THF	464	520.0	2.38	529
	DCM	457	519.1	2.39	534
P_6	C_6H_5Cl	449	512.0	2.42	526
	THF	449	509.6	2.43	524
	DCM	456	511.5	2.42	523

The absorption of the random copolymers **P_5** and **P_6** display characteristic features that reflect the contributions of their respective monomeric units. For **P_5**, the absorption spectrum shows peaks at 457 nm and 319 nm, with a shoulder at 332 nm, indicating the influence of the PPV and carbazole moieties (Figure 5. 4). In comparison, **P_6** exhibits absorption peaks at 449 nm and 318 nm, along with a shoulder at 333 nm (Figure 5. 5). The redshift observed in **P_5** relative to **P_6** is attributed to the electron-donating effect of the dioctyloxy-substituted phenylenevinylene units, which lower the electronic bandgap and enhance conjugation.

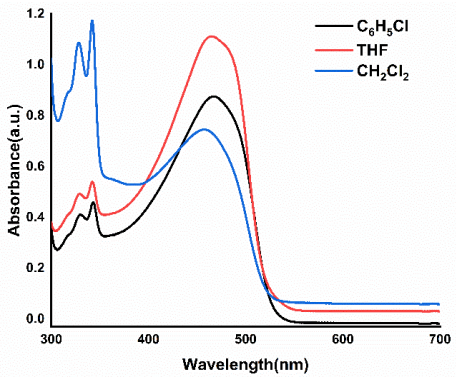

Figure 5. 4 UV of (P_5) In C_6H_5Cl & THF & DCM.

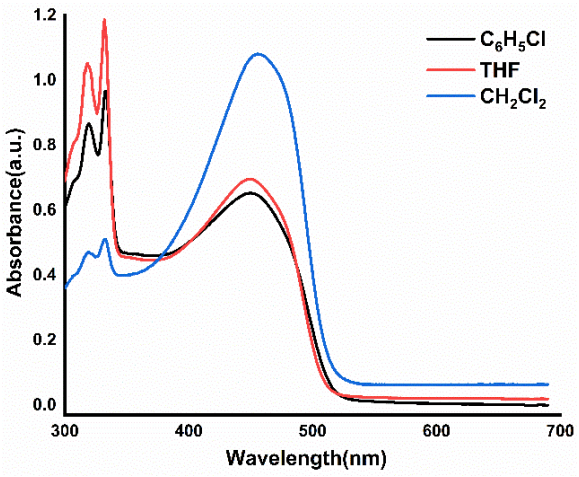

Figure 5. 5 UV of (P_6) In C_6H_5Cl & THF & DCM.

The absorption maxima (λ_{max}) for P_5 and P_6 remain relatively consistent across the three solvents, with minimal variation, suggesting limited solvent polarity effects on the electronic transitions of the polymers.

The PL spectra of P_5 and P_6 further illustrates their optoelectronic behavior. In chlorobenzene, the PL maximum of P_5 appears at 536 nm, while P_6 shows a slightly blue-shifted emission peak at 526 nm. This redshift in P_5 can be linked to the lower energy gap of the PPV backbone compared to the carbazole-NDI units in P_6. When excited at 360 nm, the random copolymers exhibit consistent emission trends in all solvents, with fluorescence peaks for P_5 observed at 536 nm (C_6H_5Cl), 529 nm (THF), and 534 nm (DCM) (Figure 5. 6), and for P_6 at 526 nm (C_6H_5Cl), 524 nm (THF), and 523 nm (DCM) (Figure 5. 7).

The solvent-dependent optical properties of P_5 and P_6 reveal negligible variations in both absorption and fluorescence emission spectra across the three solvents.

The solvent-dependent optical properties of P_5 and P_6 reveal negligible variations in both absorption and fluorescence emission spectra across the three solvents. The optical bandgaps (E_g^{op}), calculated from the onset of absorption (λ_{onset}), also remain consistent, with values ranging from 2.32 eV to 2.43 eV. This stability indicates that the copolymers' electronic structure is not significantly affected by solvent polarity, highlighting their robust optoelectronic performance.

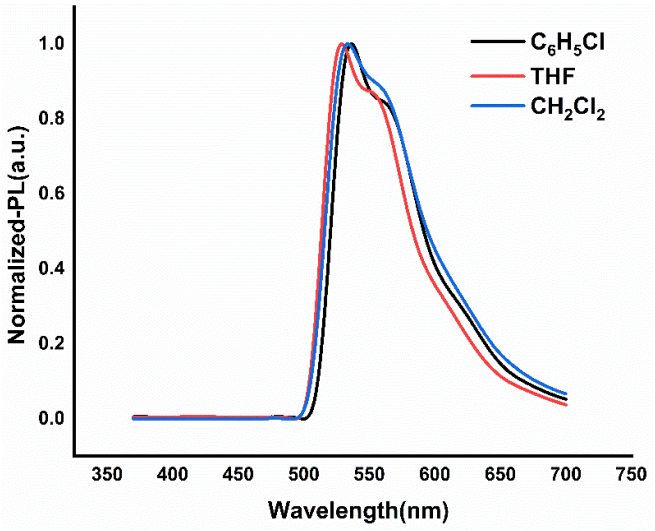

Figure 5. 6 PL of (P_5) In C_6H_5Cl &THF&DCM.

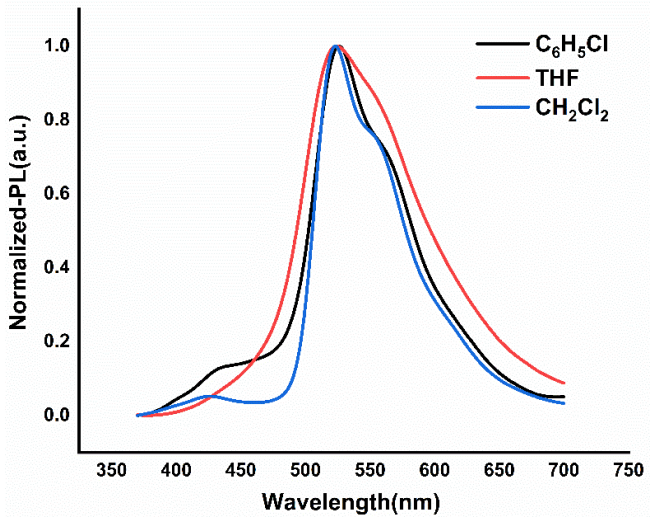

Figure 5. 7 PL of (P_6) In C_6H_5Cl &THF&DCM.

5.3.4.Electrochemical properties of the polymers (P_5 & P_6)

The electrochemical properties of polymers P_5 and P_6 were evaluated using cyclic voltammetry (CV), with results shown in (Figure 5. 8). and summarized in (Table 5. 3). The HOMO and LUMO energy levels for these polymers were derived from their oxidation and reduction onsets, leading to electrochemical band gaps of 2.33 eV for P_5, and 2.34 eV for P_6. These values align closely with those obtained from optical measurements, indicating that incorporating CA-NDI in copolymers P_5 and P_6 minimally affects the electronic structure of the PPV backbone.

Table 5. 3 Electrochemical properties of the polymers (P_5 &P_6)

Polymers	$[O]_{onset}$ (V)	$[R]_{onset}$ (V)	HOMO (eV)	LUMO (eV)	E_g (eV)
P_5	0.89	-1.44	5.69	3.36	2.33
P_6	0.93	- 1.41	5.73	3.39	2.34

This consistency in band gap confirms that our approach enhances the thermal stability of PPV derivatives without compromising their electronic properties, underscoring the potential of these modified materials in optoelectronic applications where both stability and electronic functionality are essential.

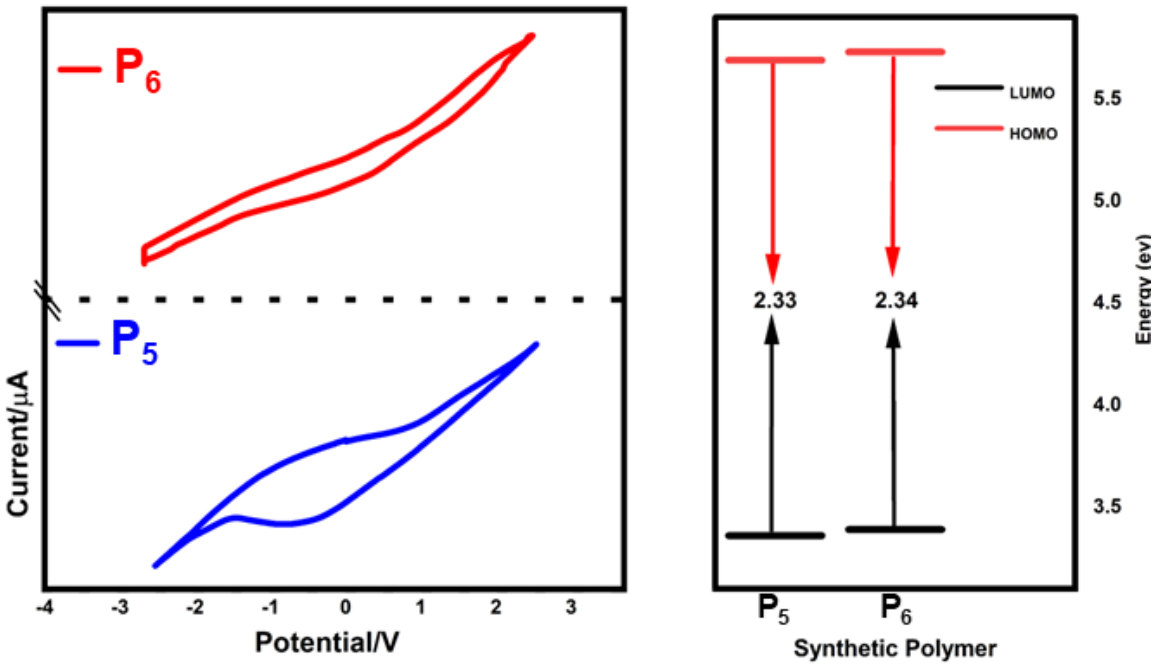

Figure 5. 8 CV curves for P_5–P_6 and band gaps.

5.3.5. Thermal behavior of the polymers (P_5&P_6)

The thermal stability of the synthesized polymers P_5 and P_6 was investigated through thermogravimetric analysis (TGA) under a nitrogen atmosphere at a heating rate of 10 °C/min. The results are presented in (Table 5. 4) and (Figure 5. 9), highlighting the thermal behavior of these polymers. copolymers P_5 and P_6, incorporating CA-NDI, were analyzed to assess the impact of copolymerization on the thermal stability of PPVs derivatives.

Table 5. 4 TGA values of the synthesized polymers (P_5&P_6)

Polymer Samples	T_{d1} (°C)	Weight Loss (%)	T_{d2} (°C)	Weight Loss (%)	Residue (%)
P_5	258.7	55.5	418.9	40.5	4
P_6	296.7	71.3	421.7	18.3	10.4

The copolymers P_5 and P_6, synthesized by incorporating CA-NDI into the PPV backbone, show improved thermal stability. The TGA results reveal two stages of decomposition. P_5 undergoes its first decomposition T_{d1} at 258.7 °C, with a 55.5 % weight loss, followed by a second stage at 418.9 °C, resulting in a further 40.5 % mass loss. The high char yield of 99.3% suggests an enhancement in backbone stability relative to P_1, P_2 in third chapter.

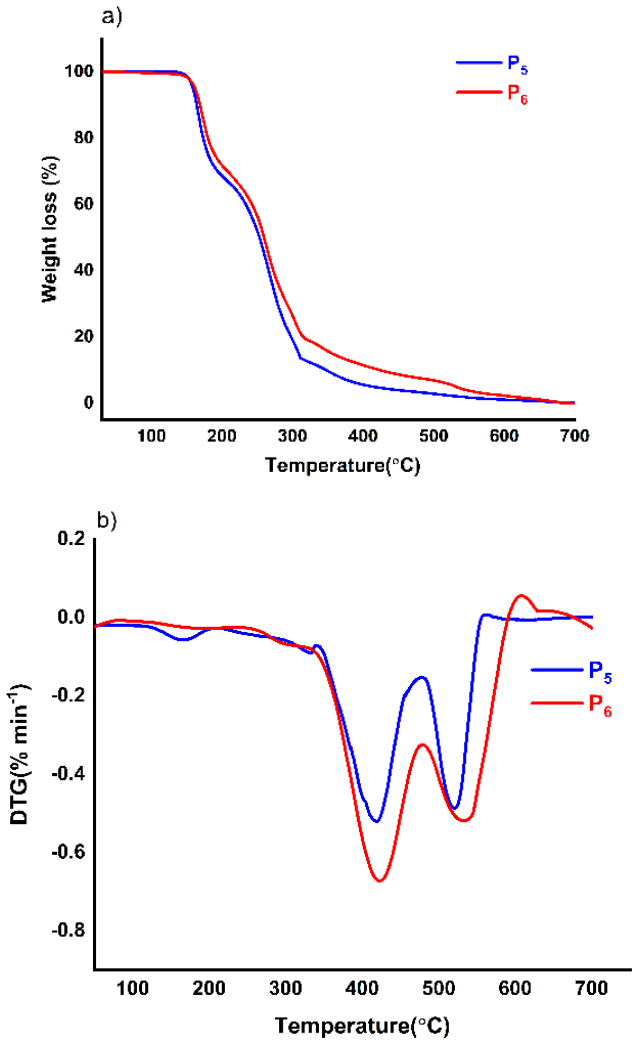

Figure 5. 9 a) TGA, and b) DTG curves for (P_5 &P_6).

P_6 displays even greater thermal resistance, with the first decomposition occurring at 296.7 °C and a weight loss of 71.3%, followed by a second degradation at 421.7 °C with an 18.3 % mass loss. A final char yield of 98.5 % further confirms the positive effect of CA-NDI copolymerization on thermal stability.

The high decomposition temperatures of P_5 and P_6 offer a notable advantage for optoelectronic devices operating at elevated temperatures, providing improved morphological and mechanical stability. The incorporation of CA-NDI into PPV derivatives has enhanced thermal stability, especially for P_5 and P_6, making them more suitable for applications requiring higher thermal resistance[38,39].

5.4.Conclusion

This investigation effectively achieved the synthesis and characterization of copolymers P_5, P_6. The implementation of ROMP enabled the production of polymers with targeted molecular weights and low polydispersity indices, illustrating the precision of the polymerization process.

The optical evaluations indicated that the incorporation of NDI into the PPV structure significantly alters the band gap, which ranged from 2.32 eV to 2.42 eV. The UV-Vis spectra revealed unique absorption profiles, with maximum absorption peaks at 457 nm for P_5, and 449 nm for P_6. The findings from cyclic voltammetry reinforced the favorable electronic characteristics of the NDI-PPV copolymers, indicating their potential for use in organic electronic devices, particularly OLEDs and OPVs. Furthermore, TGA confirmed the thermal stability of these polymers, showing decomposition temperatures between 418.9 °C and 421.7 °C for P_5 and P_6 respectively.

This research provides essential insights into the influence of molecular structural modifications on the properties of conjugated polymers, paving the way for the development of more sophisticated optoelectronic materials. Future research should focus on refining the synthesis techniques and investigating additional functionalization methods to enhance the practical use of these polymers.

Chapter 6

Synthesis, Optimization, and Copolymerization of Donor and Acceptor Polymers

This chapter presents the synthesis, characterization, and photophysical analysis of three categories of polymers designed for potential thermally activated delayed fluorescence (TADF) applications. The first category involves the synthesis of poly(carbazole hexyl-NDI) (P_7) using the CAH-NDI monomer (M_5), where the carbazole unit, attached via an alkyl linker, acts as a donor material. The second category focuses on poly(dichlorotriazine-NDI) (P_8), derived from the DCT-NDI monomer (M_6), incorporating a triazine moiety as a potential acceptor. Lastly, copolymers combining CAH-NDI and DCT-NDI in various ratios (P_9-P_{12}) were synthesized to integrate donor and acceptor functionalities within a single polymeric structure. This molecular design facilitates intramolecular charge transfer and enhances excited-state properties, making these materials potential candidates for TADF applications. The chapter provides an in-depth examination of polymerization conditions, structural characterization, and the resulting optical and electronic properties, underscoring their potential for next-generation optoelectronic devices.

6.1.Synthesis of 2-(6-(9H-carbazol-9-yl) hexyl)-3a,4,7,7a-tetrahydro-1H-4,7-methanoisoindole-1,3(2H)-dione (CAH-NDI) monomer (M_5).

The synthesis of M_5 (CAH-NDI) was carried out in a four-step process, as depicted in (Scheme 6. 1). Initially, exo-norbornene dicarboxylic anhydride (exo-NDA) (1) was prepared and subsequently reacted with urea, leading to the formation of NDI (2). In the next step, NDI underwent alkylation with 1,6-dibromohexane, yielding BrH-NDI (3). Finally, BrH-NDI was coupled with carbazole via nucleophilic substitution to afford the target monomer M5 (CAH-NDI). The synthesized structures were thoroughly characterized using 1D and 2D NMR spectroscopy to confirm the molecular framework, while mass spectrometry (MS) provided additional structural validation. The final compound was purified using column chromatography to ensure high purity. These characterization techniques confirmed the successful synthesis of M_5, which serves as a crucial donor moiety for subsequent polymerization studies.

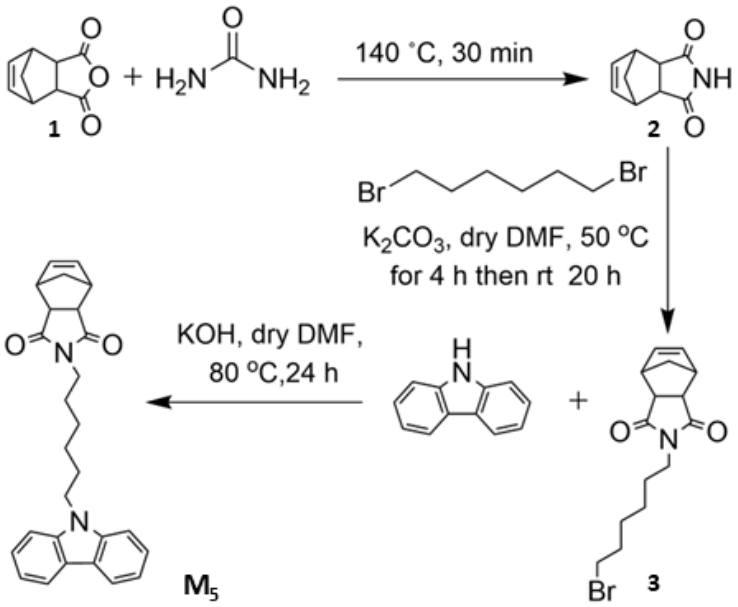

Scheme 6. 1 Synthesis of (CAH-NDI) monomer (M_5)

6.1.1.Synthesis of exo-norbornene-5,6-dicarboxylic anhydride (exo-NDA) (1).

Into a solution of maleic anhydride (90.00 g, 0.9178 mol) in *o*-dichlorobenzene (100 ml) at 200 ˚C, dicyclopentadiene (60.67 g, 0.4589 mol) was added slowly. The solution was heated for 2 hours at 200 ˚C, transferred into a beaker, and left to cool to room temperature gradually. To obtain the crystals of exo isomer, the formed precipitate was filtered, rinsed with *o*-dichlorobenzene, recrystallized three times, and dried in a vacuum oven at 50 ˚C for 12 hours to afford the white crystalline solid in 40% yield. EI-MS calculated for $C_9H_8O_3$ *m/z*: 164.16; Found: *m/z* 164. ^{1}H NMR (400 MHz, $CDCl_3$) δ: 6.30 (s, 2H), 3.41 (s, 2H), 2.98 (s, 2H), 1.63 (d, J = 10.5 Hz, 1H), 1.39 (d, J = 10.1 Hz, 1H) ppm. ^{13}C-NMR (101 MHz, $CDCl_3$) δ: 171.80, 138.02, 48.85, 46.93, 44.19 ppm (S6. 1).

*6.1.2.*Synthesis of 3a,4,7,7a-tetrahydro-1H-4,7-methanoisoindole-1,3(2H)-dione (NDI) (2).

NDI was synthesized following a previously reported procedure. A mixture of urea (1.61 g, 0.026 mol) and 5-norbornene-*exo*-2,3-dicarboxylic anhydride (4.02 g, 0.24 mol) was introduced into a 100 mL round bottom flask, the flask was fitted with a condenser. The reaction was conducted in the melt at 140°C for 1 hour, then cooled at room temperature. The crude product was purified by recrystallization from water a white crystal

precipitated. It was collected by filtration, washed with cold water and dried *under vacuum overnight* to obtain pure product of dicarboximide NDI (3.7 g, 93 %). EI-MS (EI+) calculated for $C_9H_9NO_2$: m/z 163.16; determined *m/z* 163.00. ^{1}H-NMR (400 MHz, $CDCl_3$) δ: 8.33 (s, 1H), 6.27 (s, 2H), 3.28 (s, 2H), 2.72 (s, 2H), 1.55 (d, 1H), 1.43 (d, 1H); ^{13}C-NMR (101 MHz, $CDCl_3$) δ: 178.21, 137.85, 49.01, 44.97, 42.80 ppm. ^{1}H and ^{13}C NMR signals were consistent with those reported in the literature. (S6. 2).

6.1.3.Synthesis of 2-(6-bromohexyl)-3a,4,7,7a-tetrahydro-1H-4,7-methanoisoindole-1,3(2H)-dione (BrH-NDI) (3).

1,6-dibromohexane (9.8 g, 40 mmol) and potassium carbonate (6.9 g, 50 mmol) were dissolved in dry DMF (10 mL) under nitrogen condition, and then a solution of NDI (1.7 g, 10 mmol) in dry DMF (15mL) was dropwise added to the mixture. After stirring at 50 ^{o}C for 4 hours, the mixture was stirred at room temperature for another 20 h. The reaction mixture was poured into water (200 mL) and extracted with 100 mL CH_2C_{l2} for three times. The combined organic phases were dried over Na_2SO_4. After removal of the solvent, the residue was purified by column chromatography (silica, hexane/CH_2Cl_2 *v/v* 2:1) to give colorless oil (1.9 g, 59%). EI-MS (EI+) calculated for $C_{15}H_{20}BrNO_2$: m/z 326.00; determined *m/z* 325.9. ^{1}H-NMR (400 MHz, $CDCl_3$) δ: 6.21 (s, 2H), 3.32-3.39 (m, 4H), 3.18 (s, 2H), 2.60 (s, 2H), 1.82-1.76 (2H), 1.39-1.52 (m, 5H), 1.22-1.28 (m, 1H), 1.14 (d, J = 10.1 Hz, 1H); ^{13}C-NMR (101 MHz, $CDCl_3$) δ: 177.74, 137.85, 47.59, 44.95, 42.79, 37.92, 33.78, 32.57, 27.62, 27.33, 25.92 ppm. ^{1}H and ^{13}C NMR signals were cosistant with those reported in the literature (Figure 6. 1).

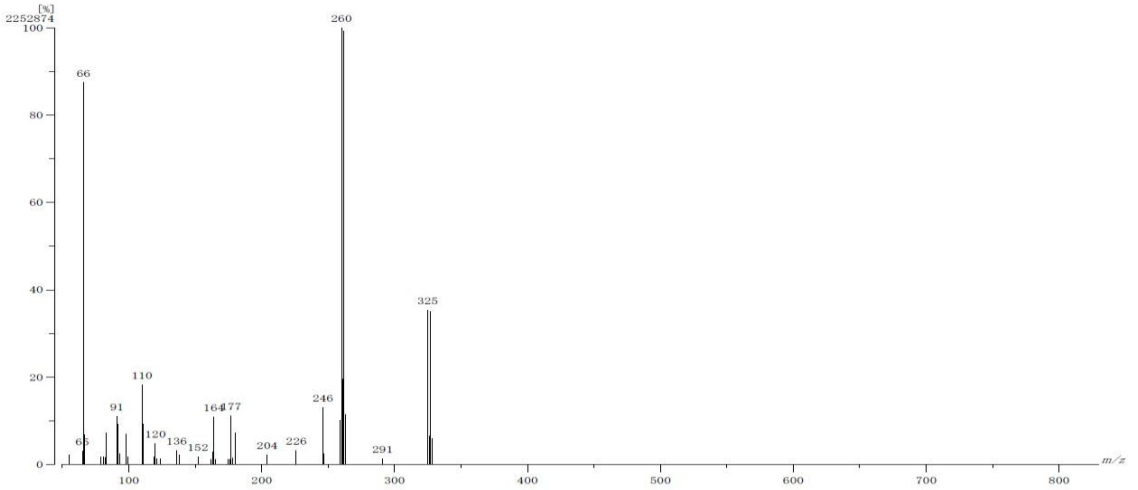

(a)

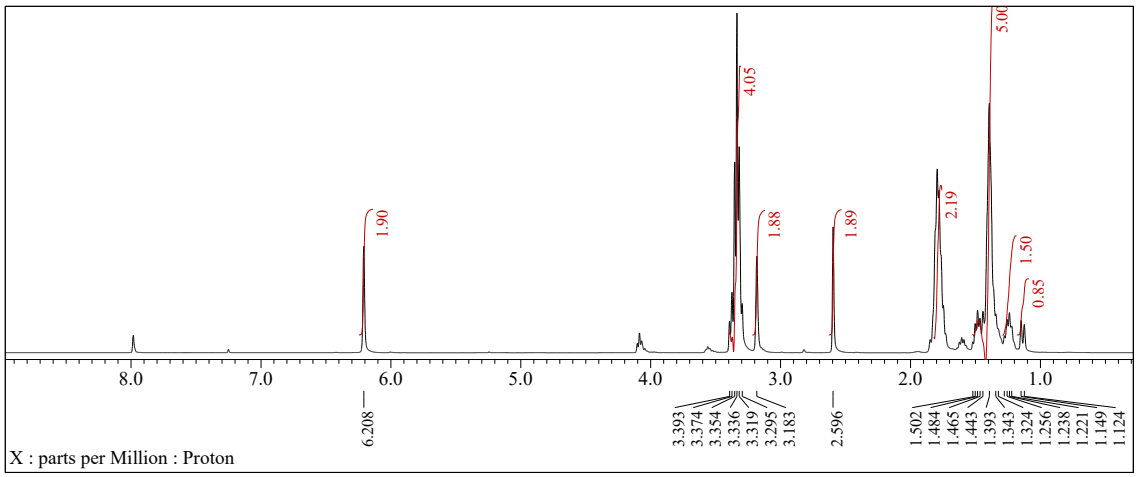

(b)

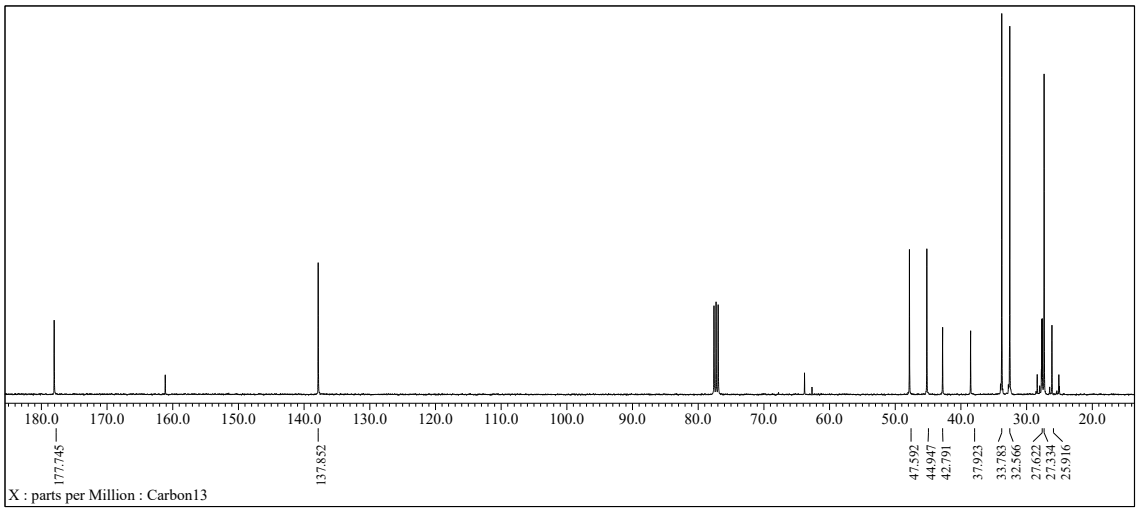

(c)

Figure 6. 1 a) EI-MS spectrum; b) ^{1}H NMR spectrum; c) ^{13}C NMR spectrum for (BrH-NDI) (3).

6.1.4. Synthesis of 2-(6-(9H-carbazol-9-yl) hexyl)-3a,4,7,7a-tetrahydro-1H-4,7-methanoisoindole-1,3(2H)-dione (CAH-NDI) monomer (M_5)

Carbazole (0.84 g, 5.0 mmol), BrH-NDI (1.6 g, 5.0 mmol) and KOH (0.33 g, 6.0 mmol) were dissolved in dry DMF (60 mL) under nitrogen condition. At 80 °C, the solution was stirred for 24 hours. After cooling to room temperature, the reaction mixture was poured into water (200 mL) and extracted with 100 mL CH_2Cl_2 for three times. The combined organic phases were dried over Na_2SO_4. After removal of the solvent, the residue was purified by column chromatography (silica, petroleum ether/CH_2Cl_2 *v/v* 10:1) to give a brown semi-solid matter (2.0 g, 96%). EI-MS (EI+) calculated for $C_{27}H_{28}N_2O_2$: m/z

413.00; determined *m/z* 412.00. ^{1}H-NMR (400 MHz, $CDCl_3$) δ: 8.09 (d, J = 17.4 Hz, 2H), 7.40 (d, J = 8.2 Hz, 4H), 7.21-7.25 (m, 2H), 6.27 (s, 2H), 4.11-4.30 (m, 2H), 3.35-3.47 (m, 2H), 3.26 (d, J = 7.3 Hz, 2H), 2.61-2.72 (m, 2H), 1.78-1.88 (m, 2H), 1.50-1.67 (m, 5H), 1.30-1.39 (m, 2H), 1.17-1.22 (m, 1H); ^{13}C-NMR (101 MHz, $CDCl_3$) δ: 178.31, 161.12, 139.53, 137.73, 125.88, 123.18, 120.21, 118.42, 108.78, 63.77, 47.90, 44.77, 42.63, 38.08, 28.08, 27.71, 26.58, 24.96 (Figure 6. 2).

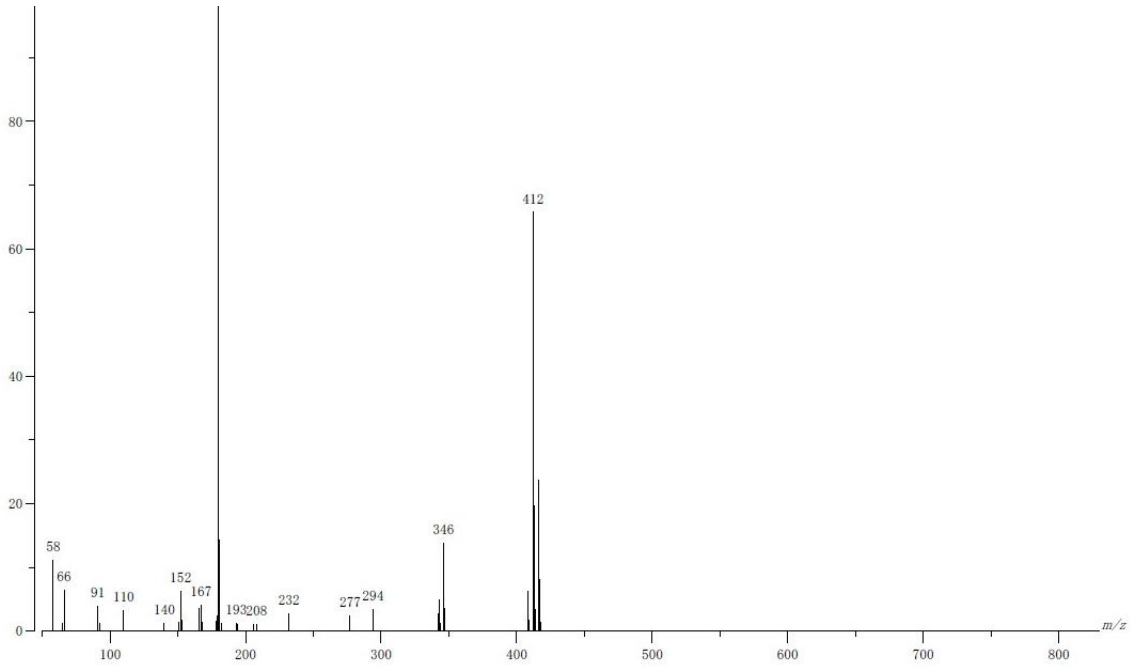

(a)

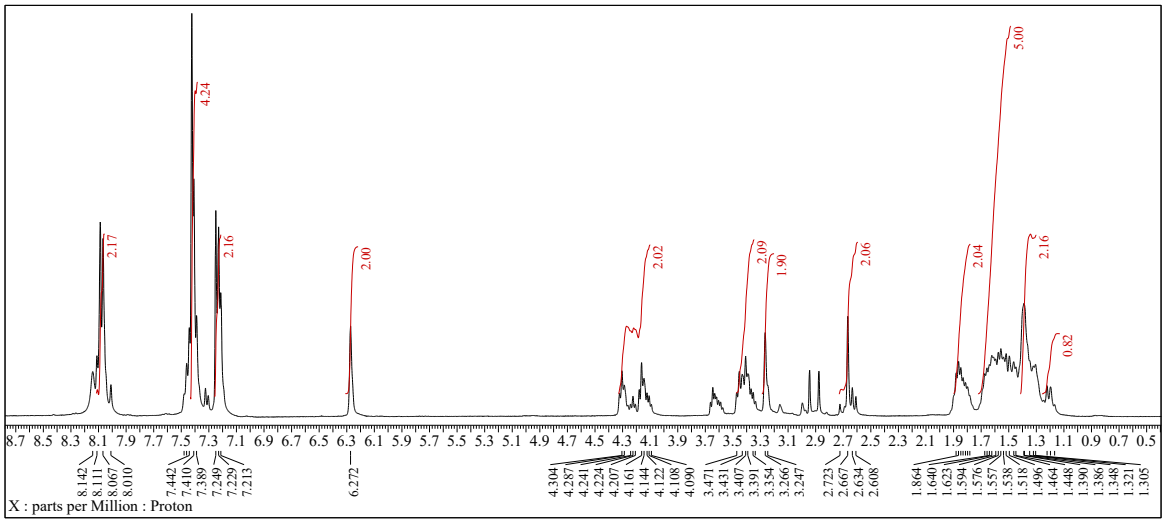

(b)

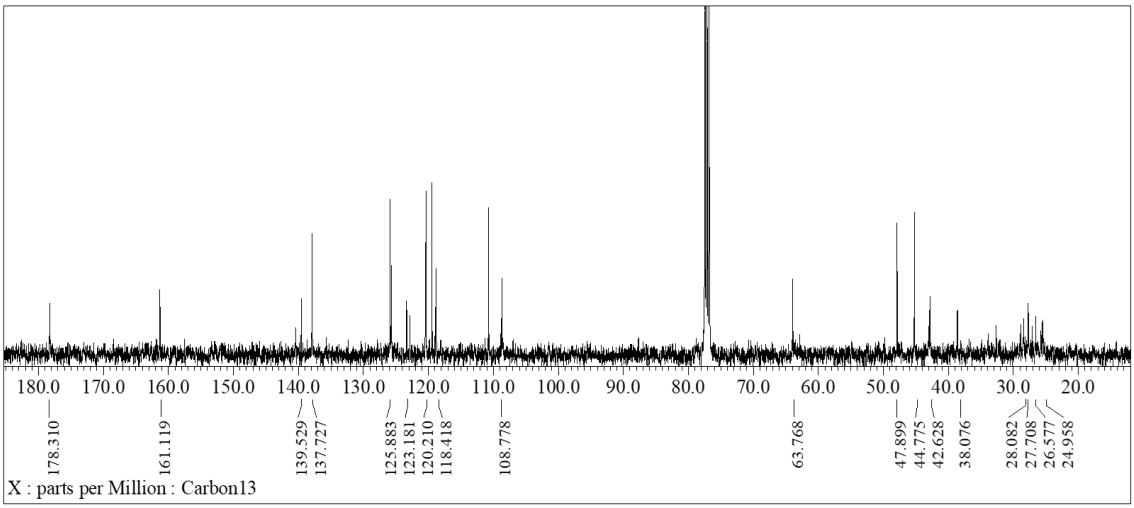

(c)

Figure 6. 2 a) EI-MS spectrum; b) ^{1}H NMR spectrum; c) ^{13}C NMR spectrum for M5.

6.2.Synthesis of poly (carbazole hexyl-norbornene dicarboximide) (CAH-NDI) (P_7)

CAH-NDI monomer (1400 mg, 0.0034 mol) was divided and placed in seven Radley's Carousel tubes each tube has (200 mg, 0.00048 mol). Anhydrous chloroform (900 µl) was added to each tube, and the solutions were stirred at room temperature for 5 minutes to ensure all monomers completely dissolve. Separately, (29.4 mg, 0.000033 mol) of the Grubbs third G3 generation initiator was dissolved in anhydrous chloroform (1400µl) and then transferred (200 µl) to each of the reaction tubes. The polymerization process was terminated by adding ethyl vinyl ether (EVE) (500µl) to each of the reaction tubes at various intervals (1, 3, 5, 10, 20, 30, and 50minutes). After quenching, the reaction was allowed to proceed for an additional 1 hour before the solvent and EVE were evaporated under vacuum. The synthesized homo-polymers were then analyzed using GPC and ^{1}H-NMR to optimize the best time for polymerization process.

6.3.Results and discussion.

6.3.1. The structural characterization of the CAH-NDI monomer M_5 & synthesized polymer P_7 by ROMP.

The synthesis of M_5 (CAH-NDI) was carried out in a four-step process, as depicted in (Scheme 6. 1). Initially, *exo*-norbornene dicarboxylic anhydride (*exo*-NDA) (1) was

prepared and subsequently reacted with urea, leading to the formation of norbornene dicarboxyimide (NDI) (2). In the next step, NDI underwent alkylation with 1,6-dibromohexane, yielding BrH-NDI (3). Finally, BrH-NDI was coupled with carbazole via nucleophilic substitution to afford the target monomer M5 (CAH-NDI).

The structural confirmation of M_5 was carried out using ^{1}H-NMR spectroscopy, revealing key characteristic peaks. The aromatic protons of the carbazole moiety appeared at 8.09 (d, J = 17.4 Hz, 2H), 7.40 (d, J = 8.2 Hz, 4H), and 7.21-7.25 (m, 4H), confirming the presence of the carbazole unit. A singlet peak at 6.27 (s, 2H) corresponded to the vinyl environment of the exo-NDI isomer, while multiple peaks at 4.11-4.30 ppm and 3.35-3.47 ppm were characteristic of the (NCH_2) methylene groups linked to the carbazole and NDI moieties, respectively. Additionally, signals below 2 ppm were attributed to aliphatic protons of the hexyl chain, except for a multiplet at 1.78-1.88 ppm, which corresponded to methylene hydrogens of the bicyclic molecule in the NDI moiety. The ^{13}C-NMR spectrum of the synthesized monomer which includes peaks at 178.3 ppm which are attributed to two carbonyl-NDI groups, six peaks from 139.5-118.4 ppm, corresponding to carbazole moiety and two peaks at 63.7, 47.8 ppm of carbon atoms adjacent to nitrogen atom of carbazole and NDI, respectively. 2D NMR techniques were also employed. Correlated Spectroscopy (COSY) revealed scalar couplings between neighboring protons, specifically between signals labeled (a, b), (k, l), and (l,m) highlighted in green, violet, and red boxes in (Figure 6. 3(a)). Heteronuclear Multiple Quantum Coherence (HMQC) spectroscopy further correlated each proton with its directly bonded carbon atom, confirming assignments such as m,l,k, a, e, and j with carbons at 120.1, 128, 118, 173.7, 63.7and 42.6 ppm, respectively (Figure 6. 3 (b)).

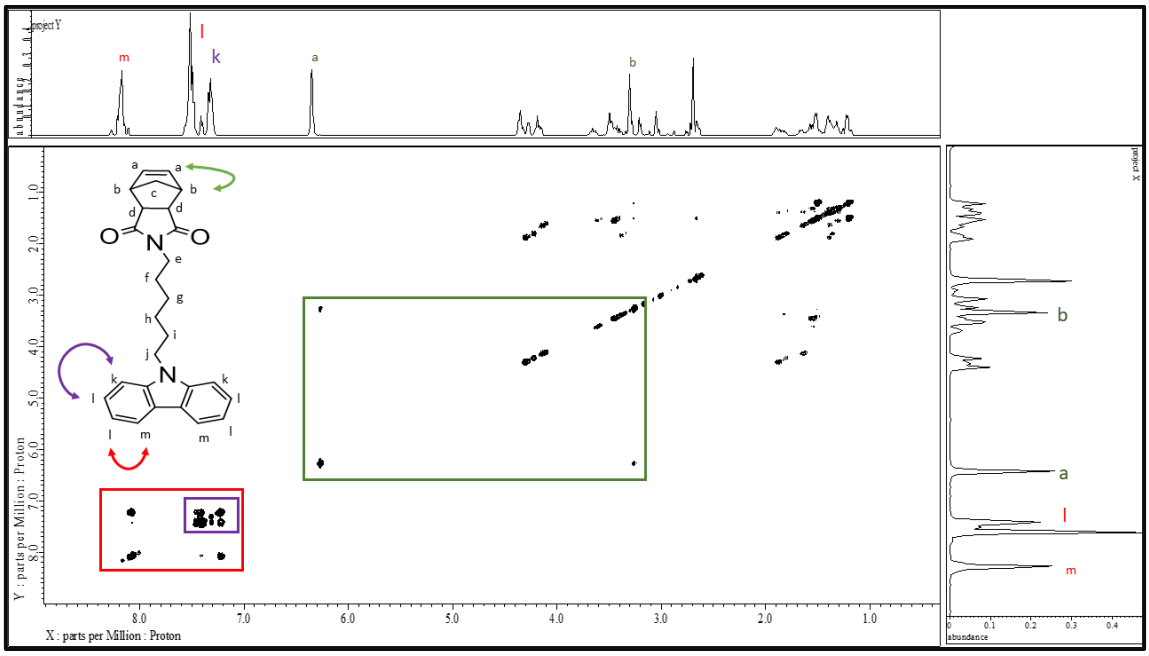

(a)

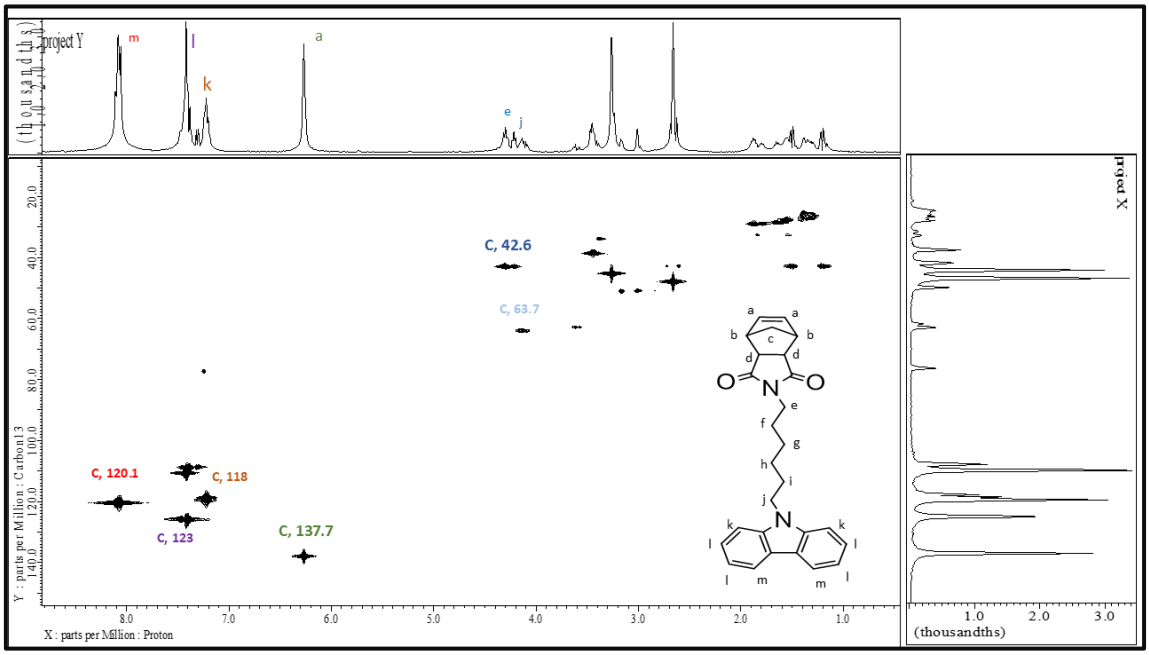

Figure 6. 3 2D NMR for monomer M5, a) COSY, b) HMQC

The monomer underwent homo-polymerization P_7 using the G3 catalyst, which was finally terminated by the addition of EVE (Scheme 6. 2).

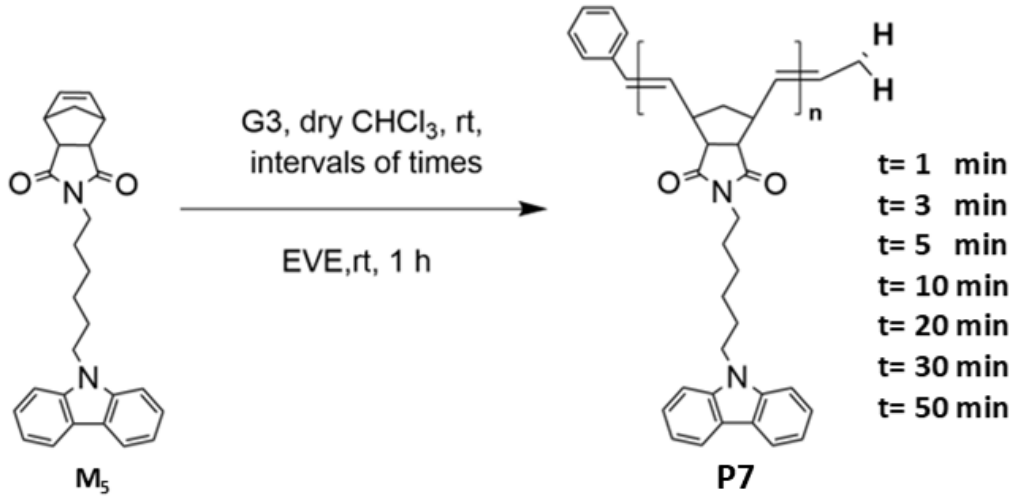

Scheme 6. 2 CAH-NDI homopolymer P_7 using the G3 catalyst.

(Figure 6. 4) highlights key regions of the P_7 proton NMR spectrum to track the polymerization process. The green box represents the olefin environment (the norbornene double bond peak) of the monomer M_5, while the blue box represents the trans-vinylene environment of P_7. As polymerization progresses and reaction time increases, the norbornene double bond peak gradually decreases in intensity and completely disappears after 20 minutes. To ensure complete conversion of the monomer to polymer chains and confirm the absence of unreacted monomer and all monomers already catalyzed, additional measurements were taken at 30 and 50 minutes. The disappearance of the norbornene double bond peak at 6.26–6.28 ppm and the appearance of new peaks at 5.4–5.8 ppm confirms the successful polymerization. Additionally, the retention of carbazole and imide characteristic peaks ensured that the functional groups remained intact post-polymerization.

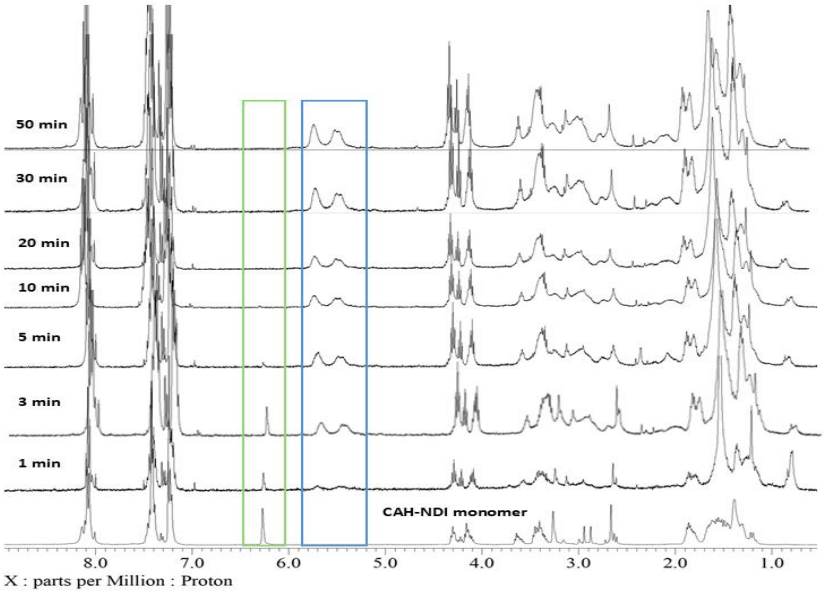

Figure 6. 4 ^{1}H-NMR Spectrum of Polymer P_7 Recorded at Various Polymerization Intervals.

The polymerization progress of P_7 was investigated through GPC analysis using THF as the eluent to determine the molecular weight of the synthesized polymer, as shown in (Figure 6. 5) and summarized in (Table 6. 1).

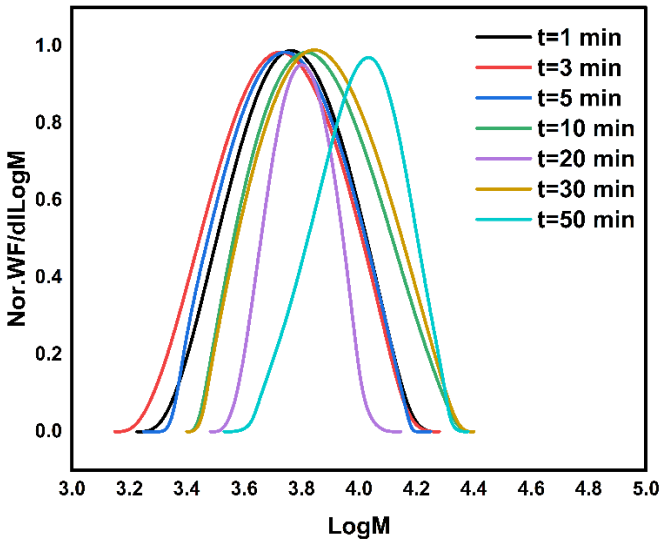

Figure 6. 5 Molecular weight distribution of polymer P_7.

Initially, at 1 minute, Mn was 4.11 kDa, with a PDI of 1.10, indicating early-stage polymer formation. As the reaction proceeded, Mn gradually increased, reaching 6.45 kDa at 20 minutes, confirming chain propagation. After 30 minutes, Mn further increased

to 6.69 kDa, with a slight broadening in molecular weight distribution (PDI = 1.22). Notably, after 50 minutes, a significant increase in Mn to 9.50 kDa was observed, along with a relatively low PDI of 1.11, indicating well-controlled polymerization.

Table 6. 1 Time-Dependent GPC Analysis of Polymer P_7

Time/ (min)	GPC Data			
	M_p /(KDa)	M_n/(KDa)	M_w/(KDa)	PDI
1	3924	4109	4562	1.10
3	4426	4298	4945	1.15
5	4534	4898	5669	1.16
10	4833	5227	6904	1.32
20	4462	6450	7716	1.20
30	5234	6686	8151	1.22
50	10637	9501	10622	1.11

M_{wt} exhibited a corresponding progression, increasing steadily over time, confirming continuous polymer growth. These results demonstrate the controlled nature of the ROMP process, with gradual molecular weight evolution and relatively narrow PDI values, ensuring uniform polymer chains.

6.3.2. Optical properties of the polymer P_7.

(Figure 6. 6) illustrates the UV–Vis absorption spectrum of polymer P_7 measured in tetrahydrofuran (THF) at a dilute concentration of 5×10^{-8} M. The absorption profile reveals three distinct peaks centered at 294 nm, 332 nm, and 346 nm. These peaks are primarily attributed to π–π* electronic transitions localized within the carbazole chromophores present along the polymer side chains. The absence of any discernible n–π* transitions suggests that there is minimal involvement of non-bonding electron pairs, and more importantly, it indicates that the extent of intramolecular charge transfer or extended π-conjugation along the polymer backbone is limited.

This observation supports the conclusion that P_7 has a non-conjugated backbone, which restricts effective electronic communication between adjacent carbazole units. As a result, the transition dipole moments remain localized, and the overall absorption intensity

remains relatively low. This weak absorption behavior is consistent with the design of the polymer, where the incorporation of the norbornene-based backbone limits the conjugation between chromophores and consequently reduces the delocalization of π-electrons. Such a structural feature can significantly influence the optoelectronic properties of the material, potentially leading to applications where controlled or isolated chromophore activity is desired, such as in optical sensors or in light-emitting devices where inter-chromophore interactions need to be minimized.

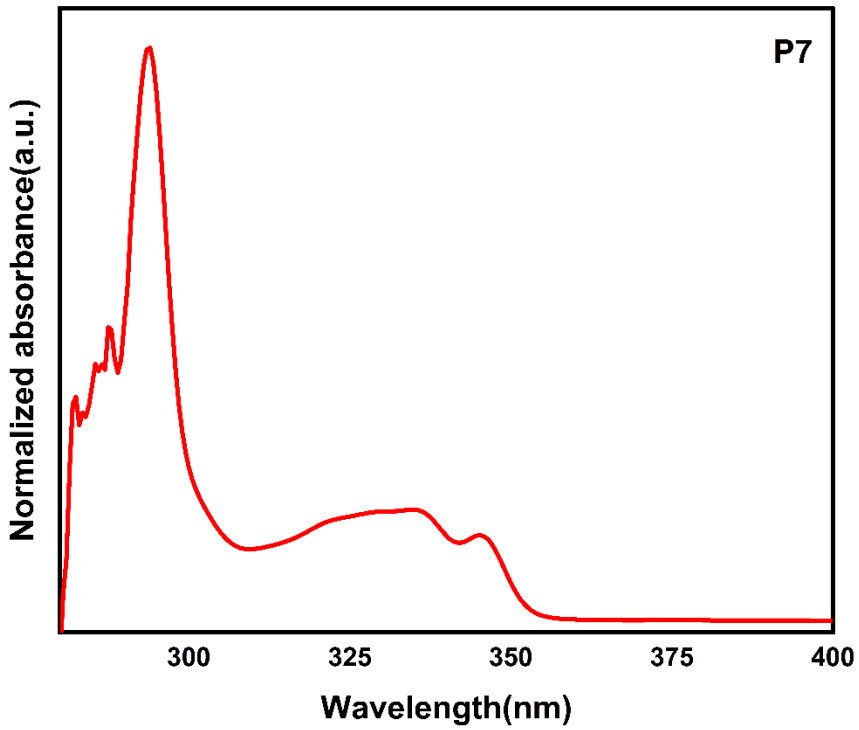

Figure 6. 6 UV for P_7.

6.4.Synthesis of 2-(2-((4,6-dichloro-1,3,5-triazin-2-yl)oxy)ethyl)-3a,4,7,7a-tetrahydro-1H-4,7-methanoisoindole-1,3(2H)-dione monomer *(DCT-NDI)* (M_6)

The preparation of M_6 (DCT-NDI) was achieved through a three-step sequence, as illustrated in (Scheme 6. 3). The process began with the synthesis of exo-*NDA* (1), which was subsequently treated with ethanolamine, leading to the formation of norbornene dicarboxyimide ethyl alcohol (NDI-OH) (4). In the subsequent transformation, NDI-OH reacted with TCT in the presence of DIPEA, which facilitated the elimination of HCl as a byproduct, ultimately yielding the target monomer M_6 (DCT-NDI). The synthesized compounds were thoroughly analyzed using 1D and 2D NMR spectroscopy to confirm

their structural integrity, while mass spectrometry (MS) provided further verification. To obtain a highly pure product, column chromatography was employed as the final purification step. The successful synthesis of M_6 establishes it as a crucial acceptor moiety for subsequent polymerization studies.

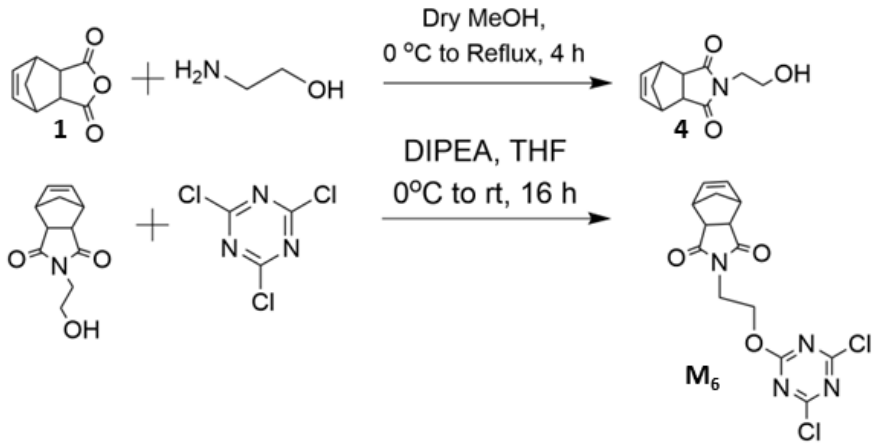

Scheme 6. 3 Synthesis of (DCT-NDI) monomer (M_6)

6.4.1. Synthesis 2-(2-hydroxyethyl)-3a,4,7,7a-tetrahydro-1H-4,7-methanoisoindole-1,3(2H)-dione (4)

The anhydride **1** (4.00 g, 0.024 mol) was suspended in dry methanol (70 mL) and the mixture cooled to 0 °C. A solution of ethanolamine (1.5 mL, 0.24mol) in 20 mL of dry methanol was added dropwise, and the resulting solution was stirred for 10 min at 0 °C, then allowed to warm to room temperature and stirred for an additional 30 minutes. Subsequently, the solution was refluxed for 4 hours. After cooling the mixture to an ambient temperature, the solvent was removed under reduced pressure, and the white residue was dissolved in 300 mL of CH_2Cl_2 and washed with 3 × 100 mL of water. The organic layer was dried over $MgSO_4$ and filtered. Removal of the solvent under reduced pressure furnished an off-white residue that was purified by flash chromatography to give **2** (2.04 g, 42% yield) as a white solid. EI-MS (EI+) calculated for $C_{11}H_{13}NO_3$: m/z 207.00; determined *m/z* 207.00. ^{1}H-NMR (400 MHz, $CDCl_3$) δ: 6.27 (dd, J = 16.5, 15.1 Hz, 2H), 3.75 (t, J = 4.8 Hz, 2H), 3.67 (t, J = 5.3 Hz, 2H), 3.26 (s, 2H), 2.70 (s, 2H), 2.37 (s, 1H), 1.48-1.54 (m, 1H), 1.33 (d, J = 10.1 Hz, 1H); ^{13}C-NMR (101 MHz, $CDCl_3$) δ: 178.90, 137.36, 60.50, 47.31, 44.98, 42.30, 40.25 ppm (Figure 6. 7).

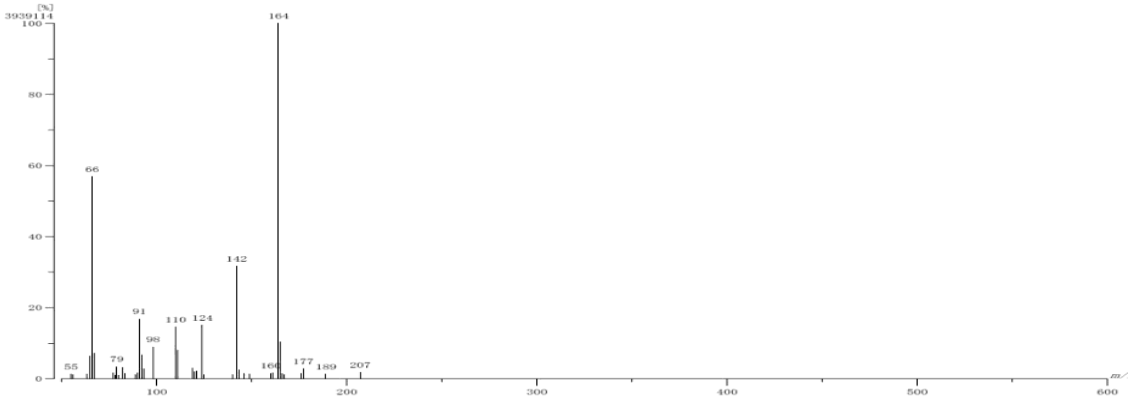

(a)

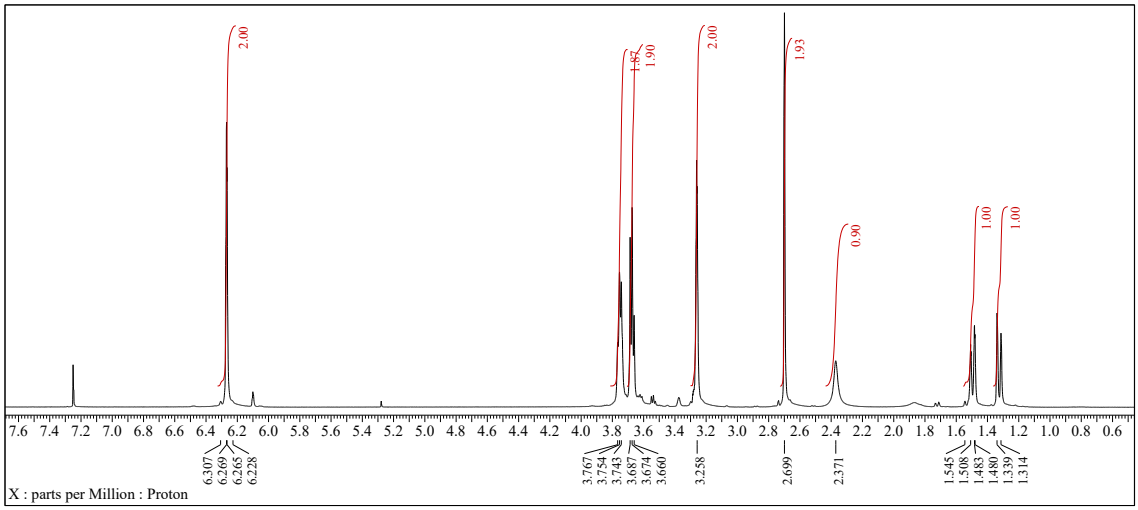

(b)

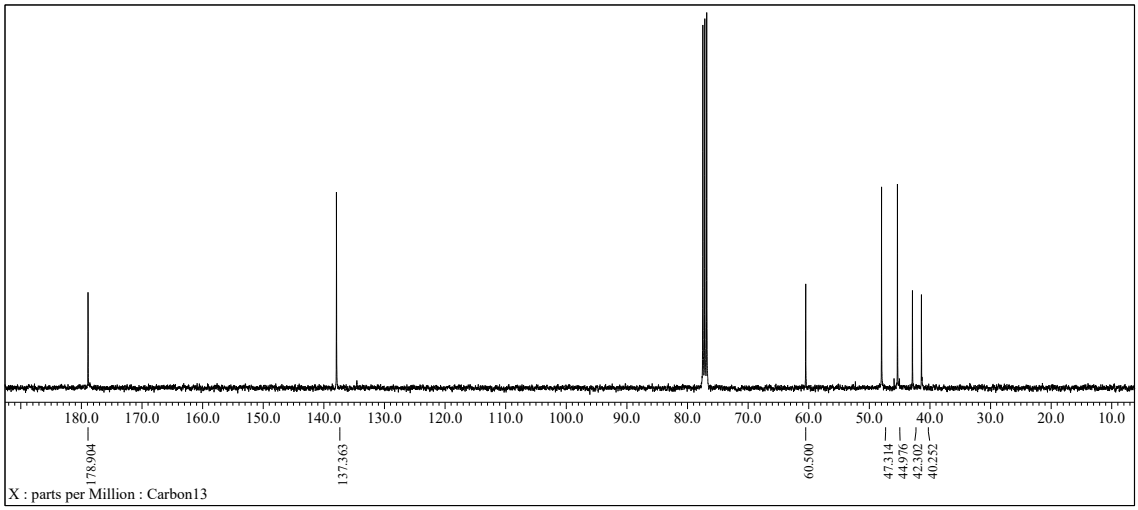

(c)

Figure 6. 7 a) EI-MS spectrum; b) ^{1}H NMR spectrum; c) ^{13}C NMR spectrum for compound 4.

6.4.2. Synthesis of 2-(2-((4,6-dichloro-1,3,5-triazin-2-yl)oxy)ethyl)-3a,4,7,7a-tetrahydro-1H-4,7-methanoisoindole-1,3(2H)-dione monomer *(DCT-NDI)* (M_6)

TCT (2.3 g, 0.012 mol) was added to a stirred solution of **1** (1.29 g, 0.006 mol) and DIPEA (2.2 mL, 0.012 mol) in THF at 0 ℃. The solution was stirred at 0 ℃ for 3 h, warmed to room temperature, and stirred for an additional 16 h. At the end of this period, the solvent was removed under reduced pressure. The residue was dissolved in DCM, and the resulting salt was removed by filtration before extraction with 3 × 100 mL of water. The collected organic layers were dried over anhydrous $MgSO_4$, and the solvent was removed under reduced pressure. The residue was washed with the mixture of DCM:diethyl ether (1:10) to give the product as a pale yellow powder (1.7 g, 76% yield). EI-MS (EI+) calculated for $C_{14}H_{12}Cl_2N_4O_3$: *m/z* 354; determined m/z 354.00. ^{1}H-NMR (400 MHz, $CDCl_3$) δ: 6.28 (s, 2H), 4.66 (t, J = 5.5 Hz, 2H), 3.93 (t, J = 5.5 Hz, 2H), 3.28 (s, 2H), 2.71 (d, J = 0.7 Hz, 2H), 1.59 (s, 1H), 1.28 (d, J = 10.1 Hz, 1H)); ^{13}C-NMR (101 MHz, $CDCl_3$) δ: 177.81, 172.44, 137.28, 65.90, 48.09, 45.23, 42.61, 36.58ppm (Figure 6. 8).

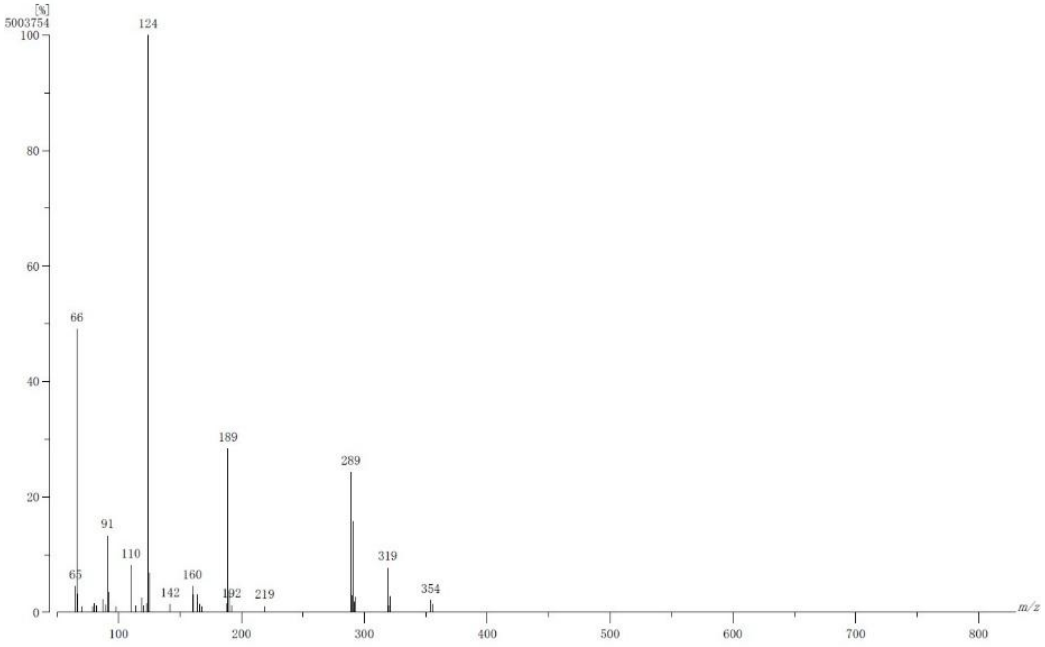

(a)

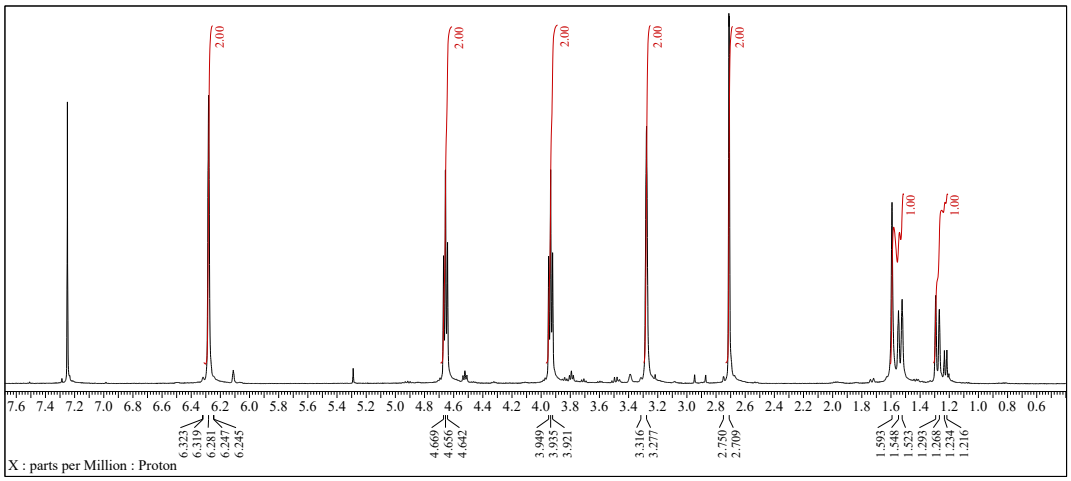

(b)

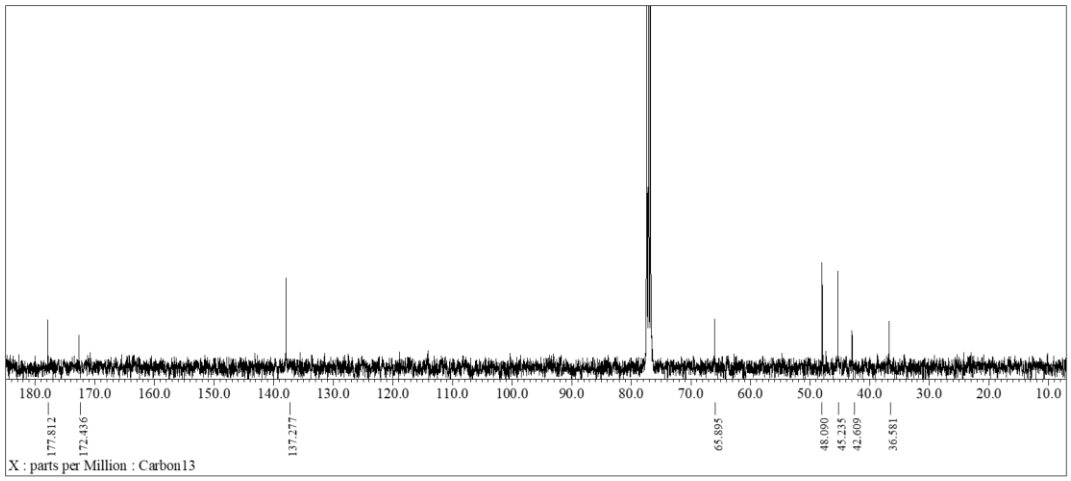

(c)

Figure 6. 8 a) EI-MS spectrum; b) ^{1}H NMR spectrum; c) ^{13}C NMR spectrum for (M_6).

6.5. Synthesis of poly (dichlorotriazine-norbornene dicarboxyimide) (DCT-NDI) (P_8)

DCT-NDI monomer (1400 mg, 0.0039 mol) was divided and placed in seven Radley's Carousel tubes each tube has (200 mg, 0.00056 mol). Anhydrous chloroform (900 µl) was added to each tube, and the solutions were stirred at room temperature for 5 minutes to ensure all monomers completely dissolve. Separately, (35 mg, 0.000039 mol) of the Grubbs third G3 generation initiator was dissolved in anhydrous chloroform (1400µl) and then transferred (200 µl) to each of the reaction tubes. The polymerization process was terminated by adding ethyl vinyl ether (EVE) (500µl) to each of the reaction tubes at

various intervals (1, 3, 5, 10, 20, 30, and 50 minutes). After quenching, the reaction was allowed to proceed for an additional 1 hour before the solvent and EVE were evaporated under vacuum. The synthesized homo-polymers were then analyzed using GPC and ^{1}H-NMR to optimize the best time for polymerization process

6.6.Results and discussion.

6.6.1.The structural characterization of the (DCT-NDI) monomer M6 & synthesized polymer P_8 by ROMP.

The synthesis of the DCT-NDI monomer M_6 involved a three-step process. Initially, exo-norbornene dicarboxylic anhydride (exo-NDA) was converted to an intermediate, NDI-OH, through a reaction with ethanolamine in anhydrous methanol. Subsequently, NDI-OH was reacted with trichlorotriazine (TCT) in the presence of *N,N*-diisopropylethylamine (DIPEA), affording the target monomer M_6. The identity and purity of M_6 were confirmed through various spectroscopic techniques. Electron ionization mass spectrometry (EI-MS) revealed a molecular ion peak at m/z 354, aligning well with the expected molecular weight. ^{1}H-NMR spectra showed key resonances, including a multiplet at 6.28 ppm (2H), assigned to the vinylic protons of the norbornene unit. Additional signals at 4.66 and 3.93 ppm were attributed to methylene protons adjacent to oxygen and nitrogen, respectively. Peaks observed at 3.28 and 2.71 ppm were associated with ring-bridged hydrogens, while broader multiplets at 1.52–1.59 ppm and 1.22–1.29 ppm corresponded to methylene groups within the NDI framework.

Further structural confirmation was provided by ^{13}C-NMR, which displayed characteristic peaks at 177.8 ppm (NDI carbonyls), 172.4 ppm (triazine ring), 65.9 ppm (O-linked CH_2), and 36.5 ppm (N-linked CH_2). To enhance confidence in the structural assignment, 2D NMR techniques were also employed. Correlated Spectroscopy (COSY) revealed scalar couplings between neighboring protons, specifically between signals labeled a and b, and e and f, highlighted in green and violet boxes in (Figure 6. 9(a)). Heteronuclear Multiple Quantum Coherence (HMQC) spectroscopy further correlated each proton with its directly bonded carbon atom, confirming assignments such as e, c, b, d, f, and a with carbons at 36.5, 42.6, 45.2, 48, 65.9, and 137 ppm, respectively (Figure 6. 9(b)). Additionally, DEPT analysis helped differentiate carbon types: the absence of

signals at 177.8 and 172.4 ppm indicated quaternary carbon centers (non-protonated), while upright peaks at 137, 48, and 45.28 ppm were consistent with tertiary CH groups. In contrast, signals at 65.9, 42.6, and 36.5 ppm were inverted, confirming the presence of secondary CH_2 groups (Figure 6. 9(c)). Together, these spectroscopic results conclusively support the successful synthesis and detailed structural elucidation of the DCT-NDI monomerM_6.

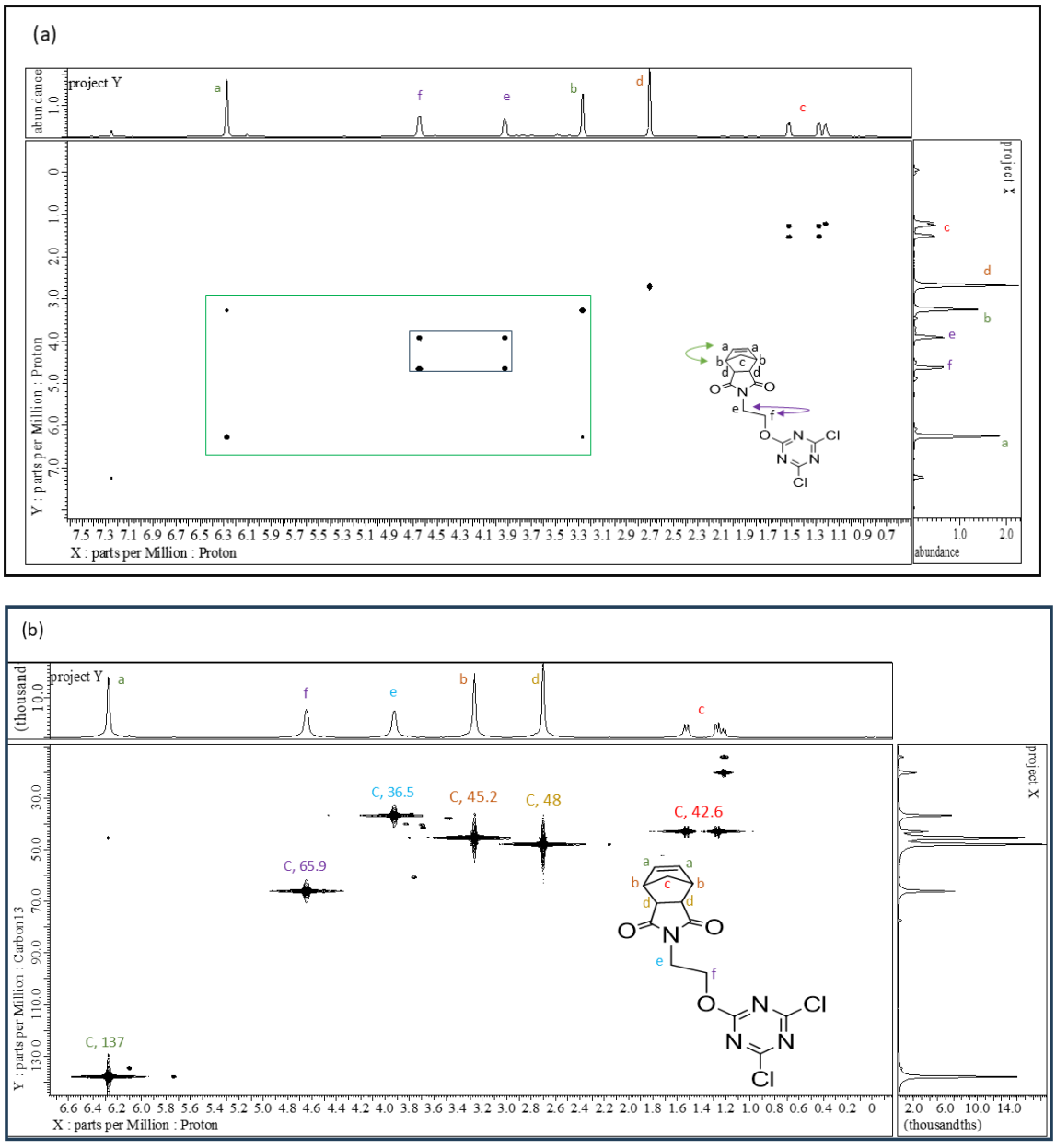

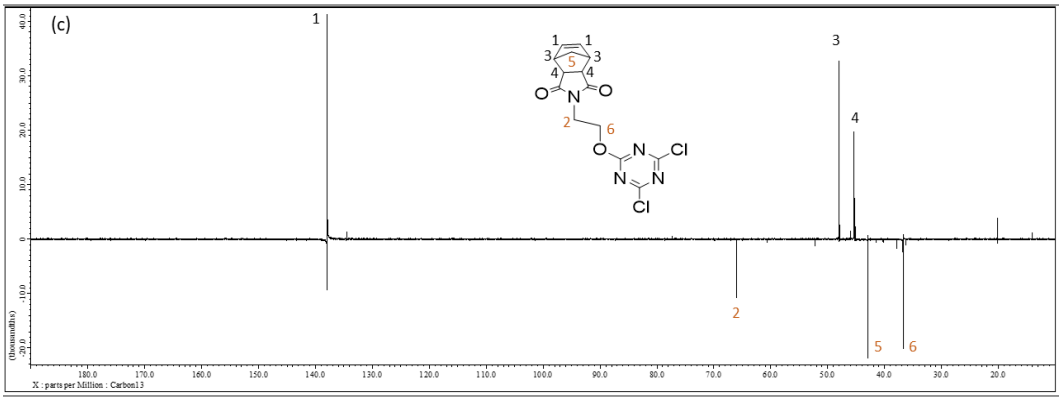

Figure 6. 9 2D NMR for monomer M6, a) COSY, b) HMQC, and c) DEPT.

The homopolymer P_8 was prepared through ROMP utilizing the G3 catalyst, resulting in polymers with a low PDI and a nearly equal distribution of *trans* and *cis* vinylene units. The polymerization process was concluded by introducing ethyl vinyl ether (EVE) (Scheme 6. 4).

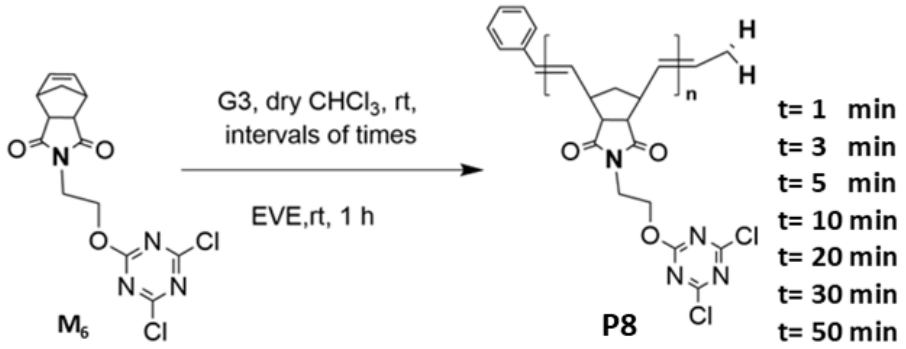

Scheme 6. 4 DCT-NDI homopolymer P_8 using the G3 catalyst.

(Figure 6. 10) highlights key regions of the P_8 proton NMR spectrum to track the polymerization process. The green box represents the olefin environment (the norbornene double bond peak) of the monomer M_6, while the blue box represents the *trans*, *cis*-vinylene environment of P_8. As polymerization progresses and reaction time increases, the norbornene double bond peak gradually decreases in intensity and completely disappears after 3 minutes. To ensure complete conversion of the monomer to polymer chains and confirm the absence of unreacted monomer and all monomers already catalyzed, additional measurements were taken at intervals times. The disappearance of

the norbornene double bond peak at 6.28 ppm and the appearance of new peaks at 5.42–5.76 ppm attributed to *trans* and *cis* form which confirms the successful polymerization.

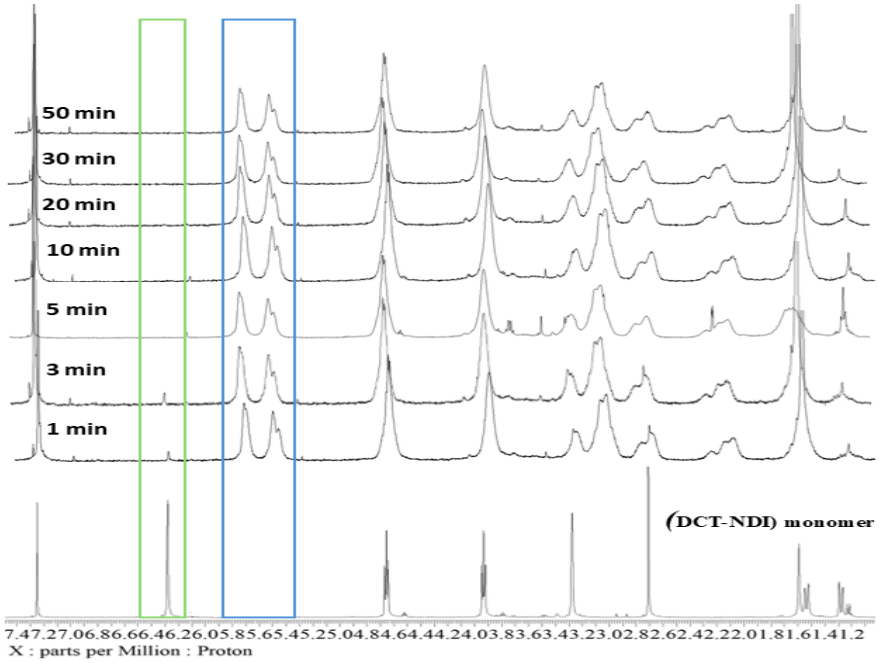

Figure 6. 10 ^{1}H-NMR Spectrum of Polymer P8 Recorded at Various Polymerization Intervals.

The polymerization progress of P_8 was investigated through GPC analysis using THF as the eluent to determine the molecular weight of the synthesized polymer, as shown in (Figure 6. 11) and summarized in (Table 6. 2).

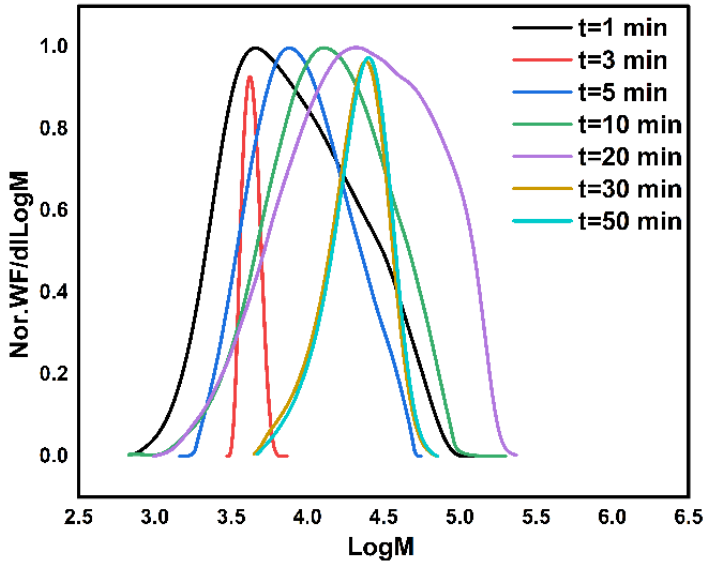

Figure 6. 11 Molecular weight distribution of polymer P_8.

The molecular weight distribution of P_8 exhibited a clear growth trend with increasing reaction time. Initially, at 1 minute, Mn was recorded at 3.96 KDa with a PDI of 1.26. As polymerization progressed, Mn steadily increased, reaching 11.49 KDa at 10 minutes and 19.24 KDa at 50 minutes. Mw followed a similar pattern, rising from 4.99 KDa at 1 minute to 23.55 KDa at 50 minutes.

Table 6. 2 Time-Dependent GPC Analysis of Polymer P_8.

Time/ (hours) t	GPC Data			
	M_p /(KDa)	M_n/(KDa)	M_w/(KDa)	PDI
1	4620	3961	4993	1.26
3	5651	4236	4354	1.02
5	8205	5933	6850	1.15
10	12778	11494	15727	1.37
20	21040	11951	16350	1.37
30	24458	17948	22474	1.16
50	25602	19243	23552	1.22

The PDI values remained within a controlled range, indicating a relatively uniform polymerization process. Notably, the most notable increase in molecular weight was observed between 10 and 30 minutes, indicating a prolonged propagation phase before stabilizing. These findings confirm the successful polymerization of P_8, demonstrating well-regulated molecular weight progression with increasing reaction time.

6.6.2. Optical Properties of Polymer P_8

Figure 6. 12 presents the UV–Vis absorption spectrum of polymer P_8 recorded in tetrahydrofuran (THF) at a concentration of 5×10^{-8} M. The spectrum shows two distinct absorption bands located at 228 nm and 255 nm. These peaks are characteristic of π–π* electronic transitions associated with the aromatic dichlorotriazine and imide moieties within the polymer side chains. The sharp absorption at 228 nm is attributed to transitions within the triazine ring system, while the band at 255 nm likely originates from the electron-deficient naphthalene diimide (NDI) core.

Compared to polymers with extended π-conjugated systems, the absorption features of P_8 appear in the higher energy (shorter wavelength) region, reflecting the localized nature of electronic transitions. The absence of lower-energy absorptions suggests that the electronic communication along the backbone is significantly suppressed, likely due to the non-conjugated norbornene framework which interrupts π-conjugation between side-chain chromophores. This structural isolation limits exciton delocalization, resulting in lower absorption intensity and high-energy transitions.

The optical behavior of P_8 underscores the effect of molecular design on its photophysical properties. The integration of electron-deficient units such as triazine and NDI without a conjugated polymer backbone leads to absorption features dominated by individual chromophore units, rather than extended delocalized systems. Such materials can be promising candidates in applications where well-defined localized excitation is necessary, such as in fluorescence tagging, controlled energy transfer systems, or as insulating matrix components in optoelectronic devices.

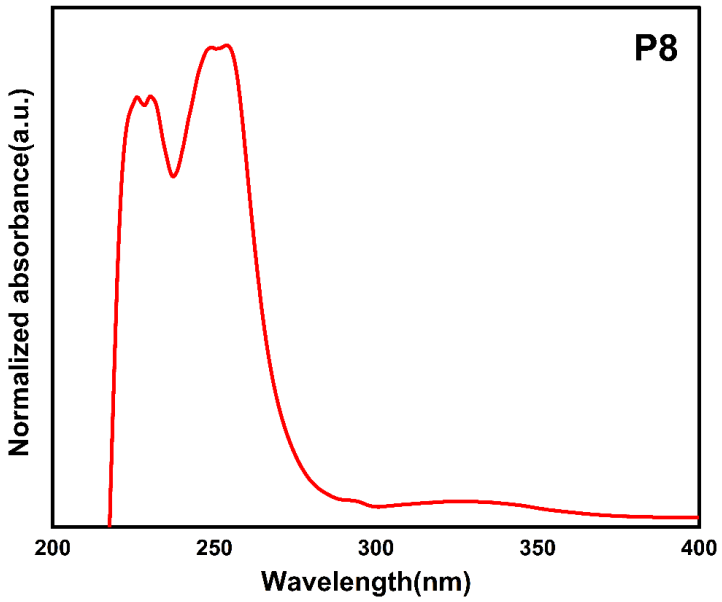

Figure 6. 12 UV for P_8.

6.7. ROMP Copolymerization of CAH-NDI and DCT-NDI Monomers.

The copolymerization was carried out following the standard Ring-ROMP protocol (Scheme 6. 5). Under an inert nitrogen atmosphere, varying molar ratios of CAH-NDI

(M_5) (0.9, 0.7, 0.5, 0.3) and DCT-NDI (M_6) (0.1, 0.3, 0.5, 0.7) were separately allocated into four Radley's Carousel reaction tubes. To each tube, 800 µL of anhydrous chloroform was added, and the mixtures were stirred at room temperature for 5 minutes to ensure complete dissolution of the monomers.

In a separate vial, 35 mg of G3 catalyst was dissolved in 1000 µL of anhydrous chloroform. A 250 µL aliquot of this catalyst solution was then transferred into each reaction tube to initiate the polymerization. The reaction was allowed to proceed for 1 hour, after which it was terminated by adding 300 µL of ethyl vinyl ether (EVE) to each tube. Following termination, the reaction mixtures were left to stir for another hour, ensuring complete quenching. The resulting polymer solutions were then concentrated by evaporating the solvent and EVE under vacuum.

The synthesized Copolymers were subsequently characterized using GPC and UV.

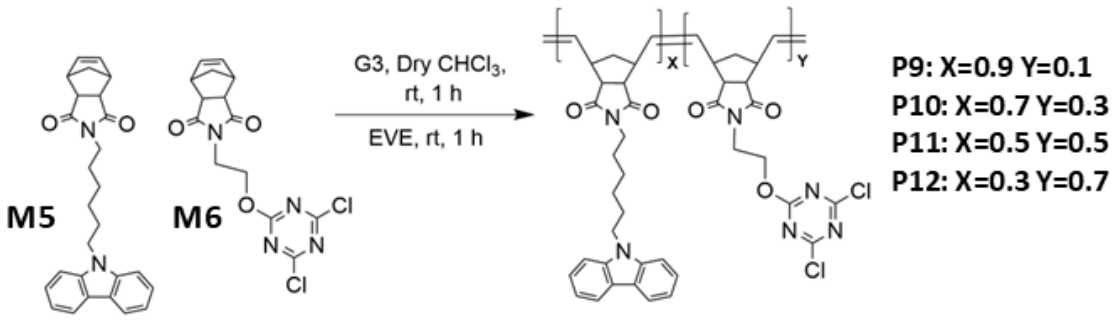

Scheme 6. 5 Synthesis of Copolymer (P_9-P_{12}).

The molecular weights of the synthesized copolymers P_9 to P_{12} were evaluated by GPC, with Mn values of 4388 kDa, 4781 kDa, 6995 kDa, and 10636 kDa, respectively (Figure 6. 13)(Table 6. 3).

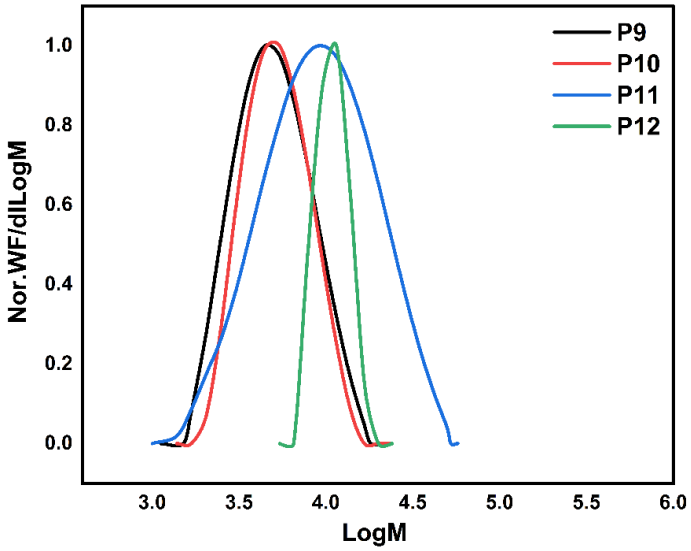

Figure 6. 13 Molecular weight distribution of Copolymer (P_9-P_{12}).

As the feed ratio of DCT-NDI increased from P_9 to P_{12}, a gradual rise in Mn was observed, with P_{12} exhibiting the highest value.

Table 6. 3 GPC analysis for Co-Polymers (P_9-P_{12})

Co-Polymer	GPC Data				
	M1:M2	M_p /(KDa)	M_n/(KDa)	M_w/(KDa)	PDI
P_9	0.9 : 0.1	4185	4388	5586	1.27
P_{10}	0.7 : 0.3	4053	4781	5699	1.19
P_{11}	0.5 : 0.5	8151	6995	11671	1.67
P_{12}	0.3 : 0.7	1248	10636	11092	1.04

This significant increase in Mn for P_{12} can be attributed to the higher content of the DCT-NDI monomer (70%), which appears to exhibit greater reactivity under ROMP conditions. The electron-withdrawing dichlorotriazine group in DCT-NDI may enhance coordination with the G3 catalyst, facilitating more efficient polymer chain propagation. Additionally, the relatively smaller steric hindrance of DCT-NDI compared to CAH-NDI likely allows for smoother monomer incorporation during polymerization. These combined electronic and steric effects contribute to the formation of longer polymer chains, resulting in a

higher Mn. The low PDI value of P_{12} (1.04) further supports the notion of a well-controlled polymerization process.

6.8. Optical Properties of Copolymers P_9–P_{12}.

The UV–Vis absorption spectra of the copolymers P_9–P_{12}, composed of varying ratios of CAH-NDI and DCT-NDI units, were recorded in THF (Figure 6. 14). These copolymers exhibit absorption features that reflect the combined contributions of the two parent chromophores, with the molar ratio of CAH-NDI decreasing progressively from P_9 to P_{12}. Across all four copolymers, a set of consistent absorption peaks is observed at 283, 293, 332, and 345 nm, which correspond to the π–π* transitions of the carbazole moieties originating from the CAH-NDI units. These bands closely resemble those observed for the CAH-NDI homopolymer (P_7), confirming the presence of the carbazole chromophore in the copolymer backbones. However, the intensity of these absorption peaks systematically decreases as the CAH-NDI content is reduced from P_9 to P_{12}, following the feed ratio trend (CAH-NDI: 370 → 280 → 200 → 120 mg). This indicates that the chromophore density directly affects the light absorption strength in this region.

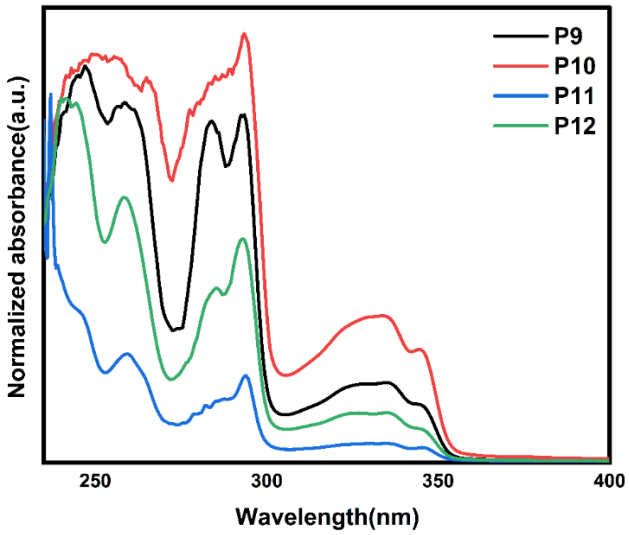

Figure 6. 14 UV for P_9-P_{12}.

In addition to carbazole-related features, the copolymers also display absorption bands at 246 and 259 nm, attributed to the DCT-NDI component. Compared to the DCT-NDI homopolymer (P_8), which shows absorptions at 228 and 255 nm, the peaks in the copolymers are slightly red-shifted (bathochromic shift). This shift may arise from altered

electronic environments or weak through-space interactions between the triazine and carbazole groups, brought about by their close proximity in the polymer chain. As the proportion of DCT-NDI increases toward P_{12}, this bathochromic effect becomes slightly more pronounced, suggesting enhanced interchromophoric interactions.

The observed spectral evolution from P_9 to P_{12} demonstrates the tunability of optical properties through compositional control. The consistent position of the CAH-NDI peaks alongside diminishing intensity confirms the retention of carbazole optical characteristics with predictable modulation. Meanwhile, the shifted triazine peaks point to subtle environmental or conformational influences introduced by copolymerization. These findings are significant for designing functional materials where optical absorption can be tailored by simply adjusting monomer feed ratios, a promising strategy for light-harvesting or electronic applications.

6.9. Thermal Behavior of Homopolymers and Copolymers (P_7–P_{12})

The thermal characteristics of the synthesized homopolymers (P_7 and P_8) and copolymers (P_9–P_{12}) were examined using differential scanning calorimetry (DSC) to determine their glass transition temperatures (Tg), a key parameter indicating polymer chain mobility and thermal stability. Measurements were performed under a nitrogen atmosphere, with samples heated from 50 °C to 250 °C at a rate of 10 °C/min. As illustrated in (Figure 6. 15) to (Figure 6. 17), the homopolymer P_7 exhibited a Tg at 117.8 °C, while P_8 displayed a slightly lower Tg of 106 °C. The relatively high Tg values, along with the broad, featureless curves, suggest that both homopolymers are amorphous in nature and lack significant crystallinity.

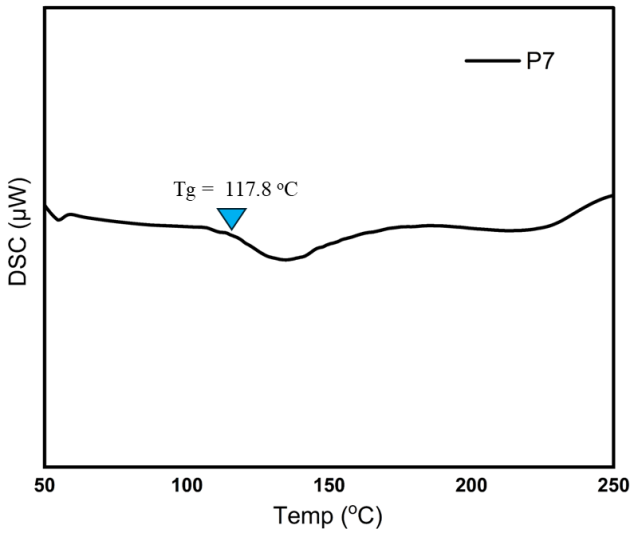

Figure 6. 15 DSC analysis of homopolymer P_7

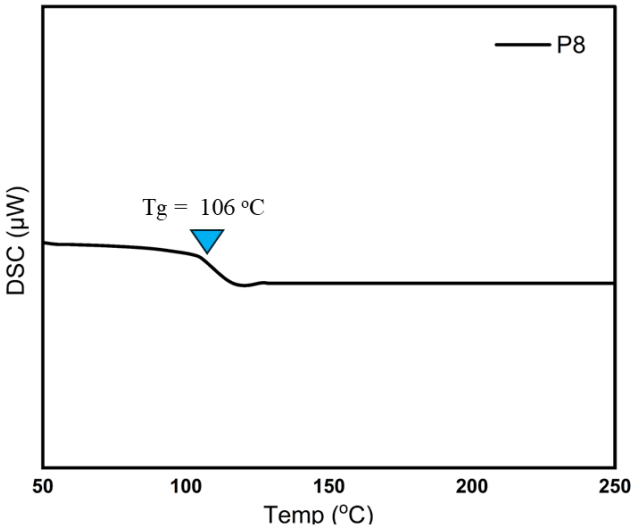

Figure 6. 16 DSC analysis of homopolymer P_8

For the copolymer series, the Tg values were more varied: 60 °C for P_9, 71.5 °C for P_{10}, 105 °C for P_{11}, and 90 °C for P_{12}. A clear trend can be observed where Tg increases with higher content of the CAH-NDI unit, known for its more rigid and thermally stable carbazole-based structure. Specifically, P_9, which contains the lowest CAH-NDI content, showed the lowest Tg, while P_{11}, with equal parts CAH-NDI and DCT-NDI, exhibited a Tg almost comparable to the homopolymers. Interestingly, P_{12}, with the highest DCT-NDI content, displayed a moderate Tg (90 °C), which may reflect a compromise between flexibility from the triazine-based units and structural integrity from the imide linkage.

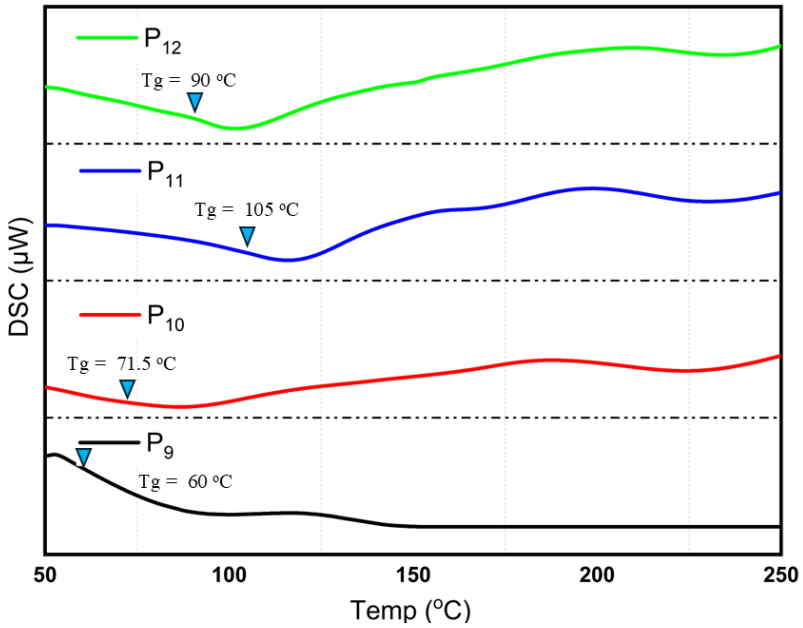

Figure 6. 17 DSC analysis of copolymers P_9 -P_{12}

Additionally, the DSC thermograms of all copolymers revealed broader transitions with no distinct melting points, indicating that they are also amorphous. However, the shape of the curves differed from those of the homopolymers and suggested the presence of a crosslinked network structure, particularly in P_{11} and P_{12}. This behavior can be attributed to the multifunctional nature of the monomers and potential intermolecular interactions, which limit segmental motion and raise thermal resistance. These results confirm that by altering the monomer feed ratio, it is possible to tailor the thermal properties of the resulting copolymers to suit specific material applications.

6.10. Conclusion

This chapter detailed the successful synthesis of donor (CAH-NDI, M_5) and acceptor (DCT-NDI, M_6) monomers, confirmed through comprehensive characterization via NMR and mass spectrometry. Controlled ROMP polymerization of these monomers yielded homopolymers (P_7, P_8) and copolymers (P_9–P_{12}), with GPC analysis verifying the well-regulated growth of polymer chains and narrow dispersity (Đ). While the UV-Vis spectra of the polymers revealed characteristic absorption bands of the constituent monomers, no emergent optoelectronic properties (e.g., intramolecular charge transfer) were observed, likely due to the non-conjugated backbone limiting electronic communication between side-chain chromophores. Nevertheless, the systematic optimization of polymerization

conditions and the modular copolymerization strategy established a robust platform for future structural modifications aimed at enhancing optoelectronic performance. These findings underscore the importance of backbone design in governing material properties and provide a foundation for further exploration of side-chain engineering to achieve functional TADF polymers

Chapter 7

Conclusions, Recommendations, and Future Work

7.1. Conclusions

This thesis, titled "Synthesis and Characterization of Homopolymers and Copolymers via ROMP Based on High-Strain Cyclic Alkenes as Potential Candidates for Organic Electronics and Electro-Optic Device Applications", presented the design, synthesis, and thorough characterization of a range of functional polymers prepared via ROMP. By utilizing high-strain cyclic alkenes such as norbornene derivatives and cyclophanediene, we established a modular platform for constructing well-defined homopolymers and copolymers with tunable optoelectronic properties.

The study began with the synthesis of soluble poly(*p*-phenylenevinylene) (PPV) derivatives P_1 and P_2 based on cyclophanediene monomers, which showed excellent solubility, narrow polydispersity, and favorable optical characteristics. In the next phase, poly (NDI) derivatives P_3 and P_4 were developed using monomers bearing functional groups such as carbazole and adamantane, which offered enhanced thermal stability and structural versatility.

Random copolymers P_5 and P_6 were synthesized by integrating PPV and NDI-based units, effectively combining the optical activity of conjugated systems with the robustness of NDI segments. The final stage involved donor–acceptor polymer design, where carbazole (donor) and trichlorotriazine (acceptor) units were incorporated into homopolymers (P_7 and P_8) and copolymers (P_9–P_{12}) through ROMP. These materials displayed composition-dependent photophysical properties, providing insights into how monomer feed ratios influence the resulting polymer behavior.

Overall, this work demonstrates the power of ROMP in synthesizing functional macromolecules from high-strain monomers. The findings validate the potential of these tailored polymers as promising materials for organic electronics and electro-optic device applications, paving the way for further exploration in material design and performance optimization.

7.2. Recommendations

- The ROMP method proved efficient and modular; it is recommended to further exploit this technique using other functional monomers to explore a broader range of properties.

- For device-related applications, such as OLEDs or OPVs, it is recommended to proceed with thin-film device fabrication and performance testing to validate the practical potential of the synthesized polymers.
- Improved monomer design, particularly through fine-tuning donor–acceptor strengths and side chain engineering, is advised to further optimize solubility, thermal stability, and emission properties.

7.3.Future Work

Building on the findings of this thesis, future research will explore the design and synthesis of solution-processable multi-resonance thermally activated delayed fluorescence (MR-TADF) pendant polymers via ROMP for application in ultra-low power consumption OLEDs. The strategy involves incorporating MR-TADF chromophores as pendant units onto non-conjugated polymer backbones to overcome limitations in solubility and processability commonly associated with rigid, planar emitters. By tuning the polymer architecture, chromophore density, and backbone flexibility, the goal is to achieve narrowband emission, high photoluminescence quantum yields (PLQYs), and excellent film-forming properties. Additionally, these materials will be evaluated for compatibility with scalable solution-processing techniques such as spin coating and inkjet printing, with a focus on developing high-efficiency OLEDs that meet the demands of next-generation display and lighting technologies.

Bibliography

[1] T. Perumal, C. Krebs de Souza, T.C. Nihues, P. Jain, K.K. Gaikwad, S. Roy, A review on biopolymer-based oil and water-resistant functional paper coating for food packaging, Food Biosci. 63 (2025) 105656. https://doi.org/10.1016/j.fbio.2024.105656.

[2] Y. Guo, D. Qiao, S. Zhao, B. Zhang, F. Xie, Advanced functional chitosan-based nanocomposite materials for performance-demanding applications, Prog. Polym. Sci. 157 (2024) 101872. https://doi.org/10.1016/j.progpolymsci.2024.101872.

[3] Q. Zhang, Y. Jin, S. Qi, Q. Ma, Z. Wang, P. Lv, F. Shi, W. Wei, Overview of fiber-shaped energy storage devices: From fabrication to application, Nano Energy 128 (2024). https://doi.org/10.1016/j.nanoen.2024.109896.

[4] K. Yaemsunthorn, W. Macyk, J. Ortyl, Semiconductor photocatalysts in photopolymerization processes: Mechanistic insights, recent advances, and future prospects, Prog. Polym. Sci. 158 (2024) 101891. https://doi.org/10.1016/j.progpolymsci.2024.101891.

[5] Y. Bae, D. Kim, S. Li, Y. Choi, S.Y. Son, T. Park, L. Ye, Stability of Intrinsically Stretchable Polymer Photovoltaics: Fundamentals, Achievements, and Perspectives, Prog. Polym. Sci. 159 (2024). https://doi.org/10.1016/j.progpolymsci.2024.101899.

[6] P. Siwach, L. Gaba, S. Dahiya, R. Punia, A.S. Maan, K. Singh, A. Ohlan, Recent progress in conjugated polymers composites with metal-organic frameworks as electrode materials for supercapacitors, Appl. Surf. Sci. Adv. 19 (2024) 100555. https://doi.org/10.1016/j.apsadv.2023.100555.

[7] C.S. Dziewior, K. Godwin, N.G. Judge, N.Z. Dreger, M.L. Becker, Poly(ester urea)s: Synthesis, material properties, and biomedical applications, Prog. Polym. Sci. 156 (2024). https://doi.org/10.1016/j.progpolymsci.2024.101866.

[8] H. Shirakawa, E.J. Louis, A.G. MacDiarmid, C.K. Chiang, A.J. Heeger, Synthesis of electrically conducting organic polymers: Halogen derivatives of polyacetylene, (CH)x, J. Chem. Soc. Chem. Commun. (1977) 578–580. https://doi.org/10.1039/C39770000578.

[9] M. Audenaert, G. Gusman, R. Deltour, Electrical conductivity of I2-doped polyacetylene, Phys. Rev. B 24 (1981) 7380–7382. https://doi.org/10.1103/PhysRevB.24.7380.

[10] H. Jiang, P. Taranekar, J.R. Reynolds, K.S. Schanze, Conjugated polyelectrolytes: Synthesis, photophysics, and applications, Angew. Chemie - Int. Ed. 48 (2009) 4300–4316. https://doi.org/10.1002/anie.200805456.

[11] Y. He, W. Hong, Y. Li, New building blocks for π-conjugated polymer semiconductors for organic thin film transistors and photovoltaics, J. Mater. Chem. C 2 (2014) 8651–8661. https://doi.org/10.1039/c4tc01201a.

[12] A.H. Malik, S. Hussain, S.R. Chowdhury, P.K. Iyer, Conjugated Polymers for Disease Diagnosis and Theranostics Medicine, Conjug. Polym. Biol. Biomed. Appl. (2018) 321–358. https://doi.org/10.1002/9783527342747.ch12.

[13] X. Chen, S. Hussain, A. Abbas, Y. Hao, A.H. Malik, X. Tian, H. Song, R. Gao, Conjugated polymer nanoparticles and their nanohybrids as smart photoluminescent and photoresponsive material for biosensing, imaging, and theranostics, Springer Vienna, 2022. https://doi.org/10.1007/s00604-021-05153-w.

[14] L. Ding, Z. Di Yu, X.Y. Wang, Z.F. Yao, Y. Lu, C.Y. Yang, J.Y. Wang, J. Pei, Polymer Semiconductors: Synthesis, Processing, and Applications, Chem. Rev. 123 (2023) 7421–7497. https://doi.org/10.1021/acs.chemrev.2c00696.

[15] A. Uva, S. Michailovich, N.S.Y. Hsu, H. Tran, Degradable π-Conjugated Polymers, J. Am. Chem. Soc. 146 (2024) 12271–12287. https://doi.org/10.1021/JACS.4C03194.

[16] Q. Yang, A. Vriza, C.A. Castro Rubio, H. Chan, Y. Wu, J. Xu, Artificial Intelligence for Conjugated Polymers, Chem. Mater. 36 (2024) 2602–2622. https://doi.org/10.1021/acs.chemmater.3c02358.

[17] Z. Chen, X. Ding, J. Wang, X. Guo, S. Shao, K. Feng, π-Conjugated Polymers for High-Performance Organic Electrochemical Transistors: Molecular Design Strategies, Applications and Perspectives, Angew. Chemie - Int. Ed. 202423013 (2025). https://doi.org/10.1002/anie.202423013.

[18] N.T. Debele, H.G. Menge, T.G. Weldemhret, A.T. Reda, Y.T. Park, Conjugated Polymer-Based Multilayer Thin-Film Triboelectric Nanogenerators via Continuous Layer-By-Layer Coating Process, ACS Appl. Mater. Interfaces (2024). https://doi.org/10.1021/acsami.4c18480.

[19] L. Han, F. He, Controllable Self-Assembly Morphologies of PPV-Based Block Copolymers, Chem. - A Eur. J. 202404380 (2025). https://doi.org/10.1002/chem.202404380.

[20] N. Donthu, S. Kumar, D. Mukherjee, N. Pandey, W.M. Lim, How to conduct a bibliometric analysis: An overview and guidelines, J. Bus. Res. 133 (2021) 285–296. https://doi.org/10.1016/j.jbusres.2021.04.070.

[21] K. Yokawa, T. Higashihara, Recent progress in nonstoichiometric step-growth polymerization, Polym. Chem. (2024) 11–26. https://doi.org/10.1039/d4py01091d.

[22] Addition Polymerization - an overview | ScienceDirect Topics, (n.d.). https://www.sciencedirect.com/topics/chemical-engineering/addition-polymerization (accessed March 21, 2025).

[23] K. Nishimori, M. Ouchi, AB-alternating copolymers: Via chain-growth polymerization: Synthesis, characterization, self-assembly, and functions, Chem. Commun. 56 (2020) 3473–3483. https://doi.org/10.1039/d0cc00275e.

[24] A.C. Grimsdale, K.L. Chan, R.E. Martin, P.G. Jokisz, A.B. Holmes, Synthesis of light-emitting conjugated polymers for applications in electroluminescent devices, Chem. Rev. 109 (2009) 897–1091. https://doi.org/10.1021/cr000013v.

[25] S.W. Thomas, G.D. Joly, T.M. Swager, Chemical sensors based on amplifying fluorescent conjugated polymers, Chem. Rev. 107 (2007) 1339–1386. https://doi.org/10.1021/cr0501339.

[26] A.H. Malik, F. Habib, M.J. Qazi, M.A. Ganayee, Z. Ahmad, M.A. Yatoo, A short review article on conjugated polymers, J. Polym. Res. 30 (2023) 1–15. https://doi.org/10.1007/s10965-023-03451-w.

[27] C.J.M. Stirling, Sulfonium Salts, Org. Chem. Sulfur 66 (1977) 473–525. https://doi.org/10.1007/978-1-4684-2049-4_9.

[28] H.G. Gilch, W.L. Wheelwright, Polymerization of α-halogenated p -xylenes with base , J. Polym. Sci. Part A-1 Polym. Chem. 4 (1966) 1337–1349. https://doi.org/10.1002/pol.1966.150040602.

[29] T. Schwalm, J. Wiesecke, S. Immel, M. Rehahn, Toward controlled Gilch synthesis of poly(p-phenylene vinylenes): Anionic vs radical chain propagation, a mechanistic reinvestigation, Macromolecules 40 (2007) 8842–8854. https://doi.org/10.1021/ma071337p.

[30] J.A. Mikroyannidis, Synthesis by Heck coupling of soluble, blue-light-emitting fully conjugated poly(p-phenylenevinylene)s with highly phenylated side groups, Macromolecules 35 (2002) 9289–9295. https://doi.org/10.1021/ma021242h.

[31] A. Mann, M.D. Hannigan, M. Weck, Cyclophanediene and Cyclophanetriene-Based Conjugated Polymers, Macromol. Chem. Phys. 224 (2023) 1–17. https://doi.org/10.1002/macp.202200397.

[32] M.Z. Basyouni, M.E. Abdu, M.F. Radwan, A.M. Spring, Ring-Opening Metathesis Polymerization of Homo- and Copolymers Based on p-Phenylenevinylene and Norbornene-Dicarboximide: Enhanced Thermal Stability for Optoelectronic Applications, J. Mol. Struct. (2025) 142296. https://doi.org/10.1016/J.MOLSTRUC.2025.142296.

[33] D.J. Gaspar, E. Polikarpov, OLED fundamentals: Materials, devices, and processing of organic light-emitting diodes, 2015. https://doi.org/10.1201/b18485.

[34] C.W. Tang, S.A. Vanslyke, Organic electroluminescent diodes, Appl. Phys. Lett. 51 (1987) 913–915. https://doi.org/10.1063/1.98799.

[35] I. Edition, Chemie, (n.d.). https://doi.org/10.1002/anie.202505608.

[36] C. Pasgrimaud, A.H.G. David, D. Maria, E. Chatir, O. Al, M. Legros, L. Le Bras, E. Levillain, A. Goujon, Synthesis of Electron-Deficient BisAzaCoroneneDiimide-Conjugated Polymers by Light-Locking Dynamic Covalent Bonds^, (2025). https://doi.org/10.1021/jacs.5c01351.

[37] L. Hua, H. Wu, Z. Xia, M. Li, Y. Liu, S. Yan, W. Zhu, J.Y. Lee, Z. Ren, Y. Wang, Narrowband Emissive Solution-Processed Polymer Organic Light-Emitting Diodes with External Quantum Efficiency Above 30%, Adv. Mater. 2502180 (2025) 1–8. https://doi.org/10.1002/adma.202502180.

[38] N. Wang, H. Zhong, M. Duan, X. Gao, Z. Tan, J. Deng, B. Zhao, Hierarchical Chirality Transfer and Amplification within Conjugated Helical Polymers for Efficient Circularly Polarized Organic Light-Emitting Diodes and Photodetectors, ACS Appl. Mater. Interfaces (2025). https://doi.org/10.1021/acsami.5c01915.

[39] T. Wang, S. Wang, J. Dong, G. Chen, J. Liu, M. Huang, Z. Chen, Z. Huang, C. Yang, Blue Multiresonance Thermally Activated Delayed Fluorescence Conjugated Polymers for Solution-Processable Narrowband Blue Organic Light-Emitting Diodes with High Color-Purity, Macromolecules (2024). https://doi.org/10.1021/acs.macromol.4c02674.

[40] K. Youssef, A. Gasonoo, C. Cougnon, M. Loumaigne, H. Melville, L. Sanguinet, G.C. Welch, F. Gohier, Optoelectronic properties study of arylamine-functionalized benzothiophenes and benzothiophene S,S-Dioxides. Application in

solution-processed organic light-emitting diodes, Dye. Pigment. 232 (2025). https://doi.org/10.1016/j.dyepig.2024.112468.

[41] M. Wei, D.F. Perepichka, Benzodithiophene-based polymer donors for organic photovoltaics, J. Mater. Chem. A (2025) 12785–12807. https://doi.org/10.1039/d4ta07020h.

[42] A. Al Shafe, S. Raza, R. Henry, J. Liu, B.T. O'Connor, Improving Adhesion in Organic Photovoltaic Cells with Self-Assembled Monolayers, ACS Energy Lett. (2025) 1865–1873. https://doi.org/10.1021/acsenergylett.5c00490.

[43] K. Ahmad Mustamin, M. Sani Sarjadi, S.M. Sarkar, S. Kumar, M.L. Rahman, Optimization of Polymers for Organic Solar Cells: Effects of Alkyl, Fluorinated and Thiophenated Chains, Chem. - An Asian J. 202401406 (2025) 1–11. https://doi.org/10.1002/asia.202401406.

[44] C.H. Chung, Y.C. Huang, S.W. Su, C.J. Su, U.S. Jeng, J.Y. Chen, Y.C. Lin, Partially Degradable N-Type Conjugated Random Copolymers for Intrinsically Stretchable Organic Field-Effect Transistors, Macromol. Rapid Commun. 2401057 (2025) 1–11. https://doi.org/10.1002/marc.202401057.

[45] Y. Son, T. Kim, H. Kim, Y. Kim, Pronounced Light Insensitivity in Low-Voltage n-Channel Organic Field-Effect Transistors with Channel Layers of Dinitrobenzothiadiazole-Containing Conjugated Polymer, ACS Appl. Electron. Mater. (2024). https://doi.org/10.1021/acsaelm.4c01473.

[46] H. Chen, R. Xie, J. Tang, X. Liu, J. Li, C. Liu, Y. Qiang, C. Yang, L. Zhang, J. Chen, X. Liu, Charge Polarity Modulation and Efficient Electron Transport in Quinoid-Donor-Acceptor Polymers by Acceptor Engineering for High-Performance Transistors, Macromolecules (2025). https://doi.org/10.1021/acs.macromol.4c02596.

[47] J.Y. Lin, F.C. Hsu, Y.C. Chao, C.C. Ho, M.C. Lai, T.Y. Li, Y.F. Chen, High-Performance Organic Field-Effect Transistors Based on a Self-Assembled Polar Dielectric Monolayer, ACS Appl. Electron. Mater. (2025). https://doi.org/10.1021/acsaelm.5c00088.

[48] S. Liu, Z. You, T. Wu, Y. Feng, J. Cao, L. Hou, Z. Yu, Toward Eco-Friendly Solvent-Processable DPP-Based Conjugated Polymers with Siloxane Branched Side Chains: Synthesis, Properties, and Ambipolar Field-Effect Transistor Characteristics, ACS Appl. Electron. Mater. (2025). https://doi.org/10.1021/acsaelm.4c02364.

[49] J. Sun, T. Huang, Z. Wang, Multiple Scattering-Enhanced Fluorescence Within Randomly Oriented Low-Index Polymer Nanofiber Sensors, Biosensors 15 (2025) 1–14. https://doi.org/10.3390/bios15020097.

[50] C. Amoah, W.G. Skene, Survey of Sustainable Wearable Strain Sensors Enabled by Biopolymers and Conductive Organic Polymers, Gels 11 (2025). https://doi.org/10.3390/gels11040235.

[51] R. Zhao, W. Wang, Y. Liu, P. Petkov, A.H. Khan, L. Gao, P. Zhang, E. Brunner, H.I. Wang, S. Singh, S. Huang, L.A. Panes-ruiz, Y. Vaynzof, M. Bonn, G. Cuniberti, M. Wang, X. Feng, Communication A Donor – Acceptor-Type Two-Dimensional Poly (Arylene Vinylene) for Efficient Electron Transport and Sensitive Chemiresistors, (2025). https://doi.org/10.1002/anie.202504302.

[52] T. Pradhan, D.K. Chelike, D. Roy, T. Pramanik, S. Dolui, Stimuli-Responsive Multiacceptor Conjugated Polymers: Recent Trend and Future Direction, ACS Polym. Au (2025). https://doi.org/10.1021/acspolymersau.4c00082.

[53] N. Zhao, S.J. Jeon, Y. Yuan, S. Venkateswarlu, A. Stella, J. Papazotos, Y. Li, Full Conjugation in a Polymer with Non-conjugated Piperazine-2,5-dione Units via Energy-minimized Lactam-to-Lactim Tautomerization Enables Water-gated Transistor Fluoride Sensors, Angew. Chemie - Int. Ed. 202419314 (2024). https://doi.org/10.1002/anie.202419314.

[54] J. Asrar, Metathesis Polymerization of N-Phenylnorbornenedicarboximide, Macromolecules 25 (1992) 5150–5156. https://doi.org/10.1021/ma00046a006.

[55] J.B. Williamson, S.E. Lewis, R.R. Johnson, I.M. Manning, F.A. Leibfarth, C−H Functionalization of Commodity Polymers, Angew. Chemie - Int. Ed. 58 (2019) 8654–8668. https://doi.org/10.1002/anie.201810970.

[56] A.J. Hackett, J. Malmström, J. Travas-Sejdic, Functionalization of conducting polymers for biointerface applications, Prog. Polym. Sci. 70 (2017) 18–33. https://doi.org/10.1016/j.progpolymsci.2017.03.004.

[57] P.L. dos Santos, P. Stachelek, Y. Takeda, P. Pander, Recent advances in highly-efficient near infrared OLED emitters, Mater. Chem. Front. (2024) 1731–1766. https://doi.org/10.1039/d3qm01067h.

[58] J. Lyu, C.W. Bielawski, New classes of functionalized parylenes and poly(phenylene vinylene)s: Via coupling of dihaloxylyl diesters, Polym. Chem. 13 (2022) 613–621. https://doi.org/10.1039/d1py01063h.

[59] D.M. Bobrowska, K. Gdula, J. Breczko, A. Basa, K.H. Markiewicz, K. Winkler, Poly(p-phenylene vinylene) incorporated into carbon nanostructures, J. Nanoparticle Res. 24 (2022). https://doi.org/10.1007/s11051-022-05589-y.

[60] M.M. Szindler, M. Szindler, Comparison of the optical and electrical energy band gap of a thin layer of polyelectrolyte based on MEH-PPV and KI, IOP Conf. Ser. Mater. Sci. Eng. 1178 (2021) 012055. https://doi.org/10.1088/1757-899x/1178/1/012055.

[61] K. Namsheer, C.S. Rout, Conducting polymers: a comprehensive review on recent advances in synthesis, properties and applications, RSC Adv. 11 (2021) 5659–5697. https://doi.org/10.1039/d0ra07800j.

[62] Y. Sun, T. Liu, Y. Kan, K. Gao, B. Tang, Y. Li, Flexible Organic Solar Cells: Progress and Challenges, Small Sci. 1 (2021). https://doi.org/10.1002/smsc.202100001.

[63] J.D. Feist, Y. Xia, Enol Ethers Are Effective Monomers for Ring-Opening Metathesis Polymerization: Synthesis of Degradable and Depolymerizable Poly(2,3-dihydrofuran), J. Am. Chem. Soc. 142 (2020) 1186–1189. https://doi.org/10.1021/jacs.9b11834.

[64] T. Tang, G. Ahumada, C.W. Bielawski, Direct laser writing of poly(phenylene vinylene) on poly(barrelene), Polym. Chem. 11 (2020) 5437–5443. https://doi.org/10.1039/d0py00869a.

[65] R. O'Shea, W.W.H. Wong, Simple improvements to Gilch synthesis and molecular weight modulation of MEH-PPV, Polym. Chem. 11 (2020) 2831–2837. https://doi.org/10.1039/d0py00072h.

[66] F. Koch, W. Heitz, Soluble poly(1,4-phenylenevinylene)s and poly(1,4-phenyleneethynylene)s via Suzuki coupling, Macromol. Chem. Phys. 198 (1997) 1531–1544. https://doi.org/10.1002/macp.1997.021980517.

[67] M. Rehahn, A. Schlüter, Soluble poly(p -phenylenevinylene)s from 2,5-dihexylterephthalaldehyde using the improved McMurry reagent , Die Makromol. Chemie, Rapid Commun. 11 (1990) 375–379. https://doi.org/10.1002/marc.1990.030110806.

[68] P. Damlin, C. Kvarnström, A. Petr, A. Neudeck, L. Dunsch, A. Ivaska, In situ spectroelectrochemical and rotating ring-disk electrode studies on the initial states in the reductive electropolymerization of poly(p-phenylene vinylene), Macromolecules 35 (2002) 5789–5795. https://doi.org/10.1021/ma0118116.

[69] M. Rimmele, K. Ableidinger, A. V. Marsh, N.J. Cheetham, M.J. Taublaender, A. Buchner, J. Prinz, J. Fröhlich, M.M. Unterlass, M. Heeney, F. Glöcklhofer, Thioalkyl- and sulfone-substituted poly(: P -phenylene vinylene)s, Polym. Chem. 10 (2019) 738–750. https://doi.org/10.1039/c8py01717d.

[70] E. Elacqua, G.T. Geberth, D.A. Vanden Bout, M. Weck, Synthesis and folding behaviour of poly(p-phenylene vinylene)-based β-sheet polychromophores, Chem. Sci. 10 (2019) 2144–2152. https://doi.org/10.1039/c8sc05111a.

[71] T. Schwalm, J. Wiesecke, S. Immel, M. Rehahn, The gilch synthesis of poly(p-phenylene vinylenes): Mechanistic knowledge in the service of advanced materials, Macromol. Rapid Commun. 30 (2009) 1295–1322. https://doi.org/10.1002/marc.200900104.

[72] S. Pfeiffer, H. Ho, alkenylidene) s by applying the Horner-reaction for condensation polymerization, Synthesis (Stuttg). 1878 (1999) 1870–1878.

[73] K.L. Makovetsky, E.S. Finkel'shtein, I.Y. Ostrovskaya, E.B. Portnykh, L.I. Gorbacheva, A.I. Golberg, N. V. Ushakov, Y.P. Yampolsky, Ring-opening metathesis polymerization of substituted norbornenes, J. Mol. Catal. 76 (1992) 107–121. https://doi.org/10.1016/0304-5102(92)80150-F.

[74] M.Z. Basyouni, M.E. Abdu, M.F. Radwan, A.M. Spring, Ring-opening metathesis polymerization of homo- and copolymers Based on p -phenylenevinylene and norbornene-dicarboximide : Enhanced thermal stability for optoelectronic applications, J. Mol. Struct. 1338 (2025) 142296. https://doi.org/10.1016/j.molstruc.2025.142296.

[75] M.E. Abdu, M.F. Radwan, D.A. Elsayed, W.S. Shehab, W.A. Zordok, M.Z. Basyouni, A.M. Spring, Controlled synthesis , characterization and computational studies of novel homo and random Co-polymers from carbazolovinylene and phenothiazinovinylene via ROMP chemistry, Polymer (Guildf). 333 (2025) 128590. https://doi.org/10.1016/j.polymer.2025.128590.

[76] M.Z. Basyouni, K. Nomura, Y. Goroumaru, M.F. Radwan, M.E. Abdu, Controlled synthesis of PPV oligomers by ROMP : impact on optical , structural , and thermal properties, Chem. Pap. (2025). https://doi.org/10.1007/s11696-025-04091-8.

[77] J. Pecher, S. Mecking, Nanoparticles of conjugated polymers, Chem. Rev. 110 (2010) 6260–6279. https://doi.org/10.1021/cr100132y.

[78] N. Nurwidiana, B.M. Sopha, A. Widyaparaga, Modelling photovoltaic system adoption for households: A systematic literature review, Evergreen 8 (2021) 69–81. https://doi.org/10.5109/4372262.

[79] A. Mann, M. Weck, Synthesis and Polymerization of an ortho- para-Substituted Tetraalkoxy [2.2]Paracyclophane-1,9-diene, ACS Macro Lett. 11 (2022) 1055–1059. https://doi.org/10.1021/acsmacrolett.2c00398.

[80] V. Komanduri, D.J. Tate, R. Marcial-Hernandez, D.R. Kumar, M.L. Turner, Synthesis and ROMP of Benzothiadiazole Paracyclophane-1,9-Dienes to Donor-Acceptor Alternating Arylenevinylene Copolymers, Macromolecules 52 (2019) 7137–7144. https://doi.org/10.1021/acs.macromol.9b01244.

[81] K.H. Yoon, K.O. Kim, M. Schaefer, D.Y. Yoon, Synthesis and characterization of hydrogenated poly(norbornene endo-dicarboximide)s prepared by ring opening metathesis polymerization, Polymer (Guildf). 53 (2012) 2290–2297. https://doi.org/10.1016/j.polymer.2012.02.047.

[82] A.M. Spring, F. Qiu, S. Yokoyama, High stability poly(N-adamantyl-exo-norbornene-5,6-dicarboximide) and phenyl vinylene thiophene electro-optic host-guest system, Eur. Polym. J. 84 (2016) 89–99. https://doi.org/10.1016/j.eurpolymj.2016.09.012.

[83] I. Mandal, A.F.M. Kilbinger, A Versatile Reversible, Degenerative Chain Transfer Mechanism for the Catalytic Living Ring-Opening Metathesis Polymerization, Angew. Chemie Int. Ed. (2024). https://doi.org/10.1002/anie.202409781.

[84] F.A. Feist, G. Tommaseo, T. Basché, Single-molecule spectroscopy of MEH-PPV polymer molecules in different host matrices', J. Phys. Chem. C 113 (2009) 11484–11490. https://doi.org/10.1021/jp901816q.

[85] Z. Gao, X. Zhao, G. Luo, W. Yang, W. Zhang, H. Wang, C. Zong, L. Lei, H. Li, Anti-fouling amphiphilic surfaces from norbornene-based fluorinated copolymers with excellent mechanical properties, Prog. Org. Coatings 190 (2024) 108361. https://doi.org/10.1016/j.porgcoat.2024.108361.

[86] B.R. Kordes, G. Mourgas, M. Steinmann, T. Schneck, I. Elser, M.R. Buchmeiser, Ring-Opening Metathesis Polymerization-Derived Poly(dicyclopentadiene)/Fiber Composites Using Latent Pre-Catalysts, Macromol. Mater. Eng. 309 (2024) 1–6. https://doi.org/10.1002/mame.202300367.

[87] M.H. Kabir, S. Kannan, K.A. Veetil, E.K. Sun, T.H. Kim, Enhancing CO2 Transport Across the PEG/PPG-Based Crosslinked Rubbery Polymer Membranes

with a Sterically Bulky Carbazole-Based ROMP Comonomer, Macromol. Rapid Commun. 2400296 (2024) 1–12. https://doi.org/10.1002/marc.202400296.

[88] Y. Yan, X. Zhang, Y. Wang, S. Xue, S. Liu, Q. Ye, F. Zhou, W. Liu, Grafting Poly(Ionic Liquid)s on Covalent Organic Frameworks via Surface-Initiated Ring-Opening Metathesis Polymerization for Enhancing Lubrication Performance, ACS Appl. Polym. Mater. 6 (2024) 10072–10082. https://doi.org/10.1021/acsapm.4c01654.

[89] Q. Zhang, J. Zhao, X. Shi, Y. Zhang, J. Wang, J. Wei, J. Li, C. Ma, Y. Du, High Voltage and Cycling Stable Norbornene-Based Polycarbonate Electrolyte for Lithium Metal Battery, ACS Mater. Lett. 6 (2024) 3675–3682. https://doi.org/10.1021/acsmaterialslett.4c00987.

[90] C.J. Liu, C.C. Wang, D.L. Kuo, C.Y. Yu, Carbazolevinylene and phenylenevinylene polymers by ring-opening metathesis polymerization and their characterization, nanoaggregates and optical and electrochemical properties, Polymer (Guildf). 181 (2019) 121770. https://doi.org/10.1016/j.polymer.2019.121770.

[91] B. Alkan, B.A. Temel, H. Durmaz, G. Temel, Preparation of poly(oxanorbornene) based single and double-folding polymers via nucleophilic aromatic substitution reaction, Eur. Polym. J. 203 (2024) 112694. https://doi.org/10.1016/j.eurpolymj.2023.112694.

[92] A. Mann, C. Wang, B.L. Dumlao, M. Weck, Functionalized [2.2]Paracyclophanedienes as Monomers for Poly(p-phenylenevinylene)s, ACS Macro Lett. (2024) 112–117. https://doi.org/10.1021/acsmacrolett.3c00714.

[93] Y. Janpatompong, V. Komanduri, R.U. Khan, M.L. Turner, Synthesis and ring-opening metathesis polymerisation of o-alkoxy benzothiadiazole paracyclophane-1,9-dienes, Org. Biomol. Chem. 21 (2023) 3245–3250. https://doi.org/10.1039/d2ob01989b.

[94] Z. Hassan, E. Spuling, D.M. Knoll, S. Bräse, Regioselective Functionalization of [2.2]Paracyclophanes: Recent Synthetic Progress and Perspectives, Angew. Chemie - Int. Ed. 59 (2020) 2156–2170. https://doi.org/10.1002/anie.201904863.

[95] M. Peters, N. Zaquen, L. D'Olieslaeger, H. Bové, D. Vanderzande, N. Hellings, T. Junkers, A. Ethirajan, PPV-Based Conjugated Polymer Nanoparticles as a Versatile Bioimaging Probe: A Closer Look at the Inherent Optical Properties and

Nanoparticle-Cell Interactions, Biomacromolecules 17 (2016) 2562–2571. https://doi.org/10.1021/acs.biomac.6b00574.

[96] M.Z. Basyouni, J. Ye, A.M. Spring, Conjugated Polymers and ROMP: Synthesis, Applications, and Prospects for Technological Innovations, Int. Exch. Innov. Conf. Eng. Sci. 9 (2023) 405–411. https://doi.org/10.5109/7158031.

[97] M.F. Radwan, E.E. Elboray, H.M. Dardeer, Y. Kobayashi, T. Furuta, S. Hamada, T. Dohi, M.F. Aly, 1,3-Dipolar Cycloaddition of 3-Chromonyl-Substituted Glycine Imino Esters with Arylidenes and in situ Diastereodivergent via Retrocycloaddition, Chem. - An Asian J. 18 (2023). https://doi.org/10.1002/asia.202300215.

[98] A.A. El-Shehawy, M.E. Abdu, M.M. El-Hendawy, M. El-Khouly, M.H. Sherif, H.Y. Moustafa, Synthesis, photophysical, and theoretical studies on π-conjugated copolymers based on benzothiadiazole and cyanopyridine acceptor moieties along with other π-bridge units, J. Phys. Org. Chem. 34 (2021) 1–15. https://doi.org/10.1002/poc.4158.

[99] E. Elacqua, M. Gregor, Poly(arylenevinylene)s through Ring-Opening Metathesis Polymerization of an Unsymmetrical Donor-Acceptor Cyclophane, Angew. Chemie - Int. Ed. 58 (2019) 9527–9532. https://doi.org/10.1002/anie.201905137.

[100] V. Komanduri, D.R. Kumar, D.J. Tate, R. Marcial-Hernandez, B.J. Lidster, M.L. Turner, Bidirectional ROMP of paracylophane-1,9-dienes to tri- and penta-block: P -phenylenevinylene copolymers, Polym. Chem. 10 (2019) 3497–3502. https://doi.org/10.1039/c9py00147f.

[101] C.Y. Yu, Y.C. Chen, C.C. Wang, Synthesis and ring opening reaction of octaoctyl substituted [2.2.2.2](2,7)-fluorenophanetetraene by photooxidation, New J. Chem. 41 (2017) 14116–14121. https://doi.org/10.1039/c7nj02735d.

[102] D.R. Kumar, B.J. Lidster, R.W. Adams, M.L. Turner, Mechanistic investigation of the ring opening metathesis polymerisation of alkoxy and alkyl substituted paracyclophanedienes, Polym. Chem. 8 (2017) 3186–3194. https://doi.org/10.1039/c7py00543a.

[103] E. Elacqua, K.B. Manning, D.S. Lye, S.K. Pomarico, F. Morgia, M. Weck, Supramolecular Multiblock Copolymers Featuring Complex Secondary Structures, J. Am. Chem. Soc. 139 (2017) 12240–12250. https://doi.org/10.1021/jacs.7b06201.

[104] B.J. Lidster, D.R. Kumar, A.M. Spring, C.Y. Yu, M. Helliwell, J. Raftery, M.L. Turner, Alkyl substituted [2.2]paracyclophane-1,9-dienes, Org. Biomol. Chem. 14 (2016) 6079–6087. https://doi.org/10.1039/c6ob00885b.

[105] M. Li, F. Yang, X. Zhou, J. Du, D. Ding, J. Chu, J. Weng, Y.F. Yang, Y. She, J. Jia, Third-order nonlinear optical properties of phenothiazine-based imine covalent organic framework films, Mater. Today Chem. 38 (2024) 102137. https://doi.org/10.1016/j.mtchem.2024.102137.

[106] B.J. Lidster, S. Hirata, S. Matsuda, T. Yamamoto, V. Komanduri, D.R. Kumar, Y. Tezuka, M. Vacha, M.L. Turner, Macrocyclic poly(: P -phenylenevinylene)s by ring expansion metathesis polymerisation and their characterisation by single-molecule spectroscopy, Chem. Sci. 9 (2018) 2934–2941. https://doi.org/10.1039/c7sc03945j.

[107] T. Tsagaantsooj, X. Tang, T. Zhang, Y.T. Lee, R. Walia, X.K. Chen, C. Adachi, Peripheral Engineering of Multiple-Resonance Framework Targeting Efficient Organic Lasers, Angew. Chemie - Int. Ed. (2025). https://doi.org/10.1002/anie.202504652.

[108] F. Menk, S. Shin, K.O. Kim, M. Scherer, D. Gehrig, F. Laquai, T.L. Choi, R. Zentel, Synthesis of Functional Block Copolymers Carrying One Poly(p-phenylenevinylene) and One Nonconjugated Block in a Facile One-Pot Procedure, Macromolecules 49 (2016) 2085–2095. https://doi.org/10.1021/acs.macromol.5b02529.

[109] M.Z. Basyouni, M.F. Radwan, M.E. Abdu, A.M. Spring, Synthesis, Characterization, and Optical Properties of Carbazole-Functionalized Poly(norbornene-dicarboximide) by ROMP, Evergreen 11 (2024) 207–213.

[110] L. Caire Da Silva, S. Cao, K. Landfester, Bursting and Reassembly of Giant Double Emulsion Drops Form Polymer Vesicles, ACS Macro Lett. 10 (2021) 401–405. https://doi.org/10.1021/acsmacrolett.0c00849.

[111] C.Y. Yu, Y.C. Lai, Synthesis, aggregation induced emission and through space conjugation of triphenylvinylphenyl substituted [2.2]paracyclophane-1,9-diene, RSC Adv. 8 (2018) 19341–19347. https://doi.org/10.1039/c8ra03025a.

[112] F. Menk, M. Mondeshki, D. Dudenko, S. Shin, D. Schollmeyer, O. Ceyhun, T.L. Choi, R. Zentel, Reactivity Studies of Alkoxy-Substituted [2.2]Paracyclophane-1,9-dienes and Specific Coordination of the Monomer Repeating Unit during

ROMP, Macromolecules 48 (2015) 7435–7445. https://doi.org/10.1021/acs.macromol.5b01737.

[113] D. Mäker, C. Maier, K. Brödner, U.H.F. Bunz, Paracyclophane-trienes-attractive monomers for ROMP, ACS Macro Lett. 3 (2014) 415–418. https://doi.org/10.1021/mz500135s.

[114] S. Shin, K.Y. Yoon, T.L. Choi, Simple preparation of various nanostructures via in situ nanoparticlization of polyacetylene blocklike copolymers by one-shot polymerization, Macromolecules 48 (2015) 1390–1397. https://doi.org/10.1021/ma502530x.

[115] G. Park, C.W. Bielawski, Ring Opening Metathesis Polymerization of Cyclic Allenes, Macromolecules 54 (2021) 6135–6143. https://doi.org/10.1021/acs.macromol.1c00571.

[116] A.A. Lyapkov, L.S. Soroka, R. V. Ashirov, D.I. Zemlyakov, D.A. Rusakov, F. Verpoort, Kinetics of Dicyclopentadiene Polymerization in the Presence of the Second Generation Hoveyda-Grubbs Catalyst with N-Chelating Ligand, Polym. Sci. - Ser. C 61 (2019) 41–48. https://doi.org/10.1134/S1811238219010107.

[117] Y. Janpatompong, A.M. Spring, V. Komanduri, R.U. Khan, M.L. Turner, Synthesis and Ring-Opening Metathesis Polymerization of o-Dialkoxy Paracyclophanedienes, Macromolecules 55 (2022) 10854–10864. https://doi.org/10.1021/acs.macromol.2c02111.

[118] J.A. Love, J.P. Morgan, T.M. Trnka, R.H. Grubbs, A practical and highly active ruthenium-based catalyst that effects the cross metathesis of acrylonitrile, Angew. Chemie - Int. Ed. 41 (2002) 4035–4037. https://doi.org/10.1002/1521-3773(20021104)41:21<4087::AID-ANIE4087>3.0.CO;2-X.

[119] S.K. Pomarico, D.S. Lye, E. Elacqua, M. Weck, Synthesis of sheet-coil-helix and coil-sheet-helix triblock copolymers by combining ROMP with palladium-mediated isocyanide polymerization, Polym. Chem. 9 (2018) 5655–5659. https://doi.org/10.1039/c8py01361f.

[120] S. Mekcham, K. Nomura, Synthesis of Bottlebrush Polymers by Z-/E-Specific Living Ring-Opening Metathesis Polymerization, Exhibiting Different Thermal Properties, J. Am. Chem. Soc. 145 (2023) 17001–17006. https://doi.org/10.1021/jacs.3c05795.

[121] J. Wu, Y. Fu, W. Liu, X. Liao, M. Xie, R. Sun, Synthesis and properties of tricarbazole-functionalized poly(norbornene-dicarboximide), Eur. Polym. J. 76 (2016) 110–121. https://doi.org/10.1016/j.eurpolymj.2016.01.037.

Appendix

Appendix: Representative Spectra and Supporting Data for Chapter 3

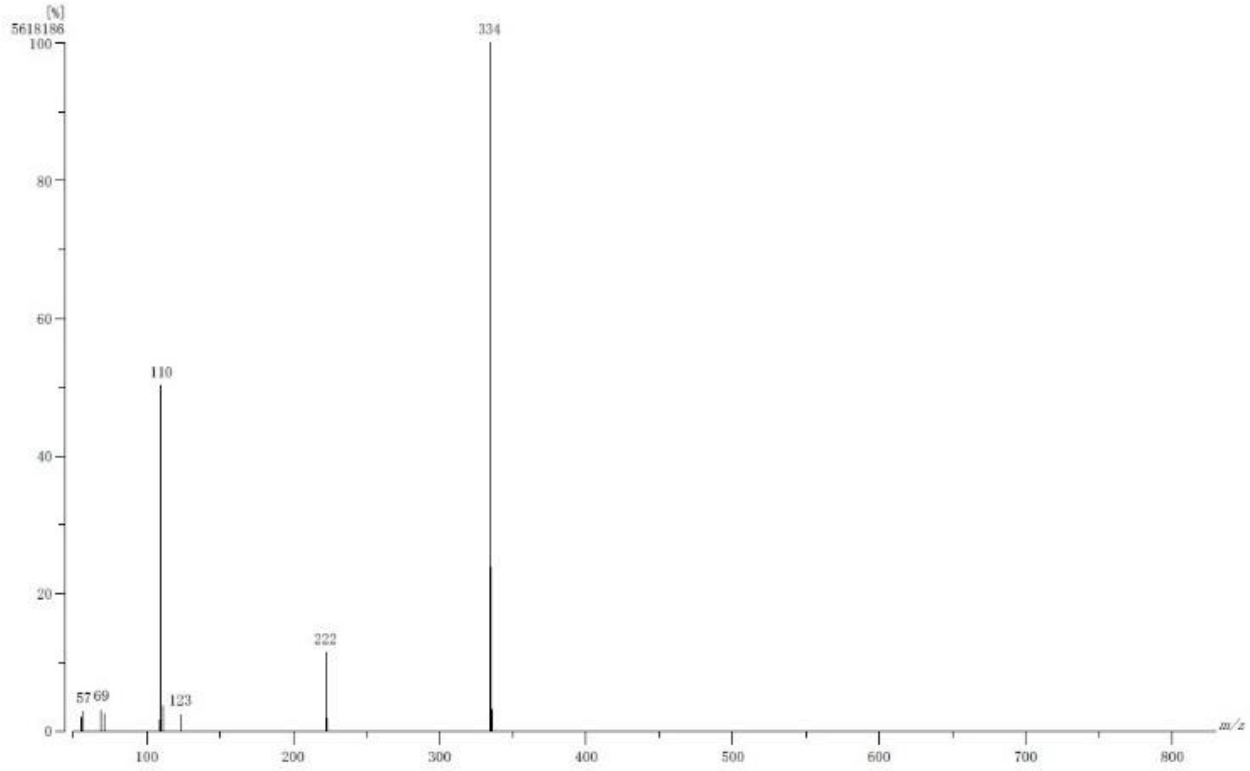

(a)

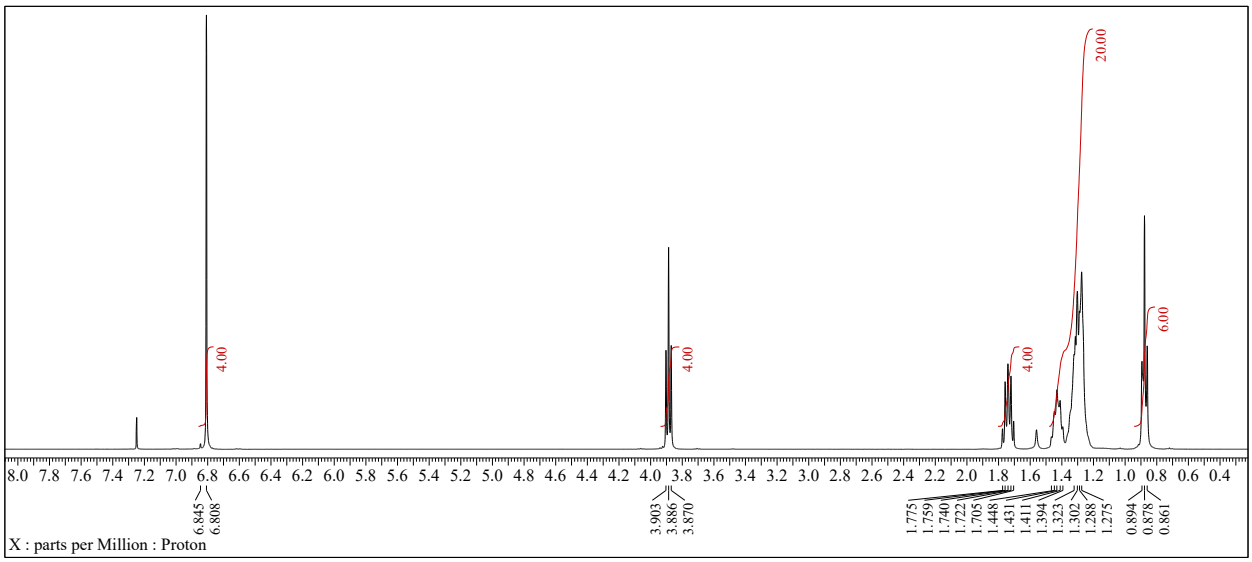

(b)

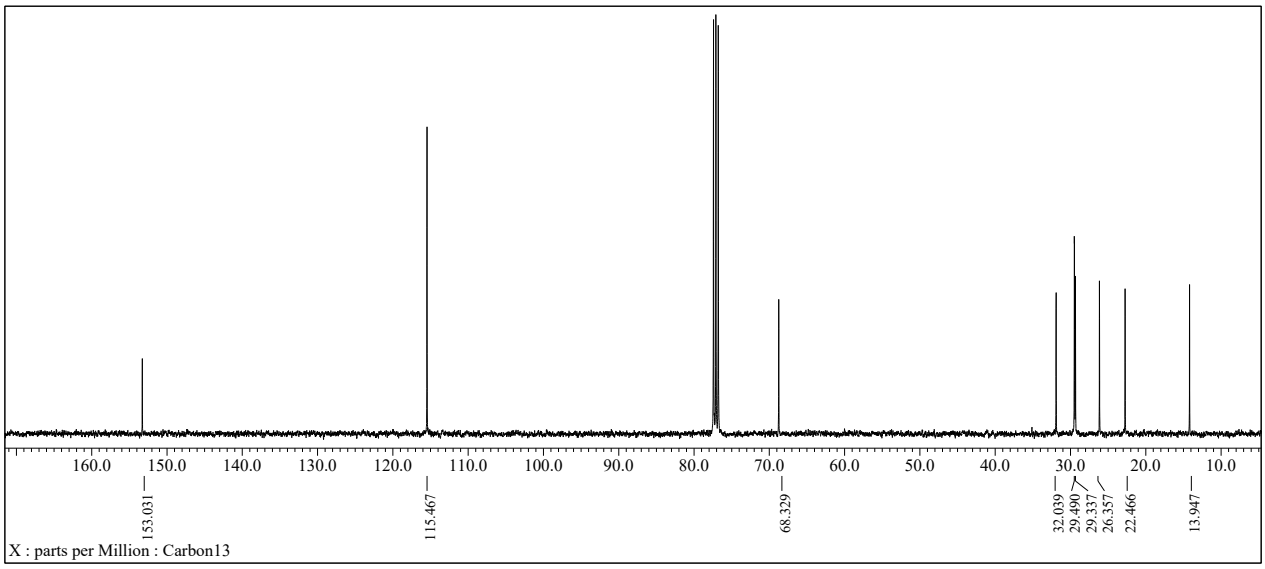

(c)

S3. 1 a) EI-MS spectrum of compound 1. b) ^{1}H NMR spectrum. C) ^{13}C NMR spectrum.

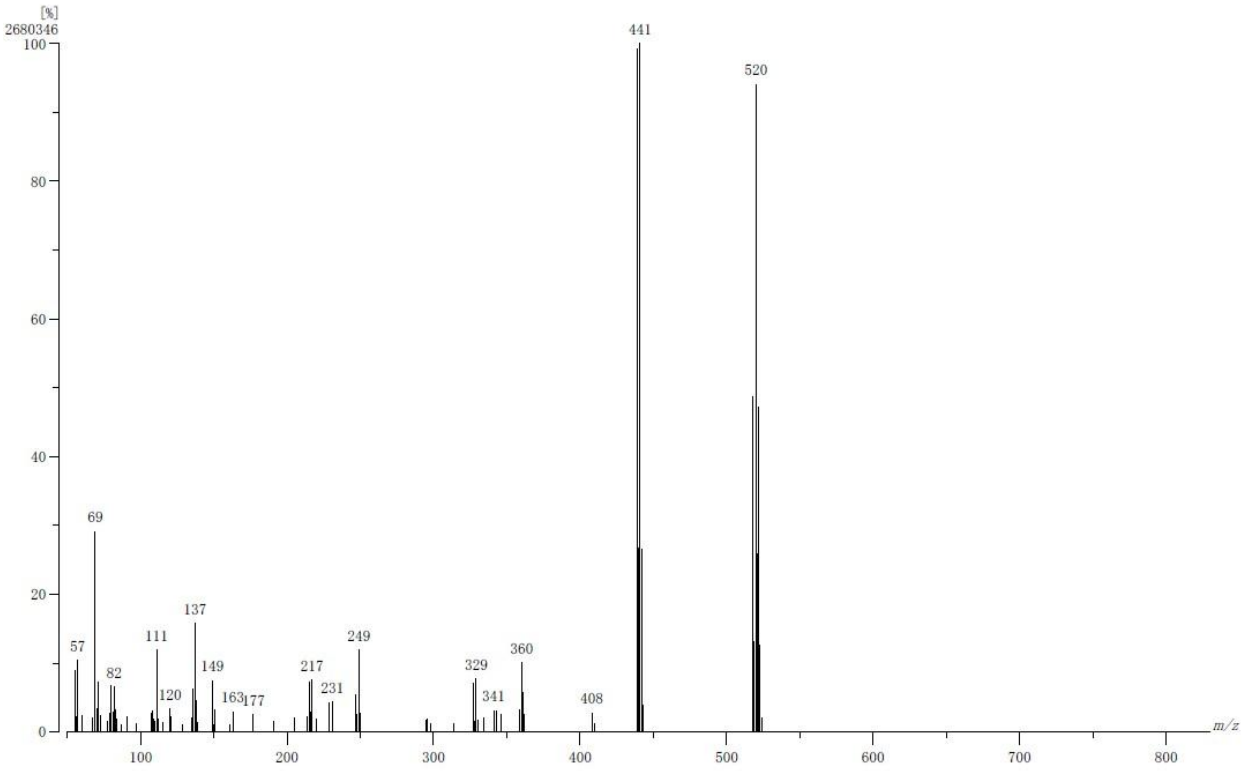

(a)

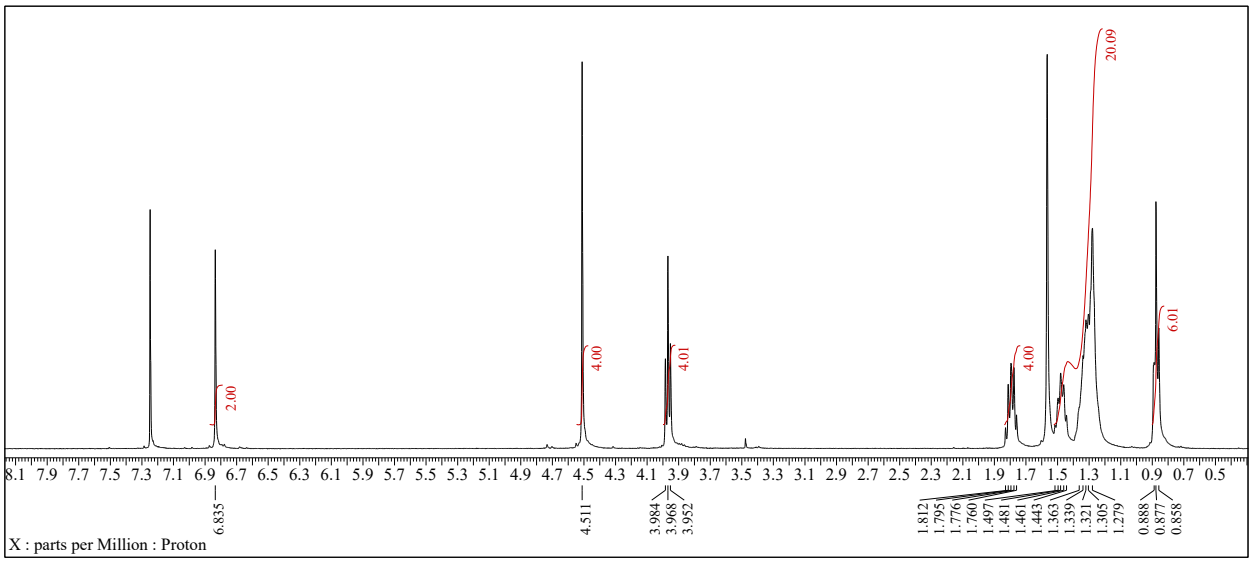

(b)

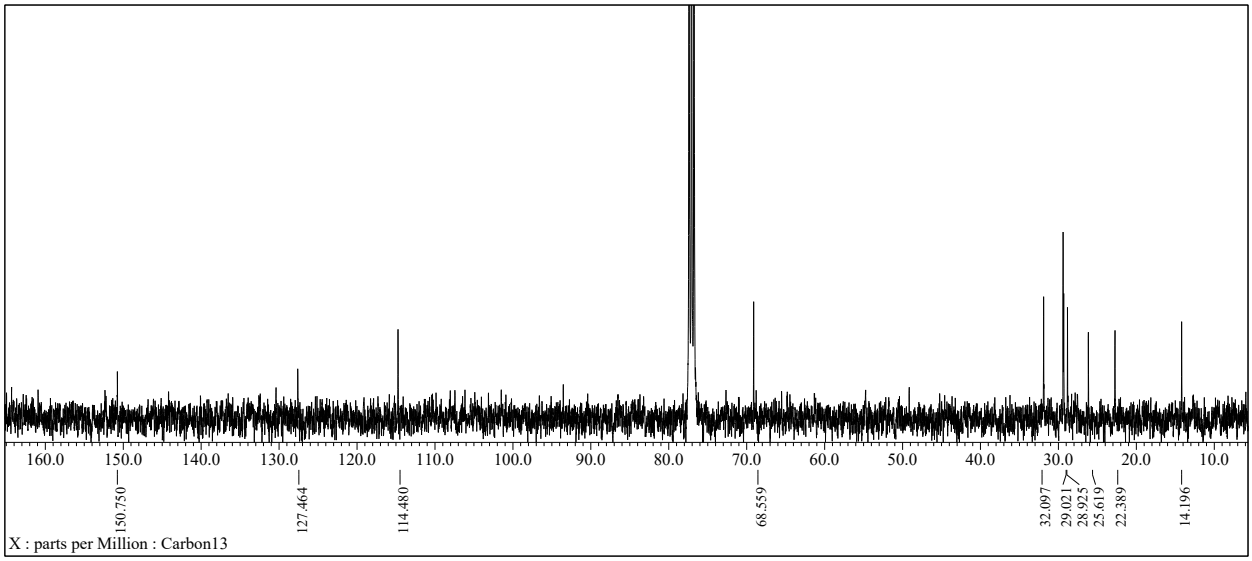

(c)

S3. 2 a) EI-MS spectrum of compound 2. b) ^{1}H NMR spectrum. C) ^{13}C NMR spectrum.

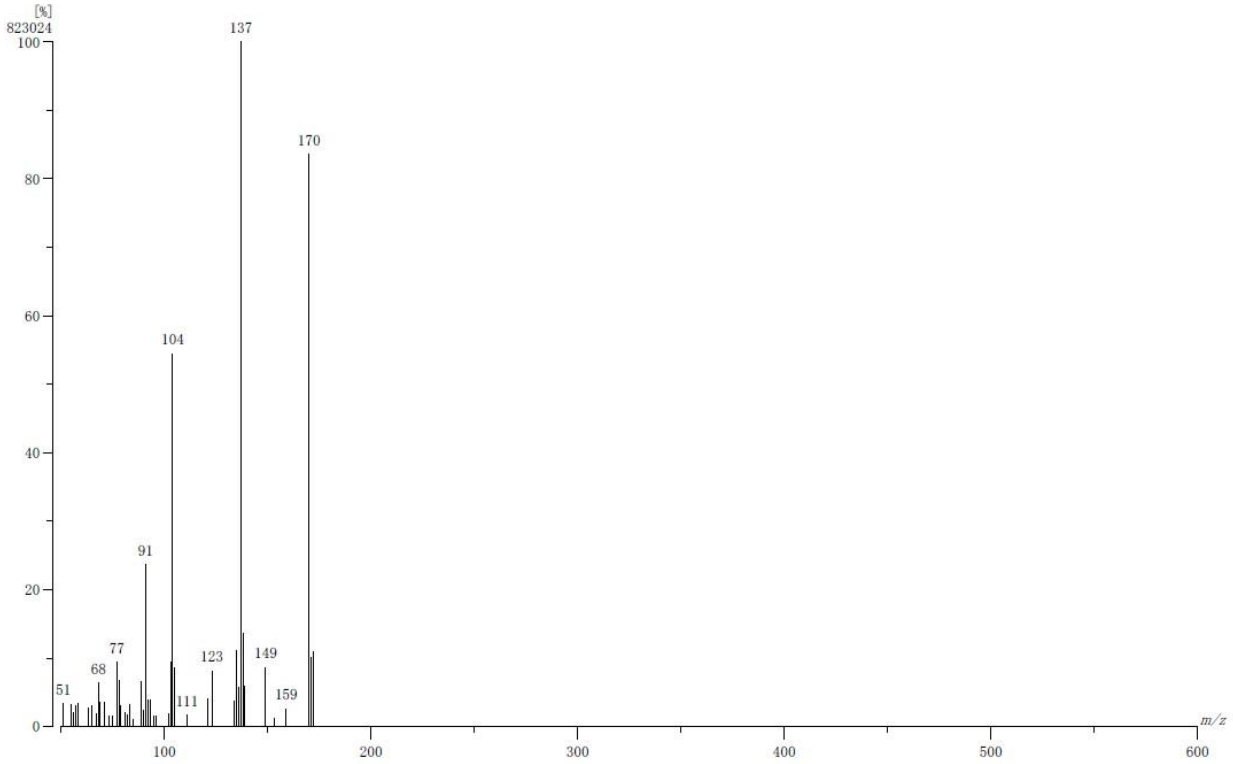
[%]
823024
100
80
60
40
20
0
137
170
104
91
77
68
51
123
149
111
159
100
200
300
400
500
600
m/z

(a)

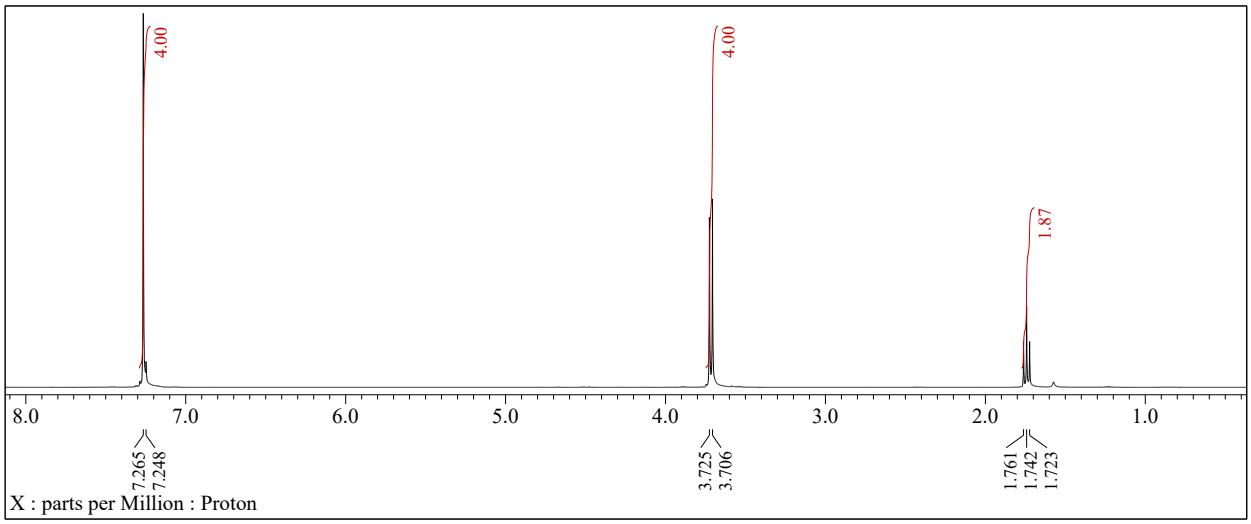
4.00
4.00
1.87
8.0
7.0
6.0
5.0
4.0
3.0
2.0
1.0
7.265
7.248
3.725
3.706
1.761
1.742
1.723
X : parts per Million : Proton

(b)

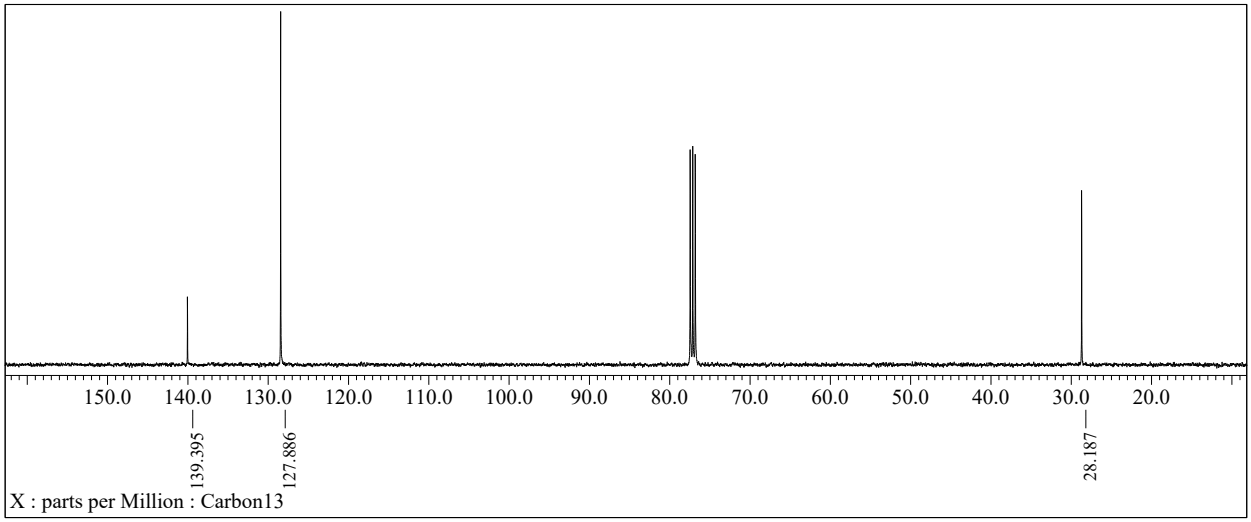

(c)

S3. 3 a) EI-MS spectrum of compound 3. b) ^{1}H NMR spectrum. C) ^{13}C NMR spectrum.

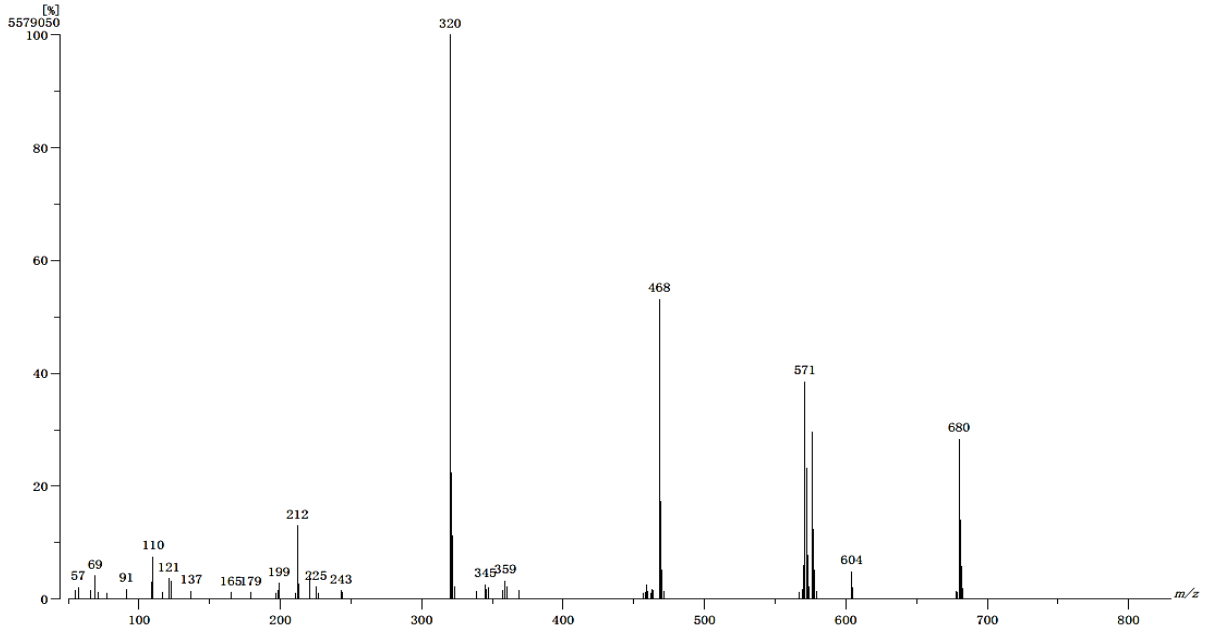

(a)

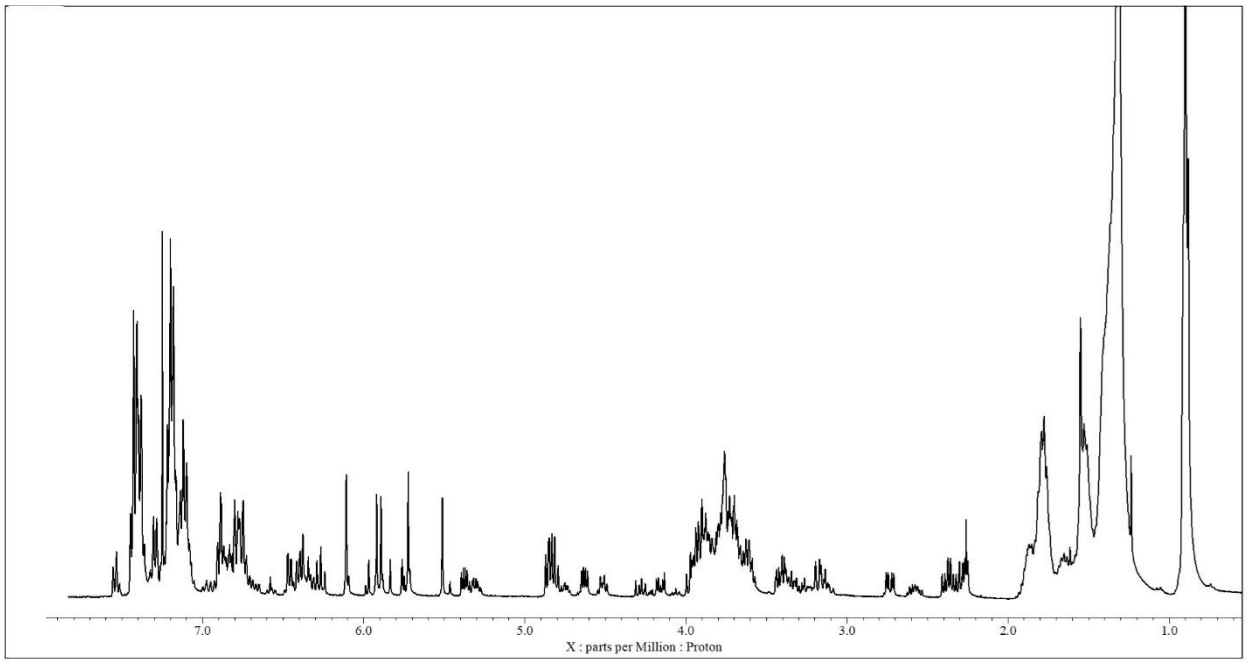

(b)

S3. 4 a) EI-MS spectrum of compound 5. b) ^{1}H NMR spectrum of intermediate 5.

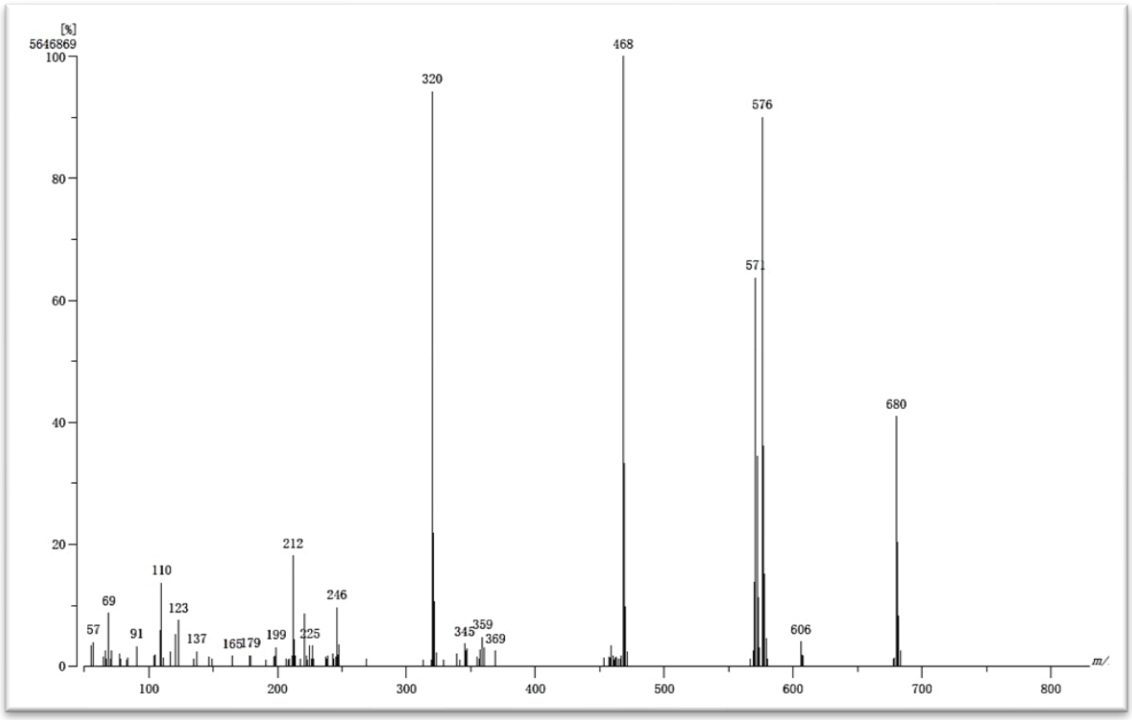

S3. 5 EI-MS spectrum of compound 6.

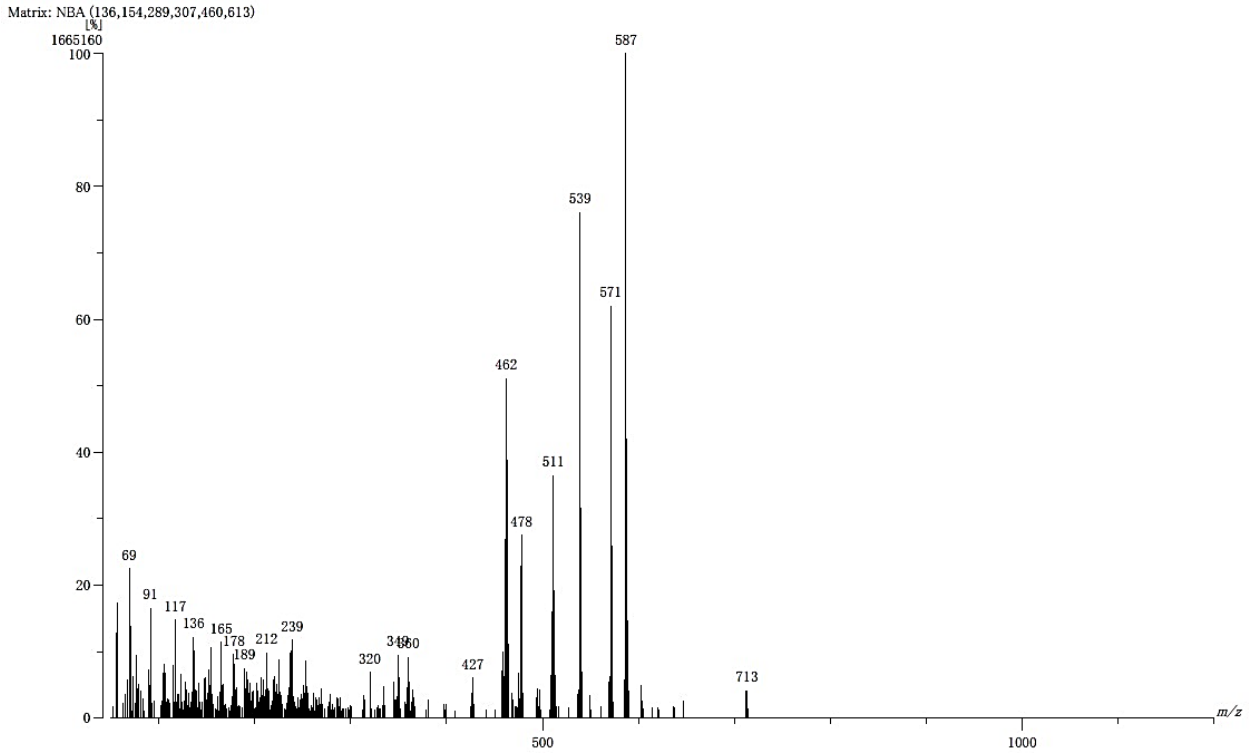

(a)

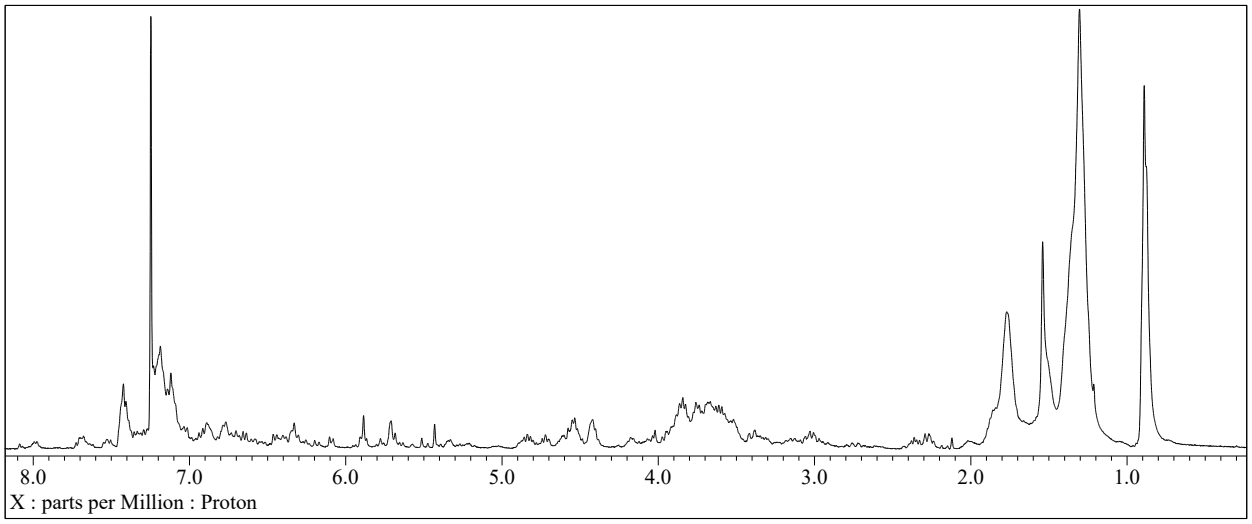

(b)

S3. 6 a) EI-MS spectrum of compound 7. b) ^{1}H NMR spectrum of intermediate 7.

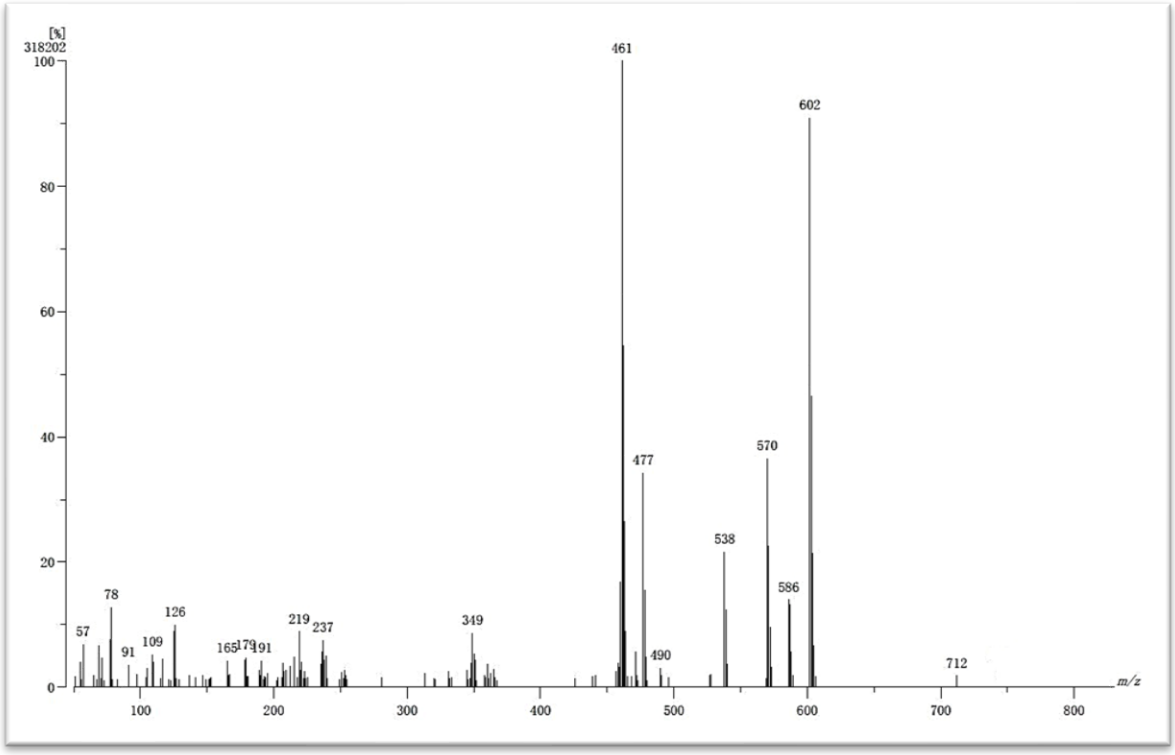

S3. 7 EI-MS spectrum of intermediate 8.

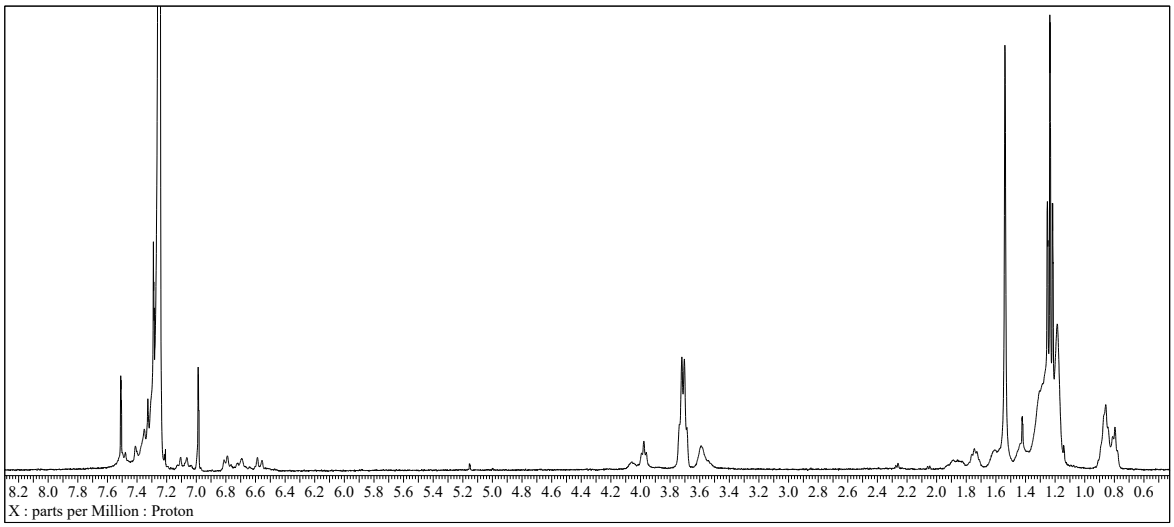

(a)

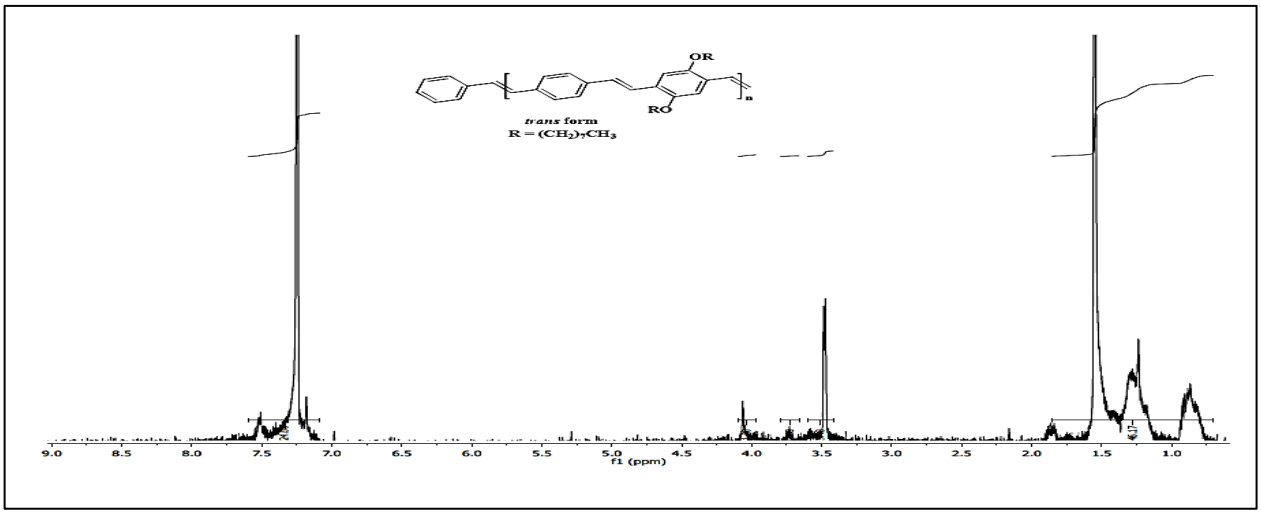

(b)

S3. 8 Compound 11 (P_1) a) ^{1}H NMR spectrum of *cis and trans* structure. b) ^{1}H NMR spectrum of *trans* structure.

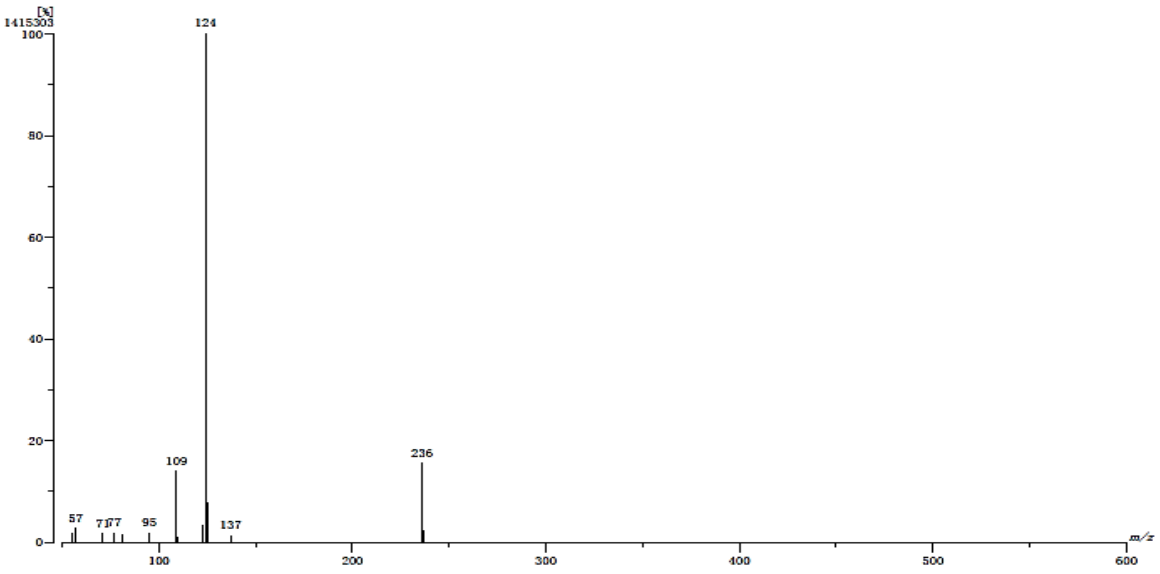

(a)

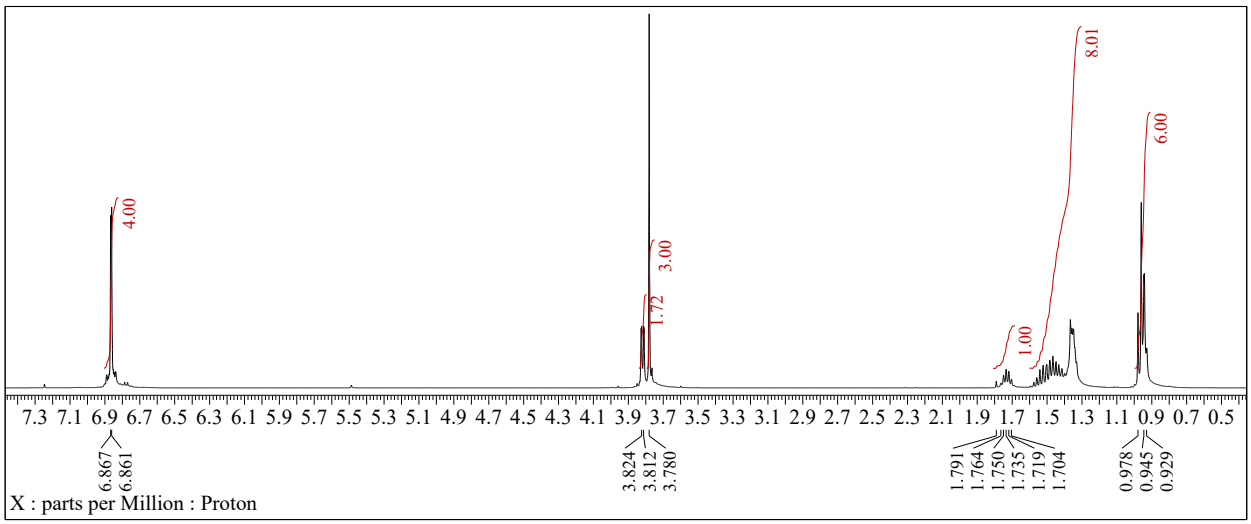

(b)

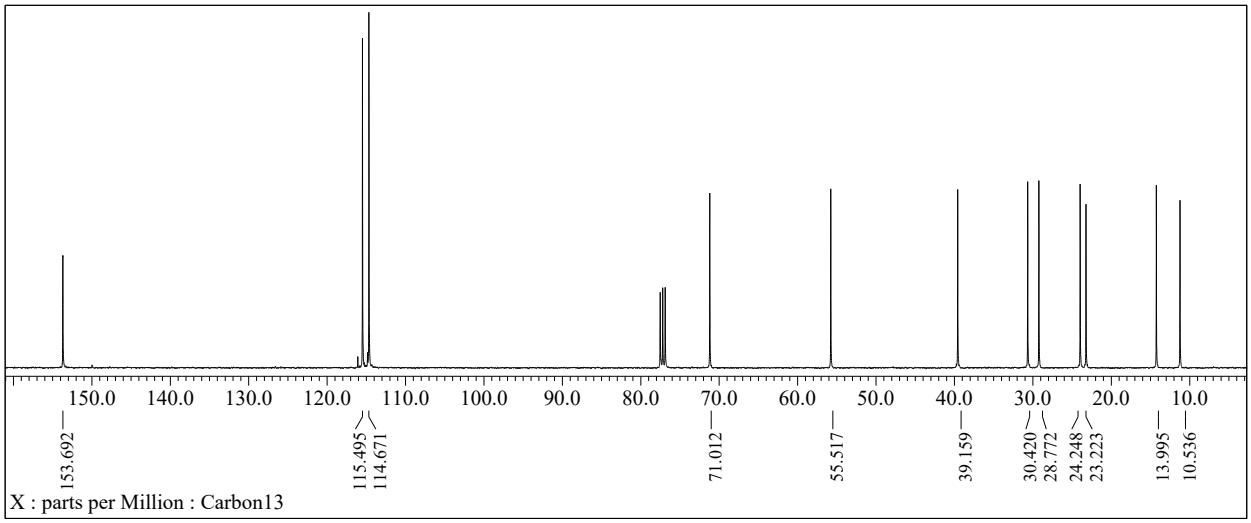

(c)

S3. 9 Compound 12 a) EI-MS spectrum; b) ^{1}H NMR spectrum; c) ^{13}C NMR spectrum.

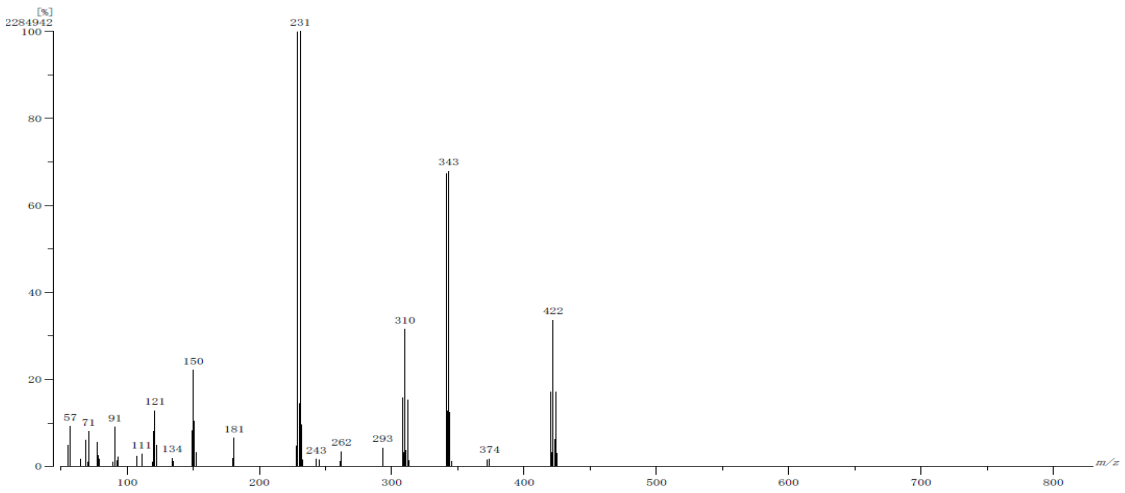

(a)

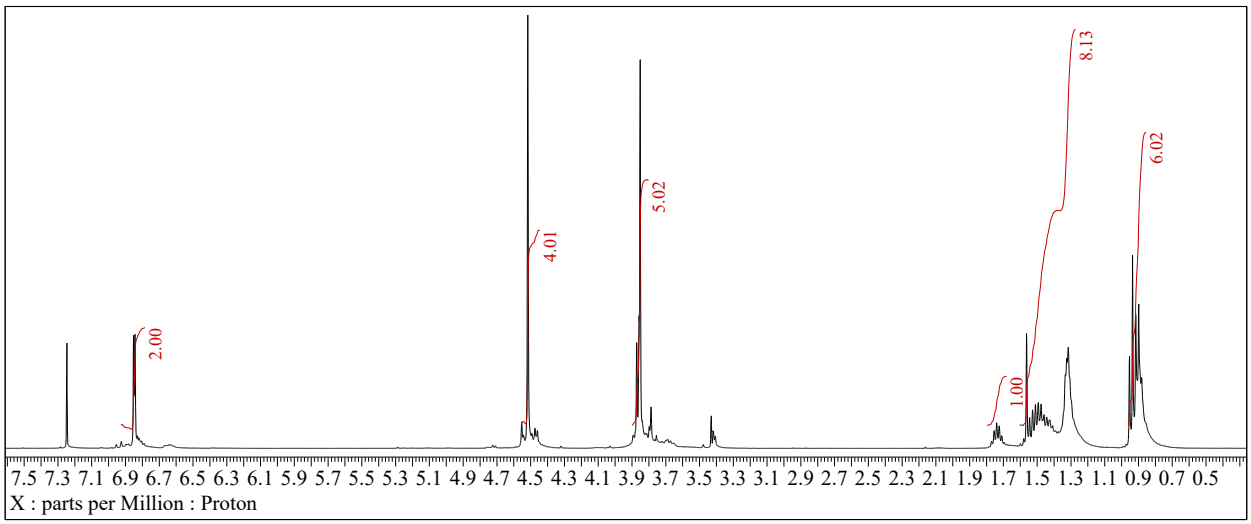

(b)

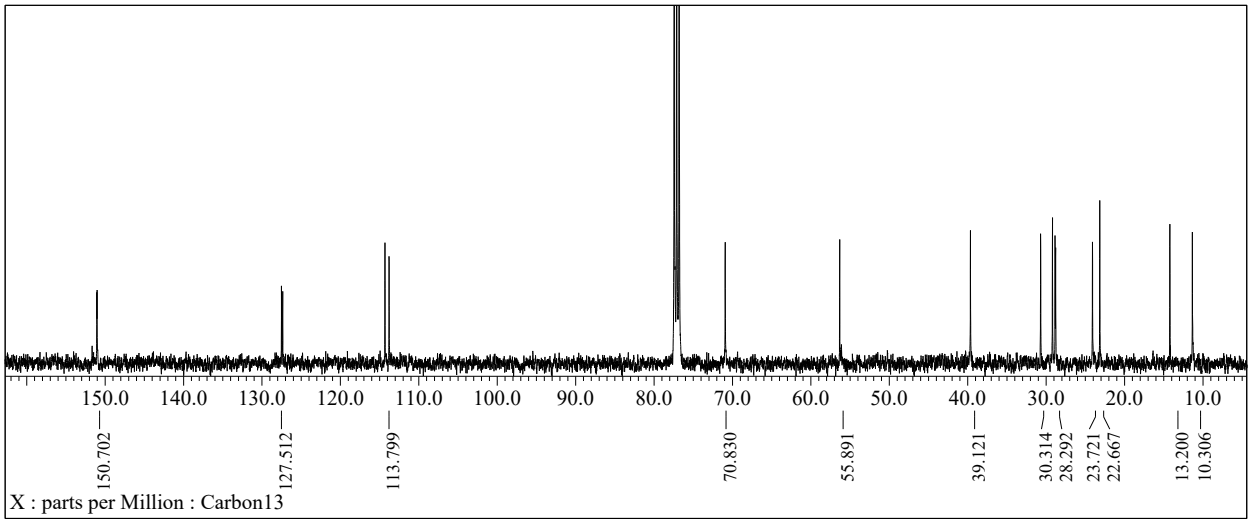

(c)

S3. 10 Compound 13 a) EI-MS spectrum; b) ^{1}H NMR spectrum; c) ^{13}C NMR spectrum.

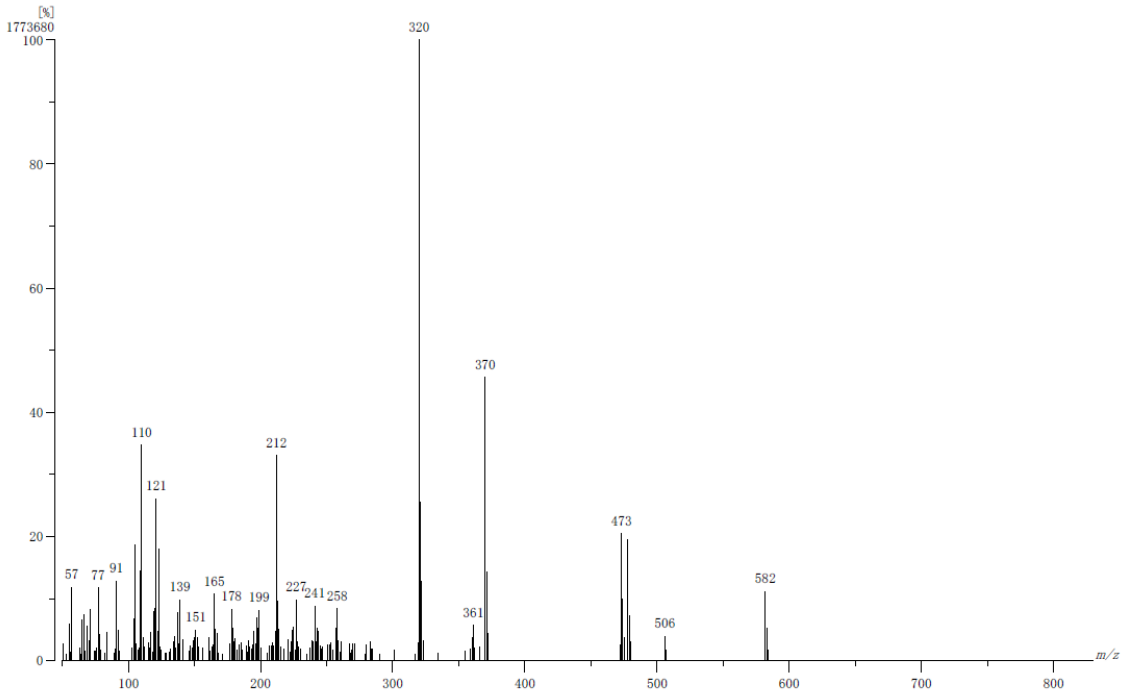

S3. 11 EI-MS spectrum for compound 15.

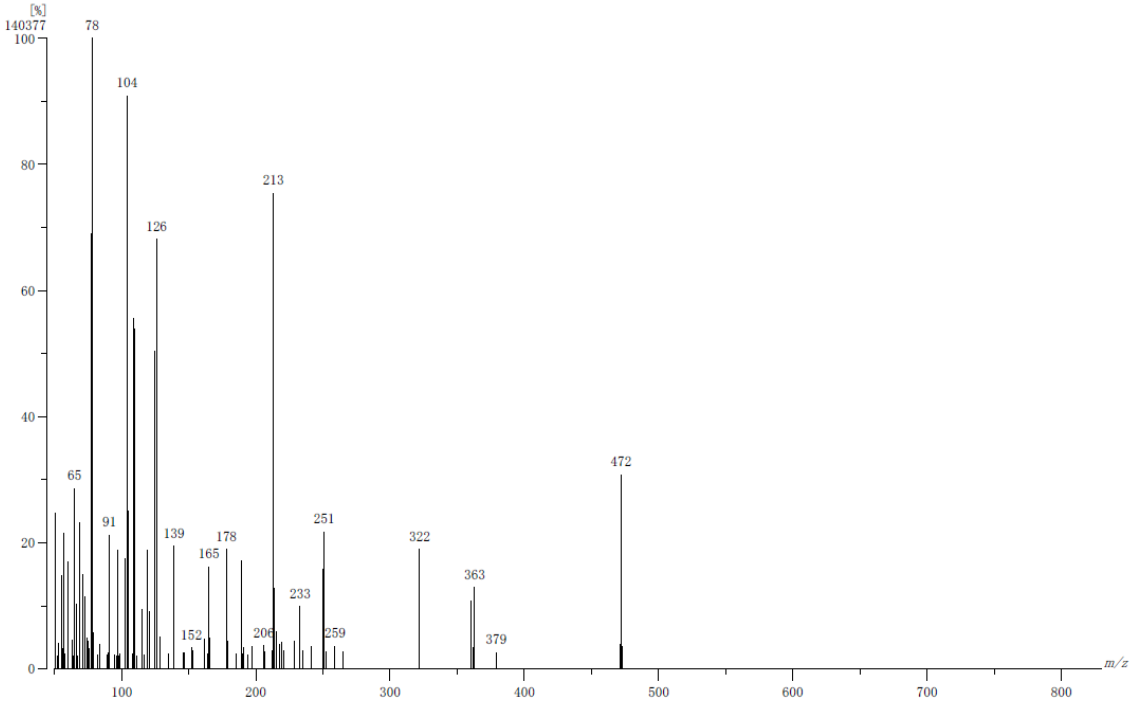

S3. 12 EI-MS spectrum for compound 16

Appendix: Representative Spectra and Supporting Data for Chapter 4

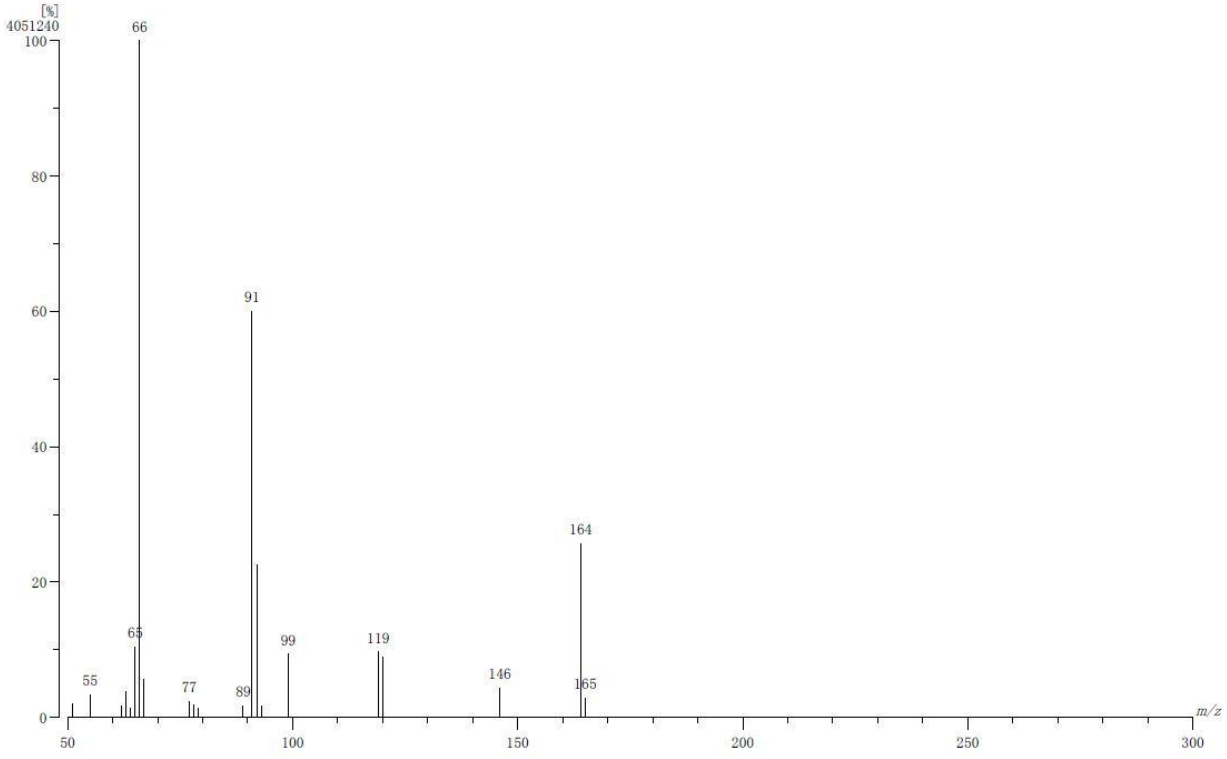

(a)

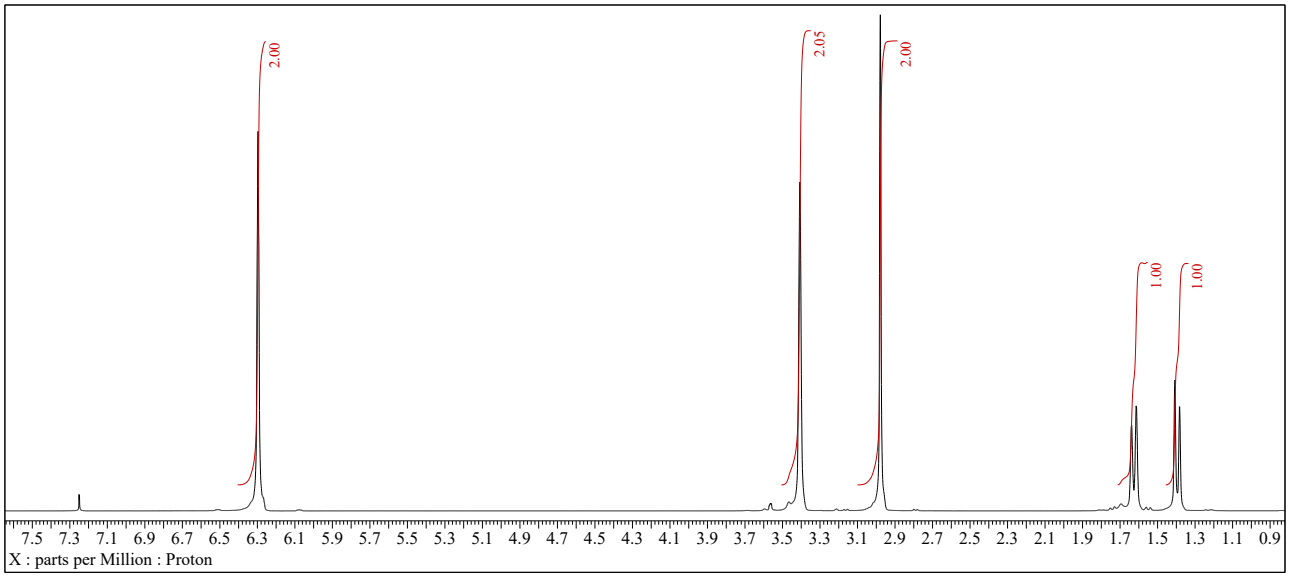

(b)

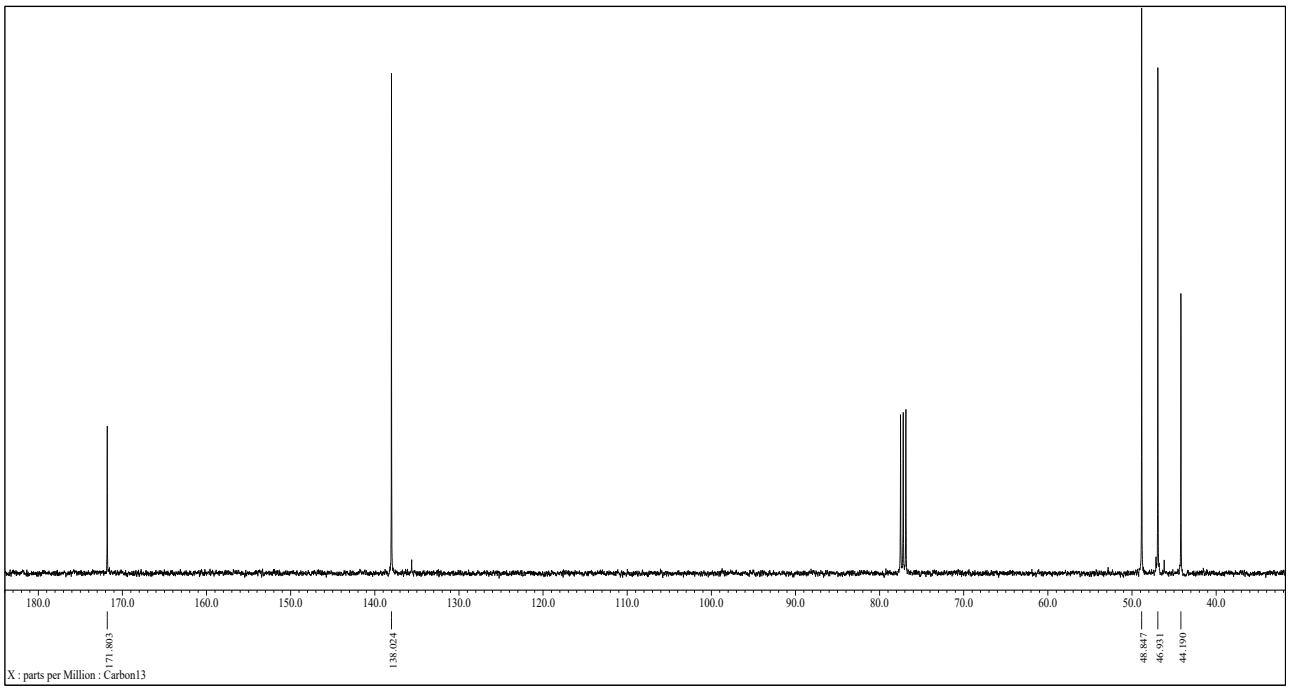

(c)

S4. 1 a) EI-MS spectrum, b) ^{1}H NMR spectrum, and C) ^{13}C NMR spectrum of precursor 1

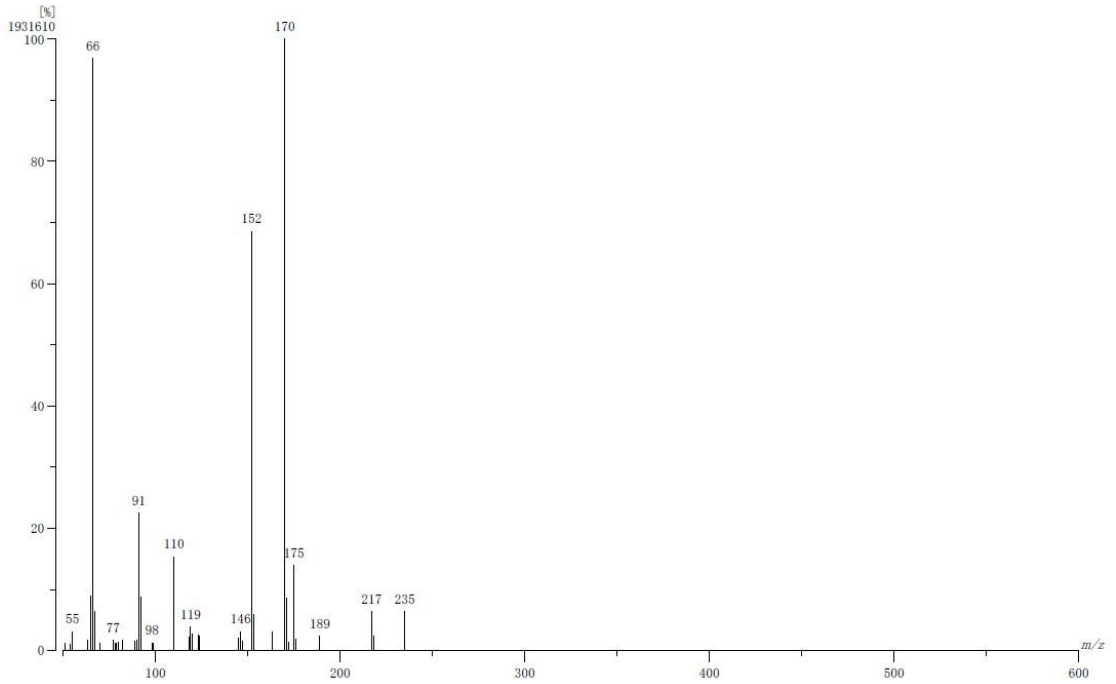

(a)

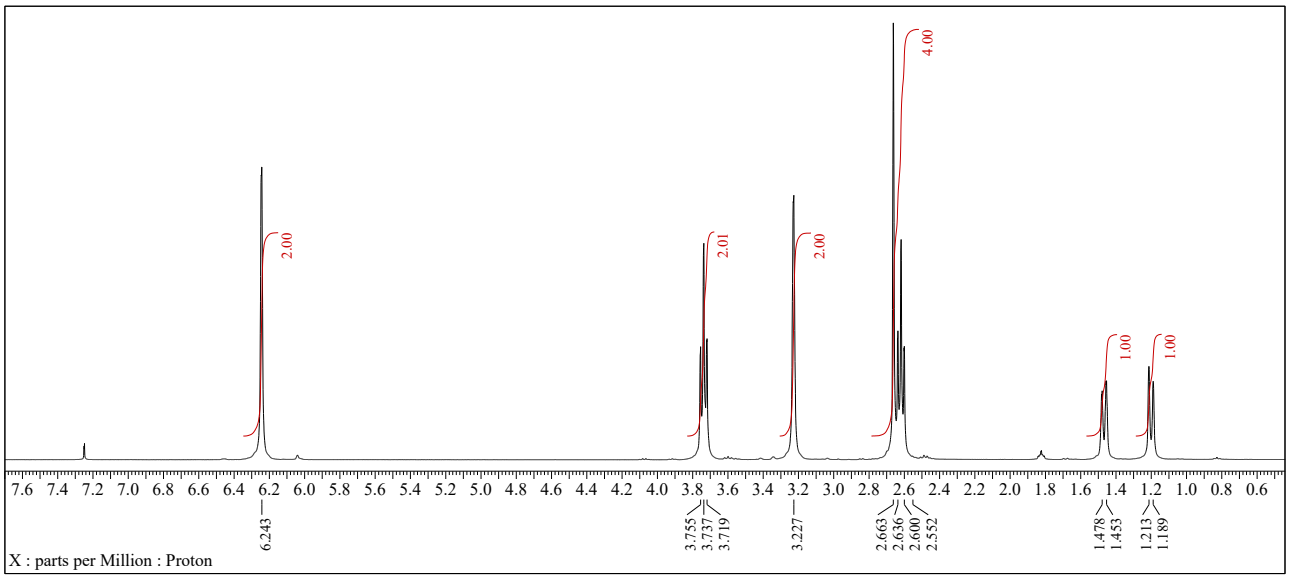

(b)

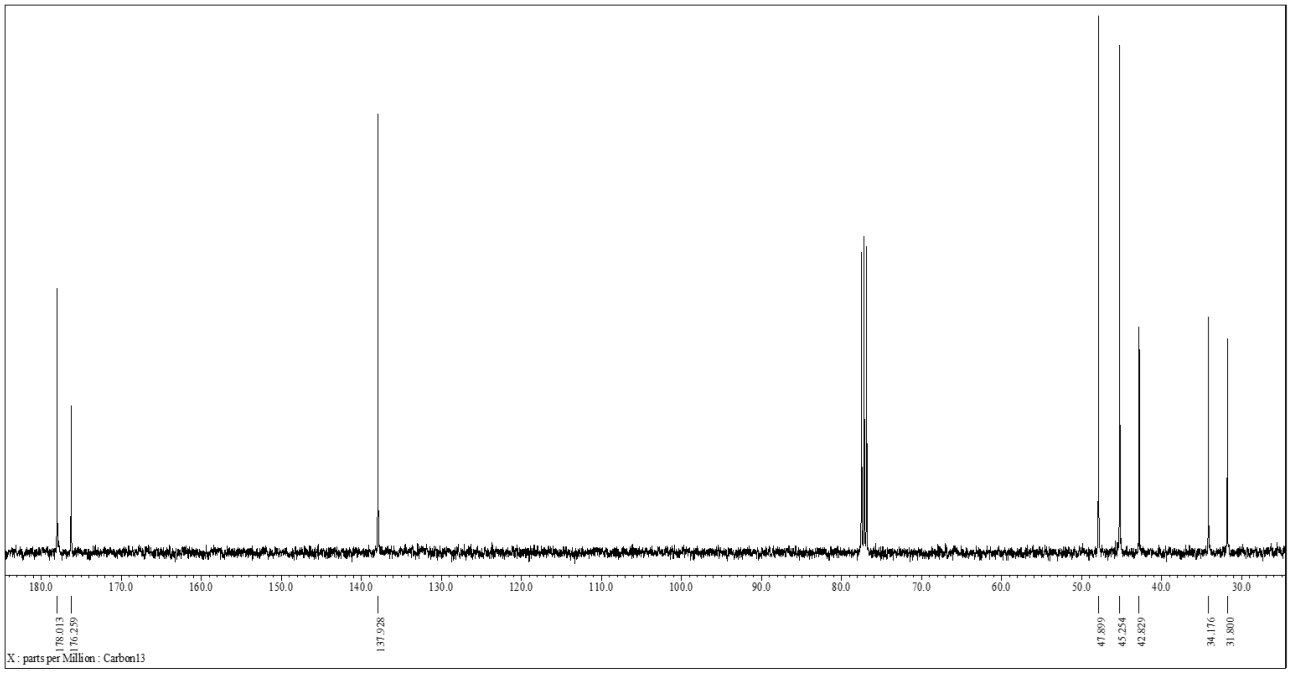

(c)

S4. 2 a) EI-MS spectrum, b) ^{1}H NMR spectrum, and C) ^{13}C NMR spectrum of precursor 2.

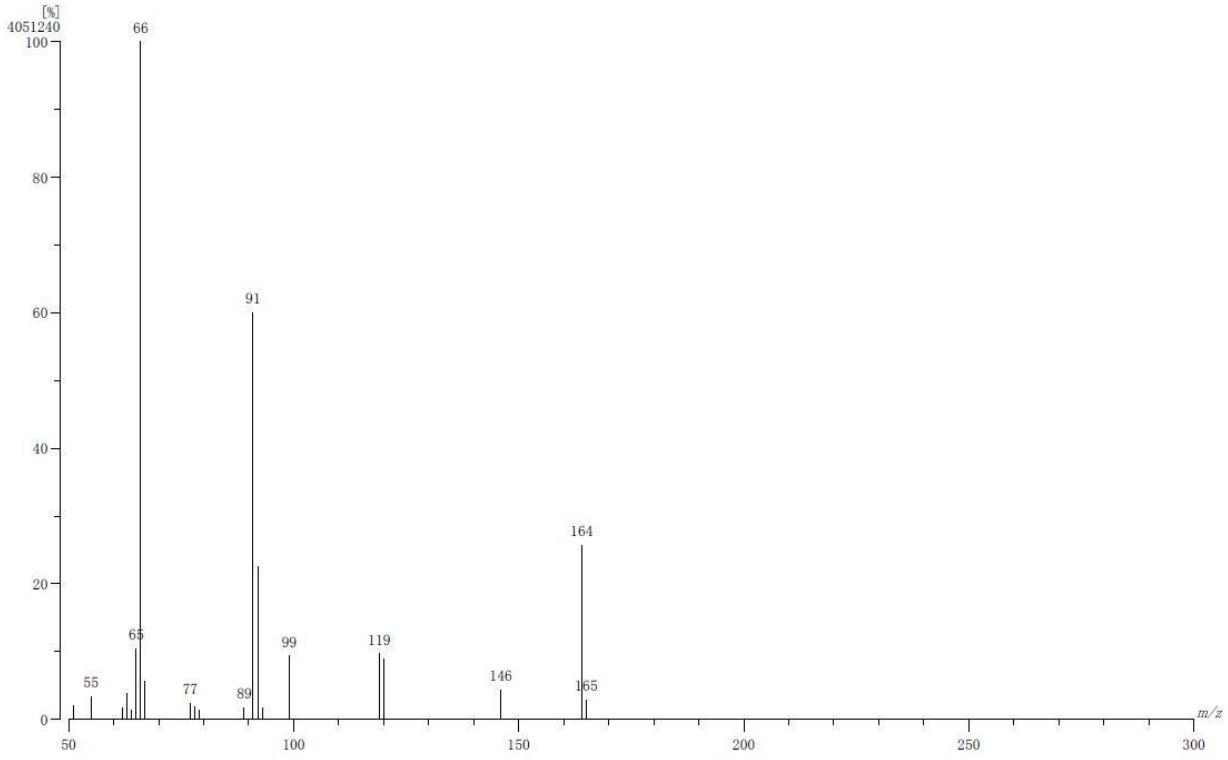
[%]
4051240
100
80
60
40
20
0
66
91
164
65
99
119
146
55
77
89
165
m/z
50
100
150
200
250
300

(a)

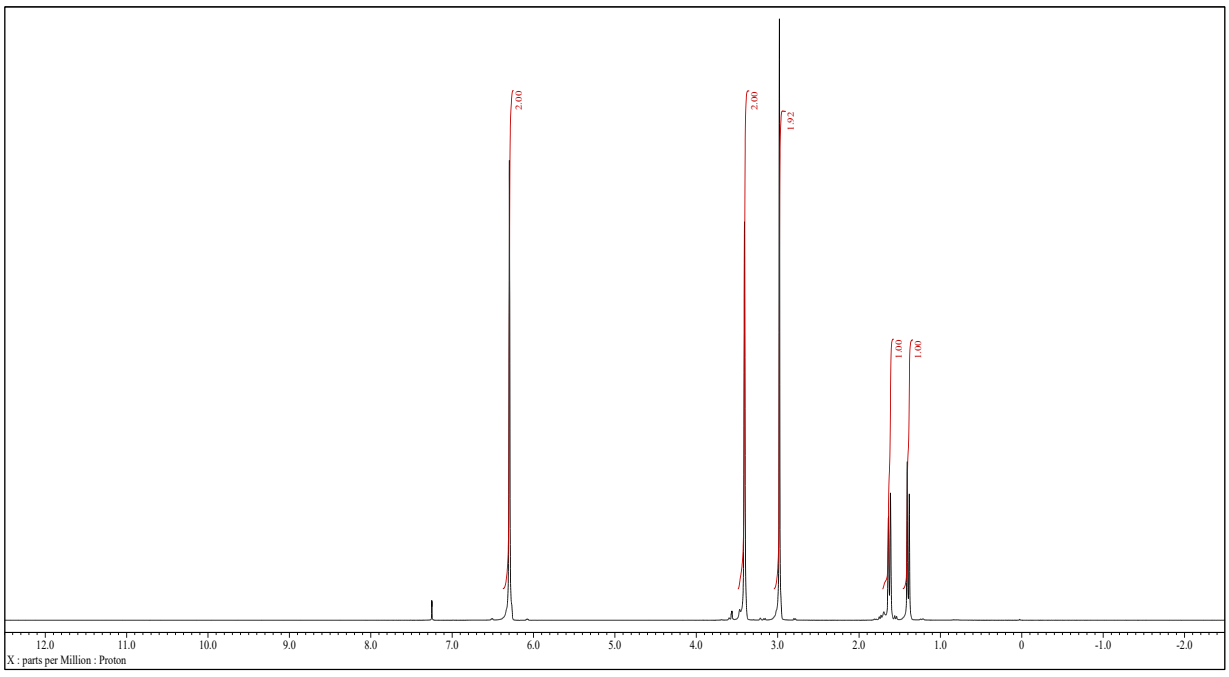
2.00
2.00
1.92
1.00
1.00
12.0
11.0
10.0
9.0
8.0
7.0
6.0
5.0
4.0
3.0
2.0
1.0
0
-1.0
-2.0
X : parts per Million : Proton

(b)

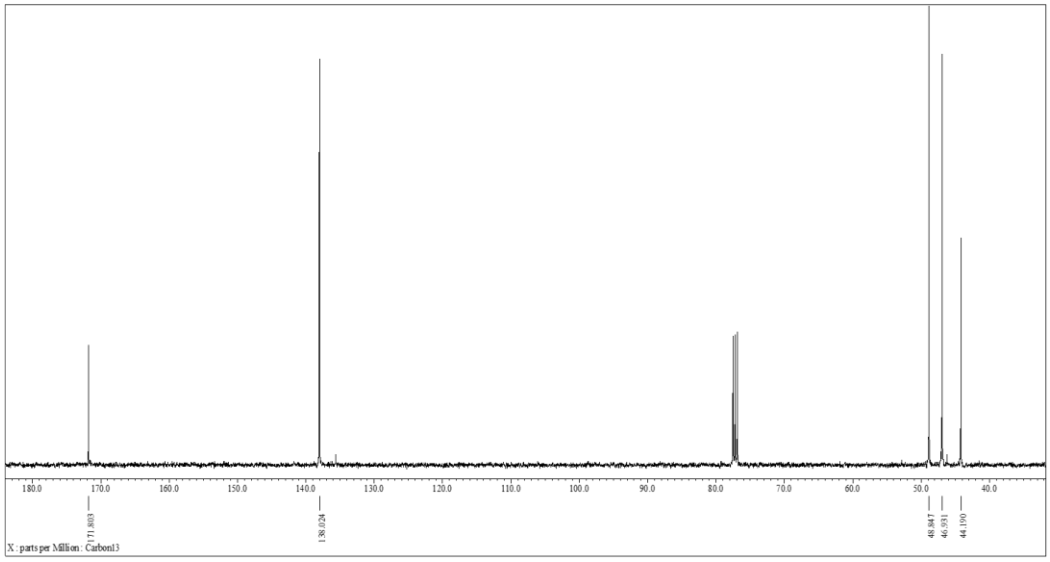

(c)

S4. 3 a) EI-MS spectrum, b) ^{1}H NMR spectrum, and C) ^{13}C NMR spectrum of precursor 5

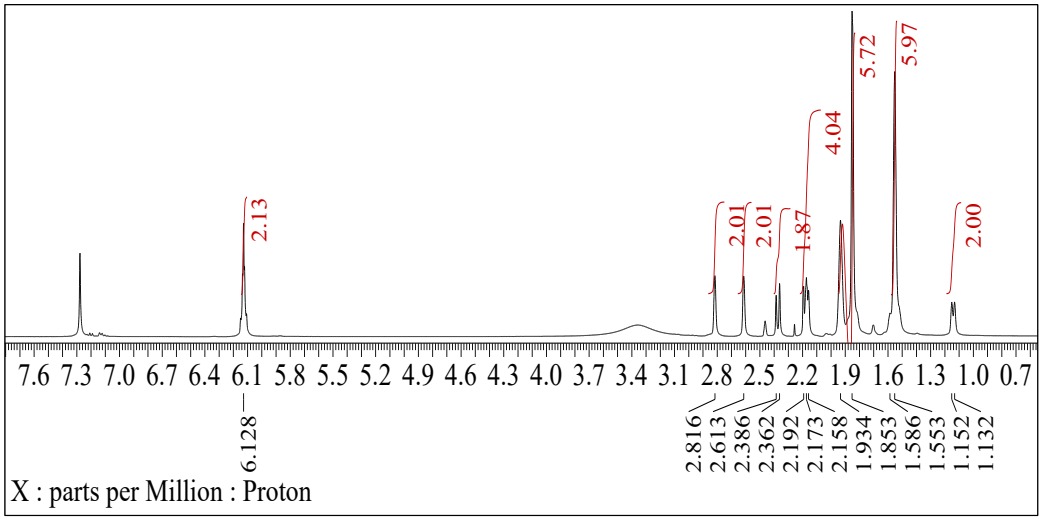

(a)

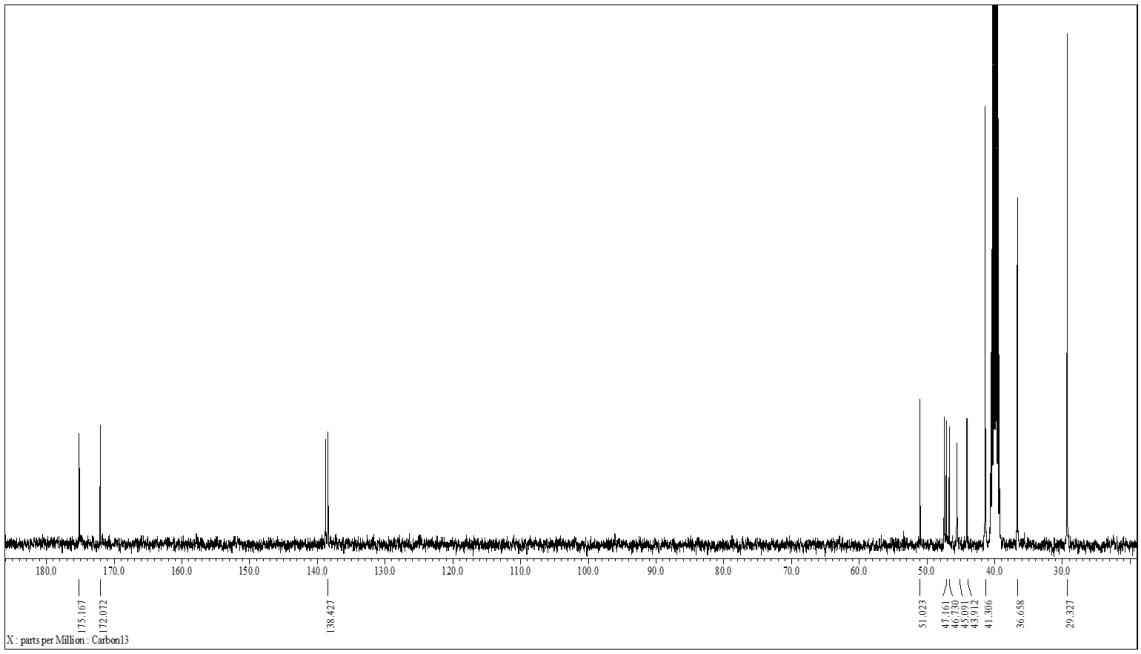

(b)

S4. 4 a) ^{1}H NMR spectrum and b) ^{13}C NMR spectrum of precursor 6.

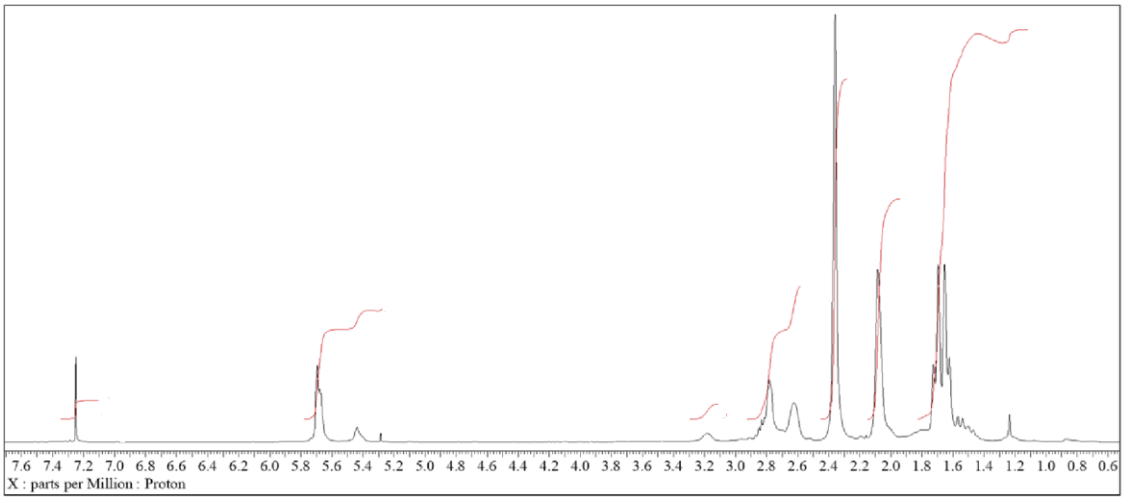

S4. 5 1H NMR spectrum of P4

Appendix: Representative Spectra and Supporting Data for Chapter 6

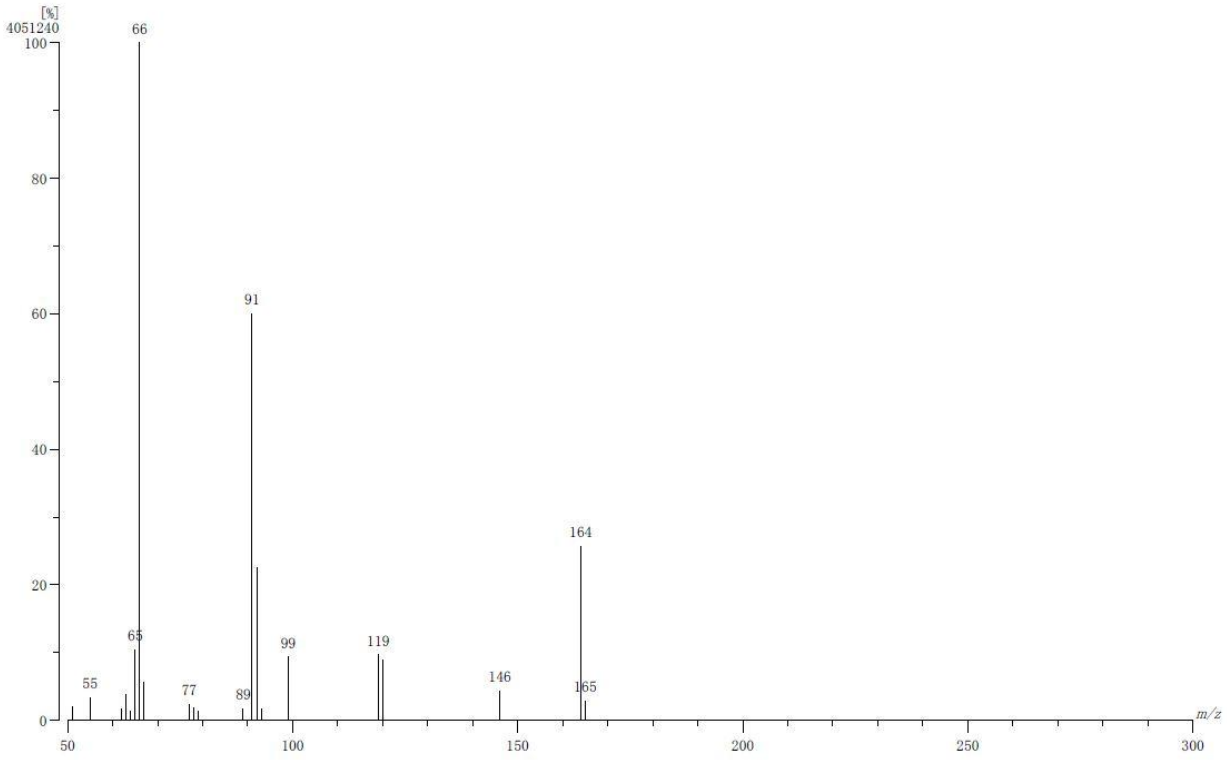

(a)

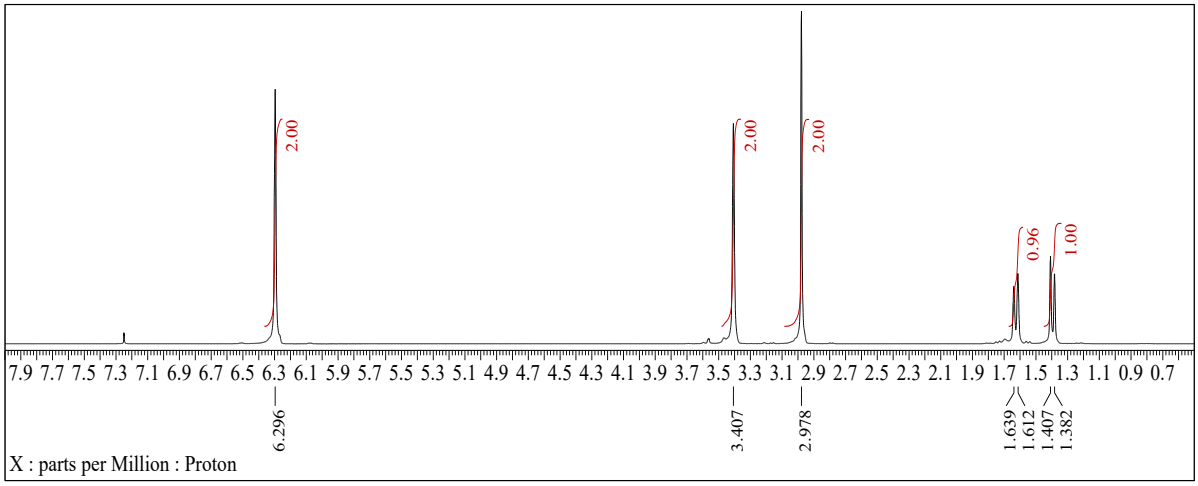

(b)

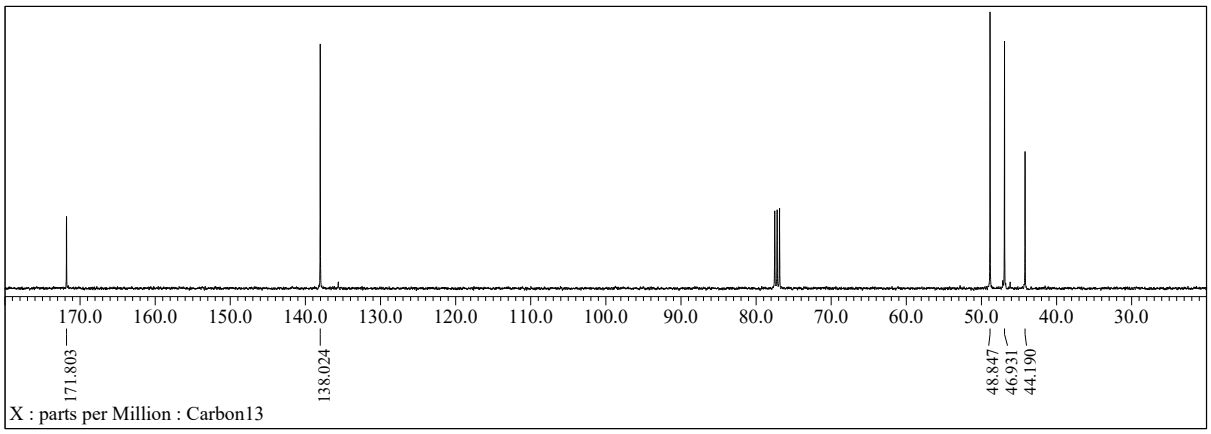

(c)

S6. 1 a) EI-MS, b) ^{1}H NMR, and c) ^{13}C NMR FOR (exo-NDA) (1).

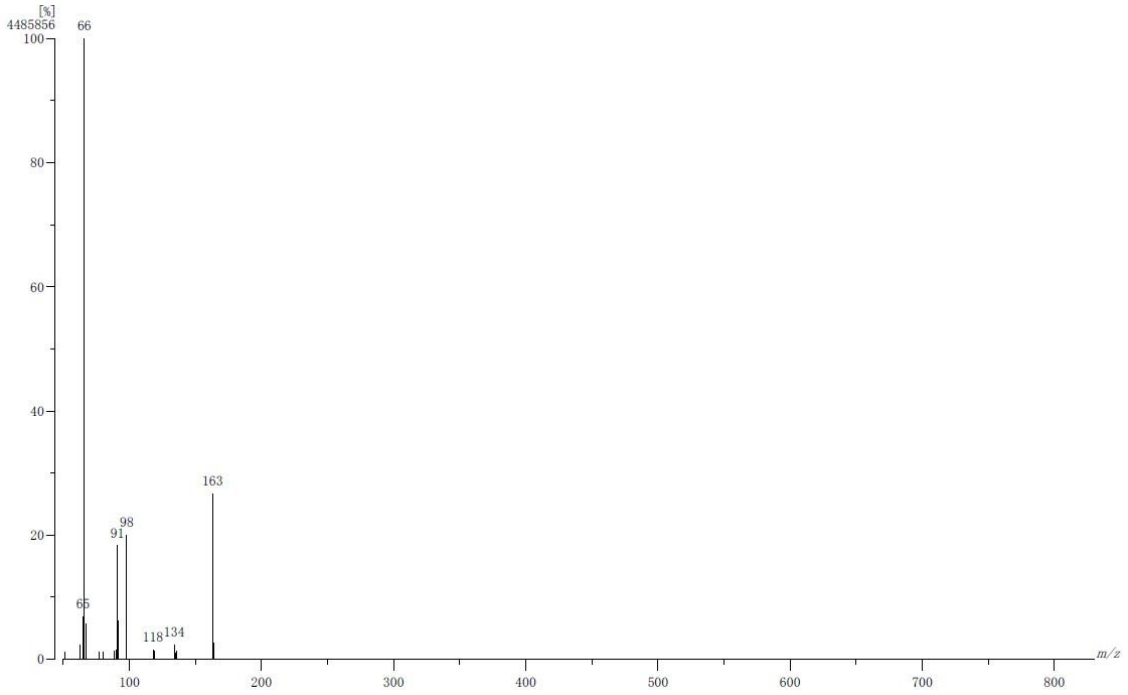

(a)

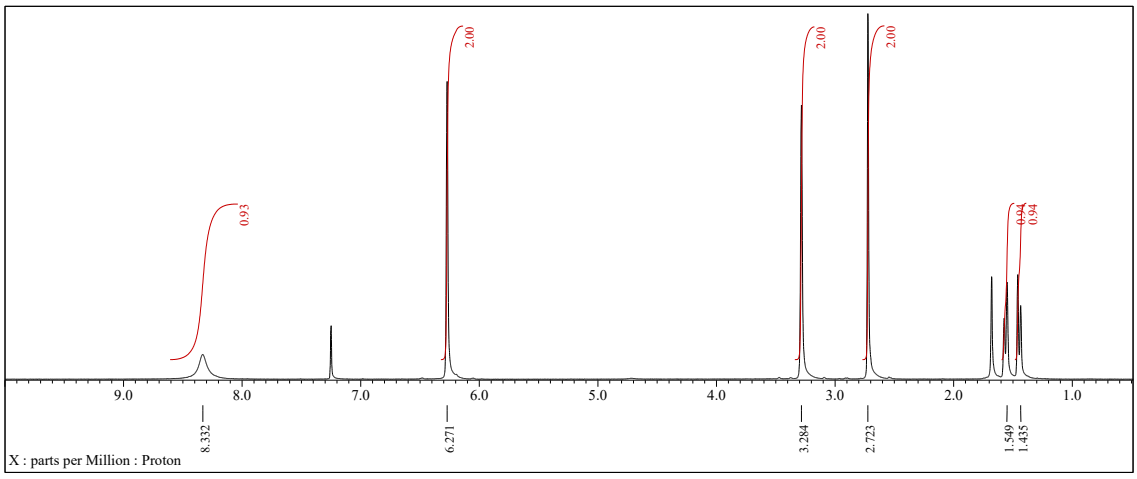

(b)

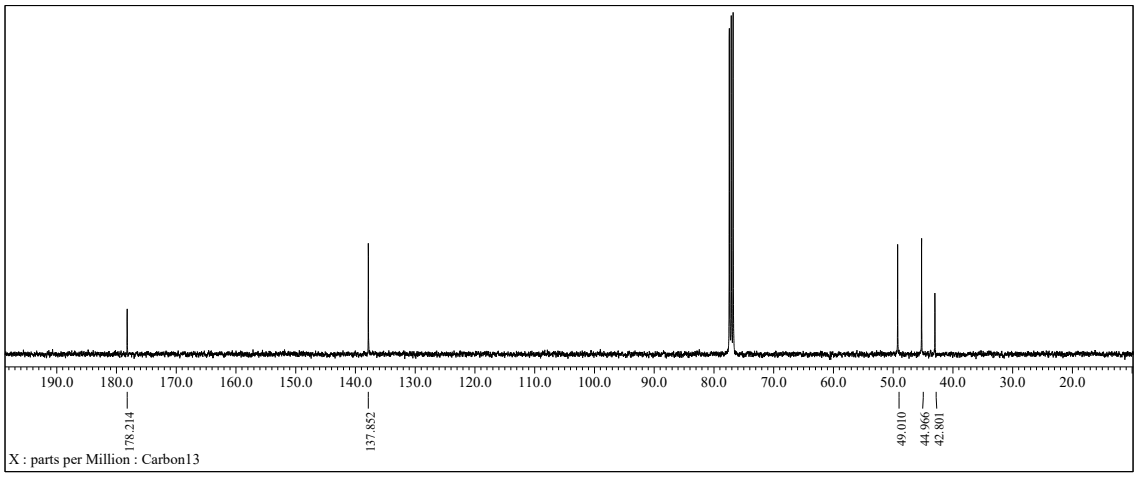

(c)

S6. 2 a) EI-MS spectrum; b) ^{1}H NMR spectrum; c) ^{13}C NMR spectrum for (NDI) (2).